

WestminsterResearch

<http://www.westminster.ac.uk/westminsterresearch>

Nerve tissue engineering using blends of Polyhydroxyalkanoates

Lizarraga Valderrama, L.

This is an electronic version of a PhD thesis awarded by the University of Westminster.
© Ms Lorena Lizarraga Valderrama, 2017.

The WestminsterResearch online digital archive at the University of Westminster aims to make the research output of the University available to a wider audience. Copyright and Moral Rights remain with the authors and/or copyright owners.

Whilst further distribution of specific materials from within this archive is forbidden, you may freely distribute the URL of WestminsterResearch: (<http://westminsterresearch.wmin.ac.uk/>).

In case of abuse or copyright appearing without permission e-mail repository@westminster.ac.uk

NERVE TISSUE ENGINEERING USING BLENDS OF POLYHYDROXYALKANOATES

Lorena del Rosario Lizarraga Valderrama

A thesis submitted in partial fulfilment of the requirements of the University of
Westminster for the degree of Doctor of Philosophy

January 2017

Abstract

PHAs are a family of linear polyesters consisting of 3, 4, 5 and 6-hydroxyacids, synthesized by a variety of bacterial species. They can be produced from renewable carbon sources, they are biodegradable, biocompatible and exhibit thermoplastic and elastomeric properties. Therefore, PHAs are a potential substitute for petroleum-derived plastics and have a wide range of biomedical applications, particularly in tissue engineering and drug delivery. The properties of PHA devices can be successfully modified through the fabrication of composites and blends. Such modifications allow for further tailoring of properties such as biocompatibility, mechanical properties and degradation times required for specific physiological conditions. PHAs have been used for the manufacture of a wide variety of surgical materials and implants in the areas of skin, nerve, dental, cardiac and bone tissue engineering. The latter two fields being where the PHAs have been the most extensively explored. These unique polymers possess significant advantages compared to their chemically-synthesized counterparts. Their structural diversity, adaptable properties, controllable surface degradation and biocompatibility with a wide range of cells, place PHAs as a biomaterial with immense potential for biomedical applications.

The main aim of this project was to explore the use of Polyhydroxyalkanoates in nerve tissue engineering ultimately leading to the development of novel PHA-based nerve guidance conduits (NGCs). Production of the scl-PHA, P(3HB) and the mcl-PHA, P(3HO) through bacterial fermentation was performed to obtain appropriate amounts of polymer for chemical characterisation and further manufacturing of scaffolds for nerve tissue engineering applications. The average polymer yields achieved using a 20 L fermenter were 42.27 % dcw of P(3HO) using *Pseudomonas mendocina* CH50 and 49.22 % dcw of P(3HO) using *Bacillus cereus* SPV respectively.

Novel PHA blends as resorbable biomaterials for use in the manufacture of NGCs were fabricated. PHA blend films with varying ratios of poly(3-hydroxyoctanoate)/poly(3-hydroxybutyrate), (P(3HO)/P(3HB)), were produced using the solvent-casting method. Neat films of P(3HO) and P(3HB) along with 25:75, 50:50 and 75:25 blend films of P(3HO)/P(3HB) were characterised with respect to their chemical, material and biological properties in order to evaluate them as potential base materials for nerve tissue engineering. In the surface analysis the blends exhibited higher values of roughness compared with the neat films. The DSC characterisation of the blends confirmed that P(3HO) and P(3HB) formed immiscible blends. FTIR and XRD analysis of the blends showed a decrease in the crystallinity with increase in the proportion of P(3HO). An increase in the stiffness of the blends was observed when the proportion of P(3HB) increased. Although all of the blends were biocompatible with

NG108-15 neuronal cells, the 25:75 P(3HO)/P(3HB) blend showed significantly better support for the growth and differentiation of these cells. Mechanical properties of PHA blends corresponded to the reported properties of peripheral nerves providing potential materials for their use as base material for the manufacture of NGCs.

The 25:75 P(3HO)/P(3HB) blend was used for the manufacturing of electrospun fibres as resorbable scaffolds for their use in the manufacture of NGCs as lumen structure. The biocompatibility of these fibres with NG108-15 neuronal cells as well as the influence of RN22 Schwann cells on their growth and differentiation was studied. Highly aligned and uniform fibres with varying diameters were successfully fabricated by controlling electrospinning parameters. The resulting fibre diameters were $2.42 \pm 0.34 \mu\text{m}$, $3.68 \pm 0.26 \mu\text{m}$ and $13.50 \pm 2.33 \mu\text{m}$ for small, medium and large fibres respectively. The effect of the fibers on the growth of neuronal cells NG108-15 was investigated by live/dead cell test. Cell migration observed on the electrospun fibres showed directional alignment in accordance with the direction of the fibres. The correlation between 25:75 P(3HO)/P(3HB) micro-fibre diameter and neuronal growth under two conditions; individually and in co-culture with RN22 Schwann cells were evaluated. This was investigated using two types of cell staining; live/dead cell test and anti-beta tubulin immunolabelling. Results displayed from both assays revealed that all 25:75 P(3HO)/P(3HB) blend fibre groups were able to support growth and guide aligned distribution of neuronal cells when grown individually and in the presence of RN22 Schwann cells. Results also revealed a direct correlation between fiber diameter and neuronal growth and differentiation. Although neuronal cell viability was similar for all the substrates (approximately 99%) except on glass, large fibres supported the highest number of live neuronal cells grown individually compared to the rest of substrates.

Biocompatibility and neuron regenerating properties of various Bioactive glasse (BG)/PHA blend composites were assessed in order to study their suitability for peripheral nerve tissue applications. BG/PHA blend composites were fabricated using Bioglass® 45S5 (BG1) and BG 1393 (BG2) along with 25:75 P(3HO)/P(3HB) blend. Different proportions of each BG (0.5, 1.0 and 2.5 % w/v) were used to determine the BG concentration that resulted in superior neuronal growth and differentiation of NG108-15 in single culture and in co-culture system with Schwannoma RN22 cells. NG108-15 cells displayed good growth and differentiation performance on all the PHA blend composites showing that both BGs (BG1 and BG2) have good biocompatibility at 2.5, 1.0 and 0.5 % w/v in the PHA blend solution. The Young's modulus values displayed by all the PHA blend/BG composites ranged from 385.6 MPa to 1792.6 MPa, which are much higher than that of peripheral nerves. However, the tensile strength obtained in PHA blend/BG1 (1% w/v) ($10.0 \pm 0.6 \text{ MPa}$) was found to be similar to that of rabbit peroneal nerve measured in another study. Therefore, although PHA

blend/BG1 (1% w/v) does not provide the adequate elasticity, it has the appropriate strength that NGCs require. PHA blend/BG1 (1% w/v) showed the best performance in supporting growth and neuronal differentiation of NG108-15 amongst all the substrates in all the cell culture experiments (Live/dead cell test, neurite outgrowth assessment on NG108-15 neuronal cell and on NG108-15/Schwann cell co-cultures). Moreover, neurite extension found on the PHA blend/BG1 (1% w/v) was remarkable as neurites formed a complex connection network. No correlation was found between the surface characteristics (roughness, hydrophilicity and pore size) of PHA blend/BGs at different concentrations of BG and cell growth and differentiation.

Two prototypes of NGCs were fabricated using blends of PHAs as base materials. Since 75:25 P(3HO)/P(3HB) blend films have shown to possess the required flexibility to be implanted in peripheral nerves, this polymer blend was chosen for manufacturing of NGCs. The NGC prototype 1 consisted of a nerve guidance conduit made from 75:25 P(3HO)/P(3HB) blend with luminal electrospun aligned fibres fabricated with 25:75 P(3HO)/P(3HB) blend. The prototype 2 comprised of a hollow tube made from 75:25 P(3HO)/P(3HB) blend manufactured by dip-moulding using various dipping conditions. The NGC prototype 2 was implanted in rats for *in vivo* work, which was carried out in *Neuroscience Institute Cavalieri Ottolenghi, Italy*. The regenerated nerves were removed and processed for high-resolution light microscopy, transmission electron microscopy and immunohistochemistry analysis. Myelinated and unmyelinated fibres, Schwann cells, connective tissue and vessels were observed in the middle of NGCs through transmission electron microscopy. Although, quantitative estimation of myelinated and unmyelinated nerve fibres was not carried out, these preliminary *in vivo* results revealed the potential of 75:25 P(3HO)/P(3HB) NGCs to support regeneration.

To summarize, the biocompatibility and mechanical properties of the P(3HO)/P(3HB) blends made these polymers excellent materials for nerve tissue engineering and for the manufacture of novel nerve guidance conduits.

Presentations and Publications

Conference Presentations

Presentation at the 8th Conference on Polymer and Fiber Biotechnology. Braga, Portugal 2014

Presentation at the 26th Annual Conference European Society for Biomaterials. Liverpool, UK 2014

Presentation at the Conference Material Science and Engineering 2014. Darmstadt, Germany 2014

Presentation at the Peripheral Nerve Society Meeting. Quebec, Canada 2015

Journal Publications

Lizarraga-Valderrama, L. R., Nigmatullin R., Taylor, C., Haycock, J. W., Claeysens, F., Roy, I. Nerve tissue engineering using blends of polyhydroxyalkanoates for peripheral nerve regeneration. *Eng. Life Sci.* 2015, 15, 612-621. DOI: 10.1002/elsc.201400151
Book Chapter

Lizarraga-Valderrama, L. R., Panchal, B., Thomas, C., Boccaccini A. R., and Roy, I. (2015). Biomedical Applications of Polyhydroxyalkanoates, in Neves, N. (Ed.), *Biomaterials from Nature for Advanced Devices and Therapies*, John Wiley & Sons, 2014, pp 500.

Conference Publications

Lizarraga-Valderrama, L. R., Percy, L., Roy, I. 'Nerve tissue engineering using blends of Polyhydroxyalkanoates', In *Proceedings of 8th International Conference on Polymer and Fiber Biotechnology*, May 2014, Braga, Portugal.

Lizarraga-Valderrama, L. R., Nigmatullin, R., Taylor, C., Claeysens, F., Haycock, J. W., Roy, I. Nerve tissue engineering using blends of Polyhydroxyalkanoates', In *Proceedings of*

26th Annual Conference European Society for Biomaterials, September 2014, Liverpool, UK
2014

Lizarraga-Valderrama, L. R., Nigmatullin, R., Taylor, C., Claeysens, F., Haycock, J. W.,
Roy, I. Nerve tissue engineering using blends of Polyhydroxyalkanoates', In Proceedings of
Conference Material Science and Engineering, October 2014, Darmstadt, Germany.

Lizarraga-Valderrama, L. R., Nigmatullin, R., Taylor, C., Claeysens, F., Haycock, J. W.,
Roy, I. Nerve tissue engineering using blends of Polyhydroxyalkanoates', In Proceedings of
Peripheral Nerve Society meeting, July 2015, Quebec, Canada.

Authors' declaration

I declare that the present research work has been performed in accordance with the guidelines and regulation of the University of Westminster. This PhD thesis is original excepting when indicated by related references.

This research work is not significantly similar to either any that I have previously submitted or I am currently making whether unpublished or published version, for a degree, diploma or any similar qualification at any other university or similar institution.

Until the result of the application of this work to the University of Westminster is known, this work will not be submitted for any similar qualification at any other university or institution.

All the views expressed in this work are those of the author and no way represent those of the University of Westminster.

Signed: Lorena Lizarraga

Date: 31-01-17

Acknowledgements

I would like to express my sincere gratitude to my supervisor, Professor Ipsita Roy for her support and motivation during the performance of this research work. Her trust and faith in me inspired to give my best. I would like to thank Gilchrist Educational Trust for its generous grant that help me to pursue my PhD studies here at the University of Westminster. I would also like to thank to my external supervisors Professor John Haycock and Professor Frederik Claeysens for their constant support and guidance. I would like to acknowledge to my colleagues at Kroto research Institute, Caroline Tailor and Dr. Adam Glen for their technical assistance with NG-10815 neuronal cell studies and moral support. I also would like to thank to my loving colleague Sabiniano Roman for his help and moral support.

I would like to acknowledge to the staff of University Collage of London, specially to Dr. Nicola Mordan for her assistance with SEM analysis, Dr. George Georgiou and Dr. Graham for their assistance with XRD and drop shape analysis respectively.

I also wish to express my most sincere gratitude to Prof. Aldo R. Boccaccini for his guidance and support with the application of bioactive glasses in Nerve Tissue Engineering, and to the staff of University of Westminster, particularly to Dr. Thakor Tandel and Neville Antonio for their technical support. I would like to thank to Dr. Stefano Geuna and and Giulia Ronchi from Neuroscience Institute Cavalieri Ottolenghi for their excellent collaboration with *in vivo* work.

I also wish to thank from the bottom of my heart to my friends Christy Thomas, Carlos Enrique Balcazar Lopez, Barbara Lukasiewicz, Bryan Ladino, Juan Ignacio Cadiz Miranda and for their moral support and help for the completion of my thesis. I would also like to thank to my colleagues of the University of Westminster, Himma Puthussery, Pooja Basnet and Prachi Dubbey for their support during my PhD.

Finally, I would like to wholeheartedly thank to my loving parents Rosa Angelica Lizarraga Valderrama and Raul Guillermo Lizarraga Mora for their financial, moral, and unconditional support during these years. The accomplishment of my PhD thesis would not be possible without their special support. I also would like to thank to my loving brothers Andres Alonzo Lizarraga Valderrama and Leonardo Santiago Lizarraga Valderrama for believing in me. Their belief has encouraged me to work hard and improve constantly.

List of Abbreviations

3HB	3-hydroxybutyrate
3HD	3-hydroxydecanoate
3HHp	3-hydroxyheptanoate
3HV	3-hydroxyvalerate
AEM	Acellular extracellular matrix
aFGF	Fibroblast growth factor acidic
AFM	Atomic Force Microscopy
bFGF	Fibroblast growth factor
bFGF	Fibroblast growth factor basic
BG1	Bioactive glass 1
BG2	Bioactive glass 2
BSA	Bovine serum albumin
CHO-K1	Chinese Hamster Ovary cells
CNTF	Ciliary neurotrophic factor
CoA	Coenzyme A
COLI	Collagen type I
COLIII	Collagen type III
DAPI	4', 6-diamidino-2-phenylindole dihydrochloride
dcw	Dry cell weight
DMA	Dynamic Mechanical analysis
DMEM	Dulbecco's modified Eagle's medium
DSC	Differential Scanning Calorimetry
ECM	Extracellular matrix
FBS	Foetal bovine serum
FTIR	Fourier Transform Infrared
GC-MS	Gas Chromatography- Mass Spectrometry
GDNF	Glial cell-line derived neurotrophic factor
GGF	Glial growth factor
HA	Hydroxyapatite
HAEC	Human aortic endothelial cells
HEK-293	Human embryonic kidney cells
HMEC-1	Human dermal microvascular endothelial cells
HPLC	High Performance Liquid Chromatography
HUVEC	Human umbilical vein endothelial cells

IGF-1	Insuline-like growth factor 1
LIF	Leukemia inhibitory factor
LPS	Lipopolysaccharides
mcl-PHA	Medium chain length polyhydroxyalkanoate
MSC	Mesenchymal stem cells
MSM	Mineral salt medium
MTT	(3-(4,5-Dimethylthiazol-2-yl)-2,5
nBG	Nanobioglass particles
NGF	Nerve growth factor
NMR	Nuclear Magnetic Resonance
NR	Not reported
NSC	Neural stem cell
NT-3	Neurotrophin-3
O.D.	Optical density
P(3HB-co-3HHx)	Poly(3-hydroxybutyrate-co-3-hydroxyhexanoate)
P(3HB-co-3HO)	Poly(3-hydroxybutyrate-co-3-hydroxyoctanoate)
P(3HB-co-3HV)	Poly(3-hydroxybutyrate-co-3-hydroxyvalerate)
P(3HB-co-4HB)	Poly(3-hydroxybutyrate-co-4-hydroxybutyrate)
P(3HB)	Poly(3-hydroxybutyrate)
P(3HHx)	Poly(3-hydroxyhexanoate)
P(3HO-co-3HHx)	Poly(3-hydroxyoctanoate-co-3-hydroxyhexanoate)
P(3HO)	Poly(3-hydroxyoctanoate)
P(4HB)	Poly(4-hydroxybutyrate)
P(BHETE)	Poly((bis(hydroxyethyl) terephthalate-ethylphosphoester)
PAN/MA	Poly(acrylonitrile-co-methylacrylate)
PAN/PVC	Poly(acrylonitrile-co-vinylchloride)
PBS	Phosphate buffer saline
PBS	Phosphate-buffered saline
PCL	Poly(ϵ -caprolactone)
PCL	Polycaprolactones
PCLEEP	Poly (caprolactone-co-ethyl ethylene phosphate)
PDFG	Platelet-derived growth factor
PDI	Polydispersity index
PDI	Polydispersity index
PDLLA	Poly(DL-lactic acid)
PDLLA	Poly(D,L-lactide)

PDLLC	Poly(DL-lactide- ϵ -caprolactone)
PDMS	Poly(dimethylsiloxane)
PDMS	Polydimethylsiloxane
PEG	Polyethylene glycol
PEO	Poly(ethylene oxide)
PEO	Polyethylene oxide
PET	Polyethylene terephthalate
PEVA	Poly(ethylene-co-vinyl acetate)
PGA	Poly(glycolic acid)
PGA	Polyglycolic acid
PHA	Polyhydroxyalkanoates
PHB	Poly(3-hydroxybutyrate)
PHEMA-MMA hydrogel	Poly (2- hydroxyethyl methacrylate-co-methyl methacrylate)
PIP	Poly(cis-1,4-isoprene)
PLA	Poly(lactic acid)
PLAEEP	Poly(lactide-co-ethyl ethylene phosphate)
PLCL	Poly(DL-lactide- ϵ -caprolactone)
PLGA	Poly(lactic-co-glycolic)acid
PLGA	Poly(lactic-co-glycolic acid)
PLLA	Poly(L-lactic acid)
PPE	Poly(phosphoester)
PTCA	Percutaneous transluminal coronary angioplasty
PTFE	Poly(tetrafluroethylene)
PTFE	Polytetrafluroethylene
PU-PLCL	Polyurethane - poly(L-lactide-co-caprolactone)
PU	Polyuretanes
PVA	Polyvinyl alcohol
PVA-g-PLGA	Polyvinyl alcohol grafted poly(lactic-co-glycolactic)
PVA	Polyvinyl alcohol
PVDF-TEE	Poly(vinylidene fluoride)-trifluorethylene
RMS	Root mean square
rpm	Revolutions per minute
Rt	Retention time
scl-PHA	Short chain length polyhydroxyalkanoate
SD	Standard deviation
SEM	Standard Error of the Mean

SGBG	Sol-gel bioactive glass
TC	Crystallisation temperature
T_g	Glass transition temperature
T_m	Melting temperature
UV	Ultraviolet
VEGF	Vascular endothelial growth factor
wt%	Weight percentage
XRD	X-ray diffraction
μm	Micrometre

TABLE OF FIGURES

Chapter 1	18
1 Introduction	1
1.1 The Peripheral nervous system	3
1.1.1 Cellular composition of the human nervous system	3
1.1.2 Anatomy of the peripheral nervous system	4
1.1.3 The myelin sheath	5
1.1.4 Function of the nerve	7
1.1.5 Neuron-Glia Communication.....	7
1.1.6 Regeneration of the peripheral nervous system and injury responses	9
1.1.7 Incidence and types of injury.....	10
1.1.8 Interventional and therapeutic strategies	12
1.2 <i>Nerve Tissue Engineering and Nerve Guidance Conduits</i>	13
1.3 <i>PHAs as biomaterials for tissue engineering</i>	18
1.4 <i>Bioglasses as biomaterials for tissue engineering</i>	21
1.4.1 Angiogenesis	22
1.4.2 Application of bioglass in nerve tissue engineering.....	23
1.5 <i>Electrospinning</i>	25
1.6 <i>Aims and objectives</i>	26
2 Production and characterization of P(3HO) and P(3HB)	29
2.1 <i>Production of Poly(3-hydroxyoctanoate)</i>	29
2.2 <i>Production of poly(3-hydroxybutyrate)</i>	30
2.3 <i>Extraction and purification of PHAs</i>	30
2.4 <i>Gas chromatography – mass spectroscopy</i>	31
2.5 <i>Nuclear Magnetic Resonance Spectroscopy (NMR)</i>	32
2.6 <i>Fourier transform infrared spectroscopy (FTIR) of the polymers and films</i>	32
2.7 <i>Film preparation</i>	32
2.8 <i>Composite film preparation</i>	33
2.9 <i>Scanning electron microscopy of films, scaffolds and PHAs/bioactive glass composites</i>	33
2.10 <i>Profilometric surface analysis</i>	33
2.11 <i>Surface wettability of the films</i>	33
2.12 <i>Static tensile test of the films</i>	34
2.13 <i>Manufacturing of aligned P(3HO)/P(3HB) blends fibres by electrospinning</i>	34
2.14 <i>Characterization of aligned P(3HO)/P(3HB) blends fibres by scanning electron microscopy</i>	35
2.15 <i>NG108-15 neuronal cell culture</i>	36
2.16 <i>Live/ dead measurement of NG108-15 neuronal cells</i>	36
2.17 <i>Immunolabelling of NG108-15 neuronal cells and RN22 Schwann cells</i>	37
2.18 <i>Manufacture of aligned PHA microfibers by electrospinning</i>	37
2.19 <i>Manufacture of nerve guidance conduits (NGCs)</i>	38
2.20 <i>Statistical analysis</i>	39
Chapter 3	40
3 Production and characterization of P(3HO) and P(3HB)	41
3.1 <i>Introduction</i>	41
3.2 <i>Results</i>	43
3.2.1 Production of P(3HO) using sodium octanoate as the carbon source	43
3.2.2 Production of P(3HB) using glucose as carbon source	44
3.2.3 Characterization of P(3HO) and P(3HB)	46
3.2.3.1 Fourier Transform Infrared Spectroscopy (FTIR) of P(3HO) and P(3HB).....	46

3.2.3.2 Gas Chromatography Mass Spectroscopy of P(3HO) and P(3HB)	47
3.3 Discussion	53
Chapter 4.....	56
4 Fabrication, chemical and biological characterization of P(3HO)/P(3HB) blend films	58
.....	
4.1 Introduction.....	58
4.2 Results	59
4.2.1 Scanning electron microscopy of PHA films.....	59
4.2.2 Profilometric surface analysis	59
4.2.3 X - Ray diffraction analysis	60
4.2.4 DSC.....	61
4.2.5 FTIR	63
4.2.6 Surface wettability.....	65
4.2.7 Static tensile test of the films.....	65
4.2.8 Live/dead measurement of NG-108-15 neuronal cells	66
4.2.9 Neurite outgrowth assessment.....	68
4.3 Discussion	70
Chapter 5	74
5 Fabrication, chemical and biological characterization of electrospun fibres using P(3HO)/P(3HB) blends	75
5.1 Introduction.....	75
5.2 Results	77
5.2.1 Fabrication of aligned P(3HO)/P(3HB) blend microfibrils by using electrospinning. Optimization of varying P(3HO)/P(3HB) blends solution concentration for electrospinning aligned microfibrils	77
5.2.2 Live/dead measurement of NG-108-15 neuronal cells on electrospun fibres....	83
5.2.3 Fabrication of aligned 25:75 P(3HO)/P(3HB) blend with different fibre diameters	86
5.2.4 Physical characterization of aligned 25:75 P(3HO)/P(3HB) blend microfibrils by scanning electron microscopy	89
5.2.5 Live/dead measurement of NG108-15 neuronal cells on PHA blend electrospun fibres	92
5.2.6 Neurite outgrowth assessment on NG108-15 neuronal cell culture grown on PHA blend electrospun fibres	95
5.2.7 Neurite outgrowth assessment on NG108-15 neuronal cell/Schwann cell co-cultures grown on PHA blend electrospun fibres	98
5.3 Discussion	102
Chapter 6	105
6 Fabrication, chemical and biological characterization of of 25:75 P(3HO)/P(3HB) blend/BGs composites	106
6.1 Introduction.....	106
6.2 Results	108
6.2.1 Fabrication of PHA blend/BGs composites	108
6.2 Characterization of the PHA blend/BGs composites	109
6.2.2 Scanning electron microscopy of PHA blend/BG composites.....	109
6.2.3 Profilometric surface analysis of PHA blend/BG composites.....	112
6.2.4 Determination of water contact angle of PHA blend/BG composites	113
6.2.4 Static tensile test of the films.....	115
6.2.4 Differential scanning calorimetry of composites	115

6.3	<i>Live/dead measurement of NG-108-15 neuronal cells on PHA blend/BG composites</i>	116
6.4	<i>Neurite outgrowth assessment on NG108-15 neuronal cell culture grown on PHA blend/BG composites</i>	118
6.6	<i>Neurite outgrowth assessment on NG108-15 neuronal cell/Schwann cell co-cultures grown on PHA blend/BG composites</i>	123
6.7	<i>Discussion</i>	129
Chapter 7	136
7	Fabrication of nerve guidance conduits	137
7.1	<i>Introduction</i>	137
7.2	<i>Results</i>	139
7.2.1	Nerve guidance conduits manufacturing.....	139
7.2.1.1	Fabrication of nerve guidance conduits by rolling and ligation of PHA films.....	139
7.2.1.2	Fabrication of nerve guidance conduit by dip-moulding.....	140
7.3	<i>Discussion</i>	141
Chapter 8	143
8	Conclusions.....	145
Chapter 9	148
9	Future Perspectives.....	149
Chapter 10	152
10	References	153

List of Figures

1.1 Single lumen nerve tube	2
1.2 Neuron structure	4
1.3 Anatomy of Nerve fibre	5
1.4 Myelin sheath	6
1.5 Action potential propagation	9
1.6 Regeneration of the peripheral nervous system after peripheral nerve injury	11
1.7 Schematic of the electrospinning process	26
2.1 Two stage culture for P(3HO) production, its purification and characterization	30
2.2 Electrospinning setup used for fabrication of aligned 25:75 electrospun fibres	37
3.1 Temporal profile of the fermentation of <i>P. mendocina</i> CH50 at shaken flask level	42
3.2 Extracted and purified P(3HO)	43
3.3 Temporal profile of the fermentation of <i>B. cereus</i> SPV at shaken flask level	44
3.4 Extracted and purified P(3HB)	45
3.5 FTIR of purified PHAs	46
3.6 Gas chromatography mass spectroscopy of P(3HO)	47
3.7 Gas chromatography mass spectroscopy of P(3HB)	48
3.8 NMR of purified P(3HO) extracted from <i>P. mendocina</i> CH50	49
3.9 NMR of purified P(3HB) extracted from <i>B. cereus</i> SVP	51
4.1 Characterization of the surface topography of P(3HO)/P(3HB) films by scanning electron microscopy analysis	59
4.2 XRD spectra and DSC thermograms of neat polymers and P(3HO)/P(3HB) blends	61
4.3 FTIR spectra of P(3HO)/P(3HB) films showing the characteristic peaks of P(3HO) and P(3HB)	62
4.4 Static water contact angle of P(3HO)/P(3HB) films	64
4.5 Confocal micrographs of NG108-15 neuronal cells labelled with propidium iodide (red) and Syto-9 (green) after four days in culture on P(3HO)/P(3HB) films and PCL	66

4.6 Confocal micrographs of NG108-15 neuronal cells immunolabelled for beta-III tubulin after four days in culture on P(3HO)/P(3HB) films and PCL	68
5.1 Bead formation made using 5% (w/v) 25:75 P(3HO/P3HB) blend	77
5.2 Electrospun fibres of neat P(3HO) 10 % (w/v)	78
5.3 Beaded electrospun fibres of 10 % w/v 75:25 P(3HO/P3HB) blends	79
5.4 Electrospun fibres of 10 % w/v 50:50 P(3HO/P3HB) blends	80
5.5 Electrospun fibres of 10 % w/v 25:75 P(3HO/P3HB) blends	80
5.6 Electrospun fibres of 10 % w/v P(3HB)	81
5.7 Micrographs of aligned 25:75 P(3HO)/P(3HB) blend electrospun fibres observed at different magnifications	82
5.8 A-D) Confocal micrographs of NG108-15 neuronal cells labelled with propidium iodide (red) and Syto-9 (green) after four days in culture on both films and electrospun aligned fibres made from 25:75 P(3HO)/P(3HB) using a PCL film and glass as controls	83
5.9 Electrospun fibres of 20 % w/v 25:75 P(3HO/P3HB) blends	85
5.10 Aligned electrospun fibres using 15% w/v of 25:75 P(3HO)/P(3HB) blend	87
5.11 Aligned electrospun fibres using 25% w/v of 25:75 P(3HO)/P(3HB) blend	88
5.12 Aligned electrospun fibres using 30% w/v of 25:75 P(3HO)/P(3HB) blend	89
5.13 Characterization of electrospun 25:75 P(3HO)/P(3HB) fibres by scanning electron microscopy. Diameter, density and alignment of fibres were determined by image analysis	90
5.14 Fibre characterization	91
5.15 Confocal micrographs of NG108-15 neuronal cells labelled with propidium iodide (red) and Syto-9 (green) after four days in culture on aligned 25:75 P(3HO)/P(3HB) fibres	92
5.16 Live and dead cell test on fibres with varying diameters	93
5.17 Confocal micrographs of NG108-15 neuronal cells immunolabelled for beta-III tubulin after four days in culture on aligned 25:75 P(3HO)/P(3HB) fibres, flat PHA flat film, PCL and glass.	94
5.18 Number of cells with neurites on P(3HO)/P(3HB) fibres, PCL and glass (control)	95
5.19 Confocal micrographs of NG108-15 neuronal cells immunolabelled for beta-III tubulin after four days in culture on aligned 25:75 P(3HO)/P(3HB) fibres.	96

5.20 Confocal micrographs of NG108-15 neuronal cells immunolabelled for beta-III tubulin + DAPI after four days in culture on PHB blend flat film, PCL and glass	97
5.21 Confocal micrographs of NG108-15 neuronal cells (red) grown with RN22 Schwann cells (green) immunolabelled for beta-III tubulin and stained with phalloidin and DAPI after four days in culture on aligned 25:75 P(3HO)/P(3HB) fibres	98
5.22 Confocal micrographs of NG108-15 neuronal cells (red) grown with RN22 Schwann cells (green) immunolabelled for beta-III tubulin and stained with phalloidin and DAPI after four days in culture on flat substrates	99
5.23 Differentiated cells NG108-15 cells in co-culture with RN22 cells	100
6.1 Scanning electron microscopy of PHA blend/BG1 composites	109
6.2 Scanning electron microscopy of PHA blend/BG2 composites	110
6.3 Scanning electron microscopy of PHA blend and PCL film	111
6.4. Root mean square roughness (Rq) of PHA blend/BG composites and controls	112
6.5 Water contact angles of PHA blend/BG composites and controls	113
6.6 Confocal micrographs of NG108-15 neuronal cells labelled with propidium iodide (red) and Syto-9 (green) after four days in culture on P(3HO)/P(3HB)/BG composites and controls PHB blend, PCL and glass	116
6.7 Live and dead tests of neuronal cells on PHA blend/BG substrates	117
6.8 Micrographs of NG108-15 neuronal cells immunocytochemically-labelled for beta-III tubulin after 4 days culture on PHA blend composites	118
6.9 Number of differentiated NG108-15 neuronal cells	119
6.10 Confocal microscopy images of NG108-15 neuronal cells immunocytochemically-labelled for beta-III tubulin after 4 days culture on PHA blend/BG1 composites	120
6.11 Confocal microscopy images of NG108-15 neuronal cells immunocytochemically-labelled for beta-III tubulin after 4 days culture on PHA blend/BG2 (0.5wt %) composite	121
6.12 Confocal microscopy images of PHA blend/BG1 (0.5wt %)	123
6.13 Confocal microscopy images of neuronal cells grown on PHA blend/BG1 (1 wt %) and PHA blend/BG1 (2.5 wt %)	124
6.14 Micrographs of NG108-15 neuronal cells immunolabelled for beta-III tubulin (red) grown in co-culture with RN22 cells stained with phalloidin (green) after 4 days on PHA blend/BG composites.	125

6.15. Number of NG108-15 neuronal cells grown on varying substrates with and without RN22 cells	126
6.16 Confocal microscopy images of neuronal cells grown on PHA blend/BG2.	127
7.1. A nerve guidance conduit with luminal electrospun aligned fibres	139
7.2. Manufacturing of NGCs by dip-moulding	140

List of Tables

1.1 Commercially available nerve conduits	14
1.2 Synthetic materials used in nerve conduits	15
1.3 Natural materials used in nerve conduits	17
2.1. Second stage seed medium and production medium	29
2.3 Kannan & Rehacek media composition	30
2.4 Summary of electrospinning conditions used for the manufacturing of aligned 20 % w/v P(3HO)/P(3HB) blend fibres of varying diameters.	34
2.5 Summary of electrospinning conditions used to manufacture aligned P(3HO)/P(3HB) blend fibers of varying diameters using different polymer concentrations.	35
2.6 Varying dip-moulding conditions used for fabrication of NGCs	38
3.1 Differential scanning calorimetry results for the PHAs	50
4.1 Roughness of PHA blend films	59
4.2 Assignments of the peaks in the FTIR spectra of the blends of P(3HO)/P(3HB)	63
4.3 Mechanical analysis of the P(3HO)/P(3HB) films	65
5.1 Summary of electrospinning parameters used to determine the optimal conditions for the manufacture of aligned blend fibres using 10% w/v of polymer blends	77
5.2 Summary of electrospinning parameters used to determine the optimal conditions for the manufacture of aligned blend fibres using 20% w/v of 25:75 P(3HO)/P(3HB) blend	84
5.3 Summary of fibre diameters obtained using different polymer concentrations of 25:75 P(3HO)/P(3HB) blend and electrospinning conditions.	86
6.1 Porous size of PHA blend/BGs composites and controls	108
6.2 Roughness of PHA blend/BGs composites and controls	112
6.3 Water contact angles of PHA blend/BG composites and controls	113
6.4 Mechanical analysis of the P(3HO)/P(3HB) films	114

6.5 Differential scanning calorimetry of PHA blend/BG composites	115
7.1 Varying dip-moulding conditions used for fabrication of NGCs	139

Chapter 1

Introduction

1 INTRODUCTION

Regeneration of the nervous system is a complex biological process that imposes formidable challenges in the field of nerve tissue engineering. The specific approach used to repair nerve injuries depends on the type of nerve that has been damaged. Peripheral nerve injury (PNI) affects 2.8% of trauma patients, many of whom suffer life-long disability (Midha, 2006). In Europe, 300,000 PNI cases are reported each year (Huang *et al.*, 2012). The regeneration of the Central Nervous System (CNS) is inhibited by biological factors and unfortunately there is currently no treatment available to adequately restore its functionality. Injuries within the CNS form an inhibitory glial scar produced by astrocytes. Therefore, efforts for CNS regeneration focus on providing the nerves with a suitable environment. Unlike the CNS, peripheral nerves are able to repair themselves when the injuries are small; typically, when the nerve has a gap of less than 5 mm to bridge (Jiang *et al.*, 2010; Schmidt and Leach, 2003).

However, even in this case, axonal regeneration may not necessarily mean that nerve functionality is recovered completely. Unfortunately, a common problem in the process of regeneration is the misdirection of the axons, even across short distances (Jiang *et al.*, 2010). When the injuries are more severe, consisting of gaps less than 3 cm, treatment is most commonly attempted using autologous nerve graft repair (Babu *et al.*, 2008; de Ruitter *et al.*, 2009). When nerve damage is even more extreme and gaps exceed this distance, allografts, vascularised nerve grafts and nerve grafts without blood vessels are used (Babu *et al.*, 2008). New approaches to peripheral nerve repair focus on the development of alternatives to nerve autografts such as nerve tubes, guides or conduits that can facilitate axon-growth and bridge larger nerve gaps (de Ruitter *et al.* 2009; Schmidt and Leach, 2003).

Peripheral nerve repair using nerve autografts has various limitations including donor site morbidity, scar tissue invasion, lack of donor nerves, inadequate return of function and aberrant regeneration (Babu *et al.*, 2008; Huang *et al.*, 2012). Currently, there are several clinically approved artificial nerve conduits made from various biomaterials possessing distinctive properties and a wide range of manufacturing techniques are used for their production (Fig. 1.1).

Although these methods have overcome some of the limitations of nerve autografts, they still present many shortcomings and there is no solution available for a completely successful treatment (Babu *et al.*, 2008; de Ruitter *et al.*, 2009). The drawbacks of using synthetic tubes or conduits include their tendency to trigger immune responses, their tendency to induce scar tissue, the difficulty in their surgical application, and their tendency to release

degradation products that are detrimental to the regeneration process. If the conduit is made from a non-biodegradable material, follow-up surgery is typically required for the removal of the conduit.

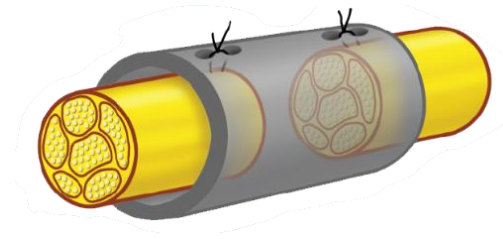


Figure 1.1. Single lumen nerve tube (Ruiter *et al.*, 2009)

Biodegradable nerve guidance conduits have been shown to result in comparatively less aberrant axonal growth, reduced fibrous scar tissue and reduced risk of neuromas (Badu *et al.*, 2008). Generally, the parameters to consider, when choosing specific materials and a manufacturing technique for the production of artificial nerve conduits are; biodegradability, toxicity, reactivity to the immune system, permeability or porosity, flexibility, degree of swelling, degradation rate, resistance to high temperatures and usability by the surgeon. Biodegradable materials are better than non-biodegradable materials as they prevent chronic nerve compression and fibrotic reactions and eliminate the need for surgery to remove the implant after completing the treatment (Babu *et al.*, 2008; Midha, 2006).

A conduit needs to be permeable in order to allow the diffusion of nutrients and oxygen, which contribute towards the viability of supportive cells and favour the formation of fibrin in the initial stages of regeneration. The flexibility of the structure is especially important in the repair of larger gaps because the ends may not lie in the same plane. Degradation and swelling of nerve conduits are important properties and need to be taken into consideration. High degradation rates might cause swelling which could block the lumen and consequently prevent regeneration. This swelling is caused generally by water uptake following the formation of by-products that might increase the osmotic pressure within the conduit. Too slow degradation rates can induce both compression of regenerated axons or a chronic immune reaction. The degradation kinetics of the tube should match the nerve regeneration rate. With an ideal degradation rate, the nerve tube should remain intact, with minimal swelling until the axons regenerate across the nerve gap. Also, the material needs to be resistant to high temperatures so that its properties remain unaffected after sterilization. The material should be easy to handle and suture, preferably be transparent (de Ruiter *et al.*, 2009). Additionally, the ideal conduit should have a simple and easily reproducible manufacturing process (Jiang *et al.*, 2010).

1.1 THE PERIPHERAL NERVOUS SYSTEM

The nervous system in mammals comprises of both the central nervous system (CNS) and the peripheral nervous system (PNS). The CNS consists of the brain, spinal cord, optic nerves, olfactory system and the auditory system. It conducts and interprets signals and provides excitatory stimuli to the PNS. The PNS includes the sensory nerve cell bodies and the nerves arising from the brain and spinal cord. These nerves innervate muscle tissue, transmitting sensory and excitatory inputs to and from the spinal column (Schmidt and Leach, 2003). Nerves connect the CNS with all parts of the body and they are the most conspicuous components of the PNS. The cell bodies of neurons in the CNS are located in regions known as gray matter, whereas the regions that do not contain cell bodies are called white matter. The neuronal cell bodies in the PNS exist in nodular structures called the ganglia (Kiernan and Rajakumar, 2014).

1.1.1 CELLULAR COMPOSITION OF THE HUMAN NERVOUS SYSTEM

The nervous system is composed of two cells types; neurons and glial cells or neuroglia. Neurons consist of a cell body also called soma or perikaryon and its branched extensions, which are called neurites (Fig. 1.2 B) (Schmidt and Leach, 2003). The neurites in higher animals are specialized and known as dendrites and axons. The cell body is large and has an euchromatic nucleus with a well-developed nucleolus and contains chromatophilic substance known as Nissl bodies. These bodies are large masses of free polysomes and rough endoplasmic reticulum (RER), which indicate the cell's rate of protein synthesis (Mescher, 2010). Dendrites transmit electrical signals to the cell body whereas axons conduit these signals away (Fig. 1.2 B). The ends of the neurites are known as synaptic terminals, and the cell-to-cell contact they make are called synapses (Kiernan and Rajakumar, 2014). The ends of axons usually have many small branches called terminal arborizations, each of which usually have a swollen end called bouton which forms a functional connection (synapse) with another neuron or other cell (Mescher, 2010). Figure 1.2 shows a micrograph of a motor neuron. Evenly dispersed Nissl bodies can be seen throughout the cell body. The narrow periodic gaps between the ends of segments of myelin are called neurofibril nodes or nodes of Ranvier. The nodes of Ranvier are uninsulated and are highly enriched in ion channels that participate in the ions exchange required to regenerate the action potential.

Glia are supporting cells that work alongside neurons (Schmidt and Leach, 2003). There are three kinds of glial cells; Schwann cells, oligodendrocytes and astrocytes. Schwann cells and oligodendrocytes are the myelin-forming cells of the PNS and CNS respectively. The layers of myelin membrane wrapped around axons serve to insulate them, allowing the

conduction of electrical impulses. Astrocytes do not produce myelin and are closely related with neurons in the brain. They associate with nodes of Ranvier, ensheath synaptic junctions and trigger responses to diseases and injuries. Therefore, in the PNS, Schwann cells carry out the functions of astrocytes and oligodendrocytes; ensheathing synaptic junctions, forming myelin and bundling axons (Fields and Stevens-Graham, 2002). Neurons are less abundant than glial cells as they cannot divide by mitosis. However, neurons can regenerate a damaged portion under certain conditions (Schmidt and Leach, 2003)

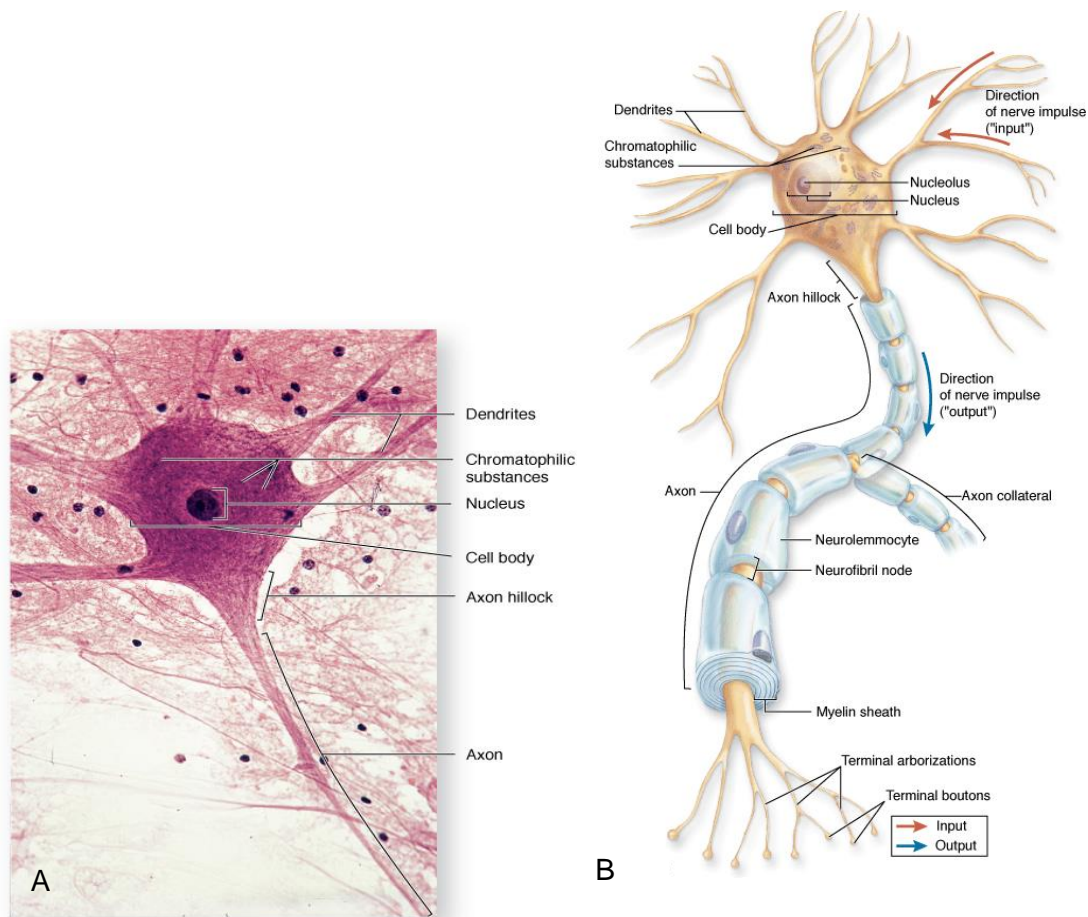


Figure 1.2. Neuron structure. A) Micrograph of a motor neuron. B) Structure of a neuron (Taken from Mescher, 2010).

1.1.2 ANATOMY OF THE PERIPHERAL NERVOUS SYSTEM

The peripheral nerves are arranged in fascicles bundled together by connective tissue sheaths to form a trunk (Fig. 1.3). The entire nerve is surrounded by the epineurium or outer sheath, which is composed of loose fibro-collagenous tissue (connective tissue) and fills spaces between fascicles. Undulations in these collagen fibres around fascicles allow for the nerve stretching during flexion of joints and other movements (Kierman and Rajakumar, 2014).

The perineurium is the sheath that encloses bundles of axons to form fascicles and consist of several layers of flattened cells and collagen. Within the perineurium, individual axons along with Schwann cells are surrounded by the endoneurium, which is composed of oriented collagen fibres (Schmidt and Leach, 2003). Within the endoneurium, Schwann cells surround all the axons with sheaths of myelin.

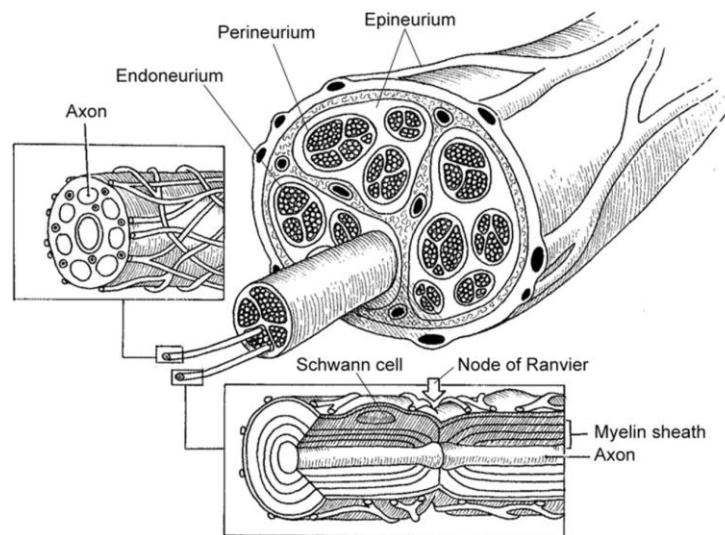


Figure 1.3. Anatomy of Nerve fibre (Taken from Griffin *et al.*, 2013)

1.1.3 THE MYELIN SHEATH

The myelin sheath is a modified and extended cytoplasmic membrane, which is wrapped around the nerve axon in spiral shape (Fig.1.4). The myelin membranes originate from Schwann cells and oligodendrocytes in the PNS and CNS respectively. Each of these cells furnish myelin for only one segment of the axon in such a way that some portions of the axon are left uncovered by myelin. These unmyelinated portions are known as the nodes of Ranvier and are essential for facilitating conduction in axons (Morell and Quarles, 2016). Voltage-gated sodium channels are present in the plasma membrane of axons only at the nodes. This arrangement allows the action potential to skip electrically from node to node (Kiernan and Rajakumar, 2014).

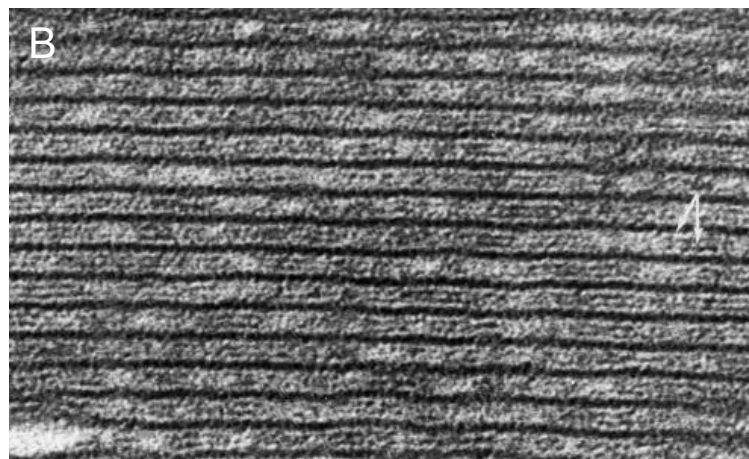
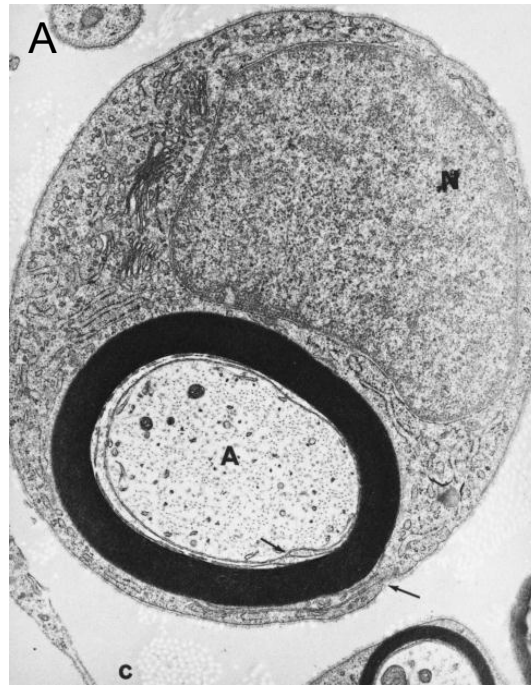


Figure 1.4. Myelin sheath. A) A myelinated PNS axon surrounded by a Schwann cell is observed in the endoneurial space. Nucleus (N), and unstained collagen (c) are also observed. X 20,000. B) Magnification of the myelin sheath. X 350,000. (Modified from Siegel *et al.*, 1999)

The distance between the nodes depends on the thickness of the fibre and varies from 100 μm to about 1 mm. There is one Schwann cell for each internode (space between nodes of Ranvier) (Kiernan and Rajakumar, 2014). The local circuit generated in the excited membrane at the node cannot flow through because of the high resistance of the sheath. This propagation of the active excitation from node to node is called saltatory conduction and it is much more rapid than in unmyelinated axons, in which the circuits flow through the adjacent piece of membrane (Morell and Quarles, 2016). Conduction velocities in myelinated fibres are

proportional to the nerve fibre diameter, whereas in unmyelinated fibres these velocities are proportional to the square root of the fibre diameter. The ratio of the inner axonal diameter to the total outer diameter is known as g-ratio and it is used as a structural index of optimal axonal myelination. Waxman and Bennett (1972); and Chomiak and Hu (2009) have shown that axons have an optimal g-ratio of 0.6. It has been shown that if the thickness of myelin deviates from this value in either way, with higher or lower g-ratios, the velocity of conduction drops (Snaidero and Simons, 2014).

1.1.4 FUNCTION OF THE NERVE

The main function of neurons is to transfer information rapidly from one part of an animal's body to another. This allows organisms to communicate, coordinate, react to stimulus and carry messages to the brain. Two coupled activities are necessary for neuronal communication; conduction of a signal from one part of the cell to another; and synaptic transmission. Synaptic transmission is the biological process by which a neuron communicates with a target cell across a synapse. There are two kinds of synaptic transmissions; chemical and electrical. Chemical synaptic transmission involves the release of a neurotransmitter from a pre-synaptic neuron, which binds to specific post-synaptic receptors. Electrical synapse transmission involves the transfer of electrical signals through the nodes of Ranvier.

If a stimulus is applied to one part of the neuron, an impulse is initiated and will travel to the rest of the cell. This impulse is known as the action potential, which is a wave of electrical depolarization that propagates within the surface membrane of the neuron (Kierman and Rajakumar, 2014). The arrival of an impulse at synaptic terminals generates synaptic transmission, which commonly involves the release of a neurotransmitter from the neuronal cytoplasm triggering a response in the postsynaptic cell (Kierman and Rajakumar, 2014).

Cells can be classified based on the kind of message they transmit as sensory nerve cells, motor nerve cells and association nerve cell. Sensory nerve cells transfer information from inside and outside of the body to the CNS. The information transmitted can be different stimuli such as light, heat or chemical compounds. Motor nerve cells transmit instructions from the CNS to other parts of the body such as muscles or glands. Association nerve cells are connected to sensory and motor neurons (Kierman and Rajakumar, 2014).

1.1.5 NEURON-GLIA COMMUNICATION

Communication between neurons and glia is essential for axonal conduction, synaptic transmission and processing of information. Signals between neurons and glia include ion

fluxes, neurotransmitters, cell adhesion molecules and specialized signaling molecules released from both synaptic and non-synaptic regions of the neuron. Communication between glial cells is carried out through intracellular waves of calcium and via intercellular diffusion of chemical messengers. Glia can affect synaptic transmission and neuronal excitability through the release of neurotransmitters and other extracellular signaling molecules (Fields and Stevens-Graham, 2002).

Although neurotransmitter receptors and voltage-sensitive ion channels are found in both, neurons and glia, the membrane properties required to fire action potentials are absent in glial cells. However, it has been demonstrated that these ion channels allow glia to sense the level of neuronal activity and that communication between glial cells and glial cells with neurons is mainly performed through chemical signals rather than electrical signals. Glia may participate in information processing among neurons, can control synaptic strength and regulate synapse formation. On the other hand, neural activity controls various glial activities such as myelination, proliferation and differentiation (Fields and Stevens-Graham, 2002).

1.1.5.1 GLIAL REGULATION OF SYNAPSIS

The Ca^{2+} responses to action potentials in the CNS are detected in hippocampal astrocytes, whereas in the PNS these responses are observed in terminal Schwann cells. Schwann cells monitor synaptic activity by detecting neuron-glia signaling molecules and control the strength of synaptic transmission by regulating the release of neurotransmitters from the nerve terminal. This process begins when the neurotransmitter acetylcholine (ACh), adenosine or extracellular ATP are released from the nerve terminal and activate G-protein-coupled receptors on the Schwann cells (Fields and Stevens-Graham, 2002). This activation induces an increase in the Ca^{2+} level in terminal Schwann cells enhancing nerve-evoked transmitter release. This increase in Ca^{2+} level is known as Ca^{2+} transient and triggers glutamate release from the Schwann cells. As a result, metabotropic receptors are activated on the postsynaptic muscle membrane, which stimulates synthesis of NO in the muscle. The produced NO diffuses to the nerve terminal provoking the depression of transmitter release (Sugiura and Lin, 2011).

1.1.5.2 NODE OF RANVIER

Neuron-glia interactions at the Node of Ranvier (Fig.1.2 B and Fig. 1.3) are essential for rapid impulse conduction. Nodes of Ranvier are exposed areas of axons and are situated at regular intervals along axons acting as repeating amplifiers to propagate neural impulse over long distances. Nodes of Ranvier are rich in voltage-gated Na^+ channels, where Na^+ ions

cross and depolarize the membrane between segments of compacted myelin. K^+ channels are highly concentrated in the juxtaparanodal region of the axon and allow K^+ ions to exit from the axon restoring the membrane potential after the impulse.

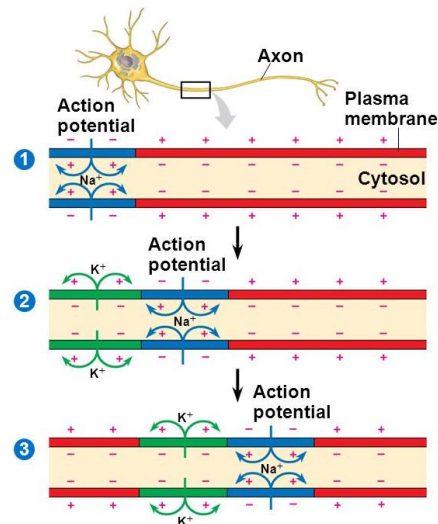


Figure 1.5 Action potential propagation (Campbell and Reece, 2008).

1.1.6 REGENERATION OF THE PERIPHERAL NERVOUS SYSTEM AND INJURY RESPONSES

Axonal regeneration in the central nervous system (CNS) is remarkably different to the regeneration in the peripheral nervous system (PNS). After injury, the regeneration in the CNS is extremely limited as there is no spontaneous regeneration as in the PNS. After a peripheral nerve is transected, axons regenerate spontaneously (Fig. 1.6). After 24-36 h of a lesion, the distal axon, which is the portion of the axon disconnected from the cell body, undergoes Wallerian degeneration (Huebner and Strittmatter, 2009). During this process the axon is fragmented and disintegrated while the basement membrane and Schwann cells remain intact. Myelin and axonal debris are then removed by glial cells and macrophages. Consecutively, proximal axons regenerate and re-innervate their targets which could lead to the recovery of function (Fig. 1.6).

Soon after a nerve is severed, a cascade of reactions occur for the next 24 h (Fig. 1.6). Firstly, the distal portion begins to degenerate as a consequence of protease activity as well as separation from the metabolic resources of the cell body. The cytoskeleton begins to breakdown, followed by the dissolution of the cell membrane. After degradation of the cytoskeleton and membrane, denervated myelinated Schwann cells release their myelin lipids (Schmidt and Leach, 2003). These Schwann cells then proliferate within their basal lamina tubes, produce cytokines/trophic factors and phagocytose detached debris. Additionally, the

reaction within the cell body begins, which is characterized by cell soma hypertrophy, displacement of the nucleus to an eccentric position and dissolution of Nissl's granules. After this first stage, Wallerian degeneration takes place for one week. Wallerian degeneration consists of a series of stereotyped, synchronized changes that occur in the distal segment of a peripheral nerve after this structure has been separated from its associated neuronal cell bodies by trauma (axotomy) (Carrol, 2009). As a result, injured axons produce soluble factors that activate resident macrophages which leads to the recruitment of hematogenous macrophages. These activated macrophages clear myelin and axon debris efficiently and produce factors that enhance axon growth and facilitate Schwann cell migration.

In the next phase (weeks to months) Schwann cells align and axons regenerate after a lag period. Regeneration begins at the proximal end and continues towards the distal stump. Injured axons form a growth cone and begin to regenerate along bands of Büngner, which are formed by Schwann cells. These tubes provide the growth environment and guide extending axons towards potential peripheral targets. New axonal sprouts usually emanate from the nodes of Ranvier. Schwann cells that have been chronically denervated are more likely to undergo apoptosis. Finally, the axon can connect with peripheral targets if it is able to traverse the injury site and its environment supports its growth along the entire distal stump (Fig. 1.6) (Gaudet *et al.*, 2011). Axon regeneration in humans occurs at a rate of 2-5mm/day, therefore, considerable injuries can take several months to heal (Schmidt and Leach, 2003). Although myelinated Schwann cells remyelinate the regenerated portion of the axon, the myelin sheath is thinner and the nodal length is shorter compared to the uninjured portion of the axon (Gaudet *et al.*, 2011).

1.1.7 INCIDENCE AND TYPES OF INJURY

Nerve injuries may cause transection of axons with resulting loss of nerve function. When the nerve has been injured but not transected, there may be a failure of conduction known as neuropraxia. Patients with this condition can recover quickly although neuropraxia can also be permanent in some cases for unknown reasons. Damage of a nerve by a penetrating wound can cause causalgia, which is a type of complex regional pain syndrome. Patients with this syndrome suffer from severe pain in the limb and changes in skin texture. This is due to the formation of abnormal excitatory contacts between sensory and sympathetic axons. The common treatment for causalgia consist of surgical removal of the sympathetic ganglia that supply the affected skin (Kiernan and Rajakumar, 2014).

When a nerve is transected, axons regenerate and associate with glial cells to form a neuroma, in which many abnormal contacts are generated between the surfaces of axons and other cells. Neuroma refers to the abnormal growth of nervous tissue and can be very painful.

The neuroma can cause phantom limb pain, which is a pain perceived from the amputated limb and includes feelings of size, position and movement (Kiernan and Rajakumar, 2014).

A pressed nerve can result in entrapment syndrome, which includes sensory disturbances in the area of distribution of the nerve. As nerve roots lack an epineurium, they are more fragile than nerves. They may be compressed by either inflamed meningitis, by bony irregularities (spinal osteoarthritis) or by abnormally protruding parts of intervertebral discs (spondylosis) (Kiernan and Rajakumar, 2014).

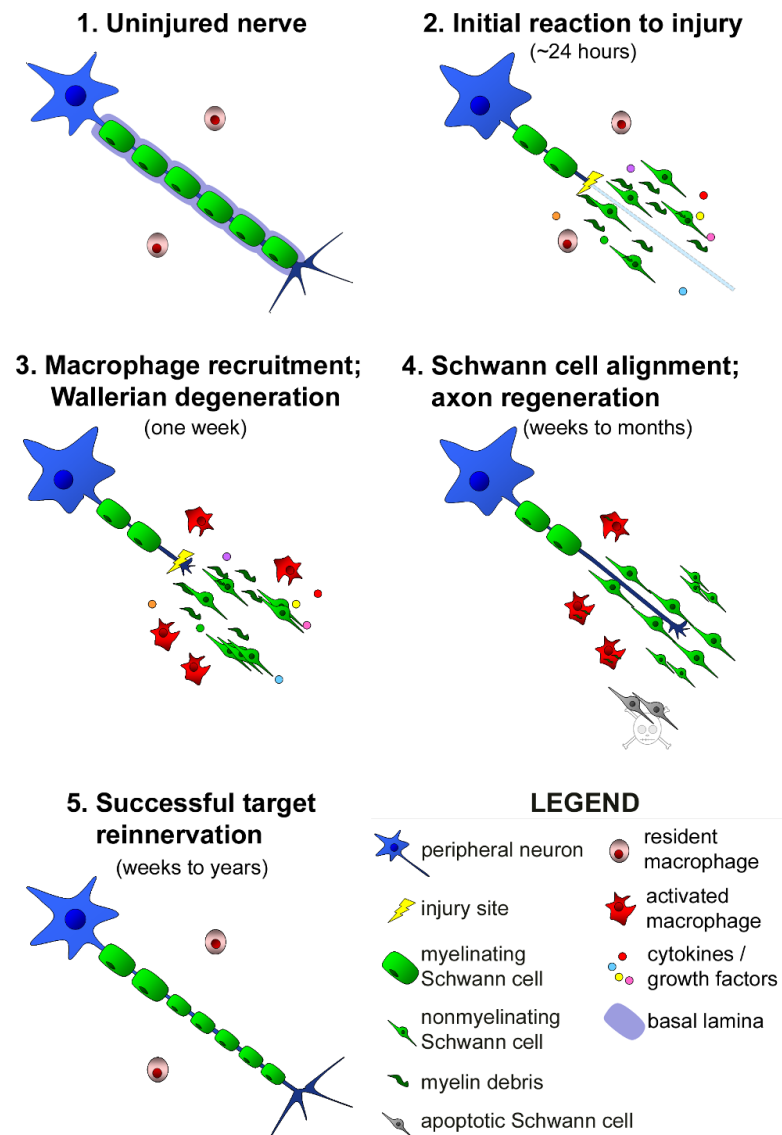


Figure 1.6. Regeneration of the peripheral nervous system after peripheral nerve injury (Taken from Gaudet *et al.*, 2011)

1.1.8 INTERVENTIONAL AND THERAPEUTIC STRATEGIES

Regeneration of peripheral nerves is a major topic in both neuroscience and clinical research. Although peripheral nerves can regenerate naturally, efficiency of nerve regeneration decreases as the length of the injury gap increases. Axon regeneration is significantly impeded by surrounding scar tissue, which may lead to the formation of neuroma (Liu *et al.*, 2015).

Peripheral nerve repair methods include nerve transfer, anastomosis, cell transplantation, use of tissue engineering material, use of neurotrophic factors and genetic engineering. In this context, anastomosis refers to a connection made surgically between adjacent nerve fibres. Nerve transfer is the first choice for treatment of peripheral nerve injury and autografting is the most commonly used method. Despite the extensive use of a wide variety of strategies for peripheral nerve repair, the maximum neurological recovery is still only approximately 70%. Therefore, development of novel methods or improvement of existing strategies are urgently required (Liu *et al.*, 2015).

Nerve autografts are still the gold standard method for repairing nerve gaps that are greater than 50-mm long or cannot undergo tension-free suturing (Doolabh *et al.*, 1996; Valero-Cabre *et al.*, 2001). The use of nerve guidance conduits is suitable only for short nerve gaps (less than 10 mm in rats).

In microsurgery, the same nerve branch for anastomosis is used to achieve the best repair effect. However, the surrounding soft tissue defects is often found with peripheral nerve injuries, and the pathological process is complex. Therefore, the surgery cannot fully restore function. Generally, end-to-end anastomosis can be used in patients with minor defects or no defects, and the epineurium and perineurium are sutured. If the nerves adhere to the surrounding tissue, neurolysis may be required. The nerves should be dissociated from scar tissue to expose the normal nerve tract. Common anastomosis techniques include end-to-end, end-to-side and side-to-side anastomosis (Liu *et al.*, 2015).

Cell transplantation along with nerve growth factors and other trophic factors is a promising alternative for treating peripheral nerve injury. Seed cells are implanted in the nerve scaffold, which secrete extracellular matrix molecules and growth factors, providing a favourable microenvironment for nerve regeneration. The most common and studied functional seed cells for this application are Schwann cells, neural stem cells, mesenchymal stem cells, embryonic stem cells and olfactory ensheathing cells (Liu *et al.*, 2015).

The use of engineered scaffolds for nerve regeneration has shown promising results in clinical trials. A combination of functional seed cells along with a variety of neurotrophic factors has demonstrated an increased effectiveness of nerve regeneration. Therefore, the

combination of multiple factors along with the nerve tissue engineering scaffolds leads to synergistic results that exceed the results obtained using individual factors (Liu *et al.*, 2015).

Gene therapy is known as the therapeutic delivery of nucleic acids into cells to treat disease by either overcoming protein deficiency or inhibiting overexpression of certain genes *in vivo* (Liu *et al.*, 2015). Hu *et al.* (2010) have shown that the accuracy of sensory axon re-innervation can be enhanced by overexpression of nerve growth factor by using recombinant adenovirus encoding nerve growth factor. This finding provided evidence that the expression of a neurotrophin ameliorates the targeting of distal peripheral axons into the appropriate nerve branch. Although gene therapy is still in an early experimental stage, it has shown significant therapeutic potential for nerve regeneration.

1.2 NERVE TISSUE ENGINEERING AND NERVE GUIDANCE CONDUITS

During the past two decades a large variety of materials, nano-structures and biochemical factors have been tested in attempts to create the ideal nerve conduit, and today there are several commercial nerve conduits approved by U.S Food and Drug Administration (FDA) and Conformit Europe (CE) (Jiang *et al.*, 2010). All of the models currently available take the form of a simple hollow tube with a single lumen. They possess no internal substructure, are made from either synthetic or organic materials and are available in different designs and sizes depending on the work they need to perform (Table 1.1).

The limited success that these simple conduits have brought in aiding nerve regeneration across larger gaps has promoted more research in improving their design by giving the lumen a substructure and incorporating agents to nurture growth. Table 1.2 and 1.3 provide a list of the variety of materials and lumen structures that have been investigated. It has been demonstrated that the incorporation of growth-promoting factors are necessary for supporting axonal regeneration across wider gaps (Jiang *et al.*, 2010). These modifications are commonly employed inside the lumen of the conduit and can considerably improve regeneration. They can be classified as biochemical and physical factors. Biochemical signalling factors include growth factors, neurotrophic factors, cells, nucleic acids and extracellular matrix (ECM) molecules such as collagen, laminin and fibronectin (Jiang *et al.*, 2010). Physical modifications to the substructure of the conduit may involve luminal filaments, fibres and multichannel structures (de Ruitter *et al.*, 2009; Jiang *et al.*, 2010). Laminin-coated collagen fibres along with Schwann cells when used as luminal fillers have enabled nerve function recovery across gaps of up to 6cm in rabbit peroneal nerves (Strauch *et al.*, 2001; Zhang *et al.*, 2004) and up to 8cm in canine peroneal nerves respectively (Matsumoto *et al.*, 2000).

Table 1.1. Commercially available nerve conduits.

Composition	Production	Company	Resorption (Months)	Device type	Ref.
Synthetic Materials					
PLCL	Neurolac®	Polyganics Inc.	16	Nerve conduit	111, 102
PGA	Neurotube	Synovis	3	Nerve cuff	173, 104
PVA	Salubridge/Hydroshealth	SaluMedica	NR	Hydrogel tube	
Natural Materials					
COLI	NeuraGen	Integra NeuroSciences	48	Nerve conduit	4, 9
	Neuroflex™	Collagen Matrix Inc.	NR	Nerve conduit	7
	NeuroMatrix™	Collagen Matrix Inc.	7	Nerve conduit	25,98
	NeuroMend™	Collagen Matrix Inc.	NR	Wrap conduit	105
ECM	Avance Nerve® Graft	Axogen Inc.	NR	Nerve conduit	144
	AxoGuard®	Axogen Inc.	NR	Wrap conduit	144
	Surgisis®Nerve Cuff	Cook Biotech Products	NR	Nerve cuff	144

See Abbreviations list for the full forms of the abbreviated names of materials

Neurotrophic factors play an essential role in controlling the proliferation, differentiation, migration and survival of various neural cell types. They are currently used as luminal fillers with satisfactory results and sometimes in conjunction with drug delivery systems. The neurotrophic factors that have been shown to improve nerve regeneration include: nerve growth factor (NGF), neurotrophin-3 (NT-3), glial cell-derived neurotrophic factor (GDNF), acidic fibroblast growth factor (aFGF), basic fibroblast growth factor (bFGF), ciliary neurotrophic factor (CNTF), glial growth factor (GGF), vascular endothelial growth factor

(VEGF), brain-derived neurotrophic factor (BDNF), leukemia inhibitory factor (LIF), insulin-like growth factor (IGF-I) and platelet-derived growth factor (Table 1.2 and 1.3). Cells incorporated into the conduit can secrete neurotrophic factors and favour a microenvironment to further enhance regeneration.

Table 1.2. Synthetic materials used in nerve conduits

Composition of the tube	Incorporated features		Animal model	Gap (mm)	Ref.	
	Luminal	Lumen				
Aliphatic polyesters						
PAN-MA		PAN-MA fibres	Rat sciatic nerve	17	90	
PAN-PVC	Schwann cells		Rat sciatic nerve	8	68	
PGA	Laminin-soaked collagen fibres		Canine peroneal nerve	81	104	
	Laminin-soaked collagen sponge		Canine peroneal nerve	81	162	
Poly(lactic acids)						
PLA		PLLA filaments	Rat sciatic nerve	18	26	
PDLLA	bFGF		Rat sciatic nerve	15	171	
PLAEEP						
PLLA			Rat sciatic nerve	12	52	
	Schwann cells		Rat sciatic nerve	20	37	
PLGA	GGF, Schwann cells		Rat sciatic nerve	10,12	23, 17	
		Porous	Rat sciatic nerve	10	31, 30	
Polycaprolactones						
PCL		Micro-/macroporous	Rat peroneal nerve	6	168	
PDLLC						
PCLEEP	GDNF			15	39	
		Aligned fibres	PCLEEP	Rat sciatic nerve	15	39
PHEMA-MMA	GDNF, aFGF		Rat sciatic nerve	10	47	
PEVA	GDNF		Rat sciatic nerve	8, 15	11, 55	
PPE	NGF		Rat sciatic nerve	10	180	
P(BHETE)	Growth factors		Rat sciatic nerve	10	171, 180	
Polysulfone	Laminin		Rat sciatic nerve	10	82	
Polyurethanes (PU)						
PU-PLCL			Rat sciatic nerve	7	142	
Silicone			Rat sciatic nerve	10	56	
	NGF in PPE		Rat sciatic nerve	10	180	
	NGF with heparin-containing fibrin gel		Rat sciatic nerve	13	93	
	GDNF		Rat sciatic nerve	13	78	
	VEGF in matrigel		Rat sciatic nerve	10	74	

	PDGF in laminin-containing Biomatrix, collagen or methylcellulose gel	Rat sciatic nerve	8	175	
	CNTF in saline	Rat sciatic nerve	10	189	
	Schwann cells	Rat sciatic nerve	10	124	
	Fibroblast-like MSCs in gelatin	Rat sciatic nerve	15	33	
	Collagen fibrils	Rat sciatic nerve	5	132	
	Collagen, laminin and fibronectin adsorbed to conduit lumen			36	
		Polyamide filaments	Rat sciatic nerve	15	40
		Collagen or PLA	Rat sciatic nerve	15	82
		PLLA filaments	Rat sciatic nerve	14	26
		Bioglass 45S5 fibres bundles	Rat sciatic nerve	5	24

See Abbreviations list for the full forms of the abbreviated names of materials

Several cell types have been tested in nerve regeneration such as; Schwann cells, bone marrow stromal cells or mesenchymal stem cells (MSCs), olfactory ensheathing cells (OECs), embryonic stem cells (ESCs), neural stem cells (NSCs), fibroblasts, skin-derived stem cells (SDSCs), hair follicle stem cells (HFSCs) and ectomesenchymal stem cells (EMSCs) (Jiang *et al.*, 2010).

Gene therapy is an attractive approach to prolonging the production of the bioactive form of growth-promoting proteins. Different approaches have been used to trigger the expression of genes that encode growth factors such as gene transfection, injection of recombinant viral vectors and monoclonal antibodies.

Several ECM molecules have been tested as luminal fillers to improve nerve regeneration such as magnetically aligned fibrin matrices, hyaluronic acid, collagen fibres, laminin, and fibronectin. Although some experiments have shown that the presence of these molecules aid nerve regeneration, other research remains contradictory. There is strong evidence to suggest that this is because the way in which the fillers are distributed is pivotal to their effectiveness and can make or break the success of any regeneration process.

The principle reason for poor nerve regeneration being observed when using empty nerve conduits is the inability for non-neuronal cells to migrate across lesion gaps, especially when these gaps are large. Therefore, the need for an environment that will enable Schwann

cells to proliferate more successfully has fuelled the various design improvements to the lumen of the conduit. A host of different materials have been used to make filaments and fibres that are used as luminal fillers. Gelatin, collagen, poly(acrylonitrile-co-methylacrylate), poly (caprolactone-co-ethyl ethylene phosphate), polylactic acid (PLA) and glass fibres have all been proven to bridge 15-18mm nerve gaps effectively. Another luminal substructure that has been investigated is multichannel architecture (Yao *et al.*, 2010). Multichannel nerve conduits have internal frameworks that could potentially enhance regeneration through stabilization of the fibrin matrix that will form inside the tube. These internal structures provide a greater surface area for cell attachment and localized release of growth factors (de Ruiter *et al.*, 2009).

Table 1.3. Natural materials used in nerve conduits

Composition of the tube	Incorporated features		Animal model	Gap (mm)	Ref.
	Luminal fillers	Lumen modifications			
Collagen					
COLI		Multichannels	Rat sciatic nerve	10	183
COLI-COLIII	Schwann cells		Rat sciatic nerve	20	
Glycoproteins					
Fibronectin mats	NT-3, fibronectin		Rat sciatic nerve	10	151, 177
Polypeptides					
Gelatin		Gelatin fibres	Rat sciatic nerve	10	60
PHAs					
PHB	GGF in alginate-fibronectin hydrogel		Rabbit peroneal nerve	20, 41	123
	LIF in calcium alginate hydrogel		Rat sciatic nerve	10	70
	Schwann cells		Rat sciatic nerve	10	123
	Fibronectin conjugated to alginate hydrogel		Rat sciatic nerve	10	122

Polysaccharides						
Alginate			Rat nerve	sciatic	7	158
			Cat nerve	sciatic	51	154
Chitosan		PGA filaments	Rat nerve	sciatic	10	78
Chitosan-coated						
PDMS	NSCs					
Heparin/alginate hydrogel	bFGF		Rat nerve	sciatic	10	131
Proteins						
Silk		Silk fibres	Rat nerve	sciatic	10	182
Descellularized biomaterials						
AEM	IGF-1in delivered with osmotic bombs		Rat nerve	sciatic	20	53

See Abbreviations list for the full forms of the abbreviated names of materials

Imitating a fascicular nerve structure by subdividing the lumen into smaller guide-tubes may reduce the axon dispersion that commonly occurs in empty conduits (Stang *et al.*, 2005). Porogens and fibrous scaffolds have also been incorporated into the lumen, with the aim of controlling the permeability of the conduit. These structures can assist Schwann cell proliferation by promoting nutrient transport and blood vessel infiltration while at the same time limiting cell infiltration that can obstruct axon extension. It has also been demonstrated by Vleegert-Lankamp *et al.* (2007) that the conduit pore size has an impact on nerve generation. The main benefit of using fibrous scaffolds inside the lumen is that the combination of porosity, high surface area and topographical signals constitute an ideal environment for cell attachment and growth (Jiang *et al.*, 2010).

1.3 PHAS AS BIOMATERIALS FOR TISSUE ENGINEERING

PHAs are a family of linear polyesters consisting of 3, 4, 5 and 6-hydroxyacids, synthesized by a variety of bacterial species under nutrient-limited conditions with an excess of carbon, through the fermentation of sugars, lipids, alkanes, alkenes and alkanolic acids (Philip *et al.*, 2007). They are water-insoluble polymers produced as intracellular carbon and

energy storage compounds (Tian *et al.*, 2009) and are found as discrete cytoplasmic inclusions in bacterial cells (Philip *et al.*, 2007). They exhibit thermoplastic and elastomeric properties; they are recyclable; they can be produced from renewable carbon sources; they degrade easily and are biocompatible (Philip *et al.*, 2007). Therefore, they are potential substitutes for petroleum-derived plastics and have a wide range of biomedical applications.

PHAs can be produced and accumulated by many Gram-positive and Gram-negative bacteria from at least 75 different genera, of which *Pseudomonas*, *Ralstonia*, *Aeromonas*, *Rhodobacter* and *Bacillus* have been the most studied to date (Sangkharak and Prasertsan, 2008). They are also produced by halophilic archaeal species belonging to 10 genera, with *Haloferax* being the most well-known (Poli *et al.*, 2011). Considering the wide diversity of PHA-producing microorganisms, the study of the production of these polyesters by marine bacteria has been neglected until recently. An interest in halophilic microorganisms has started to emerge since new research revealed their remarkable potential for biotechnological PHA production. The halophilic archaeon *Haloferax mediterranei* accumulates the co-polymer poly(3-hydroxybutyrate-co-3-hydroxyvalerate) in large quantity when using glucose, starch or hydrolysed whey as a source of carbon (Lu *et al.*, 2008). Several bacterial species of the *Halomonadaceae* family have also been found to accumulate PHAs. In fact, *Halomonas boliviensis* exhibited PHA yields and volumetric productivity close to the highest reported so far (Quillaguamán *et al.*, 2010). Sangkharak and Prasertsan (2008) studied poly(3-hydroxybutyrate) P(3HB) production in the halotolerant bacteria *Rhodobacter sphaeroides* ES16 which had been isolated from a marine environment, along with two mutants of the same strain namely N20 and U7. Under optimal conditions the mutant N20 was found to be the most efficient, accumulating 88% dry cell weight (dcw) PHA. Shrivastav *et al.*, (2010) found two promising PHA-producing bacteria isolates; *Bacillus sonorensis* SM-P-1S and *Halomonas hydrothermalis* SM-P-3M which were isolated from a soil and marine environment respectively. They accumulated 71.8% and 75% dcw PHA respectively, using *Jatropha* biodiesel by-products as the carbon source.

PHAs are divided into two groups based on the number of carbon atoms in their monomer units; short-chain-length (scl) PHAs and medium-chain-length (mcl) PHAs. The former consists of monomers with 3-5 carbon atoms; they are generally stiff and brittle and have a high degree of crystallinity. The latter consists of monomers with 6-16 carbon atoms; they are flexible, have low crystallinity, low tensile strength and a low melting point. PHAs synthesized by microbes are heavily dependent on the carbon source used. Carbon sources are classified as either “related” meaning they give rise to monomers that are structurally identical to the carbon source; or “unrelated” meaning they generate monomers that are completely different in structure to the carbon source (Philip *et al.*, 2007).

PHAs with their very unique properties exhibit quite a few of the desired characteristics for nerve tissue engineering such as high biocompatibility with neuronal cells and controllable biodegradation. Hence, they are excellent candidates for use in the manufacture of conduits for peripheral nerve repair. Since PHA degrades via surface erosion, they possess a more controllable degradation than their synthetic counterparts PLA, PGA, poly(lactic-co-glycolic acid) PLGA and poly(L-lactic acid) PLLA, where the degradation mechanism is predominantly bulk erosion. Additionally, PHAs induce a reduced immune response because of the lower acidity of their by-products compared to their synthetic counterparts. Currently, poly-3-hydroxybutyrate P(3HB) is the only type of PHA that has been explored for use in nerve regeneration. P(3HB) conduits have been shown to repair nerve gaps of 10mm (Hart *et al.*, 2003; Hazari *et al.*, 1999; Mosahebi *et al.*, 2001; Mosahebi *et al.*, 2002; Mosahebi *et al.*, 2003) and 40mm (Mohanna *et al.*, 2005; Young *et al.*, 2002) in rat sciatic nerves and rabbit peroneal nerves respectively. Although the level of inflammatory infiltration was low and the reabsorption time was suitable for nerve repair, the regeneration obtained with this type of NGC was not statistically comparable with the regeneration obtained by using autologous nerve grafting. In a similar study, Young *et al.* (2002) used hollow conduits made from P(3HB) for nerve repair for 20, 30 and 40mm gaps in rabbit peroneal nerves. This study demonstrated good nerve regeneration over 63 days using this type of NGC. Although nerve regeneration was faster in the nerve autograft, the three different lengths of P(3HB) conduits did support continuous nerve growth. These results prove that P(3HB) conduits are suitable for long gap distance nerve repair. In another study, multi-block copolymers were made from poly[glycolide-co-(epsilon-caprolactone)]-diol and poly[(R)-3-hydroxybutyric acid-co-(R)-3-hydroxyvaleric acid]-diol (P(3HB-co-3HV) diol). The latter contained different amounts of P(3HB) at 41, 17 and 8 wt%. These were then used to make nerve guidance conduits of 10mm in length (Borkenhagen *et al.*, 1998). After implantation of these conduits across rat sciatic nerves with 8 mm gaps, no significant differences were observed in the degree of nerve regeneration between the different variants. The highest degree of degradation was at 24 weeks, being observed in the guidance conduit made of 8 wt% P(3HB). This result suggested that a faster complete resorption could be achieved using the lowest concentration of P(3HB) tested.

It has been shown that the use of luminal fillers have significantly improved nerve regeneration when using P(3HB) conduits. Luminal fillers such as glial growth factor (GGF), leukemia inhibitory factor (LIF), Schwann cells and fibronectin have all been used to improve the efficiency of these P(3HB) conduits. Hart *et al.* (2003) demonstrated that P(3HB) conduits can effectively deliver leukemia inhibitory factor (LIF) to enhance nerve generation after late secondary repair. In this study both nerve isografts and conduits made from P(3HB) were used

to repair 10mm gaps in rat sciatic nerves after 2 months and 4 months of axonal severance. The NGCs were filled with hydrogel comprising of fibronectin and calcium alginate with a high content of mannuronic acid, both of which served as a matrix substitute and as a carrier for the delivery of LIF. The incorporation of exogenous LIF was shown to increase the regeneration distance when using bio-artificial nerve conduits. This result was statistically comparable to that obtained when using the isograft. In an attempt to assess the viability and lac Z expression of transduced Schwann cells (SCs) during nerve regeneration, Mosahebi *et al.* (2001) incorporated these labelled syngeneic cells in a conduit made from P(3HB). The NGC was then transplanted to bridge a 10mm gap in a rat sciatic nerve. Three weeks after transplantation, the lacZ-labeled rat SCs were distinctly visible and displayed an enhanced axonal regeneration rate with a 100% improvement in comparison to conduits without SCs. Mosahebi *et al.* (2002) successfully used P(3HB) conduits to compare the effects of using allogeneic and syngenic SCs in peripheral nerve regeneration. The conduits were filled with alginate hydrogel both with and without each cellular type and were implanted in rat sciatic nerves to bridge 10mm gaps. Although the allogeneic SCs produced immune response, these cells supported axonal regeneration. These findings demonstrated the suitability of using allogenic SCs to improve nerve regeneration. The use of allogeneic cells is highly beneficial as it would mean that the extraction of autologous cells from the patient would not be necessary, allowing a simplified and more immediate transplantation procedure. In an attempt to characterize the effects of fibronectin in nerve regeneration Mosahebi *et al.* (2003) created P(3HB) conduits filled with alginate matrix containing labelled SCs to bridge 10mm gaps in rat sciatic nerves. In this experiment, it was shown that the addition of fibronectin to the alginate matrix increased the viability of SCs and subsequently improved nerve regeneration. With the aim of studying the effects of using Glial Growth Factor (GGF) and alginate matrix in nerve regeneration, Mohanna *et al.* (2005) used P(3HB) conduits to bridge gaps of 20mm and 40mm in rabbit peroneal nerves. It was shown that GGF significantly improved nerve regeneration and promoted organ re-innervation. GGF also increased the quantity of SCs, improved axonal regeneration and reduced the muscle mass percentage in comparison to both empty conduits and conduits containing purely alginate matrix.

1.4 BIOGLASSES AS BIOMATERIALS FOR TISSUE ENGINEERING

Hench *et al.* (1970) discovered the biocompatibility and use of glasses as a potential tool in bone tissue engineering. Bioglasses are a commercially available family of bioactive glasses (BGs) made from SiO₂, Na₂O, CaO and P₂O₅ in different proportions. Bioglasses present high osteoconductivity, osteostimulation and have appropriate degradation rate for

bone tissue regeneration. A high ratio of calcium to phosphorus in bioglasses promotes formation of apatite crystals whereas calcium and silica ions might act as crystallization nuclei.

Research involving bioactive glasses has focused on applications in orthopaedics and dentistry as the original bioglass composition, Bioglass 45S5TM, was developed to treat non-self-healing bone defects such as bullet trauma and cancer. Bioglass 45S5TM has a high bioactivity and it is the current golden standard for bioactive glasses. Due to the high bioactivity of BGs along with their angiogenic potential they have recently been valued for applications in soft tissue such as peripheral nerve regeneration and wound healing. This high bioactivity allows them to directly bond to bones and promote the regeneration process (Miguez-Pacheco *et al.*, 2015).

Surface reactions of BGs in contact with relevant fluids involves the release of metallic ions and precipitation of a hydroxyapatite (HA) surface layer (Miguez-Pacheco *et al.*, 2015). Metallic ions contained in some BGs have shown to have a highly beneficial effect on bone regeneration as they upregulate genes in osteoblast cells, increase matrix mineralization and stimulate proliferation of osteoblast cells.

1.4.1 ANGIOGENESIS

Angiogenesis is the generation of new blood vessels from existing ones. It is a crucial process for tissue regeneration and repair and play a fundamental role in the development of pathogenic processes such as cancer. Angiogenesis involves the migration, growth, and differentiation of endothelial cells. This process is orchestrated by mechanical stress and chemical cues produced by surrounding tissues such as extracellular matrix proteins, growth factors and other signaling proteins (Miguez-Pacheco *et al.*, 2015).

Angiogenesis is a fundamental process for tissue engineering as adequate oxygenation and mass transport is required for the development of new tissue. One common strategy in tissue regeneration to stimulate angiogenesis in engineered constructs is the use of growth factors and signaling molecules. Nevertheless, this strategy has some limitations such as lack of understanding of their release kinetics and efficiency of delivery to surrounding tissues (Miguez-Pacheco *et al.*, 2015).

It has been shown that BG dissolution products have an angiogenic effect in both *in vitro* and *in vivo* experiments. Direct stimulation of fibroblast cells with BG dissolution products triggers the production of growth factors such as vascular endothelial growth factor (VEGF) and basic fibroblast growth factor (bFGF) (Gorustovich *et al.*, 2010). Recently, El-Gendy *et al.* (2015) studied the angiogenic effect of 45S5-Bioglass-based scaffolds on human dental pulp cells for development of bone constructs. They found increased endothelial gene expression in the functional cells that were seeded onto 3D porous scaffolds *in vitro*. They also found

formation of microvessel-like tubular structures in *in vivo* experiments using male immunocompromised mice.

The angiogenic effect of BGs in regeneration of soft tissue has also been assessed. Mao *et al.* (2015) investigated the effects of nanosized 58S and 80S BGs on growth of human umbilical vein endothelial cells (HUVECs). They found that both BGs triggered proliferation and migration of HUVECS. They enhanced the production of VEGF and bFGF and also upregulated expression of their respective receptors.

1.4.2 APPLICATION OF BIOGLASS IN NERVE TISSUE ENGINEERING

Nerve tissue engineering has focused on the development of implants such as NGCs to bridge the gaps resulting from damaged tissue. The majority of implants used for peripheral nerve regeneration are made from natural and synthetic polymeric materials. However, there has been a notable increase in the use of BGs for applications in nerve tissue engineering and especially the use of fibrous BGs.

Bunting *et al.* (2005) proved that fibres of Bioglass® 45S5 are biocompatible with rat Schwann cells and fibroblasts *in vitro*. They showed qualitative and quantitative evidence of axonal regeneration *in vivo* by using a silastic conduit filled with Bioglass® 45S5 fibres implanted in sciatic nerves of adult rats.

Vitale-Brovarone *et al.* (2012) have investigated the applicability of phosphate glass fibres coded as TiPS0, TiPS2.5 and TiPS5 in nerve regeneration. They assessed their solubility using bi-distilled water and biocompatibility using Neonatal Olfactory Bulb Ensheathing Cell Line (NOBEC) and Dorsal Root Ganglia (DRG) neurons. They found that the fibres not only maintained their structural integrity and composition during 20 days of dissolution but also supported cell adhesion and proliferation of the functional cells. Additionally, they observed that the aligned configuration of the fibres showed to provide a directional cue for the growing axons (Vitale-Brovarone *et al.*, 2012).

Kim *et al.* (2012) have manufactured NGCs consisting of aligned phosphate glass fibres wrapped with a compressed collagen gel sheet. They demonstrated in *in vitro* experiments that adult dorsal root ganglion (DRG) neurons were biocompatible with the phosphate bioglass and significant neurite outgrowth was observed along the fibres. For the *in vivo* experiments, they implanted two kinds of NGCs in rat sciatic nerves, one filled with the phosphate aligned fibres (PGf/Col) and a hollow conduit made from compressed collagen gel (Col). The parameters used to assess nerve regeneration were number of axons, muscle atrophy, motor and sensory functions, which were evaluated at 7 and 12 weeks after implantation. The PGf/Col groups showed better regeneration performance in all the evaluated

parameters when compared to Col group at week 7. However, no significant differences between the two groups were found at week 12 (Kim *et al.*, 2012).

Marquardt *et al.* (2013) fabricated two forms of degradable bioactive borate glass scaffolds to investigate their potential for nerve regeneration (bioglass microfibers and fibrin/bioglass rods). To assess the biocompatibility of the material, embryonic chick dorsal root ganglia (DRG) was seeded on both bioglass constructs. Two different cell culture conditions were used; static and transient conditions. Viability of glia and fibroblasts decreased in both bioglass constructs when compared with the fibrin scaffold control. However, the proportion of neurons in the bioglass constructs increased and became higher by the end of the experiment when compared with the fibrin scaffold control. Furthermore, neurite extension in both bioglass constructs was similar to that of control fibrin scaffolds. Also, aligned glass scaffolds were found to guide neurite extension in an oriented manner (Marquardt *et al.*, 2013).

Koudehi *et al.* (2014) developed a porous nano bioglass/gelatin NGC for peripheral nerve regeneration using the sol–gel technique. MTT assay was used to assess biocompatibility of the material, which showed to support the growth of Chinese hamster ovary cells (CHO). NGCs were implanted in male Wistar rats to regenerate 10 mm gaps in the sciatic nerve. To assess nerve regeneration, gastrocnemius muscle contractility was examined at one, two and three months after surgery using electromyography (EMAP) and compared with non-severed sciatic nerves rats. Histological and muscle contractility results obtained from the rats with the implant were statistically equivalent to those obtained from rats with non-severed sciatic nerves (Koudehi *et al.*, 2014).

Novajira *et al.* (2014) have developed a novel NGC made from resorbable phosphate glass hollow fibers in combination with a genipin-crosslinked agar/gelatin hydrogel (A/G_GP). To evaluate the biocompatibility of the material, growth of neonatal olfactory bulb ensheathing cell line (NOBEC) in the culture medium containing fibre dissolution products was measured. The expression of pro- and anti-apoptotic proteins was also measured *in vitro*. Fluorescein isothiocyanate–dextran (FD-20) was used as a growth factor model molecule for the release studies. The fibres were loaded with FD-20 using three different strategies; i) FD-20/PBS solution, ii) FD-20/hydrogel solution before gelation and iii) hydrogel before gelation, subsequently lyophilized and then filled with the FD-20/ PBS solution (A/G_GP). The different strategies used to fill the fibres resulted in different release kinetics. The slowest release was observed when the A/G_GP hydrogel was used. Finally, hollow NGCs made from PCL were fabricated by dipping and a bundle of hollow fibres with the hydrogel (A/G_GP) was inserted into the conduit (Novajira *et al.*, 2014).

Mohammadkhah *et al.* (2015) used three different composite sheets consisting of biodegradable poly- ϵ -caprolactone (PCL) and varying types of bioactive glass to investigate

nerve regeneration. The three composites consist of 50 wt.% PCL and i) 50 wt % 13–93 B3 borate glass particles, ii) 50 wt% 45S5 silicate glass particles, or iii) a blend of 25 wt % 13–93 B3 and 25 wt% 45S5 glass particles. Degradation profiles were determined for each composite and the composite 50 wt% 13–93 B3 borate glass particles had a higher degradation rate compared to the composite 50 wt% 45S5 silicate glass particles. To determine the biocompatibility, dorsal root ganglia isolated from embryonic chicks were cultured on composite sheets and neurite outgrowth was measured. The bioactive glass particles added to the composites did not showed negative effects on neurite extension (Mohammadkhah *et al.*, 2015).

1.5 ELECTROSPINNING

Electrospinning is an adaptable method used to process solutions into continuous fibres with diameters ranging from nanometers to micrometers. This technique is suitable for every soluble polymer, which can be either synthetic or natural. The polymers to be used can be mixed or modified with additives such as chromophores, nanoparticles, active agents, metals and ceramics. Complex species also can be added such as enzymes, viruses, and bacteria. A wide diversity of fibres with complex architectures can be produced such as hollow fibers, core–shell fibers by using special electrospinning methods. Different rearrangements of fibres are also possible to be produced such as single and ordered organization of fibres (Grainer and Wendorff, 2007). Electrospinning is not only used for research studies, but its applications in industry are significantly increasing. The scope of its applications are diverse and includes medicine, optoelectronics, catalysis, sensor technology and filtration.

In a typical electrospinning experiment (Fig. 1.7), a polymer solution or melt is pumped through a thin nozzle or needle (inner diameter \approx 100 μ m), which serves as an electrode. A high electric field is applied to the electrode (12-500 kV) and a distance ranging from 10 to 25 cm is kept between the tip of the needle and the grounded collector. Electrospinning can be carried out either vertically or horizontally. The solution is extruded from the needle tip at a constant rate by a syringe pump. The applied voltage causes a cone-shaped deformation of the drop of polymer solution, in the direction of the grounded collector (Grainer and Wendorff, 2007). In electrospinning, the cone angle is about 30°. If the electrostatic charge overcomes the surface tension of the solution, a polymer jet is formed and reaches the grounded collector becoming narrower in the process. On the way to the grounded collector, the solvent evaporates and solid fibres are formed. Figure 1.7 shows a schematic of a typical electrospinning set-up to collect random fibres (Fig. 1.7 A) and aligned fibres using a grounded collector and rotating drum or disc respectively (Fig.1.7 B) (Lee and Arinzeh, 2011).

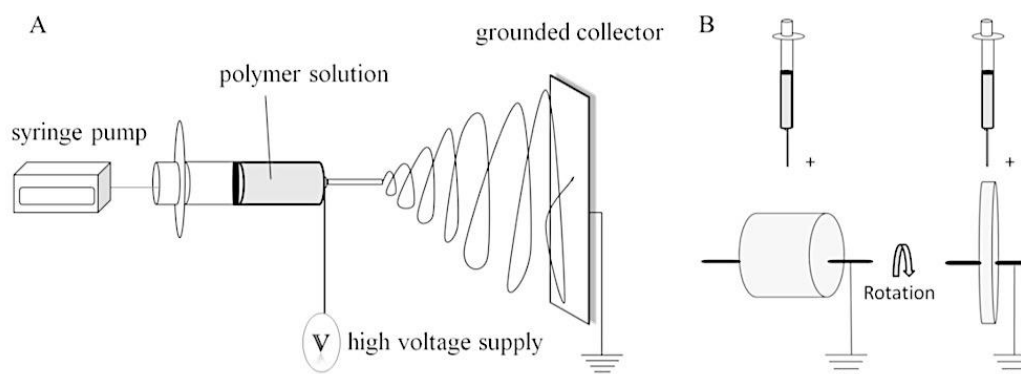


Figure 1.7 Schematic of the electrospinning process. (A) A typical electrospinning set-up to collect random fibres. (B) Collection methods for creating aligned fibrous scaffolds using a rotating drum and rotating disk (Lee and Arinzeh, 2011).

The fibre diameter depends on a wide diversity of electrospinning parameters and the properties of the polymer such as molecular weight, molecular-weight distribution, glass-transition temperature, and solubility. The characteristics of the polymer solution also have a significant effect on the fibre diameter such as viscosity, viscoelasticity, polymer concentration, surface tension, and electrical conductivity. Moreover, the solution feed rate, the field strength and geometry of the electrodes can also have an important impact on the resulting fibres. Other factors such as the relative humidity of the surroundings and the vapour pressure of the solvent play a major role in fibre formation (Grainer and Wendorff, 2007).

1.6 AIMS AND OBJECTIVES

The main aim of this project was to explore the use of polyhydroxyalkanoates in nerve tissue engineering ultimately leading to the development of novel PHA-based nerve conduits. In order to accomplish this, the following specific objectives were achieved:

1. Production of the short chain length PHA, P(3HB)) using *Bacillus cereus* SPV and medium chain length PHA, (P(3HO)) using *Pseudomonas mendocina* CH50
2. Production and characterization of films and electrospun fibres made from P(3HO), P(3HB) and varying proportions of P(3HO)/P(3HB) blends (25:75, 50:50, 75:25).
3. Determination of the biocompatibility of both flat films and electrospun fibres using NG-108-15 neuronal cells along with RN22 Schwann cells.

4. Fabrication and characterization of material properties of scaffolds made from the most biocompatible P(3HO)/P(3HB) blend and bioactive glasses
5. Determination of the effect of bioactive glasses on the biocompatibility of PHA/BG composites using NG-108-15 neuronal cells along with RN22 Schwann cells.
6. Manufacture of two different designs of NGCs: (1) hollow tube, (2) hollow tube with luminal surface of electrospun fibres.
7. Determination of nerve regeneration *in vivo* using NGCs made using PHAs.

Chapter 2

Materials and Methods

2 PRODUCTION AND CHARACTERIZATION OF P(3HO) AND P(3HB)

2.1 PRODUCTION OF POLY(3-HYDROXYOCTANOATE)

P(3HO) was produced using *Pseudomonas mendocina* via a two-stage culture preparation (Fig 2.1) at shaken-flask and fermenter level using two media compositions called second stage seed medium and production medium (Table 1.1). The P(3HO) second stage seed medium and P(3HO) production medium included minimal salt medium (MSM), magnesium sulphate ($MgSO_4$), trace element solution and sodium octanoate as the carbon source. The MSM consisted of ammonium sulfate ($(NH_4)_2SO_4$), potassium phosphate (KH_2PO_4) and sodium phosphate (Na_2HPO_4). The sodium octanoate and $MgSO_4$ were autoclaved separately and added aseptically to the MSM. Similarly, 1 mL/L of the trace element solution previously filtered was aseptically added to the MSM. The chemical compounds used for the culture media in the production of P(3HO) were purchased from Sigma–Aldrich (The Old Brickyard, New Rd, Gillingham SP8 4XT, UK), VWR (Hunter Blvd, Lutterworth LE17 4XN, UK) and Alfa Aesar (Shore Rd, Port of Heysham Industrial Park, Heysham LA3 2XY, UK).

Table 2.1. Second stage seed medium and production medium

Compounds	Concentration (g/L)	
	Second stage seed medium	Production medium
$(NH_4)_2SO_4$	0.45	0.50
KH_2PO_4	2.38	2.65
Na_2HPO_4	3.80	3.80
$MgSO_4$	0.40	0.40
Sodium octanoate	3.32	3.32

The first seed culture was prepared by inoculating a single colony of *P. mendocina* in sterile nutrient broth (NB) (Sigma–Aldrich, Gillingham, UK) and grown for 16 h at 30°C and 200 rev min⁻¹. The volume of NB was 10% of that from the seed culture volume ($V = 140$ mL). The resultant culture broth was used to inoculate the previously sterilized second stage seed culture medium. The resultant culture broth ($V = 1.4$ L) was then incubated for 48 h at 30°C and 200 rpm. When the P(3HO) second stage seed culture reached an optical density (OD) of 1.6 at 450 nm, this was inoculated in sterile P(3HO) production medium and grown for 48

h at 30°C and 200 rpm ($V = 14L$). The volume of the second stage seed culture represented 10% from the total volume of the production broth.

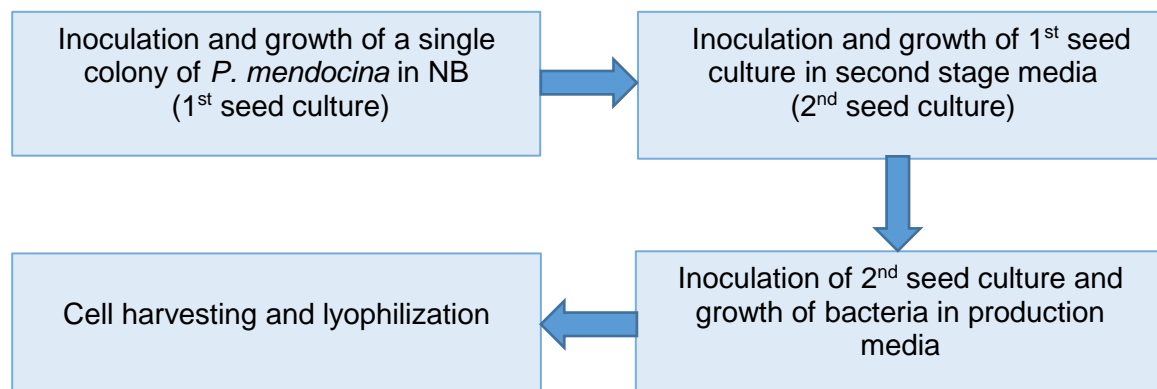


Figure 2.1. Two stage culture for P(3HO) production, its purification and characterization.

2.2 PRODUCTION OF POLY(3-HYDROXYBUTYRATE)

Batch production of P(3HB) was carried out using *B. cereus* SPV with the Kannan & Rehacek medium (Table 2.3) at both shaken-flask and fermenter level. The inoculum was prepared by inoculating a single colony of the organism in sterile NB (Sigma–Aldrich, Gillingham, UK) and grown for 16 h at 30°C and 200 rev min⁻¹. The volume of the inoculum was 10 % of the production medium volume. The obtained culture was then used to inoculate the sterile production media (Kannan & Rehacek medium) and incubated at 30°C and 200 rpm for 72 h. The chemicals used for the culture media for P(3HB) production were purchased from Sigma–Aldrich (Gillingham, UK), VWR (Lutterworth, UK) and Alfa Aesar (Heysham, UK).

Table 2.3. Kannan & Rehacek media composition

Compounds	Concentration (g/L)
Glucose	20.00
Yeast extract	2.50
Potassium chloride	3.00
Ammonium sulphate	5.00
Soybean dialysate	100 mL

2.3 EXTRACTION AND PURIFICATION OF PHAS

Prior to extraction, the cells were harvested by centrifuging the bacterial cultures at 4600 rpm for 30 min and then lyophilized for 48h. For the extraction of either P(3HO) and

P(3HB) the chloroform/sodium hypochlorite dispersion and soxhlet method were performed. For the chloroform/sodium hypochlorite dispersion, freeze-dried cells were treated with 80 % v/v hypochlorite (NaOCl) (Sigma–Aldrich, Gillingham, UK) and chloroform (CHCl₃) (Sigma–Aldrich, Gillingham, UK) in a 1:4.5 ratio and incubated for 2 h at 30°C and 150 rpm. This mixture was then centrifuged at 4600 rpm for 18 min after which three layers were formed. Both, the upper layer of NaOCl and the middle layer containing cell debris were discarded. The bottom CHCl₃, layer which contained the polymer, was concentrated using a rotatory vacuum evaporator. P(3HO) was precipitated by adding the concentrated chloroform to 10 volumes of ice-cold methanol:ethanol (1:1) (Sigma–Aldrich, Gillingham, UK), whereas P(3HB) was obtained by adding the concentrated chloroform to 10 volumes of ice-cold methanol with constant stirring. For further purification of P(3HO), the polymer was dissolved in acetone and then precipitated again in 10 volumes of ice-cold methanol:ethanol (1:1) at constant stirring. For further purification of P(3HB), the polymer was dissolved in chloroform and then precipitated again in 10 volumes of ice-cold methanol with constant stirring. This process was repeated at least three times. For soxhlet extraction cells were previously homogenised before lyophilizing. Freeze-dried cells were then refluxed in methanol for 24 h to remove the media components. Thereafter, cells were refluxed in chloroform for 48 h, after which chloroform containing polymer was concentrated using a rotatory vacuum evaporator. Precipitation of polymers was carried-out as stated above.

2.4 GAS CHROMATOGRAPHY – MASS SPECTROSCOPY

Chemical structure analysis of P(3HO) and P(3HB) was carried-out using GC-MS of the methanolysed polymer. The GCMS analysis was performed using a Varian GC/MS system consisting Chrompack CP-3800 gas chromatograph and Saturn 200 MS/MS block (Varian, 3100 Hansen Way Palo Alto, CA 94304-1038, USA). The chromatograph was equipped with a capillary column; 30 m length 0.25mm internal diameter and 0.25 film thickness (Elite-5MS, Perkin Elmer, Rd, Seer Green, Beaconsfield HP9 2FX, UK). The purified polymers were subjected to methanolysis in order to generate methyl esters of the polymers (Furrer et al., 2007). Methylene chloride (2ml) and 2– ethyl-2-hydroxybutyric acid (10 mg/ml) (Sigma–Aldrich, Gillingham, UK) were added to 20 mg of polymer and left at room temperature for 1 hour. After this, 2ml of boron trifluoride (Sigma–Aldrich, Gillingham, UK) in methanol (0.65 M) (Sigma–Aldrich, Gillingham, UK) was added to the mixture and tightly sealed, followed by vigorous shaking. This reaction mixture was then refluxed for 16 hours after which the reaction tubes were cooled on ice for 5 min. High performance liquid chromatography (HPLC) (2 ml) water was added to the reaction mixture and vortexed thoroughly for 1 min. This led to phase

separation after which the bottom organic phase containing the polymer was collected and dried using the mixture of anhydrous sodium sulphate and sodium carbonate (Furrer *et al.*, 2007). This was then filtered for GC-MS analysis. The sample (1 μ L) dissolved in chloroform (Sigma–Aldrich, Gillingham, UK) was injected with helium (1 mL.min⁻¹), which was used as the carrier gas. The injector temperature was 225°C at 18°C/min and held at the final temperature for 10 min.

2.5 NUCLEAR MAGNETIC RESONANCE SPECTROSCOPY (NMR)

Structural characterization of P(3HO) and P(3HB) was performed using ¹³C and ¹H NMR analysis (Bruker Avance III 600 Cryo, Banner Lane, Coventry CV4 9GH, UK). For this analysis, 20 mg of each purified polymer was dissolved in 1 ml of deuterated chloroform. The chemical shifts were referenced against the residual solvent signals 7.26 ppm and 77.0 ppm for ¹H and ¹³C respectively. NMR spectra were analyzed using the MestRec software package. The NMR analysis was carried-out at the Department of Chemistry, University College London, UK.

2.6 FOURIER TRANSFORM INFRARED SPECTROSCOPY (FTIR) OF THE POLYMERS AND FILMS

FTIR spectroscopy analysis was performed to determine the degree of crystallization of the structure of the PHAs and P(3HO)/P(3HB) films. The FTIR spectrum of both, PHA samples in powder form (2mg) and film samples of an area of approximately 0.7 mm² were recorded at 400 – 4600 cm⁻¹ with a resolution of 4 cm⁻¹; window material, Csl; 10 scans and resolution of 4 cm⁻¹. 2 mg samples of films were used to perform the analysis (Labram 300, Horiba Jobin Yvon, 133 Finnieston St, Glasgow Metropolitan Area G3 8HB).

2.7 FILM PREPARATION

Films of P(3HO), P(3HB) and three different blends of P(3HO)/P(3HB) were prepared using the solvent casting method. The PHAs were dissolved in chloroform (Sigma–Aldrich, Gillingham, UK) in order to obtain a total polymer concentration of 5 wt %. The P(3HO)/P(3HB) blends were prepared in ratios of 75:25, 50:50 and 25:75 by dissolving the required amounts of polymers in 10 mL of chloroform. After polymer dissolution, the solutions were homogenized by sonication and then cast in glass petri dishes that were 6 cm in diameter. The films were air dried for two weeks and their thickness was measured using a digital depth gauge. They were produced in triplicate in order to obtain a total of fifteen films with varying thicknesses ranging between 0.09 – 0.15 mm.

2.8 COMPOSITE FILM PREPARATION

Films of 25:75 P(3HO)/P(3HB) blend along with both Bioglass® (BG1) and bioactive glass 1393 (BG2) were prepared using the solvent casting method. These bioglasses were provided by The Institute of Biomaterials, University of Erlangen-Nuremberg, 91058 Erlangen, Germany). The PHAs and each bioactive glass were dissolved in chloroform (Sigma–Aldrich, Gillingham, UK) in order to obtain a total polymer concentration of 5 wt % of the 25:75 P(3HO)/P(3HB) blend and 0.5, 1.0, 2.5 and 5 wt% of each bioactive glass. The control of 25:75 P(3HO)/P(3HB) blend was prepared as described in section 2.7 (Lizarraga-Valderrama *et al.*, 2015). After polymer dissolution, the solutions were homogenised by sonication and then cast in 6-cm glass petri dishes. The films were air dried and produced in triplicate in order to obtain a total of twenty-one films including the control 25:75 P(3HO)/P(3HB) blend.

2.9 SCANNING ELECTRON MICROSCOPY OF FILMS, SCAFFOLDS AND PHAS/BIOACTIVE GLASS COMPOSITES

Surface topography of the films, electrospun fibres and the PHA/Bioglass composites was analysed using a FEI XL30 Field Emission Gun Scanning Electron Microscope (Achtseweg Noord 5, 5651 GG Eindhoven, Netherlands). All the samples were previously sputter-coated with a 20 nm film of palladium using a Polaron E5000 sputter coater. The operating pressure of the sputter coating was 5×10^{-5} bar with a deposition current of 20 mA for a duration of 1 m 30 s. The images were then recorded and the diameters of fibres were measured at different magnifications at 5kV using the FEI software. This analysis was carried out at the Eastman Dental Institute, University College London.

2.10 PROFILOMETRIC SURFACE ANALYSIS

The surface roughness of the films were analysed using a Sony Proscan 1000 Laser Profilometer (1-7-1 Konan Minato-ku, Tokyo, 108-0075 Japan). The laser used was model 131A, which had a measuring range of 400 μm , a resolution of 0.02 μm and a maximum output of 10 mW. Scans of 0.5 mm^2 were obtained from each sample. Nine random coordinates were selected from each specimen in order to measure the root mean square roughness (Rq). This analysis was carried out at the UCL Eastman Dental Institute of University College London.

2.11 SURFACE WETTABILITY OF THE FILMS

The static contact angle was measured to study the hydrophilicity of the films using a KSV Cam 200 goniometer (KSV, Laivurinkatu 43, 00150 Helsinki, Finland). About 200 μL of deionized water was dropped onto the surface of the films using a gas-tight micro-syringe. As

soon as the water droplet made contact with the sample, a total of 10 images were captured with a frame interval of one second. The analysis of the images was performed using the KSV Cam software. For each sample, three random points were analyzed to obtain a total of nine measurements for each type of film. This analysis was carried out in the UCL Eastman Dental Institute of University College London.

2.12 STATIC TENSILE TEST OF THE FILMS

Mechanical analysis of the films was conducted using a Perkin Elmer Dynamic Mechanical Analyser 7 (Perkin, 761 Main Ave, Norwalk, CT 06851, USA). The sample dimensions were 1.66 mm - 2.05 mm in width; 5 mm – 6 mm in length and had a thickness of 0.05 mm - 0.18 mm. The load was set within a range of 1 nN – 6000 mN with a rate of 200 mN/min⁻¹ at 24°C. The mechanical properties were determined using the Perkin Elmer DMA 7 software. This included analysis of Young’s modulus, ultimate tensile strength and elongation at break. This analysis was carried out in the UCL Eastman Dental Institute of University College London.

2.13 MANUFACTURING OF ALIGNED P(3HO)/P(3HB) BLENDS FIBRES BY ELECTROSPINNING.

Electrospinning was performed using a high voltage power supply (Genvolt, New Road, Bridgnorth WV16 6NN, UK) with a syringe pump (WPI, 175 Sarasota Center Blvd. Sarasota, FL 34240, USA) and a rotating cylindrical collector (IKA, Suite 1 Fountain House John Smith Drive Oxford Business Park, Oxford Oxon OX4 2JY, UK). A plastic 1 mL syringe (Intertronics, UK) with a blunt needle (20 G) connected to the power supply was used to fabricate the fibres. All the fibres were collected on a sheet of aluminium foil, which was used to wrap the electrically grounded collector. Several electrospinning conditions and various P(3HO)/P(3HB) blends were applied in order to fabricate fibres of different diameters (Table 2.4).

Table 2.4. Summary of electrospinning conditions used for the manufacturing of aligned 20 % w/v P(3HO)/P(3HB) blend fibres of varying diameters.

% Polymer (w/v)	Flow rate (ml/h)	Voltage (kV)	Rotator speed (rpm)	Diametre of 25:75 P(3HO)/P(3HB) fibres (µm)
20	1	12	2000	3.6 ± 0.6
20	1	12	1500	4.1 ± 1.1

20	1	12	1000	4.4 ± 0.2
20	1	18	2000	3.7 ± 0.6
20	1	18	1500	4.3 ± 1.6
20	1	18	1000	5.6 ± 1.0

Since the 25:75 P(3HO)/P(3HB) blend showed better biocompatibility and mechanical properties (Lizarraga-Valderrama *et al.*, 2015), it was chosen for further electrospun fibre manufacture. Appropriate quantities of purified P(3HO) and P(3HB) were dissolved in chloroform (Sigma–Aldrich, Gillingham, UK) and stirred for 24 h before electrospinning. Aligned fibres of 25:75 P(3HO)/P(3HB) blend were produced using varying polymer concentrations (15, 25 and 30 and 35 % w/v) under different voltage conditions (12 kV, 18 kV) and collector speed (1500 and 2000 rpm). All PHA solutions were electrospun at a distance of 10 cm from the collector for 1 min with a syringe pump flow rate of 1 ml/h. The electrospun sheet dimensions after electrospinning were 5 cm x 20 cm, from which squares of 1.5 cm x 1.5 cm were removed for scanning electron microscopy analysis and cell culture experiments. Table 2.5 summarizes the processing conditions used to obtain 25:75 P(3HO)/P(3HB) blend fibres with different diameters using varying polymer concentrations (15, 25, 30 and 35 %wt). Three representative diameters were chosen for cell culture studies based on the uniformity of the fibres; large ($13.5 \pm 2.3 \mu\text{m}$), intermediate ($3.7 \pm 0.3 \mu\text{m}$) and small ($2.4 \pm 0.3 \mu\text{m}$).

Table 2.5. Summary of electrospinning conditions used to manufacture aligned P(3HO)/P(3HB) blend fibers of varying diameters using different polymer concentrations.

Voltage (kV)	Collector speed (RPM)	Fibre diameter			
		Polymer concentration			
		15 % wt	25 % wt	30 % wt	35 % wt
12	2000	2.4 ± 0.3	3.5 ± 0.3	4.3 ± 0.2	12.1 ± 3.6
	1500	3.5 ± 0.4	4.1 ± 0.3	4.4 ± 0.3	13.5 ± 2.3
18	2000	3.1 ± 0.3	3.4 ± 0.3	4.4 ± 0.8	14.0 ± 3.5
	1500	3.4 ± 0.2	3.7 ± 0.3	5.1 ± 0.9	15.9 ± 8.0

2.14 CHARACTERIZATION OF ALIGNED P(3HO)/P(3HB) BLEND FIBRES BY SCANNING ELECTRON MICROSCOPY.

Three separated batches of sample of the three diameter fibre groups were characterized using scanning electron microscopy (FEI XL30 Field Emission Gun Scanning

Electron Microscope, Eindhoven, Netherlands). Three parameters were analysed: i) fibre diameter; ii) fibre density and iii) fibre alignment. An average of 27 fibres per fibre group were studied for the determination of fibre diameter and fibre alignment. The same images used to determine parameters i and iii were analysed to measure the density, which was defined as the number of fibres per area of the image.

Fibre alignment was determined by measuring the angular variance between the fibres. Therefore, a reference line was drawn parallel to a central fibre, from which the angular difference was measured with respect to each fibre across the sample. The resulting data was collected in four groups classified by their angular difference ($\pm 0^\circ$, 1° , 2° and 3°).

2.15 NG108-15 NEURONAL CELL CULTURE

NG108-15 neuronal cells were obtained from The European Collection of Cell Cultures (ECACC) and grown in Dulbecco's Modified Eagle Medium (DMEM) (Sigma–Aldrich, Gillingham, UK) under a humidified atmosphere of 5 % CO₂ at 37°C. The DMEM was supplemented with 10 % (v/v) fetal calf serum, 1 % (w/v) glutamine, 1% (w/v) penicillin/streptomycin, and 0.5% (w/v) amphotericin B. Cells were only used in the experiments once they were 80 % - 90 % confluent. Cells were trypsinised and 3×10^4 cells were seeded directly onto the PHA film samples within 12 well plates in 3 mL of DMEM. The cultures were maintained for 4 days, with half of the medium being removed and replaced with fresh serum-free DMEM on day 2 to trigger differentiation. The used NG-108-15 cells were between passages 10-20. All the cell culture experiments were performed in the Kroto Institute at the University of Sheffield.

2.16 LIVE/ DEAD MEASUREMENT OF NG108-15 NEURONAL CELLS

After growing the cells for 4 days, the culture medium was removed and replaced with fresh serum-free DMEM (Sigma–Aldrich, Gillingham, UK) containing 0.0015% (w/v) propidium iodide (Invitrogen, 55B Bridge Cl, Dartford DA2 6PT, UK) and 0.001% (w/v) Syto-9 (Invitrogen, Dartford, UK) at 37°C/5% CO₂ for 15 min. After washing with phosphate-buffered saline (PBS) (x3) (Sigma–Aldrich, Gillingham, UK), the cells were imaged with an upright Zeiss LSM 510 confocal microscope (Zeiss, Carl-Zeiss-Strasse 22, 73447 Oberkochen, Germany). A helium-neon laser was used for the detection of propidium iodide ($\lambda_{\text{ex}} = 536 \text{ nm} / \lambda_{\text{em}} = 617 \text{ nm}$) while an argon-ion laser was used for Syto 9 ($\lambda_{\text{ex}} = 494 \text{ nm} / \lambda_{\text{em}} = 515 \text{ nm}$). Three fields-of-view were imaged containing 20-500 cells per sample, so as to express the data as a percentage of live

versus dead cells \pm Standard Error of the Mean (SEM). Quantification of live and dead cells was performed using Image J.

2.17 IMMUNOLABELLING OF NG108-15 NEURONAL CELLS AND RN22 SCHWANN CELLS

To assess the differentiation of neuronal cells, samples were immunolabeled using β III-tubulin as the primary antibody and with Alexa Fluor® 488 goat anti-mouse IgG as the secondary antibody (Sigma–Aldrich, Gillingham, UK). Sample containing cultures of NG108-15 neuronal cells previously washed with PBS (x3) (Sigma–Aldrich, Gillingham, UK), were fixed with 4% (v/v) paraformaldehyde for 20 min, then permeabilized with 0.1 % (v/v) Triton X-100 (Sigma–Aldrich, Gillingham, UK) for 20 mins, before being washed with PBS (x3). Unreactive binding sites were blocked with 3% (w/v) bovine serum albumin (BSA) (Sigma–Aldrich, Gillingham, UK) with the cells being incubated overnight with mouse anti β III-tubulin antibody (1:1000) (Promega, 2800 Woods Hollow Road. Madison, WI 53711, USA) diluted in 1% BSA at 4°C. Cells were then washed three times with PBS before being incubated either with Alexa Fluor® 488 goat anti-mouse IgG antibodies (1:200 in 1 % BSA) (Sigma–Aldrich, Gillingham, UK) or Texas Red-conjugated anti-mouse IgG antibody (1:100 dilution in 1% BSA) for 90 min (Sigma–Aldrich, Gillingham, UK). After washing the cells once with PBS, 4', 6-diamidino-2-phenylindole dihydrochloride (DAPI) (1:500 dilution in PBS) (Sigma–Aldrich, Gillingham, UK) was added to label nuclei along with phalloidin-FITC (1:1000 dilution in PBS) (Sigma–Aldrich, Gillingham, UK) to label RN22 Schwann cells when required. Cells were then incubated for 30 mins at room temperature before being washed again with PBS (x3). Cells were then imaged using an upright Zeiss LSM 510 confocal microscope (Zeiss, Oberkochen, Germany) in Kroto imaging facility at University of Sheffield. Nuclei were visualized by two photon excitation using a Ti:sapphire laser (716 nm) for DAPI ($\lambda_{ex} = 358$ nm/ $\lambda_{em} = 461$ nm) (Sigma–Aldrich, Gillingham, UK). For imaging the neuronal cell body and neurites of NG108-15 helium-neon laser (543nm) was used to detect Texas Red-conjugated anti-mouse IgG antibody (1:100 dilution in 1% BSA) ($\lambda_{ex} = 589$ nm/ $\lambda_{em} = 615$ nm) (Sigma–Aldrich, Gillingham, UK) and an argon ion laser (488 nm) to detect Alexa Fluor ® 488 goat anti-mouse IgG ($\lambda_{ex} = 495$ nm/ $\lambda_{em} = 519$ nm) (Sigma–Aldrich, Gillingham, UK). For imaging RN22 Schwann cell cytoskeleton, argon ion laser (488 nm) was used to detect phalloidin-FITC ($\lambda_{ex} = 495$ nm/ $\lambda_{em} = 521$ nm) (Sigma–Aldrich, Gillingham, UK). The differentiated cells were then counted using Image J, and identified as neuronal cells expressing neurites.

2.18 MANUFACTURE OF ALIGNED PHA MICROFIBERS BY ELECTROSPINNING

Electrospinning was performed using a high voltage power supply (Genvolt, UK) with a syringe pump (WPI, USA) and a rotating cylindrical collector (IKA, UK). A plastic 1 mL syringe with a blunt needle (20G) (Intertronics, 17 Station Field Industrial Estate, Banbury Road, Kidlington OX5 1JD, UK) connected to the power supply was used to fabricate the fibres. All the fibres were collected on a sheet of aluminium foil, which was used to wrap the electrically grounded collector. Several electrospinning conditions were applied in order to fabricate fibres of different diameters. The neat P(3HO) and P(3HB) polymers and their blends were all previously dissolved in chloroform and stirred for 24 h before electrospinning. Aligned fibres of P(3HO), P(3HB) and 25:75, 50:50 and 75:25 blend films of P(3HO)/P(3HB) were produced using varying polymer concentrations (5, 10, 15, 20 % w/v), under different conditions of voltage (12 kV, 18 kV) and collector speed (1000, 1500 and 2000 rpm). All PHA solutions were electrospun at a distance of 10 cm from the collector for 1 min with a syringe pump flow rate of 1 ml/h. The electrospun sheet dimensions after electrospinning were 5 cm x 20 cm, from which squares of 1.5 cm x 1.5 cm were removed for scanning electron microscopy analysis and cell culture experiments.



Figure 2.2 Electrospinning setup used for fabrication of aligned 25:75 electrospun fibres (A) Syringe pump. (B) Blunt needle connected to an electrode. (C) Focusing ring. (D) Electrically grounded cylindrical collector. (E) Electric motor. (F) Voltage generator (Daud, 2013).

2.19 MANUFACTURE OF NERVE GUIDANCE CONDUITS (NGCs)

Nerve guidance conduits were produced by the dip-moulding technique and rolling and ligation of PHA films. For the manufacture of single lumen conduits, a mandrel (outer diameter, 1.8 mm) was submerged into PHAs solution contained in a glass tube. Inside the fume hood, the mandrel was secured to a dipping apparatus with drying oven (PTL-MMB02, 860 S 19th St, Richmond, CA 94804, USA) and dipped into the PHA solution every 10 seconds, for a total

of 10-12 dips at different rates. After dipping, the conduits were left in the fume hood for evaporation of solvent at atmospheric pressure for 10 days. Four tubes were fabricated using different conditions and shown in Table 2.6. A single lumen conduit with electrospun fibres inside was produced by wrapping the PHA film around a blunt needle (20G) (Intertronics, UK) followed by joining the ends. A sheet of 75:25 P(3HO)/P(3HB) blend film was attached to the collector and fibres were electrospun with 25:75 P(3HO)/P(3HB) blend solution (30 % wt). After one week, when the fibres were dry, a square was cut and wrapped around a mandrel and stuck using a 5 % wt 25:75 P(3HO)/P(3HB) blend solution.

Table 2.6. Varying dip-moulding conditions used for fabrication of NGCs.

NGCs	Dip-moulding conditions
1	3 dips (20 sec), 3 dips (30 sec), 3 dips (40 sec), 3 dips (50 sec)
2	3 dips (30 sec), 3 dips (30 sec), 3 dips (40 sec), 3 dips (40 sec)
3	10 dips (35 sec)
4	12 dips (35 sec)

2.20 STATISTICAL ANALYSIS

Statistical analysis was conducted using Graph Pad Prism 6 software. A Shapiro - Wilk and Bartlett's test was previously performed to verify the normality and homogeneity of the data respectively. To analyse the difference between data, a one-way ANOVA test ($p < 0.05$) was conducted followed by Turkey's – post test ($p < 0.05$). Data was reported as mean \pm SEM.

Chapter 3

Production and Characterization of P(3HO) and P(3HB)

3 PRODUCTION AND CHARACTERIZATION OF P(3HO) AND P(3HB)

3.1 INTRODUCTION

PHAs are polymers synthesized by a wide diversity of bacteria and are believed to play a role in carbon storage, energy storage and also as reducing equivalents (Madison and Huisman, 1999; Tian *et al.*, 2009). The first PHA discovered was by Maurice Lemoigne in 1927 who found that *Bacillus megaterium* produced poly(3-hydroxybutyrate), P(3HB) (Lemoigne, 1927). Since then, PHAs have been studied extensively and over 100 different hydroxyl acid monomers have been identified (Marchesini *et al.*, 2003). These biopolymers have similar properties to common chemically-synthesized plastics, but unlike these plastics, PHAs have the attractive advantage of being able to be produced from renewable carbon sources as well as being both biodegradable and biocompatible. Therefore, they are environmentally friendly and are a potential alternative for today's petroleum-derived plastics. They have been shown to have a great variety of industrial uses, however biomedical applications is one of the most economically practical field in which the advantages of PHAs can be exploited, as the benefits that their unique characteristics bring to medical science far outweigh their relatively high production cost.

During the last 20 years, the unique characteristics of polyhydroxyalkanoates have encouraged scientists from different disciplines to investigate the possible applications of these polymers in biomedicine and have developed a wide variety of medical devices. The most common PHAs used in biomedical applications are P(3HB), copolymers containing 3-hydroxybutyrate and 3-hydroxyvalerate, P(3HB-co-3HV), poly(4-hydroxybutyrate), P(4HB), copolymers containing 3-hydroxybutyrate and 3-hydroxyhexanoate, P(3HB-co-3HHx) and poly(3-hydroxyoctanoate), P(3HO), since they can all be obtained in large-enough quantities (Chen, 2010). Suitable materials for medical applications must be biocompatible, which means having the ability to support the appropriate cellular activity without eliciting any systemic responses in the patient. Similarly, the by-products generated during the degradation process of the biomaterial must elicit a minimal inflammatory response (Shoichet, 2010). *In vivo* biocompatibility studies both on various model animals and also in human blood have shown a minimal immune response towards PHAs. The response has been found to be similar to that observed when using standard materials currently used in surgical procedures such as silk or catgut (Brigham and Sinskey, 2012). The development of PHA composites allows for further tailoring of the inherent PHA properties in order to achieve the desired biocompatibility, mechanical properties and degradation times required for specific physiological conditions (Chen, 2010). The biocompatibility of PHAs can also be improved by using both, chemical and

enzymatic treatments using lipases and NaOH, or functionalization with carboxyl-ions (Chen and Wu, 2005).

Biodegradability is an essential material property required for tissue engineering and drug delivery applications. Various methods of manufacture can be used to alter the biodegradability of PHA devices such as by blending with others polymers, increasing the porosity and increasing the exposed surface area (Chen and Wu, 2005). PHAs have also been demonstrated to be suitable for use as scaffolds in tissue engineering since they are easily degradable and favour proliferation and attachment of cells. Examples of these are fibroblasts, mesenchymal stem cells, neural stem cells, chondrocytes, osteoblasts, epithelial cells, hepatocytes, adrenocortical cells and vascular smooth muscle cells. Furthermore, PHAs are ideal candidates for use as drug carriers, not only because of their biodegradability and biocompatibility but also because they can degrade through surface degradation (Chen, 2010).

PHAs have been used for the manufacture of a wide variety of surgical material and implants such as sutures, suture fasteners, meniscal repair devices, rivets, tacks, staples, screws, bone plates, surgical mesh, slings, orthopaedic pins, vein valves, bone dowels, wound dressing, implant patches and haemostats (Chen, 2010). Other biomedical applications include; intermediaries in chiral synthesis and nutritional supplements in their oligomeric and monomeric forms. Another potential application is the use of the PHA granules as protein immobilizers that can be utilized in diagnostic and therapeutic applications (Grage, 2009).

An important step forward in the research and development of biomedical devices made from PHAs has been the approval of TephaFLEX® by the U.S. Food and Drug Administration. This is significant as the product is an absorbable suture manufactured using P(4HB), which is the first PHA product to be available commercially. Moreover, there are currently four PHAs that are commercially available called Biopol, Degra pol, Nodax and Biogreen (Anjun *et al.*, 2016). Biopol is a co-polymer of poly (3-hydroxybutyrate-co-3-hydroxyvalerate) and it's currently produced by Metabolix (Cambridge, MA, USA). Nodax, developed by Procter and Gamble, consists of 3-hydroxybutyrate along with a small quantity of medium chain length monomers with side groups greater than or equal to three carbon units, which includes 3-hydroxyhexanoate, 3-hydroxyoctanoate and 3-hydroxydecanoate. Degra Pol is a polyester-urethane that consists of two blocks of polymers; polyhydroxybutyrate-diol (hard segment) and ω -dihydroxy-poly (ϵ -caprolactone-block-diethyleneglycol-block- ϵ -caprolactone) (Soft segment). Biogreen, manufactured by Japan-based Mitsubishi Gas Chemicals, consist of P(3HB) produced from methanol (Anjun *et al.*, 2016).

Due to the high cost of PHA production, several optimisation strategies are being developed that include, using of renewable carbon substrates, optimization of fermentation processes, developing of new bacterial strains and engineering new pathways. These approaches are applied not only to reduce production cost but also to significantly increase the polymeric yields of production (Liu *et al.*, 2016). This breakthrough should encourage further studies of the use of PHAs as raw materials for manufacturing medical devices.

This chapter will describe the production of the scl-PHA, P(3HB) and the unique_mcl-PHA, P(3HO), a homopolymer unlike the P(3HO) containing traces of 3-hydroxy decanoate, described by Chen, 2010, using bacterial fermentation.

3.2 RESULTS

3.2.1 PRODUCTION OF P(3HO) USING SODIUM OCTANOATE AS THE CARBON SOURCE

P. mendocina was grown in MSM for batch production of P(3HO) (Fig. 3.1) at shaken-flask level (Fig. 3.1) using octanoate as the the sole carbon source.

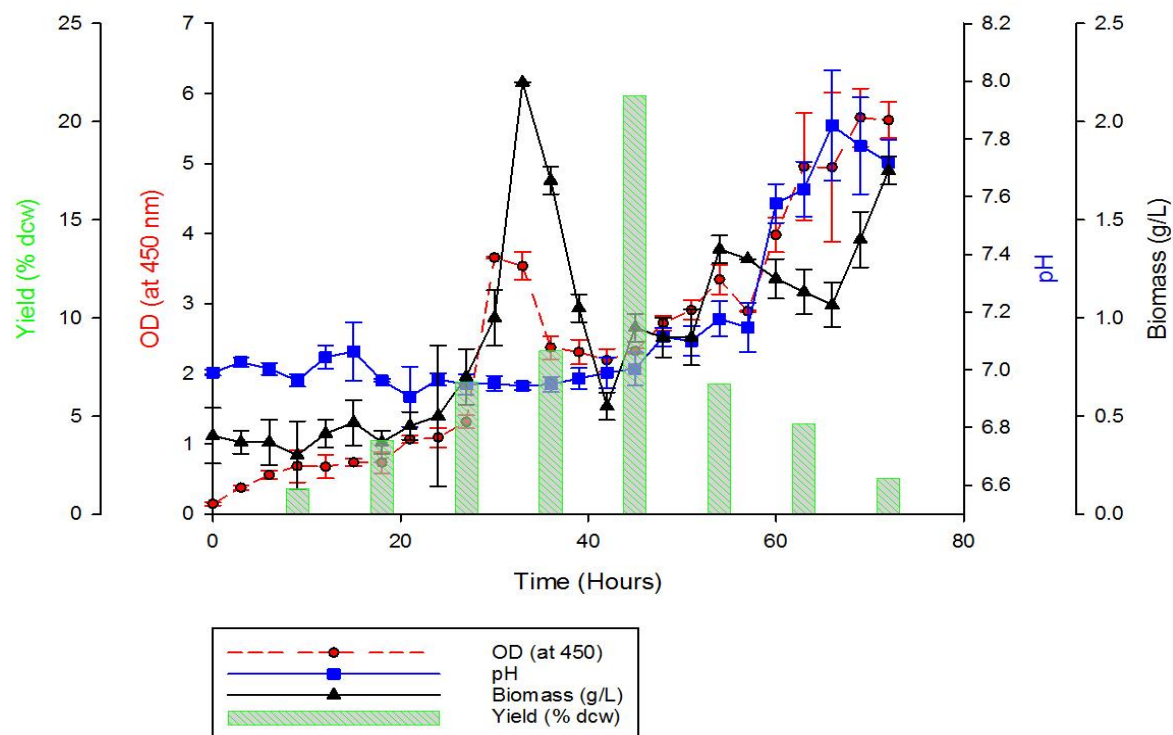


Figure 3.1 Temporal profile of the fermentation of *P. mendocina* CH50 at shaken flask level.

Fig. 3.1 shows the characteristic fermentation profile of *P. mendocina* at shaken flask level. Three samples of 1 mL were taken every 3 hours for measuring the OD, pH and biomass. The microbe grew exponentially up to 36 h, when the stationary phase started. As expected, the OD and biomass increased steadily until it reached the value of 3.5 at 36 h corresponding to the end of the exponential phase, after which these values started to decrease. The pH increased steadily until it reached the highest value of 7.84 at 66 h. The pH of the culture broth decreased slightly after 66 h and within 72 h the pH had reached 7.7. The polymer yields also increased until reaching the maximum value (22% dry cell weight, dcw) at 42 h, after which it started to decrease. The biomass increased gradually up to 36 h when the highest dry cell mass (2.3 g/L) was reached, after which it started to decrease, achieving a value of 0.5 g/L, at 42 h. The organism started to accumulate the polymer at 9 h (0.2 % dcw), from which the polymer yield increased steadily up to 42 h when the highest value (22% dcw) was achieved.

This fermentation process was then scaled up to 14 L and 50 L total media production using 20 L and 72 L fermenters respectively. The yields for the 20 L and 72 L fermenters were 42.27 % dcw and 13,59 % dcw respectively. Figure 3.2 shows neat P(3HO) extracted and purified using soxhlet extraction and ethanol:methanol (1:1) purification.



Figure 3.2 Extracted and purified P(3HO).

3.2.2 PRODUCTION OF P(3HB) USING GLUCOSE AS CARBON SOURCE

Batch production of P(3HB) using *Bacillus cereus* SPV was also carried-out at shaken-flask and fermenter level. Fig. 3.4 shows the characteristic fermentation profile of *B. cereus* SVP at shaken flask level. The organism grew rapidly over 24 hours, as indicated by the OD. The OD increased rapidly until it reached a value of 9.90 ± 0.18 at 48 h when the exponential phase finished. The maximum OD value of 13.57 ± 0.28 was reached at 63 h. Biomass

increased gradually, reaching the maximum value of 2.59 mg/L at 39 h, which then decreased to 1.77mg/L at 48 hours. The pH of the culture broth dropped sharply during the first 6 h and then increased to a value of 6.48 at 30 h, before dropping to 4.8 at 72 h. In the first 9 h, the P(3HB) yield was 16.60% dcw. This yield was doubled at 18 h after which the yield increased steadily until 72 h when it reached 47.27% dcw.

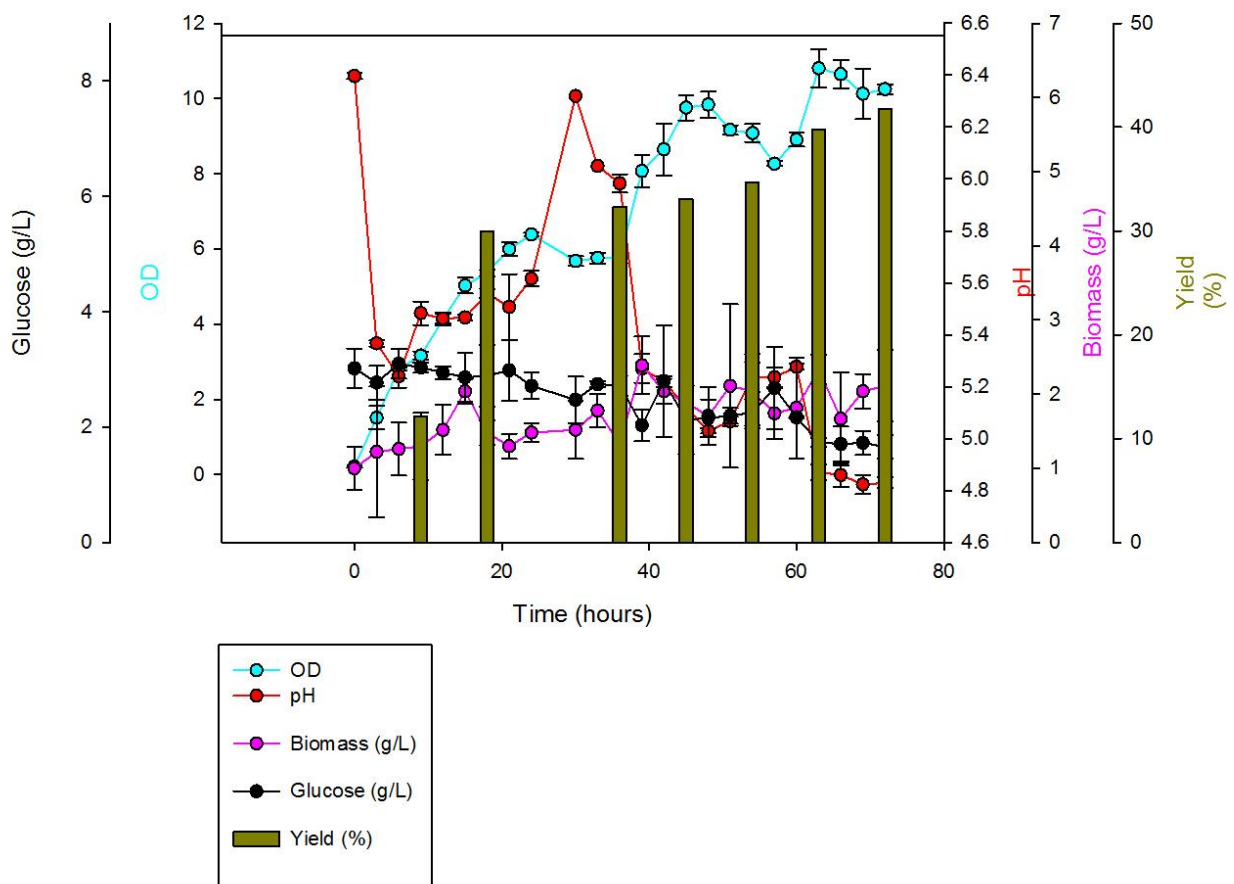


Figure 3.3 Temporal profile of the fermentation of *B. cereus* SPV at shaken flask level.

Similar to the P(3HO) production, this fermentation process was then scaled up to 14 L using a 20 L fermenter shown in Figure 3.4. The polymer yield for the 20 L fermenter was 49.22 % dcw

Figure 3.5 shows neat P(3HB) extracted and purified using soxhlet extraction and methanol purification respectively. The extracted and purified P(3HB) is characterized by its white colour. The physical appearance of P(3HB) is notably different to that of P(3HO), which is cream-coloured.

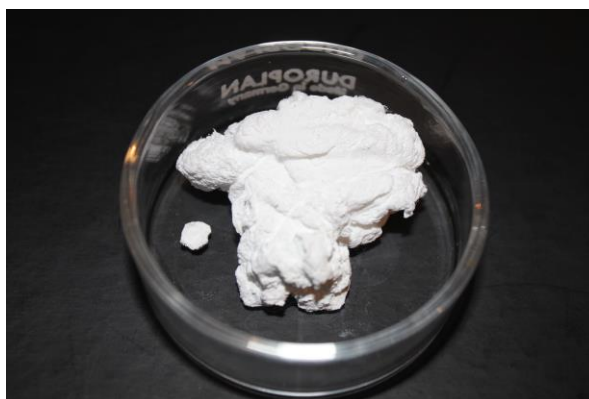


Figure 3.4 Extracted and purified P(3HB)-

3.2.3 CHARACTERIZATION OF P(3HO) AND P(3HB)

Chemical characterization of the PHAs produced by *P. mendocina* and *B. cereus* SPV was carried out by using Fourier transform infrared spectroscopy (FTIR), gas chromatography mass spectroscopy (GC-MS) and ^{13}C and ^1H NMR. Differential scanning calorimetry (DSC) was used to determine the thermal characteristics of the polymers.

3.2.3.1 FOURIER TRANSFORM INFRARED SPECTROSCOPY (FTIR) OF P(3HO) AND P(3HB)

The signature FTIR peaks that are commonly used to rapidly detect and identify PHAs are the peaks corresponding to the C=O group stretch and ester C-O-C group stretch. Furthermore, peaks corresponding to the C-O-C stretch vibrations are also useful not only for the identification of PHAs but also for the determination of the crystallinity index (CI). Figure 3.5 (A) and (B) shows the FTIR of P(3HO) and P(3HB) respectively.

As seen in Figure 3.5, the P(3HO) linked carbonyl peak was observed at 1725.45 cm^{-1} (Figure 3.12. A) whereas that linked to P(3HB) was observed at 1718.99 cm^{-1} (Figure 3.5. B). The C-O stretching bands for P(3HO) and P(3HB) were observed at 1161.12 cm^{-1} and 1179.25 cm^{-1} respectively (Figure 3.5 A and 3.5 B). Another noticeable difference between these polymers are the C-H stretching vibration bands around 2900 cm^{-1} which were stronger for P(3HO). In general, in the infrared spectra of PHAs, C=O stretch peaks are detected in the region $1719\text{-}1744\text{ cm}^{-1}$, whereas the ester C-O-C stretch bands are observed in the range of $1160\text{-}1300\text{ cm}^{-1}$. Although in the FTIR spectra, the above mentioned bands are the ones most commonly used to analyse PHAs, the peaks of other detectable groups conforming to the PHA molecules such as CH_2 and CH_3 were also identified (Noda *et al.*, 2007; Sato *et al.*, 2004; Wu *et al.*, 2001).

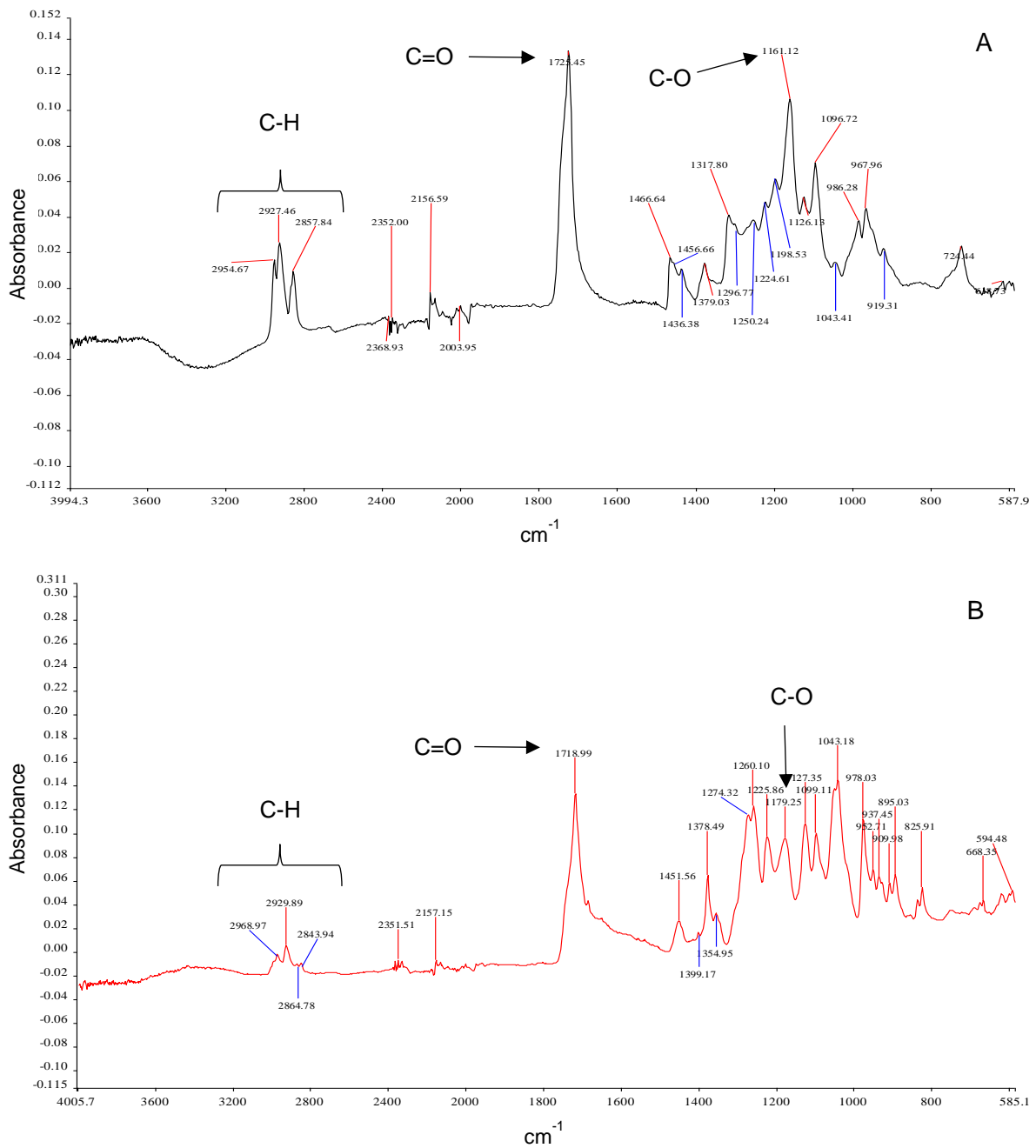


Figure 3.5 FTIR of purified PHAs. A) FTIR of purified P(3HO) extracted from *P. mendocina* CH50. B) FTIR of purified P(3HB) extracted from *B. cereus* SVP.

3.2.3.2 GAS CHROMATOGRAPHY MASS SPECTROSCOPY OF P(3HO) AND P(3HB)

The extracted polymers were methanolysed for gas chromatography mass spectroscopy in order to produce methyl esters, which can be detected using [gas chromatography](#). Figure 3.6 A and B show the gas chromatogram and the mass spectrum respectively.

The peak observed at a retention time of 8.18 min corresponded to the octanoic acid, 3-hydroxy-methylester. The internal standard 2-ethyl-2-hydroxybutyric acid exhibited a retention time of 5.33 min. The peak at 5.90 could be remaining membrane lipids from the bacteria. The mass spectrum of the peak at a retention time (Rt) of 8.18 min is shown in Figure 3.6 B. The spectrum mass observed was found to be identical to that of the methyl ester of 3-hydroxyoctanoate ($M_w = 174$) in the MS (NIST) library. This result thus confirmed that the polymer produced using *P. mendocina* CH50 had monomers 3-hydroxyoctanoic acid and hence was poly(3-hydroxyoctanoate).

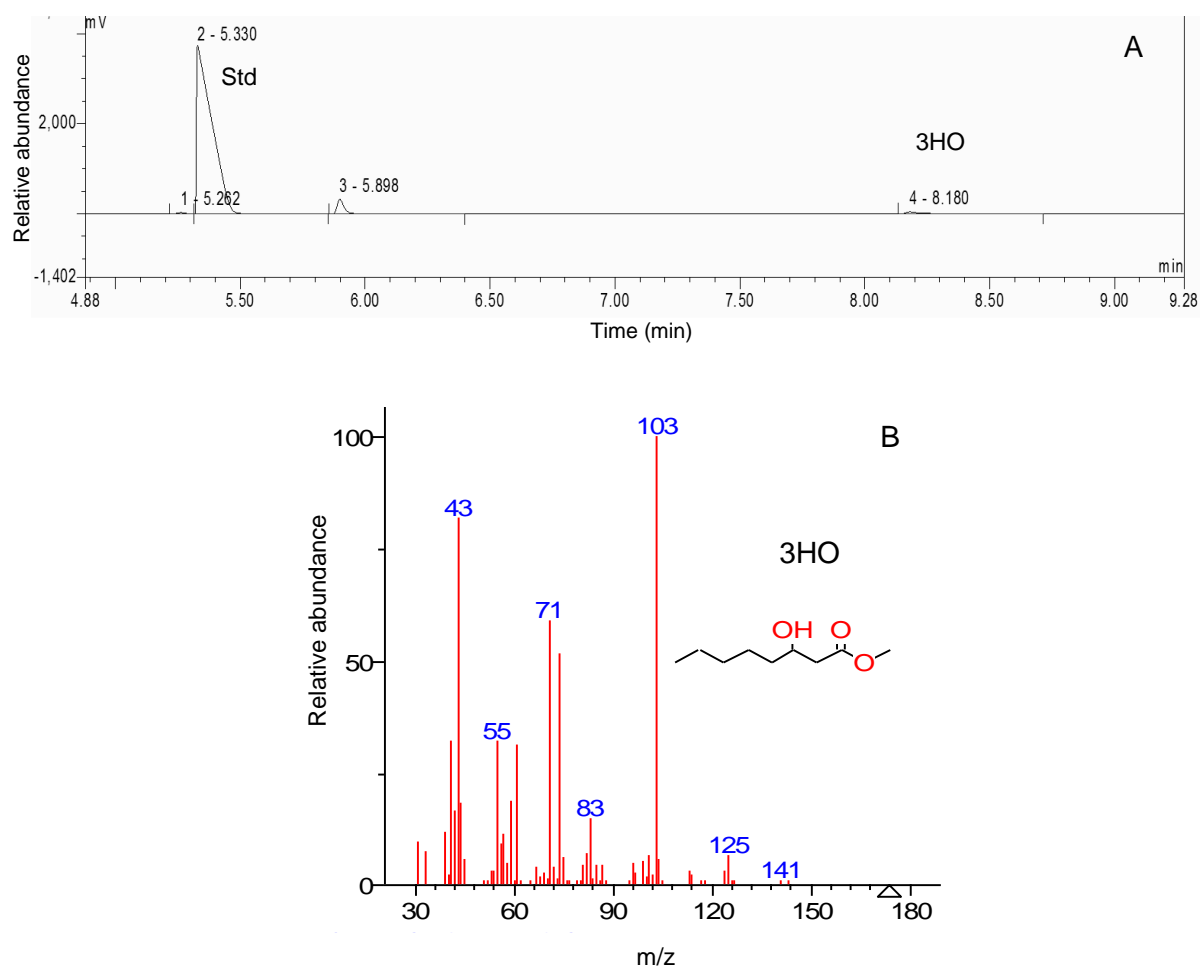


Figure 3.6 Gas chromatography mass spectroscopy of P(3HO). A) Gas chromatogram of methanolysed P(3HO). B) Mass spectroscopy of 3-hydroxy-methylester of octanoic acid.

Fig. 3.7 A shows the gas chromatogram of 3-hydroxybutyric acid. The most conspicuous peak found at a retention time (R_t) of 5.83 min corresponded to the methyl ester of 3-hydroxybutyric acid (3HB). The internal standard methyl benzoate peak was observed at a retention time (R_t) of 9.32 min. The mass spectrum of the peak at a retention time (R_t) of 5.83 is shown in Figure 3.7 B. The spectrum obtained was that of the methyl ester of 3-

hydroxybutyrate (Mw = 174) in the MS (NIST) library. This chromatography analyses thus confirmed that the polymer produced by *B. cereus* SPV using glucose as carbon source was P(3HB).

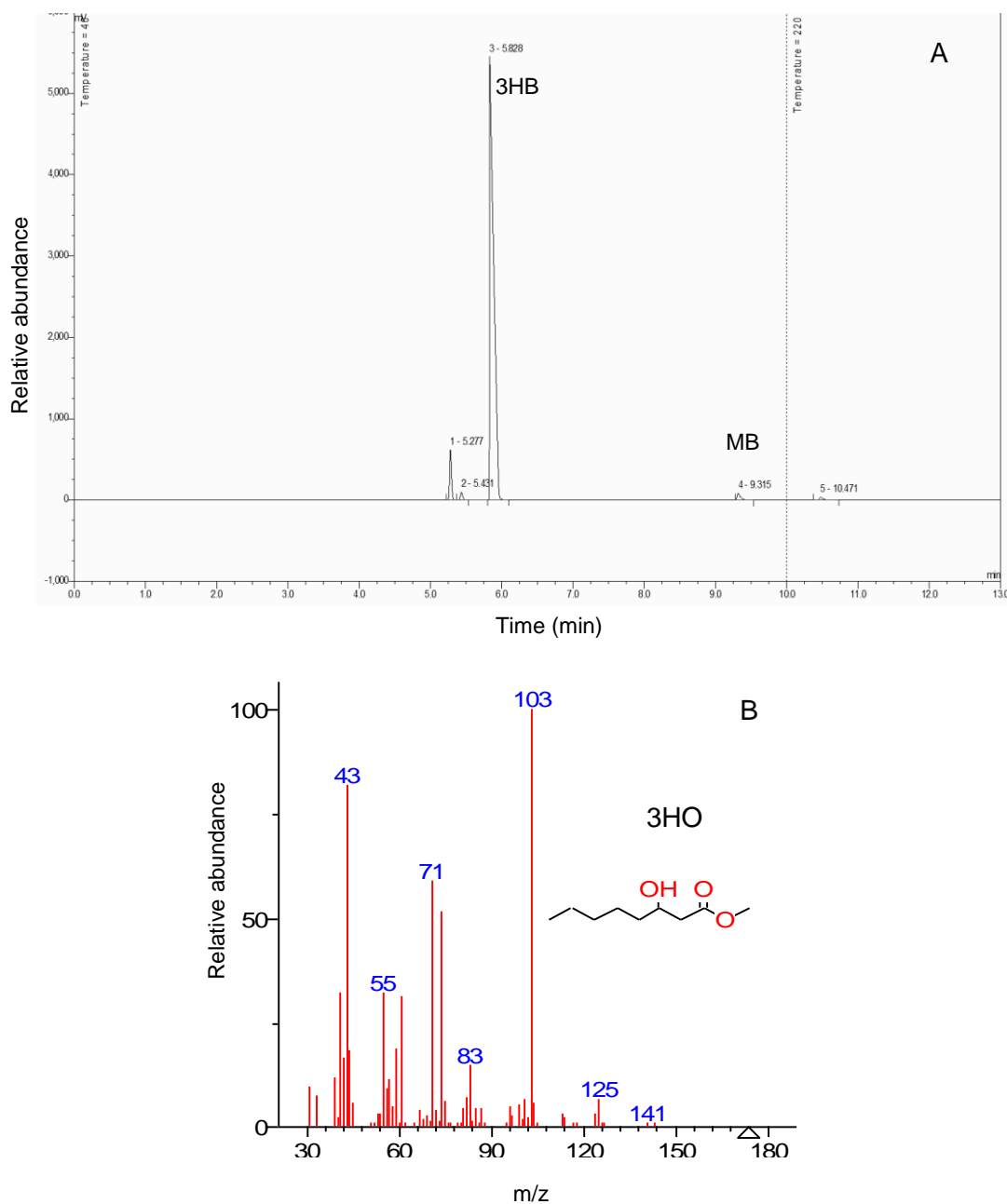


Figure 3.7 Gas chromatography mass spectroscopy of P(3HB). A) Gas chromatogram of methyl esters of 3-hydroxybutyric acid. B) Mass spectroscopy of P(3HB).

3.2.3.3 ^1H NMR AND ^{13}C NMR OF P(3HO) AND P(3HB)

The extracted polymers were purified and subjected to both ^{13}C and ^1H NMR. In the ^1H NMR spectrum of P(3HO) (Figure 3.9 A), six peaks were observed.

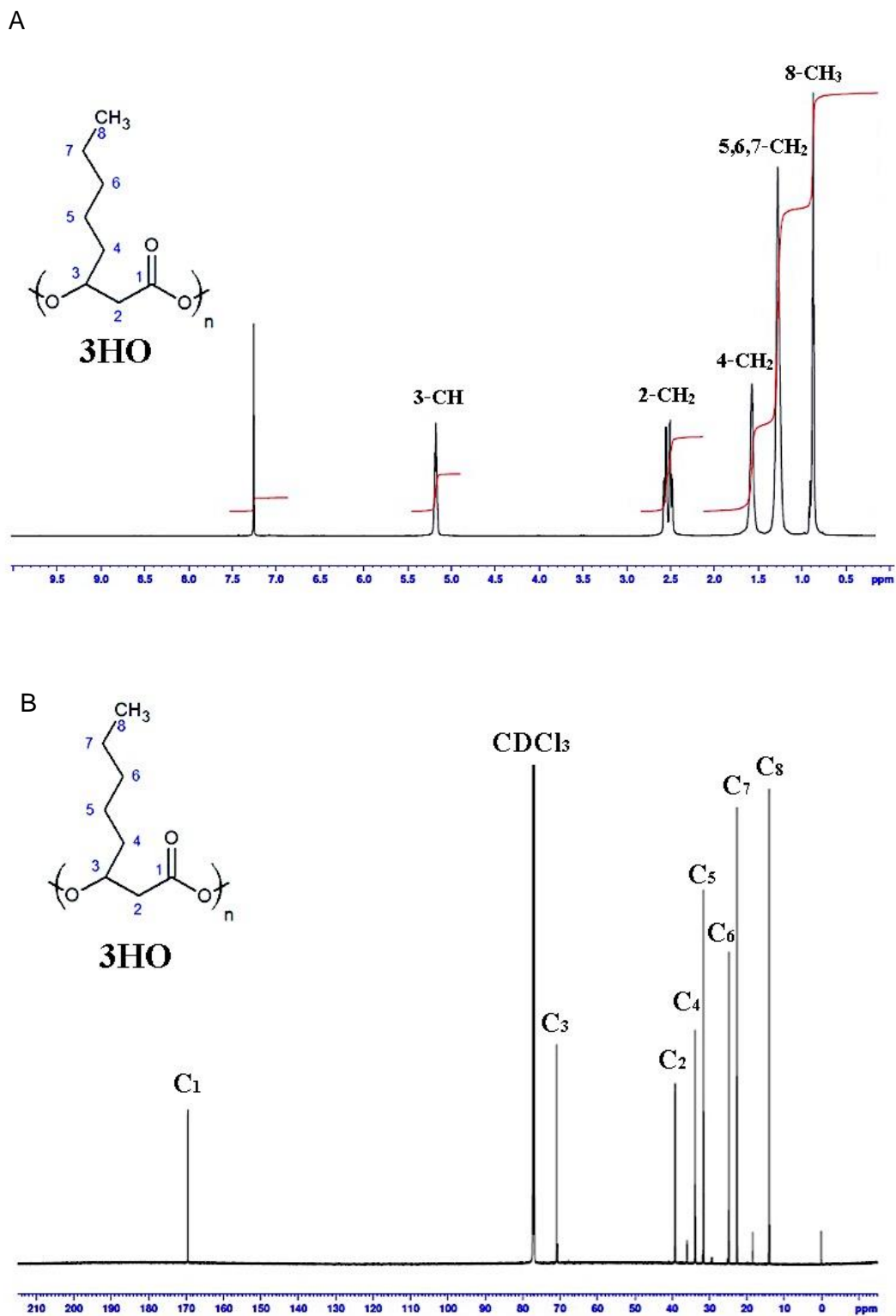


Figure 3.8 NMR of purified P(3HO) extracted from *P. mendocina* CH50 (A) ^1H NMR spectrum of 3HO showing six peaks, from which five peaks correspond to the five different protons environments in the 3HO molecule.

The peaks at the chemical shifts of 5.2, 2.5, 1.6, 1.2 and 0.8 ppm corresponded to protons bonded to C3 (-CH group), C2 (-CH group), C4 (-CH₂ group), C5, C6, C7 (-CH₂ group) and C8 (-CH₃ group) of the 3-hydroxyoctanoate respectively. As expected and previously reported, these five peaks represented the five different proton environments in the molecule. The peak at the chemical shift 7.2 corresponded to the proton of the chloroform (CHCl₃) residues.

In the ¹³C NMR spectrum of P(3HO) (Figure 3.8 B), nine peaks were observed. The peak at the chemical shift of 77.92 corresponded to the solvent CDCl₃ used to dissolve the sample. The other eight peaks corresponded to the eight carbons with different environments present in the 3-hydroxyoctanoate. The chemical shifts at 169.54, 70.94, 39.19, 33.85, 31.50, 25.18, 22.75 and 14.21 ppm corresponded to C1 (C=O group), C3 (-CH group), C3 (-CH₂ group), C4, C5, C6, C7 (-CH₂ group) and to C8 (-CH₃ group) respectively.

In the ¹H NMR spectrum of P(3HB) (Figure 3.9, A) four peaks were found. The peaks at 5.27 ppm, 1.38 ppm and the multiplet at 2.5 ppm corresponded to protons bonded to C3 (-CH group), C4 (-CH₃ group) and to C2 (-CH₂ group). Similar to ¹H NMR of P(3HO) spectrum, the peak at the chemical shift 7.2 corresponded to the proton of the chloroform residues.

In the ¹³C NMR spectrum of P(3HB) (Figure 3.9, B), 5 peaks were observed. The peak at 76.93 ppm corresponded to the solvent CDCl₃ used to prepare the sample. As expected, the other four peaks represented the four carbons with different environment in the molecule 3-hydroxybutyrate. The four peaks at 169.44, 67.79, 40.67 and 19.99 ppm corresponded to C1 (C=O group), C3 (-CH group), C2 (-CH₂ group) and C4 (-CH₃ group).

3.2.3.4 DIFFERENTIAL SCANNING CALORIMETRY

Table 3.1 shows the thermal characteristics of P(3HO) and P(3HB) respectively. The glass transition temperature (T_g) of P(3HB) was not detected.

Table 3.1. Differential scanning calorimetry results for the PHAs.

Polymer	T _g (°C)	T _m (°C)	ΔH _f (J/g)
P(3HO)	-39.46	39.94	5.79
P(3HB)	-	161.39	90.28

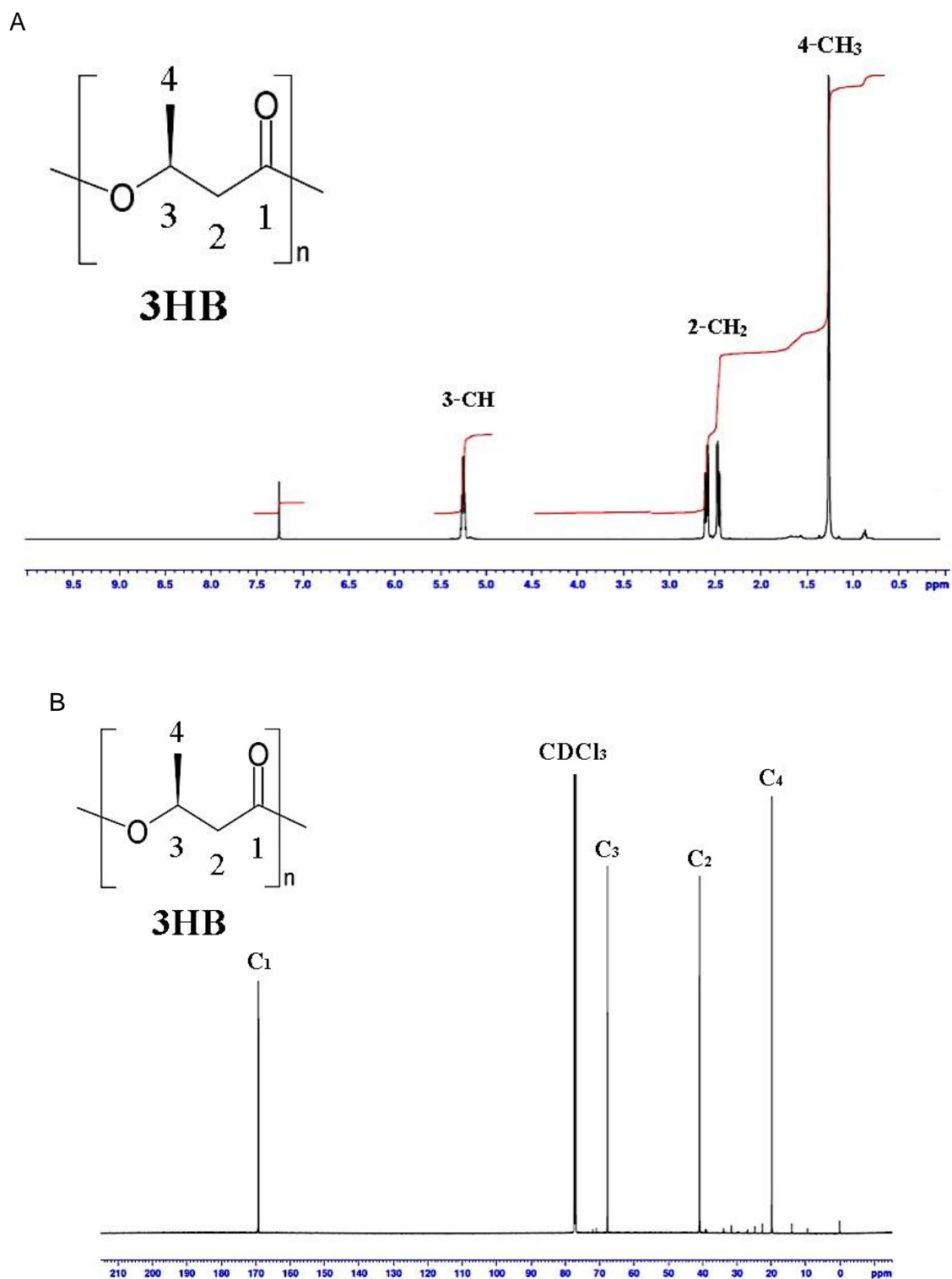


Figure 3.9 NMR of purified P(3HB) extracted from *B. cereus* SVP. A) ¹H NMR spectrum of 3HB showing five peaks, of which four peaks correspond to the four different protons environments present in the 3HB molecule. B) ¹³C NMR spectrum of 3HB showing five peaks, of which four peaks correspond to the four different carbon environments present in the 3HB molecule.

3.3 DISCUSSION

Petroleum-derived plastics have been valuable materials for modern life due to their versatile properties such as lightness, robustness, durability and resistance to degradation. These materials have a wide variety of applications in cosmetics, medical and industrial fields such as gears, packaging, furniture, machinery frames and accessories. In 2014, the production of plastic worldwide amounted to some 311 million metric tons and it was expected to continue until 2020. The worldwide dependence on petroleum derived plastics have caused serious pollution problems and a significant decrease in the crude oil reserves. Furthermore, the current disposal methods of plastic material are inefficient and present several complications. Therefore, replacement of conventional petroleum-derived plastics seems to be the most convenient solution to reduce the environmental impact of plastics. Biopolymers are the current plastic alternatives such as polylactide acids, polysaccharides, aliphatic polyesters and polyhydroxyalkanoates, which exhibit similar properties to petroleum-derived polymers.

Several bacteria synthesize and accumulate PHAs as carbon and energy storage materials and are found as discrete cytoplasmic inclusions in bacterial cells, which are typically 0.2 ± 0.5 μm in diameter (Anjum *et al.*, 2016). They exhibit thermoplastic and elastomeric properties; they are recyclable; they can be produced from renewable carbon sources; they degrade easily and are biocompatible (Philip *et al.*, 2007). Therefore, they are a potential substitute for petroleum-derived plastics and have a wide range of biomedical applications. A great amount of PHAs are composed of R(-)-3-hydroxyalkanoic acid monomers ranging from C_3 to C_{14} carbon atom containing monomers.

The principal strategy to produce PHAs is the growth of bacteria under nutritional stress such as the limitation of nitrogen, magnesium, oxygen or phosphorus, along with excess of carbon source supply. In this investigation, *P. mendocina* CH50 has been grown under conditions with excess of sodium octanoate as the carbon source. On the other hand, *B. cereus* SPV was grown with Kannan & Rehacek medium, with excess of glucose as the carbon source (Valappil *et al.*, 2007). The maximum P(3HO) yields reached were 22% dcw obtained at shaken flask level and 42.27 % dcw using a 20L fermenter. Similarly, maximum yields of P(3HB) obtained were 47.27% dcw at shaken flask level and 49.22% dcw using a 20L fermenter. The discrepancy observed in the P(3HO) yield could be attributed to the different extraction methods applied to isolate the polymers. The P(3HO) yield (22% dcw) was obtained by using the soxhlet method whereas 42.27 % dcw was achieved when the dispersion technique was used (described in Chapter 3, section 2.3). It has been shown that the polymer extraction method significantly affects the polymer yield of PHAs (Rai *et al.*, 2011).

When the dispersion method was applied, cells are disrupted by hypochlorite, which provides greater access to the accumulated intracellular granules by the chloroform in which the polymer dissolves. Moreover, the presence of CHCl_3 diminishes the degradation effect of the hypochlorite (Rai *et al.*, 2011). The resultant polymer yields obtained for both polymers, P(3HO) (42.27 % dcw) and P(3HB) (49.22 % dcw) using the 20L fermenter were higher than those obtained in previous studies. Rai *et al.*, 2011 obtained a P(3HO) yield of 31.38% whereas Valappil *et al.*, 2007 obtained 38.00 % dcw. This difference could be due to the fact that Rai *et al.* (2011) and Valappil *et al.* (2007) obtained these polymer yields from polymer production at shaken flask level, in which the aeration was less efficient than in a fermenter.

During the production of P(3HO), the pH increased slightly from 7 to 7.8 at the end of the the polymer production. In contrast, a prominent decrease in pH was detected during P(3HB) production by using *B. cereus* SPV. The initial pH was 6.8, which decreased until 4.8 at the end of the PHA production. This has been observed in previous studies (Valappil *et al.*, 2007b) and shows the acid tolerance of this *Bacillus* strain. It has been shown that the acid tolerance of *B. cereus* depends on its growth phase. During the log phase, cells have shown to be more sensitive to acid stress resulting in the development of acid resistance as the culture enters he stationary phase. The initial pH at 6.8 of the culture media permitted the establishment of the log phase of growth by the organism. The resulting acidification of the media prevented P(3HB) degradation, allowing improved yields of the polymer.

Characterization of both, P(3HO) and P(3HB) using FTIR, GC-MS and ^1H NMR and ^{13}C NMR successfully allowed the identification and confirmation of the structure these polymers. Chemical structure confirmation of the extracted polymers was firstly carried out by FTIR. In the FTIR analysis, the peaks around 1725 cm^{-1} or 1719 cm^{-1} detected in the polymers corresponded to the C=O stretching vibrations of the crystalline phase of P(3HO) and P(3HB) respectively. When scl-PHAs are in the crystalline phase, the peak corresponding to the carbonyl group is detected at around 1728 cm^{-1} , whereas in the amorphous phase this band is detected at 1743 cm^{-1} . Therefore, the peak at 1725 cm^{-1} of C=O stretching vibration of P(3HO) has shown that the majority of P(3HO) molecules were in crystalline phase. Similarly, peaks of C=O groups of scl-PHAs at around 1725 cm^{-1} are detected when the polymer is in the crystalline phase. When the scl-PHAs are in the amorphous phase the peak of C=O group is detected at 1740 cm^{-1} . Similar to P(3HO), the C=O stretching vibration of P(3HB) at 1719 cm^{-1} has shown that the majority of P(3HB) molecules were in the crystalline phase (Ouyang *et al.*, 2007; Randriamahefa *et al.*, 2003).

GC-MS resulted in the confirmation of the presence of the methyl ester of 3-hydroxyoctanoic acid and 3-hydroxybutyric acid in P(3HO) and P(3HB) respectively. The production of the homopolymer P(3HO) is quite unique since normally *P. mendocina* is known

to produce the copolymer P(3-hydroxyoctanoate-co-3-hydroxydecanoate) (Tian *et al.*, 2000). Monomer identification was performed by the direct interpretation of the spectra and comparison with known NMR spectra of P(3HO) and P(3HB) (Rai *et al.*, 2011). It is well-known that *Pseudomonas sp.* uses two different pathways depending of the carbon source present in the culture media. Fatty acid β -oxidation pathway is preferred when these bacteria are grown in structurally related carbon sources (fatty acids, alkanes, and alkenes), whereas the *de novo* fatty acid synthesis pathway is used when grown in structurally unrelated carbon sources. Therefore, *P. mendocina* is expected to have used the β -oxidation pathway of fatty acids. For the production of P(3HO), it has been previously observed that the unusual production of only P(3HO) without formation of co-polymers could be the result of the dominance of the conversion of octanoate to 3-hydroxyoctanyl-CoA over further breakdown of the 3-hydroxyoctanoate to a hexanoate derivative. Rai *et al.* (2011) explained that this preference could be due to a high affinity of the enoyl-CoA reductase, ketoacyl-CoA reductase and 3-hydroxyacyl-CoA epimerase for the octanoate. Rai *et al.* (2011) also suggested that PHA synthase in *P. mendocina* could have a higher affinity for 3-hydroxyoctanyl-CoA compared to any other 3-hydroxyacyl-CoA, resulting in the formation of the homopolymer.

Since the carbon source used in this investigation for P(3HB) production was glucose, the synthesis of P(3HB) homopolymer was expected. Furthermore, it has been shown that the production of the P(3HB) homopolymer results from the utilization of even numbered n-alkanoates as a carbon source, whereas the use of odd numbered n-alkanoates produces copolymers of 3HB and 3-hydroxyvalerate (3HV). The characterization of the polymer using FTIR, GCMS, ^1H NMR and ^{13}C NMR have confirmed the production of P(3HB) by *B. cereus* SPV. Since P(3HB) was the first PHA discovered by Lemoigne at the Institute Pasteur in 1926, it is the most extensively studied PHA. The P(3HB) biosynthetic pathway consists of three reactions catalysed by three distinct enzymes. The first reaction is the condensation of two molecules of acetyl coenzyme A (acetyl-CoA) into acetoacetyl-CoA by β -ketoacyl-CoA thiolase, which is encoded by *phbA*. The second reaction consists of the reduction of acetoacetyl-CoA to (R)-3-hydroxybutyryl-CoA by a NADPH-dependent acetoacetyl-CoA dehydrogenase, which is encoded by *phbB*. The last reaction results in the polymerization of (R)-3-hydroxybutyryl-CoA monomers into poly(3-hydroxybutyrate) by P(3HB) synthase, which is encoded by *phbC*.

In the DSC analysis, the values obtained of T_g , T_m and ΔH_f for P(3HO) and P(3HB) were similar to those reported in the literature. Rai *et al.* (2011) and Basnett *et al.* (2013) obtained a T_g for P(3HO) of $-35.81\text{ }^\circ\text{C}$ and $-30.10\text{ }^\circ\text{C}$ respectively. Similarly, the T_m for P(3HO) measured in these investigations were $39.21\text{ }^\circ\text{C}$ and $51.00\text{ }^\circ\text{C}$ with melting enthalpies of 9.77

J/g and 1.16 ± 0.3 J/g respectively. Basnett *et al.* (2013) also reported similar values of T_m (170.3 ± 0.01 °C) and ΔH_f (73.9 ± 0.1 °C) for P(3HB).

In conclusion, the culture media used for the production of both, P(3HO) and P(3HB) allowed the production of appropriate amounts of polymer for characterisation and manufacturing of scaffolds presented in the following chapters. Since PHA production is often expensive, the development of production strategies that permit high PHA productivity and yield is vital. Several methods have been performed to produce PHA at industrial level such as fed-batch and continuous cultivations (Lee, 1996; Du and Yu, 2002a; Du and Yu, 2002b; Du *et al.*, 2001b; Yu and Wang, 2001). Only four PHAs are currently produced with high productivity and yield **including** P(3HB), poly (3-hydroxybutyrate-co-3-hydroxyvalerate and poly (3-hydroxyhexanoate-co-3-hydroxyoctanoate) and P(3HO-copolymers). Also, the use of renewable and inexpensive carbon sources needs to be explored to reduce the overall cost of PHA production.

Chapter 4
Fabrication, chemical and biological
characterization of P(3HO)/P(3HB)
blend films

4 FABRICATION, CHEMICAL AND BIOLOGICAL CHARACTERIZATION OF P(3HO)/P(3HB) BLEND FILMS

4.1 INTRODUCTION

Peripheral nerve injuries (PNI) affect about 2.8% of trauma patients, many of who suffer life-long disability (Midha, 2006). Peripheral nerves are able to repair when the injuries present a gap of less than 5 mm long (Jiang *et al.*, 2010; Schmidt and Leach, 2003). For injuries resulting in nerve damage with gaps of more than 5 mm, treatment is most commonly attempted using autologous nerve graft repair (De Ruyter 2009, Babu *et al.*, 2008). When nerve damage is even more extreme and gaps exceed 3 cm, allografts, vascularized nerve grafts and nerve grafts without vessels are used (Babu *et al.*, 2008). Peripheral nerve repair using nerve autografts has several limitations including donor site morbidity, scar tissue invasion, scarcity of donor nerves, inadequate return of function and aberrant regeneration (Babu *et al.*, 2008, Huang *et al.*, 2012). Currently there are several clinically approved artificial nerve guidance conduits (NGCs) made from various biomaterials that have overcome some of the limitations of these nerve autografts. However, NGCs made from synthetic materials can trigger immune responses, induce scar tissue and can release compounds that are detrimental to the nerve regeneration process (Babu *et al.*, 2008).

During the past two decades a large variety of materials including nano-structured materials and biochemical factors have been explored in attempts to improve the quality of nerve conduits, and currently there are several commercial nerve conduits approved by U.S Food and Drug Administration (FDA) and Conformit Europe (CE) (Jiang *et al.*, 2010). All of the models currently available take the form of a simple hollow tube with a single lumen. They possess no internal substructure, are made from either synthetic or natural materials and are available in different designs and sizes (Bell and Haycock, 2012). The materials that have been used for their manufacture include poly(DL-lactide- ϵ -caprolactone) (PLCL), polyglycolic acid (PGA), polyvinyl alcohol (PVA), collagen type I (COLI) and extracellular matrix (ECM). Furthermore, a large diversity of materials have been used experimentally to produce nerve guidance conduits such as aliphatic polyesters, polylactic acids, polycaprolactones, polyurethanes, silicones, collagens, glycoproteins, polypeptides, polyhydroxyalkanoates (PHAs), polysaccharides, proteins and acellular or extracellular matrices.

PHAs have great potential as materials for use in the manufacturing of NGCs to assist axonal regeneration. Their prominent properties such as: controllable surface degradation; variability in material properties; lower acidity of degradation products and longer stability compared to their synthetic counterparts are all of special interest in this field. Currently, P(3HB) and P(3HB-co-3HHx) are the only types of PHAs that have been explored for their

use in nerve regeneration. P(3HB) conduits have been shown to repair nerve gaps of 10mm (Hart *et al.*, 2003; Hazari *et al.*, 1999; Mosahebi *et al.*, 2001; Mosahebi *et al.*, 2002; Mosahebi *et al.*, 2003) and 40mm (Mohanna *et al.*, 2005; Young *et al.*, 2002) in rat sciatic nerves and rabbit peroneal nerves respectively. Hollow P(3HB-co-3HHx) conduits have also been used to bridge 10mm defects in rat sciatic nerves (Bian *et al.*, 2009). Although these studies showed low level of inflammatory infiltration and suitable reabsorption time for nerve repair, the regeneration obtained was not statistically comparable with the regeneration obtained by using autologous nerve grafting.

The aim of this chapter was to investigate PHA blends as resorbable biomaterials for their use in the manufacture of novel NGCs. Mechanical, physical and chemical properties of P(3HO), P(3HB) and their blends were characterized. The biocompatibility of these materials with NG108-15 neuronal cells was also studied. As P(3HO) exhibits mechanical properties similar to those of the peripheral nerve and P(3HB) has been shown to be biocompatible and to have nerve regenerating properties these PHAs were chosen for evaluation as improved materials for nerve tissue engineering (Lizarraga-Valderrama *et al.*, 2015).

4.2 RESULTS

4.2.1 SCANNING ELECTRON MICROSCOPY OF PHA FILMS

Scanning electron microscopy images of the films were obtained in order to compare their surface morphology. The P(3HO) film (Fig. 4.1A) displayed the presence of pores with sizes ranging from 0.1 μ m to 5 μ m. The 75:25 P(3HO)/P(3HB) blend (Fig. 4.1B) and 25:75 P(3HO)/P(3HB) blend (Fig. 4.1D) presented smaller and less abundant pores (0.1 μ m to 3 μ m) compared to the P(3HO) film. Conversely, pores were not detected in the 50:50 P(3HO)/P(3HB) blend (Fig. 4.1C), which showed protrusions uniformly distributed on the surface. The P(3HB) film (Fig. 4.1E) displayed the smoothest and most homogenous surface without the presence of pores. It was observed that the presence of P(3HO) in the blends increased the porosity compared with the neat P(3HB) film.

4.2.2 PROFILOMETRIC SURFACE ANALYSIS

The root mean square roughness (R_q) of the films was determined using a laser profilometer. The roughness of P(3HO) and P(3HB) films were significantly different ($3.69 \pm 0.20 \mu\text{m}$ versus $2.60 \pm 0.09 \mu\text{m}$, $p < 0.05$). Although the P(3HO) film was the most porous, its roughness ($3.69 \pm 0.20 \mu\text{m}$) was not significantly different to the roughness of the 75:25 P(3HO)/P(3HB) blend, 50:50 P(3HO)/P(3HB) blend and 25:75 P(3HO)/P(3HB) blend ($4.00 \pm$

0.15 μm , $4.23 \pm 0.37 \mu\text{m}$, $4.16 \pm 0.25 \mu\text{m}$, $p > 0.05$). On the other hand, statistical analysis showed that the roughness of P(3HB) ($2.60 \pm 0.09 \mu\text{m}$) was significantly different to that of the 25:75 P(3HO)/P(3HB) blend, 50:50 P(3HO)/P(3HB) blend and 75:25 P(3HO)/P(3HB) blend ($4.00 \pm 0.15 \mu\text{m}$, $4.23 \pm 0.37 \mu\text{m}$, $4.16 \pm 0.25 \mu\text{m}$, $p < 0.05$). As expected, the neat P(3HB) film presented the lowest value of roughness, which correlated with its surface having the smoothest appearance of all the films, as can be observed in the scanning electron microscopy analysis (Fig. 4.1F). The Rq values are summarised in Table 4.1

Table 4.1 Roughness of PHA blend films

PHA blend films	Roughness Rq (μm)
P(3HO)	3.7 ± 0.2
75:25 P(3HO)/P(3HB)	4.0 ± 0.2
50:50 P(3HO)/P(3HB)	4.2 ± 0.4
25:75 P(3HO)/P(3HB)	4.2 ± 0.3
P(3HB)	2.6 ± 0.1

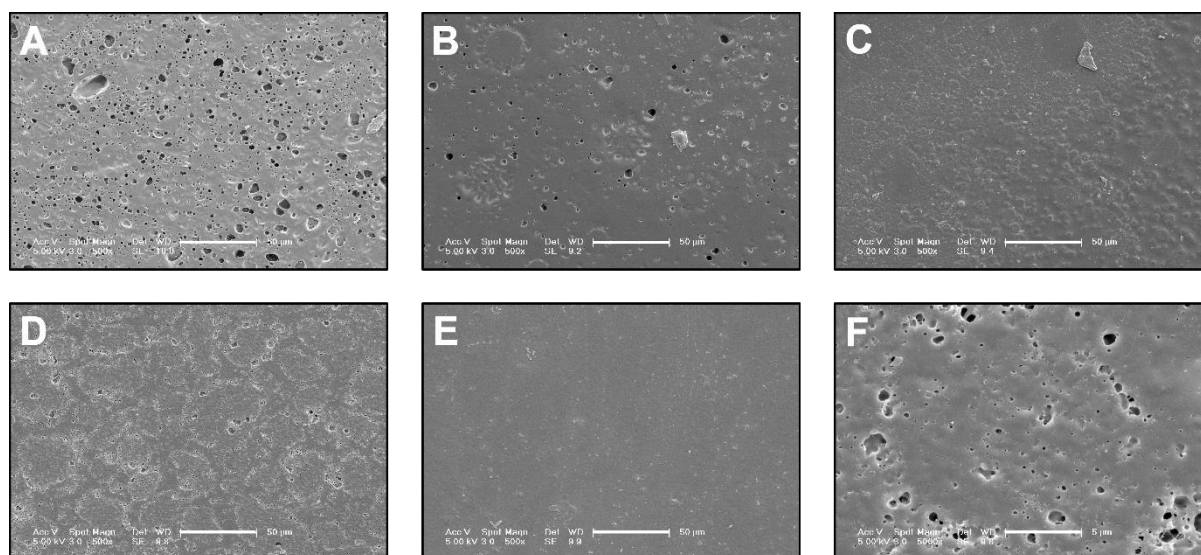


Figure 4.1. Characterization of the surface topography of P(3HO)/P(3HB) films by scanning electron microscopy analysis. (A) P(3HO); (B) 75:25 P(3HO)/P(3HB) blend; (C) 50:50 P(3HO)/P(3HB) blend; (D) 25:75 P(3HO)/P(3HB) blend, (E) P(3HB) and (F) 25:75 P(3HO)/P(3HB) blend. The films P(3HO) (A), 75:25 P(3HO)/P(3HB) blend (B) and 25:75 (D) showed porous topography whereas the P(3HB) presented smooth surface. The surface observed on the 50:50 P(3HO)/P(3HB) blend (C) presented protrusions uniformly without pores. All the figures were taken at 500X magnification excepting for Fig. F. Figure F was taken at a higher magnification (5000 X) and shows the porous structure of 25:75 P(3HO)/P(3HB) blend film.

4.2.3 X - RAY DIFFRACTION ANALYSIS

The solvent-cast films were characterised by wide-angle X-ray diffraction spectroscopy. The neat P(3HB) film exhibited two intense peaks at 2θ values of 13.5° and

16.4° (Fig. 2A). The peak positions correspond to the values obtained in previous studies of P(3HB) (Yokouchi *et al.*, 1973; Galego *et al.*, 2000) crystalline structure where they were assigned to the (020) and (110) planes of the orthorhombic unit cell. Moreover, a series of peaks were observed in the 2θ range between 18° and 34°. These peaks are most likely attributed to the crystalline lattice planes of (021), (120), (111) and (101). In contrast to neat P(3HB), the diffraction pattern of P(3HO) was characterised by the presence of a broad amorphous halo located around $2\theta=20^\circ$. However, in the P(3HO) diffractogram the amorphous halo was superposed with a series of diffraction peaks around 17°, 19° and 21°. Thus a significant fraction of the semi-crystalline P(3HO) was in the amorphous phase. X-ray diffractograms of all the blends showed intense peaks of P(3HB) (020) and (110) planes indicating that P(3HB) crystallised in the presence of P(3HO) even when the concentration of P(3HO) was 75%. However, peaks corresponding to P(3HO) crystallites were not detected in the diffractograms of the blends. Also, the weak amorphous halo was observed only in the 75:25 P(3HO)/P(3HB) blend while other blend compositions did not show the P(3HO) amorphous phase. Comparing the spectrum of pure P(3HB) with those of the blends, it was seen that peak positions corresponding to P(3HB) were constant. This indicated that the P(3HB) unit cell did not change in the blends.

4.2.4 DSC

A representative thermogram of P(3HO)/P(3HB) blends (Fig. 4.2B) shows the presence of two endothermic events with peak temperatures around 50 °C and above 150 °C corresponding to the melting temperatures (T_m) of P(3HO) and P(3HB) respectively. After erasing the thermal history and material cooling at 20°C/min, neither material, including neat P(3HO), showed the lower temperature melting event. Thus such cooling conditions do not allow crystallisation of P(3HO). The blending of these two polymers did not have any effect on the T_m of P(3HB). These PHAs have distinctive glass transition temperatures (T_g), namely -39°C and 2°C for P(3HO) and P(3HB) respectively. Blends of these polymers were characterised by the presence of two glass transition events. Similar to melting, positions of both glass transitions were not affected by the presence of the second polymer. Interestingly, cold crystallisation was observed for the blends with high P(3HO) content (50:50 and 75:25), as shown by the relatively narrow exothermal peaks between 40 to 70°C. In contrast, the cold crystallisation of neat P(3HB) and the 25:75 blend were barely detectable, they manifested as slight changes of the baseline at temperatures above 60°C lasting until the endothermic melting of the P(3HB) crystals. It appears that P(3HB) crystallises to the same degree as P(3HB) in blends with P(3HO) content up to 50%.

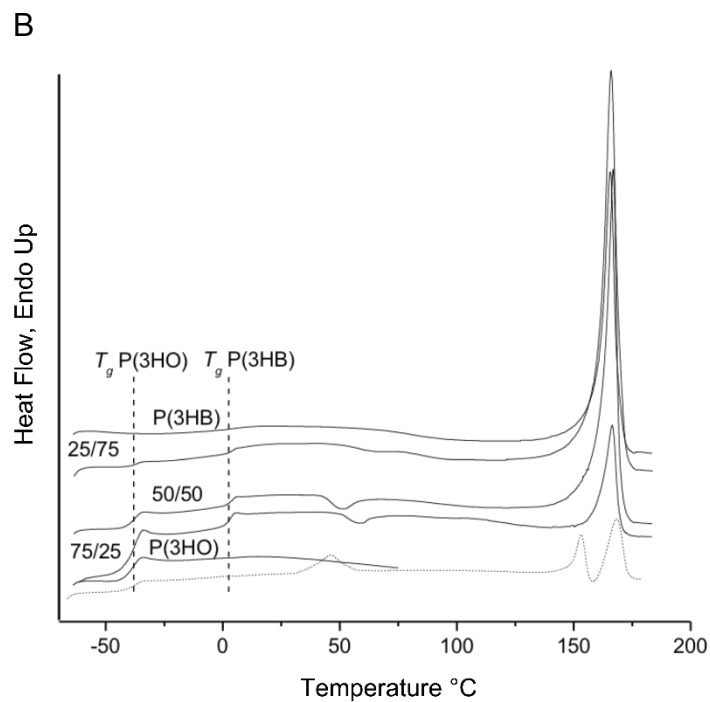
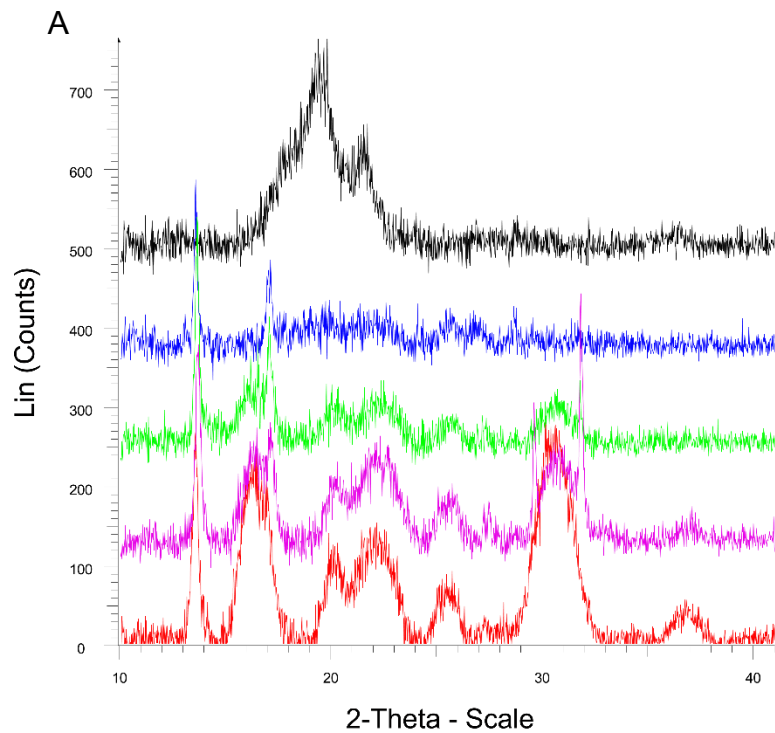


Figure 4.2. XRD spectra and DSC thermograms of neat polymers and P(3HO)/P(3HB) blends. ---- P(3HO); ---- 75:25 P(3HO)/P(3HB), ---- 50:50 P(3HO)/P(3HB), ---- 25:75P(3HO)/P(3HB), ---- P(3HB). **A)** XRD spectra of P(3HO)/P(3HB) films showing crystalline (sharp peaks) and amorphous (broad peaks) phases of the polymers. As the content of P(3HB) increased in the blend the number the peaks increased. **B)** DSC thermograms of neat polymers and their blends.

Specific enthalpy of fusion (ΔH_f) had slight fluctuations for P(3HB), 25:75 P(3HO)/P(3HB) blends, 50:50 P(3HO)/P(3HB) blends, namely 73.4, 74.4, 71.6 J/g of P(3HB) respectively. However, it significantly decreased to 28.8 J/g of P(3HB) for the 75:25 P(3HO)/P(3HB) blend.

4.2.5 FTIR

Table 4.2 summarises all the peaks observed in the FTIR spectrum of the PHA blends as seen in Figure 4.3 (Noda *et al.*, 2007; Sato *et al.*, 2004, Wu *et al.*, 2001). In the spectrum corresponding to the film made using neat P(3HO), the band corresponding to the carbonyl group was observed at 1725.45 cm^{-1} , whereas in the neat P(3HB) spectrum it was observed at 1718.99 cm^{-1} (Fig. 4.3, Table 4.2). In the 75:25 P(3HO)/P(3HB) blend, 50:50 P(3HO)/P(3HB) blend, 25:75 P(3HO)/P(3HB) blend the peak corresponding to the carbonyl group was observed at 1726.53 cm^{-1} , 1719.37 cm^{-1} and 1719.29 cm^{-1} respectively. The carbonyl group peak presented by both P(3HO) and 75:25 P(3HO)/P(3HB) blend was observed at 1725 cm^{-1} , which was characteristic of the crystalline phase of mcl-PHAs. Similarly, the C=O stretch band at around 1719 cm^{-1} observed in the spectrum corresponding to the P(3HB) film and both the 50:50 P(3HO)/P(3HB) blend and 25:75 P(3HO)/P(3HB) blend were attributed to the crystalline phase of scl-PHAs.

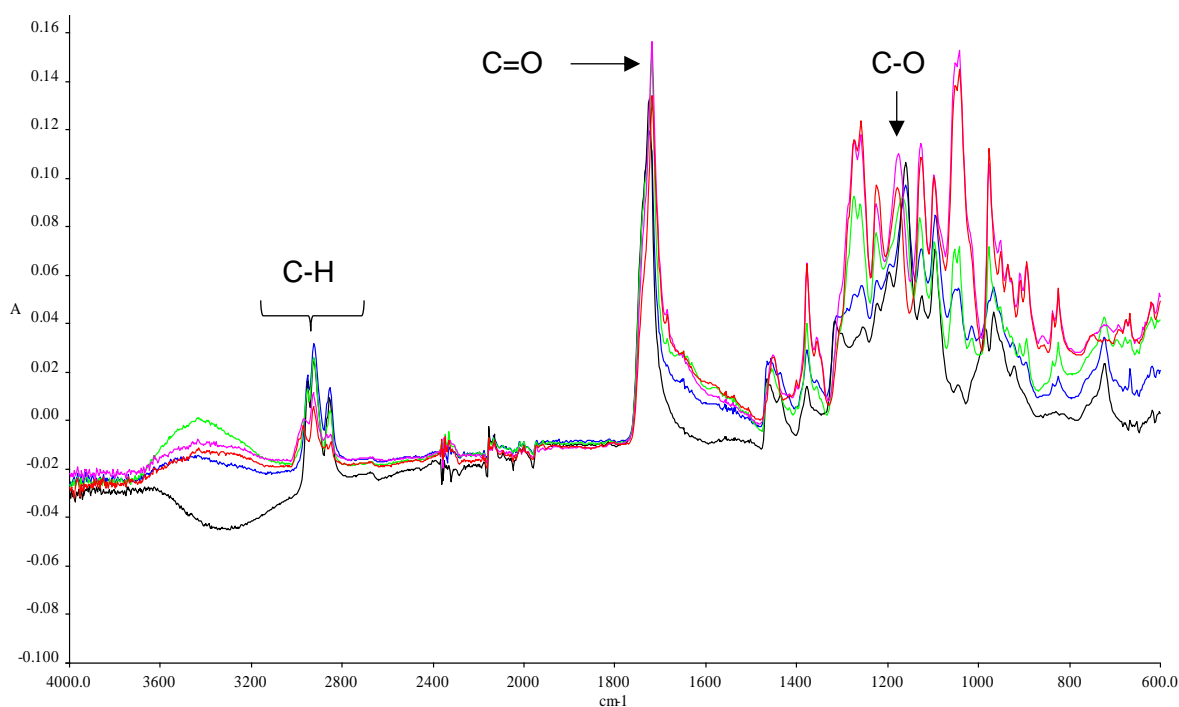


Figure 4.3 FTIR spectra of P(3HO)/P(3HB) films showing the characteristic peaks of P(3HO) and P(3HB). The FTIR spectra of the P(3HO) and 75:25 P(3HO)/P(3HB) blend showed peaks at similar wavelengths. Similarly, the films 25:75 P(3HO)/P(3HB) blend and P(3HB) presented peaks at similar wavelengths. . ---- P(3HO); ---- 75:25 P(3HO)/P(3HB), ---- 50:50 P(3HO)/P(3HB), ---- 25:75P(3HO)/P(3HB), ---- P(3HB).

In the region 1126-1317 cm^{-1} multiple bands corresponding to the C-O-C bond in the amorphous and crystalline state of the polymers were observed (Fig. 4.2, Table 4.2). The C-O-C stretch bands around 1160 cm^{-1} and 1180 cm^{-1} are the most common C-O-C fingerprints studied in the FTIR analyses of PHAs. These bands were similar for the P(3HO) (1161.12 cm^{-1}), the 75:25 P(3HO)/P(3HB) blend (1161.33 cm^{-1}) and the 50:50 P(3HO)/P(3HB) blend (1167.95 cm^{-1}). Similarly, the C-O stretch bands were also comparable for the 0:100 (1179.25 cm^{-1}) and the 25:75 (1177.57 cm^{-1}) P(3HO)/P(3HB) films. The bands around 2900 cm^{-1} correspond to the stretching vibration of the C-H aliphatic groups of the polymer backbones. As expected, these bands were stronger for P(3HO) compared with P(3HB) due to the longer aliphatic chains present in P(3HO) molecules (Fig. 4.3, Table 4).

Table 4.2 Assignments of the peaks in the FTIR spectra of the blends of P(3HO)/P(3HB)

Assignment	Wavenumbers (cm^{-1}) of P(3HO)/P(3HB) films				
	P(3HO)	75:25	50:50	25:75	P(3HB)
C-O stretching mode, ether	1043.41	1044.83	1044.31	1043.89	1043.18
	1096.72	1096.62	1098.65	1099.14	1099.11
C-O-C stretching mode, crystalline state	1126.13	1128.02	1130.47	1128.33	1127.35
C-O-C stretching mode	1161.12	1161.33	1167.95	1177.57	1179.25
C-O-C stretching mode, crystalline state	1224.61	1223.98	1226.77	1227.18	1225.86
C-O-C stretching mode, amorphous state	1250.24	1258.96	1258.84	1260.77	1260.10
C-O-C stretching mode, crystalline state	1272.12	1273.13	1275.63	1276.46	1274.32
C-O-C stretching mode, crystalline state	1296.77	1286.06	ND	ND	ND
C-O-C stretching mode, amorphous state	1317.80	1314.52	ND	ND	ND
CH ₃ symmetric deformation	1379.03	1378.82	1379.00	1378.87	1378.49
CH ₃ asymmetric deformation	1436.38	1436.09	ND	1453.50	1451.56
CH ₂ deformation	1456.66	1454.20	1457.25	ND	ND
C=O stretching mode, crystalline	1725.45	1726.53	1719.37	1719.29	1718.99
CH ₂ stretching mode	2857.84	2858.29	2855.64	2850.79	2843.94
CH ₃ symmetric stretching mode	ND	ND	ND	2871.67	2864.78
CH ₂ asymmetric stretching mode	2927.46	2928.68	2928.46	2930.67	2929.89
CH ₃ asymmetric stretching mode	2954.67	2955.19	2955.39	2965.62	2968.97

ND, band not detected in the FTIR spectrum

4.2.6 SURFACE WETTABILITY

Surface wettability of the PHA films was analyzed by measuring the water contact angle. Wettability describes the ease with which a fluid spreads or adheres across a solid surface. A high contact angle signifies low wettability, whereas a low contact angle means high wettability. When the contact angle between distilled water and the surface of a solid substrate is less than 90°, the material is said to be hydrophilic or wet. When the angle is greater than 90°, the material is said to be hydrophobic or water-repellent (Noda *et al.*, 2007). The water contact angle of the P(3HO)/P(3HB) films decreased as the content of P(3HO) decreased ((P(3HO), 103.56 ± 0.95; 75:25 P(3HO)/P(3HB), 94.41 ± 1.16; 50:50, P(3HO)/P(3HB) 84.40 ± 0.70; 25:75, P(3HO)/P(3HB) 77.36 ± 0.81; P(3HB), 69.69 ± 1.63) (Fig. 4.4). This is due to the long aliphatic chains present in P(3HO) that results in its hydrophobic character. The statistical analyses showed that the differences in water contact angle between all the P(3HO)/P(3HB) films were significant (p -value < 0.05). As the water contact angle of both the P(3HO) and the 75:25 P(3HO)/P(3HB) films were greater than 90°, they were considered to be hydrophobic in nature. In contrast, the water contact angles of the 50:50, 25:75 blend films and the P(3HB) films were less than 90° and were therefore hydrophilic in nature.

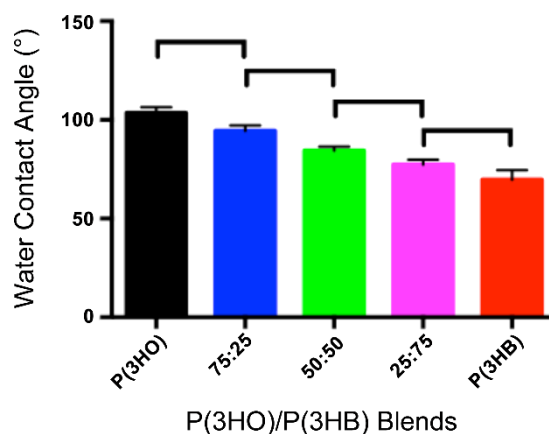


Figure 4.4 Static water contact angle of P(3HO)/P(3HB) films. The water contact increased as the content of P(3HO) increased in the blend. The water contact angle was significantly different for all the blends (mean ± SEM, $n = 9$ independent experiments, $p < 0.05$).

4.2.7 STATIC TENSILE TEST OF THE FILMS

Mechanical properties of the films were measured using the static tensile testing. Young's Modulus (E values), tensile strength and elongation at break of the different films are

shown in Table 4.3. Young's modulus, a measure of the stiffness of materials, was determined by calculating the slope of the linear region of the stress-strain curve. The tensile strength is the maximum load that a material can sustain during the test, whereas the elongation at break is the ratio between the final length before break and the initial length of the specimen. The *E* values of the blends and P(3HO) were significantly different to the *E* value of P(3HB) (*p*-value < 0.05). The tensile strength values were all significantly different when compared against each other excepting P(3HO) and the blend 75:25 P(3HO)/P(3HB) of which the difference was not significant. All the values of percentage strain were significantly different to P(3HO) percentage strain (*p*-value < 0.05). When the percentage strain values of the blends were compared against each other the only significant difference was found between the blends 50:50 P(3HO)/P(3HB) and 25:75 P(3HO)/P(3HB). When the % strain of P(3HB) was compared with the blends the only significant difference found was when compared with the 50:50 P(3HO)/P(3HB) blend. Stiffness of the blends increased when increasing the content of P(3HB) except for the 75:25 P(3HO)/P(3HB) blend. On the other hand, the pliability of the blends decreased with increase in the P(3HB) content.

Table 4.3 Mechanical analysis of the P(3HO)/P(3HB) films

P(3HO)/P(3HB) Films	<i>E</i> (MPa)	Tensile strength (MPa)	Percentage strain
100:0	1.9 ± 0.1	4.9 ± 0.3	286.4 ± 18.5
75:25	1.2 ± 0.2	0.7 ± 0.1	73.8 ± 18.1
50:50	21.8 ± 0.9	2.2 ± 0.9	94.2 ± 3.5
25:75	143.4 ± 2.1	17.8 ± 0.8	41.3 ± 1.7
0:100	1160.0 ± 185.9	28.60 ± 1.8	9.6 ± 2.6

4.2.8 LIVE/DEAD MEASUREMENT OF NG-108-15 NEURONAL CELLS

A live/dead cell measurement was conducted in order to compare the attachment and survival of NG-108-15 neuronal cells on the P(3HO)/P(3HB) films using PCL and glass as controls. Figure 4.5 shows representative confocal images of the cells grown on different substrates. Images (C) and (D) correspond to the 50:50 and 25:75 P(3HO)/P(3HB) blends respectively and displayed the highest density of cells compared with the other images.

The percentage of live cells grown on P(3HO), 75:25 P(3HO)/P(3HB) blend, 50:50 P(3HO)/P(3HB) blend, 25:75 P(3HO)/P(3HB) blend and P(3HB) films was 80.54 ± 6.26%, 89.73 ± 3.68 %, 95.12 ± 1.02 %, 95.59 ± 1.23 %, 88.40 ± 2.99 % and on PCL was 89.29 ±

3.06 % (Fig. 4.5 G). This was higher when compared with the glass substrate ($62.68 \pm 3.15\%$) (Fig 4.5 G).

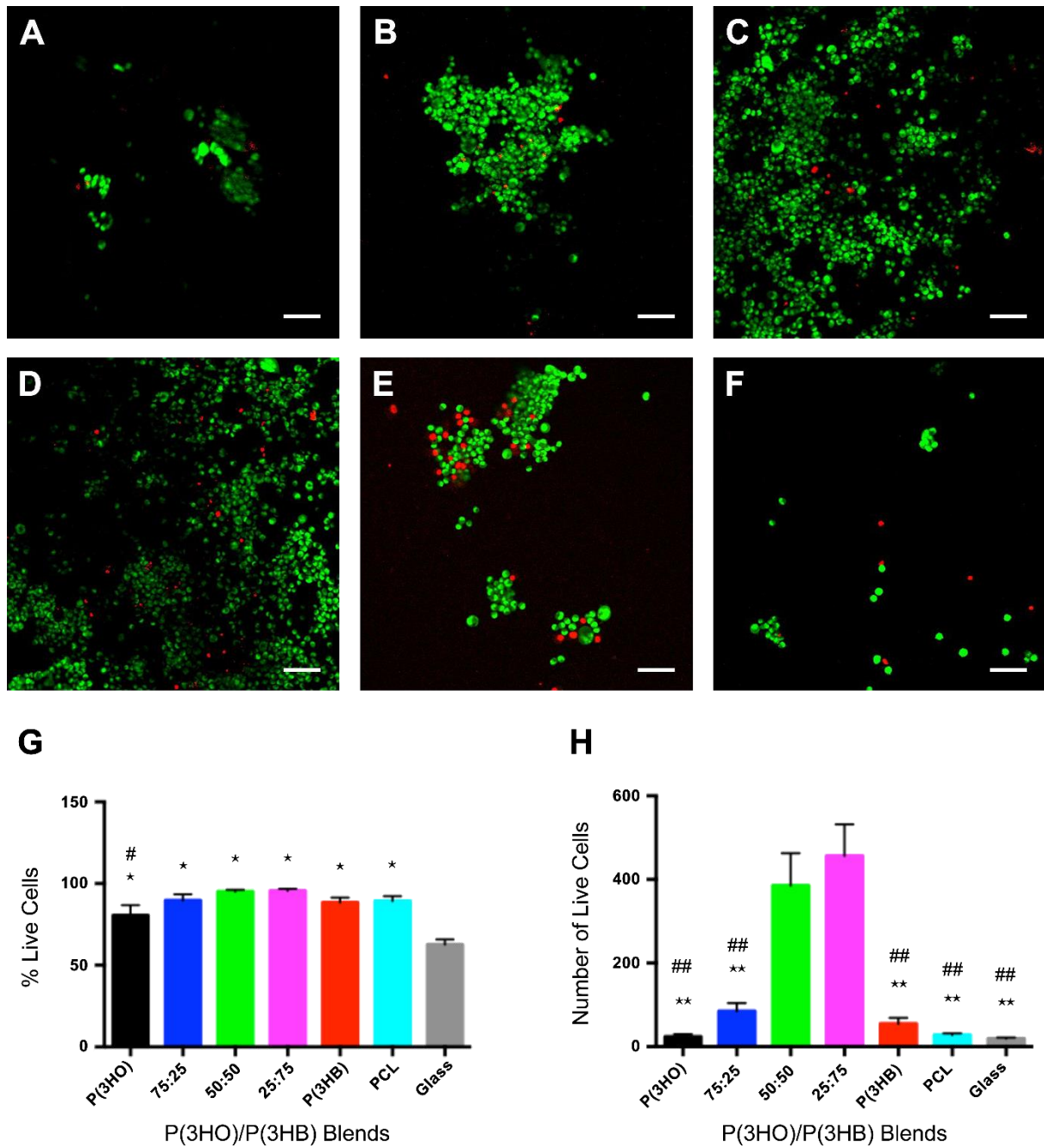


Figure 4.5 Confocal micrographs of NG108-15 neuronal cells labelled with propidium iodide (red) and Syto-9 (green) after four days in culture on P(3HO)/P(3HB) films and PCL. (A) P(3HO); (B) 75:25; (C) 50:50; (D) 25:75; (E) P(3HB) and (F) PCL. Cell growth was randomly oriented on each of the flat substrates. (G) Live/dead analysis of neuronal cells on the P(3HO)/P(3HB) blends, PCL and glass (control). (H) Number of live cells on the P(3HO)/P(3HB) blends, PCL and glass (control). (mean \pm SEM, $n = 9$ independent experiments $P < 0.05$).

Statistical analysis showed that the difference in the percentage of live cells was significant for all the substrates including PCL when compared with that of glass ($p < 0.05$). The difference in the percentage of live cells between the 75:25 P(3HO)/P(3HB), 50:50 P(3HO)/P(3HB), 25:75 P(3HO)/P(3HB) and PCL substrates was not significant ($p > 0.05$). The only significant difference in the percentage of live cells found between the substrates was when the P(3HB) ($80.54 \pm 6.26\%$) and the 25:75 blend ($95.59 \pm 1.23\%$) were compared ($p < 0.05$) (Fig 4.5 G). Hence, the percentage of live cells obtained using the 25:75 P(3HO)/P(3HB) film was significantly higher than that obtained on P(3HB). Figure 4.5 H shows the average number of cells on the different substrates. The 50:50 P(3HO)/P(3HB) blend and 25:75 P(3HO)/P(3HB) blend were associated with the highest number of adhered neuronal cells per view (385.11 ± 77.69 cells and 456.00 ± 75.67 cells respectively).

No significant differences were found in the number of adhered neuronal cells on 50:50 P(3HO)/P(3HB) and 25:75 P(3HO)/P(3HB) polymer blends. Statistical analysis demonstrated that the number of cells on the 50:50 P(3HO)/P(3HB) and 25:75 P(3HO)/P(3HB) was significantly higher than the other substrates, including PCL and glass. The difference in the number of live cells found between P(3HO), 75:25 P(3HO)/P(3HB) blend, P(3HB), PCL and glass substrates was not significant (23.78 ± 5.96 , 84.56 ± 19.92 , 54.22 ± 14.04 , 27.78 ± 4.07 , 19.00 ± 2.52).

4.2.9 NEURITE OUTGROWTH ASSESSMENT

NG108-15 neuronal cells were immunolabelled with the anti- β III-tubulin antibody to assess neurite outgrowth on the substrates (Figure 4.6). The protein β -III-tubulin is considered a neuron-specific marker as this molecule is expressed in neuronal cell bodies, dendrites, axons and axonal terminations. Therefore, this protein is widely used as an indicator of neuronal cell differentiation. Figure 4.6 (A-F) shows the confocal images of neuronal cells grown on each of the substrates, where neurite outgrowth could be clearly observed. However, two important characteristics of neuronal cells grown on the 25:75 P(3HO)/P(3HB) blend, P(3HB) and PCL films were both the presence of several neurite-bearing neurons and the appearance of longer neurites as compared with those cells grown on the P(3HO), 25:75 and 50:50 P(3HO)/P(3HB) blends.

Figure 4.6 G shows the percentage of cells with neurites on each substrate. Statistical analysis showed no significant difference in the percentage of cells with neurites for the P(3HO) ($91.42 \pm 2.99\%$), 25:75 P(3HO)/P(3HB) blend ($80.90 \pm 11.39\%$), 50:50 P(3HO)/P(3HB) blend ($86.15 \pm 5.76\%$), 25:75 P(3HO)/P(3HB) blend ($99.30 \pm 0.40\%$), P(3HB) (97.98 ± 0.73), PCL (97.00 ± 1.30) and glass (81.85 ± 9.64), ($p < 0.05$). Fig. 6H, shows the number of cells with neurites in the different substrates.

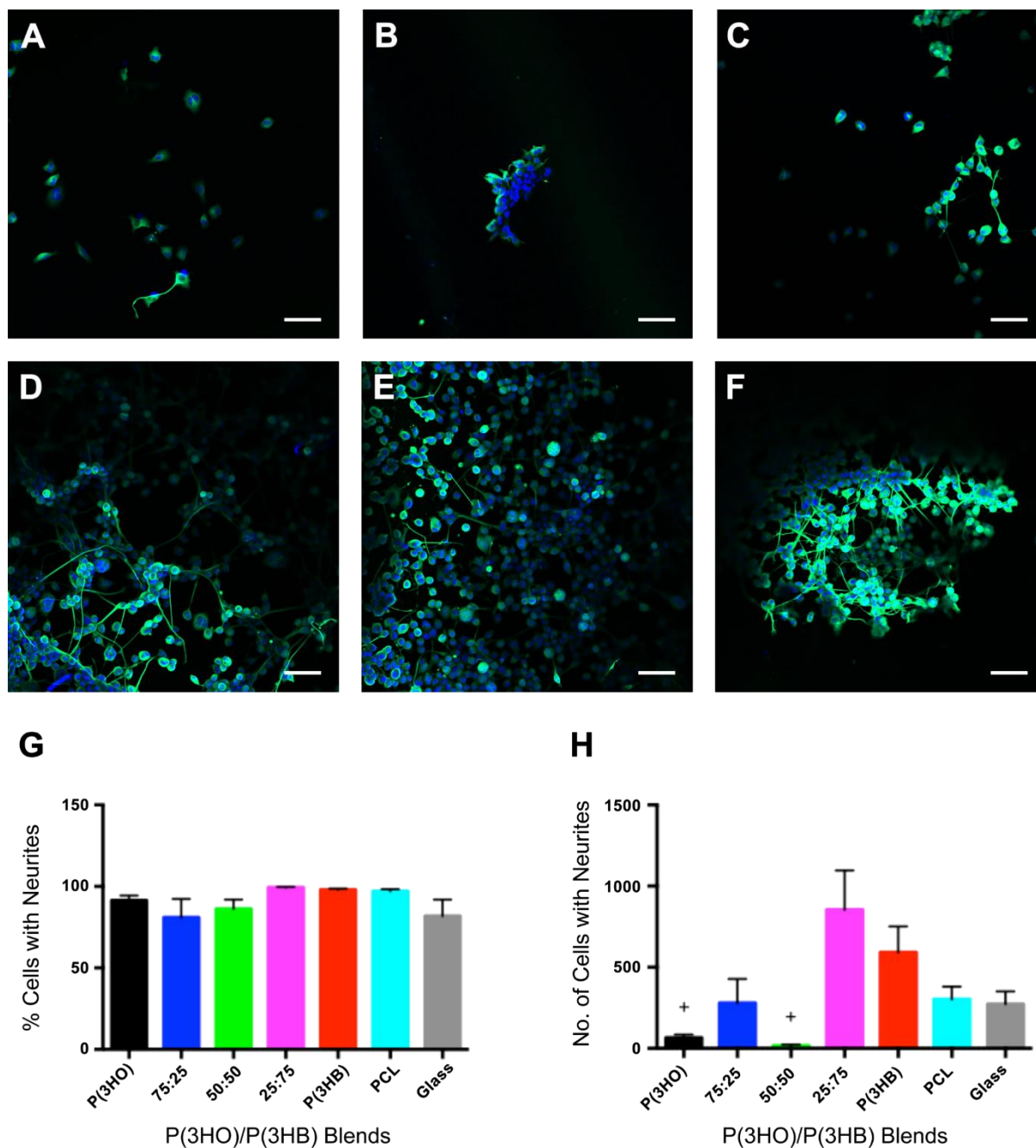


Figure 4.6 Confocal micrographs of NG108-15 neuronal cells immunolabelled for beta-III tubulin after four days in culture on P(3HO)/P(3HB) films and PCL. (A) P(3HO); (B) 75:25 P(3HO)/P(3HB) blend; (C) 50:50 P(3HO)/P(3HB) blend; (D) 25:75 P(3HO)/P(3HB) blend; and (E) P(3HB) and (F) PCL. Neurite outgrowth was randomly oriented on each of the flat substrates. (G) Percentage of cell with neurites on the P(3HO)/P(3HB) blends, PCL and glass (control). Percentage of neurites on all the blends, PCL and glass was similar (mean \pm SEM, $n = 6$ independent experiments, $P < 0.05$). (H) Number of cells with neurites on the P(3HO)/P(3HB) blends, PCL and glass (control). The number of cells with neurites on P(3HO) and 50:50 was lower in comparison to 25:75 blend (mean \pm SEM, $n = 6$ independent experiments, $+P < 0.05$).

There was no significant difference in the number of cells with neurites on PCL (303.00 ± 77.94), glass (273.00 ± 77.94), 75:25 (280.00 ± 147.31), 25:75 (854.00 ± 243.02) and

P(3HB) (591.00 ± 159.34) ($p < 0.05$). However, the number of cells with neurites on 25:75 P(3HO)/P(3HB) blend was significantly higher compared to the P(3HO) and 50:50 P(3HO)/P(3HB) blend ($p < 0.05$).

4.3 DISCUSSION

The presence of two glass transitions and melting events in P(3HO)/P(3HB) blends, which occurs at the same temperatures as neat polymers (Fig. 4.2B) indicates that the PHAs used in this study were immiscible in both amorphous and crystalline phase. The independence of specific enthalpy of fusion of P(3HB) for blends with P(3HO) content up to 50% indicated that P(3HB) crystallises as a separate phase in the presence of P(3HO). Although the aged blends show melting of P(3HO) crystals, the crystallisation was slower than P(3HB) and occurred when crystallisation of the main part of P(3HB) was complete. Apparently the presence of mcl-PHAs, a polymer with lower glass transition temperature, accelerates the kinetics of P(3HB) crystallisation. This was observed in the P(3HB) non-isothermal crystallisation, which was characterised by cold crystallisation for blends containing up to 50% of P(3HO). This influence of mcl-PHA on the crystallisation of P(3HB) could be due to the increase of polymer chain mobility in the system containing polymer in a rubbery state. However, in the 75:25 blend, crystallisation of P(3HB) was significantly suppressed.

Crystallisation of P(3HB) was also confirmed by XRD. Although intensities of the peaks in the diffractograms of P(3HO)/P(3HB) blends decreased with the increase of P(3HO) content, their positions were essentially the same as the peaks on the diffractogram of P(3HB). The peaks characteristic for P(3HO) were not detectable even in the blend with the highest P(3HO) content. That might imply that P(3HO) co-crystallised with P(3HB). However, considering that the DSC experiments showed two separate melting events exactly matching the melting temperatures of the neat polymers, it is unlikely that these two PHAs could co-crystallise. One might suggest that crystallites of P(3HO) do not develop sufficiently in the blends in order to be detectable in XRD.

The surface of the P(3HB) film was found to be smooth whereas the surface of the P(3HO) film was porous. The smooth surface observed in P(3HB) film was similar to that characterized by Wang *et al.* (2012), where the degradation of P(3HB) by polyhydroxybutyrate depolymerase was investigated (Sato *et al.*, 2004). Conversely, this smooth appearance contrasts with the porous morphology of a P(3HB) film characterised by Kai *et al.* (2003) in their study of P(3HB-co-3HH)/P(3HB) blends (Wu *et al.*, 2001). Although the surfaces of P(3HO) films have shown to be smooth and non-porous in previous studies (Rai *et al.*, 2011;

Capitan *et al.*, 2004) it is worth to highlight that there is a lack of information available relating to the characterisation of P(3HO) for comparison.

The smooth appearance shown in the SEM images of P(3HB) film was in accordance with the profilometric analysis in which this film presented the lowest root mean square roughness. The higher Rq values of P(3HO) compared to that of P(3HB) might be attributed to its porous surface. The higher Rq values of the 75:25, 50:50 and 25:75 P(3HO)/P(3HB) blend films compared to the P(3HO) and P(3HB) film corroborated the phase separation process detected in the blend films by DSC analysis. Furthermore, it has been shown that when smooth blend films are produced using a wide compositional range, the polymers have a high level of compatibility (Förch *et al.*, 2009, pp 471). Most of the Rq values of P(3HO) and P(3HB) films found in the available literature have been obtained using atomic force microscopy (AFM) and not by profilometric analysis. As it has been found that there is a discrepancy in the resultant Rq values between these two techniques, comparison with these values were not feasible (Poon and Bhushan, 1995).

It has been shown that the forces affecting the wettability in a solid substrate are the surface tension of the substrate, the surface tension of the liquid and the interfacial tension. The hydrophobicity of blend materials can change due to compositional variations and the arrangement of polymer molecules in surface layers. When polymer films are formed from polymer solutions the solution interface is exposed to the hydrophobic air environment. Thus, polymeric molecules in the surface may re-orientate their hydrophobic groups towards the surface of the material, resulting in a less wettable surface. The neat P(3HO) film was the most hydrophobic polymer. This polymer has a longer aliphatic chain per monomer unit with four more methyl groups compared with P(3HB). These methyl groups may have rotated towards the hydrophobic interface through chain rotation. This orientation is more favourable energetically and decreases the surface free energy (Kai *et al.*, 2003). Therefore, the observed decrease in the wettability of the films as the P(3HO) content increased demonstrated that higher number of hydrophobic chains were present on the films.

The Young's modulus, tensile strength and elongation at break values obtained for the P(3HO) and 50:50 blend differed slightly from the mechanical properties determined for similar films previously examined (Capitan *et al.*, 2004). The higher Young's modulus values obtained in this study for the P(3HO) and 50:50 blend could be the result of variations in the molecular weight of the polymers. It has been shown that lower molecular weights of the same polymer increase Young's modulus and tensile strength values (Al-Nasassrah *et al.*, 1998). Therefore, these results suggest that the molecular weight of the P(3HO) used in this study could be higher than that used by Basnett *et al.* (2013). It is well known that cultivation conditions can affect the molecular weight of PHAs. Tomizawa *et al.* (2011) and Agus *et al.* (2012) showed

that the molecular weight of P(3HB) decreased with an increase in culture time and temperature (Gutmann *et al.*, 2000; Poon *et al.*, 1995). The mechanical properties of P(3HB) obtained in this study agreed with values obtained in similar studies (Misra *et al.*, 2006).

The Young's modulus of the 75:25 P(3HO)/P(3HB) blend (1.25 ± 0.18 MPa) and the tensile strength (0.71 ± 0.08 MPa) were most similar to that of peripheral nerves in rats (0.58 MPa \pm 0.16 MPa and 1.4 ± 0.29 MPa respectively). However, the 25:75 P(3HO)/P(3HB) blend displayed similar percentage of strain (41.30 ± 1.73 %) to that of peripheral nerve in the same study (48 ± 11.7 %) (Borschel *et al.*, 2003). It is important to notice that the mechanical properties of nerves vary depending on the nature of the peripheral nerve being considered and the species from which the nerve was taken. In another study, the tensile strength and elongation at break of rabbit peroneal nerve were 11.7 ± 0.7 MPa and 38.5 ± 2 % respectively, which are similar to those of the 25:75 P(3HO)/P(3HB) blend (17.80 ± 0.80 MPa and 41.30 ± 1.73 % respectively) (Al-Nasassrah *et al.*, 1998). Therefore, PHA-based blends could provide the appropriate strength and elasticity that NGCs require for adequate flexibility at the site of implantation.

The superior biocompatibility displayed in the 50:50 and 25:75 P(3HO)/P(3HB) blends could be attributed to the higher roughness values featured in these films and their lower hydrophobicity compared to P(3HO) and 75:25 P(3HO)/P(3HB) films. It is well known that cell attachment is enhanced by the roughness, porosity and hydrophilicity. However, in the neurite outgrowth test, the 50:50 blend exhibited a low number of cells with neurites compared with the 25:75 P(3HO)/P(3HB) blend, which supported the highest number of cells containing neurites. Therefore, these findings indicate that the 25:75 P(3HO)/P(3HB) blend supported the growth and differentiation of NG108-15 neuronal cells significantly better than the other blends and neat polymers. Biocompatibility studies of NG108-15 neuronal cells with polyhydroxyalkanoates have only been previously performed on P(3HB) substrates. P(3HB) has demonstrated high biocompatibility not only with NG108-15 neuronal cells (Al-Nasassrah *et al.*, 1998) but also with neuronal cells in animal models (Hart *et al.*, 2003; Hazari *et al.*, 1999; Mosahebi *et al.*, 2001; Mosahebi *et al.*, 2002; Mosahebi *et al.*, 2003; Mohanna *et al.*, 2005; Young *et al.*, 2002. Armstrong *et al.* (2007) have used NGCs made from P(3HB) as a substrate to investigate the effect of Schwann cells (SC) on neurite outgrowth from NG108-15 neuronal cells showing good compatibility with both cell types (Armstrong *et al.*, 2007).

The growth of NG108-15 neuronal cells was characterized by their irregular growth in various layers on all substrates showing a random migration of cells. Neuronal migration is highly dependent on the expression of cell adhesion proteins, which can also be involved in neuronal differentiation. In neuronal cells, including NG108-15, different families of proteins regulate cell-cell and cell-substrate interactions: the Efh family, α - β -hydrolase fold family, and

three families of cell adhesion molecules (CAMs); the immunoglobulin (Ig) superfamily CAMs, cadherins and integrins (Binns *et al.*, 2000, De Jaco *et al.*, 2006, Tojima *et al.*, 2000, Charness *et al.*, 1994, Hynes *et al.*, 1992, Hynes *et al.*, 2002). It has been shown that cell adhesion to polymeric surfaces such as PHA films is mediated mainly by integrins through the interactions between proteins and the polymers (Lee *et al.*, 2004; Cargill *et al.*, 1999). Proteins coming from the serum, the surrounding medium or those produced by the cells could be adsorbed into the surface of the films and recognized by integrins through the Arg-Gly-Asp (RGD) sequence which is present in a considerable number of proteins.

In summary, although all of the P(3HO)/P(3HB) blends and P(3HO) were able to support neuronal growth, the 25:75 P(3HO)/P(3HB) and P(3HB) films supported better neurite extension. Although both 75:25 P(3HO)/P(3HB) and 25:75 P(3HO)/P(3HB) blends presented suitable tensile strength and elongation at break for their application in peripheral nerve repair, the 25:75 P(3HO)/P(3HB) blend displayed the highest biocompatibility among all the substrates.

Chapter 5
Fabrication, chemical and biological
characterization of electrospun fibres
using P(3HO)/P(3HB) blends

5 FABRICATION, CHEMICAL AND BIOLOGICAL CHARACTERIZATION OF ELECTROSPUN FIBRES USING P(3HO)/P(3HB) BLENDS

5.1 INTRODUCTION

Engineered scaffolds are designed to closely mimic the topography, spatial distribution and chemical cues corresponding to the native extracellular matrix (ECM) of the intended tissue in order to support cell growth and differentiation. In tissue engineering both three-dimensional and two-dimensional cell cultures are used. Porous scaffolds provide adhesion sites; facilitate mass transfer, spatial control and exchange of nutrients, metabolites and gases. Although the use of scaffolds with co-cultures in three-dimensional cultures have been widely applied to regenerate a broad variety of tissues, these techniques have been scarcely used in nerve tissue regeneration. Three dimensional culture techniques would not only allow a better understanding of neurons-glia cells communication but also could contribute to the development of scaffolds for peripheral nerve regeneration (Daud *et al.*, 2012).

The use of nerve guidance conduits (NGCs) to re-connect peripheral nerve gaps has been extensively investigated in the last 20 years. Notable efforts have been made to overcome the limitations of using the standard treatment, autografting, including donor site morbidity, scar tissue formation, scarcity of donor nerves, inadequate return of function and aberrant regeneration. Although some NGCs made from natural and synthetic materials have been clinically approved, the regeneration obtained with them is only comparable with that using autologous grafts when the gaps are short (5 mm). Commercial NGCs are all hollow tubes and can induce scar tissue and release compounds that are detrimental for the nerve regeneration process. Several research groups have investigated the use of lumen structures to improve neuronal regeneration such as luminal filaments, fibres and multichannel structures (de Ruyter *et al.* 2009; Jiang *et al.*, 2010).

Schwann cells are the glial cells of the peripheral nervous system. They wrap layers of myelin membrane around axons to insulate them, permitting impulse conduction (Fields and Stevens-Graham, 2002). It is well-known that a two-way communication between neurons and glial cells is crucial for normal functioning of the nervous system. Axonal conduction, synaptic transmission and information processing are controlled by neurons-glia cells interaction (Fields and Stevens-Graham, 2002). Neurons and glia communicate through cell adhesion molecules, neurotransmitters, ion fluxes and specialized signaling molecules whereas glial cells rely on intracellular waves of calcium and intracellular diffusion of chemical messengers (Fields and Stevens-Graham, 2002).

As the design of scaffolds should reproduce the tissue of interest, the native environment of neurons must be taken into consideration (Haycock, 2011). Although tissue

engineered scaffolds may not exactly reproduce the target tissue, they have shown to provide a “nucleation structure” that triggers cellular self-organization (Sun *et al.*, 2006). In tissue engineering the main approach is to generate this “nucleating environment” in which 3D structures contain enough information for permitting cellular adhesion, proliferation and differentiation, so then the scaffold can become a mature and functioning construct (Haycock, 2011). In nature, axons are surrounded by uniaxial aligned lipoprotein sheaths of myelin. (Haycock, 2011). For this reason, majority of the scaffolds used in nerve tissue engineering consist of 3D structures based on aligned fibres. Electrospinning is a versatile manufacturing method used to produce random or aligned fibres with either nano- or micro-scale diameters using a vast diversity of materials. Therefore, electrospinning is an ideal technique to reproduce aligned fibres to mimic the extracellular matrix environment of neuronal cells and serve as a nucleating environment. Additionally, this technique is used to produce fibrous structures with random distribution characteristic of the native ECM fibres found in the majority of tissues such as breast, liver, bladder and lung, etc. (Cai *et al.*, 2013)

It has been shown that hollow NGCs are able to bridge nerve stumps resulting from severed nerves when the gaps are less than 10 mm by permitting the formation of a fibrin cable. This fibrin cable supports the migration of Schwann cells permitting the recreation of longitudinally oriented bands of Büngner, which are aligned columns of Schwann cells and laminin. In this way, bands of Büngner serve not only as a source of neurotrophic factors but also as a guiding substrate that promotes axonal regrowth (Kim *et al.*, 2008).

In vitro cells have shown to respond differently to diverse topographic scales, eg., nano-, micro- and macro scales (Sun *et al.*, 2006). Changes in the topography of a substrate can alter the biological behavior due to different sensitivity scales of cells as a consequence of the variability in cell sizes, cell matrix and filopodia (Sun *et al.*, 2006). Several studies have demonstrated that aligned electrospun fibres can provide contact guidance to cultured cells, particularly leading to the elongation and alignment of cells along the axes of fibres. It has been found that the resulting elongation along the fibres emulate the structure of bands of Büngner (Chew *et al.*, 2007). Furthermore, it has been shown that aligned fibres are able to induce orientation of focal adhesion contacts and the cell actin cytoskeleton through contact guidance (Badami *et al.*, 2006).

A wide diversity of biodegradable materials have been used for the manufacturing of scaffolds for nerve tissue engineering applications. Fibres of both, synthetic polymers (aliphatic polyesters, polylactic acids and polycaprolactones) and natural polymers (gelatin and silk) have been already used as lumen modifications of NGCs. The use of biodegradable polymers for the manufacture of implants avoid second surgeries after implantation. After the implant is sutured at the nerve stumps, the scaffold is populated and remodeled by neuronal

cells and eventually replaced by native tissue, hence the original function might be restored. Although PHAs, in particular P(3HB) have also been investigated for peripheral nerve regeneration applications (Hart *et al.*, 2003; Hazari *et al.*, 1999; Mosahebi *et al.*, 2001; Mosahebi *et al.*, 2002; Mosahebi *et al.*, 2003; Mohanna *et al.*, 2005; Yong *et al.*, 2002), studies have focused on the fabrication of hollow NGCs without lumen modifications.

The aim of this chapter was to investigate 25:75 P(3HO)/P(3HB) blend electrospun fibres as resorbable scaffolds for their use in the manufacture of NGCs. The biocompatibility of these fibres with NG108-15 neuronal cells as well as the influence of RN22 cells on their growth and differentiation was studied. As the 25:75 P(3HO)/P(3HB) blend has been shown to be biocompatible to neuronal cells in a previous study (Lizarraga-Valderrama *et al.*, 2015, Chapter 4), this PHA blend was chosen for evaluation as lumen modifiers for NGC manufacturing. These biodegradable polymers would permit the manufacture of a functioning implant containing a temporary biodegradable scaffold. Furthermore, the biodegradation products resulting from the breakdown of P(3HO) and P(3HB) have shown minimal toxicity and immunogenic response in animal models.

5.2 RESULTS

5.2.1 FABRICATION OF ALIGNED P(3HO)/P(3HB) BLEND MICROFIBRES BY USING ELECTROSPINNING. OPTIMIZATION OF VARYING P(3HO)/P(3HB) BLENDS SOLUTION CONCENTRATION FOR ELECTROSPINNING ALIGNED MICROFIBRES

In this preliminary stage, different proportions and concentrations of P(3HO) and P(3HB) were used to determine the optimal concentration required to obtain varying fibre diameters for application in nerve tissue engineering. Polymer concentrations of 5% (w/v) and 10% (w/v) were studied for microfibre manufacturing using the neat polymers P(3HO) and P(3HB) along with three different P(3HO)/P(3HB) blends; 75:25, 50:50 and 25:75 P(3HO)/P(3HB) (Table 5.1). Two different applied voltages were used (12kV and 18 kV) combined with three rotator speeds (2000, 1500 and 1000 rpm) whereas the other electrospinning conditions such as flow rate, needle-to-collector distance and needle diameter were kept constant.

For 5 % (w/v) P(3HO)/P(3HB) blend concentration, no fibre formation was observed (Fig. 5.1) in any of the P(3HO)/P(3HB) blends for any of the different electrospinning conditions applied. Instead of fibres, clusters of polymer beads were formed (Fig. 5.1).

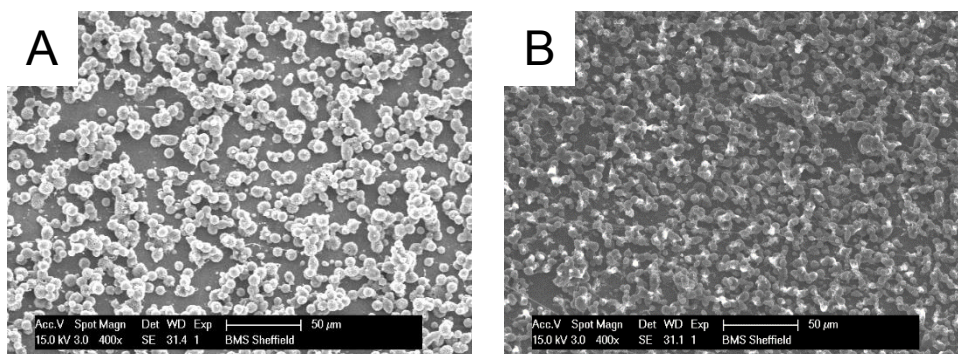


Figure 5.1. Bead formation made using 5% (w/v) 25:75 P(3HO/P3HB) blend. A) Beads made from 5% w/v 25:75 P(3HO/P3HB) blend using a voltage of 12kV and 1000 rpm. B) Beads made from 5% w/v 25:75 P(3HO/P3HB) blend using a voltage of 18kV and 1500 rpm. No fibre formation was observed by using 5% (w/v) 25:75 P(3HO/P3HB) blend under varying electrospinning conditions. Under both conditions similar beads were obtained instead of fibres.

For 10 % (w/v) P(3HO)/P(3HB) blend concentration, fibres of varying diameters were obtained (Table 5.1). When 10% (w/v) neat P(3HO) was electrospun, only fibres were obtained when the voltage was 12kV (Fig. 5.2. A-C, table 5.1). Although the fibres obtained were aligned, they all contained beads under the three different rotator speeds (1000, 1500 and 2000 rpm) (Fig.5.2, A, B and C respectively). Increment in the fibre diameter was observed when the rotator speed was decreased to 0.81 ± 0.24 ; 2.34 ± 0.67 ; $2.36 \pm 1.24 \mu\text{m}$ for 2000, 1500, 1000 rpm respectively.

Table 5.1 Summary of electrospinning parameters used to determine the optimal conditions for the manufacture of aligned blend fibres using 10% w/v of polymer blends.

% Polymer (w/v)	Voltage (kV)	Flow rate (ml/h)	Rotator speed (rpm)	Diameter of P(3HO)/P(3HB) fibres (μm)				
				100:0	75:25	50:50	25:75	0:100
10	12	1	2000	0.8 ± 0.2	0.3 ± 0.1	0.1 ± 0.1	1.2 ± 0.2	1.0 ± 0.1
10	12	1	1500	2.3 ± 0.7	0.4 ± 0.1	0.5 ± 0.1	1.5 ± 0.4	5.4 ± 1.9
10	12	1	1000	2.4 ± 1.2	0.5 ± 0.1	1.0 ± 0.2	2.5 ± 1.2	2.2 ± 1.8
10	18	1	2000	NF	0.3 ± 0.0	0.9 ± 0.1	1.5 ± 0.7	2.2 ± 1.8
10	18	1	1500	NF	0.4 ± 0.1	1.1 ± 0.1	1.7 ± 0.5	1.4 ± 0.4
10	18	1	1000	NF	0.5 ± 0.2	1.3 ± 0.4	2.8 ± 0.4	3.4 ± 0.9

NF: no fibres formation

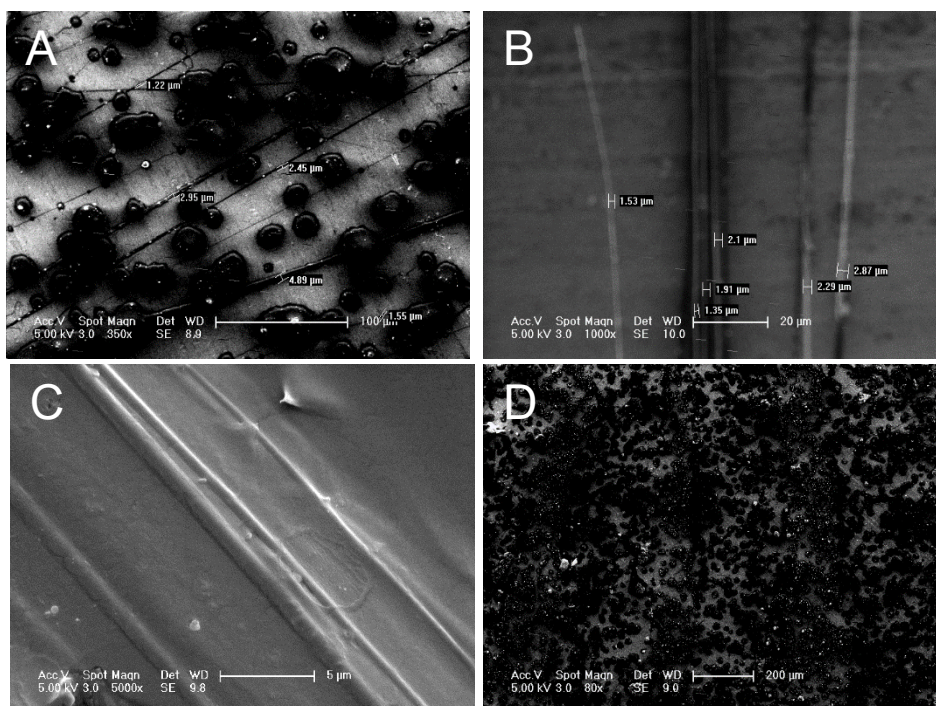


Figure 5.2. Electrospun fibres of neat P(3HO) 10 % (w/v). A) Neat P(3HO) 10% w/v fibres using 12 kV and 1000 rpm. The fibre diameter was $2.36 \pm 1.24 \mu\text{m}$ and polymer beads were observed B) Neat P(3HO) 10% w/v fibres using 12 kV and 1500 rpm. The measured fibre diameter was higher ($2.34 \pm 0.67 \mu\text{m}$) when compared with fibres shown in Fig. 5.2.A. C) Neat P(3HO) 10% w/v fibres using 12 kV and 2000 rpm. The fibres obtained were aligned ($2.36 \pm 1.24 \mu\text{m}$) and less beads were observed compared to Fig.5.2. A and Fig.5.2.B. D) Neat P(3HO) (10% w/v) beads using 18 kV and 1500 rpm.

For the 10% (w/v) 75:25 P(3HO)/P(3HB) blend, fibres were obtained for all voltages and rotator speeds. The fibre diameters increased when the rotator speed decreased for both voltages (12kV and 18kV). When the voltage applied was 12kV fibre diameters of 0.31 ± 0.06 , 0.44 ± 0.08 and $0.50 \pm 0.10 \mu\text{m}$ were obtained for rotator speeds of 2000 (Fig. 5.3.A,B), 1500 and 1000 rpm respectively. Similarly, when the voltage applied was 18kV fibre diameters of 0.35 ± 0.04 , 0.45 ± 0.05 , $0.47 \pm 0.25 \mu\text{m}$ were obtained for rotator speeds of 2000, 1500 and 1000 rpm (Fig.5.3.C,D) respectively. All the fibres obtained under these electrospinning conditions had random distribution and contained beads and polymer crystals.

When the polymeric solution of 10% (w/v) 50:50 P(3HO)/P(3HB) blend was electrospun, fibres with varying diameters were also obtained for each combination of voltages and rotator speeds. When the voltage applied was 12kV, no trend was detected in the fibre diameter. For this voltage fibre diameters of 0.89 ± 0.09 , 0.46 ± 0.10 and $1.01 \pm 0.21 \mu\text{m}$ were obtained when the rotator speeds were 2000, 1500 and 1000 rpm (Table 5.1, Fig. 5.4.A,B). When the voltage applied was 18 kV, the fibre diameters increased when the rotator speed decreased. The resulting fibre diameters when applying a voltage of 18kV, fibre diameters of

0.90 ± 0.09 , 1.11 ± 0.15 , $1.34 \pm 0.37 \mu\text{m}$ were obtained for rotator speeds of 2000, 1500 and 1000 rpm respectively (Table 5.1). The fibres obtained under all applied electrospinning conditions had a random distribution and contained beads.

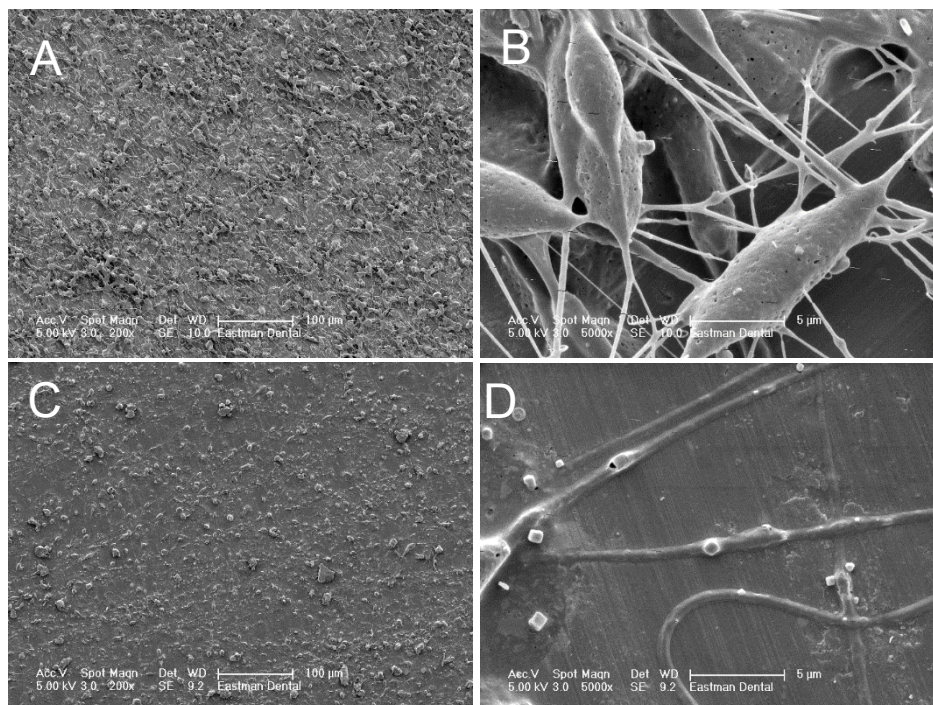


Figure 5.3 Beaded electrospun fibres of 10 % w/v 75:25 P(3HO)/P(3HB) blends. A and B) Random 10% w/v 75:25 P(3HO)/P(3HB) fibres using 12 kV and 2000 rpm. The fibrous sheet (A) contained random fibres of $0.31 \pm 0.06 \mu\text{m}$ diameter. Polymer beads were found on the fibrous sheet. C) and D) Random 10% (w/v) 75:25 P(3HO)/P(3HB) fibres using 18 kV and 1000 rpm. The fibrous sheet (C) contained random fibres of $0.47 \pm 0.25 \mu\text{m}$ diameter. Polymer crystals were found in all the fibres.

When the polymeric solution of 10% (w/v) 50:50 P(3HO)/P(3HB) blend was electrospun, fibres with varying diameters were also obtained for each combination of voltages and rotator speeds. When the voltage applied was 12kV, no trend was detected in the fibre diameter. For voltage of 12 kV, fibre diameters of 0.89 ± 0.09 , 0.46 ± 0.10 and $1.01 \pm 0.21 \mu\text{m}$ were obtained when the rotator speeds were 2000, 1500 and 1000 rpm respectively (Table 5.1, Fig. 5.4.A,B). When the voltage applied was 18 kV, the fibre diameters increased when the rotator speed decreased. When a voltage of 18kV was applied, fibre diameters of 0.90 ± 0.09 , 1.11 ± 0.15 , $1.34 \pm 0.37 \mu\text{m}$ were obtained for rotator speeds of 2000, 1500 and 1000 rpm respectively (Table 5.1). The fibres obtained under all applied electrospinning conditions had a random distribution and contained beads.

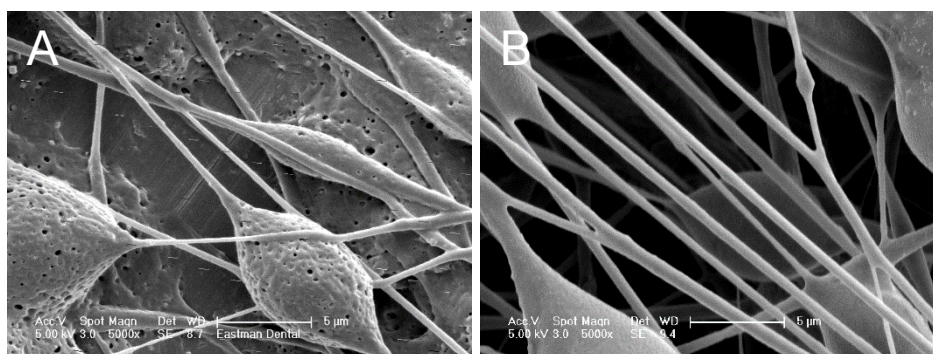


Figure 5.4 Electrospun fibres of 10 % w/v 50:50 P(3HO)/P(3HB) blends. A) Random 50:50 P(3HO)/P(3HB) fibres (10% w/v) using 12 kV and 1500 rpm. B) Random 50:50 P(3HO)/P(3HB) fibres (10% w/v) using 12 kV and 2000 rpm. The fibrous sheet shown in A contained fibres of $0.46 \pm 0.10 \mu\text{m}$ diameter. The fibrous sheet shown in B contained random fibres of $0.89 \pm 0.09 \mu\text{m}$ diameter.

Fibres made from 10% (w/v) 25:75 P(3HO)/P(3HB) blend were more aligned and had larger diameter than those obtained with the other polymeric solutions of 0:100, 75:25, and 50:50 P(3HO)/P(3HB) (Fig. 5.2, 5.3, 5.4 and 5.5). The fibre diameters increased when the rotator speed decreased for both voltages (12 and 18kV) (Table 5.1). For applied voltage of 12kV, the resulting fibre diameters were 1.20 ± 0.25 , 1.46 ± 0.40 and $2.54 \pm 1.22 \mu\text{m}$ for rotator speeds of 2000, 1500 and 1000 rpm respectively. When the voltage applied was 18kV fibre diameters of 1.55 ± 0.70 , 1.69 ± 0.53 , $2.80 \pm 0.36 \mu\text{m}$ were obtained for rotator speeds of 2000, 1500 and 1000 rpm (Fig.5.5.A,B) (Table 5.1) correspondingly. All the fibres obtained under these electrospinning conditions contained less beads compared to the 0:100, 75:25, 50:50 and 0:100 P(3HO)/P(3HB) fibres.

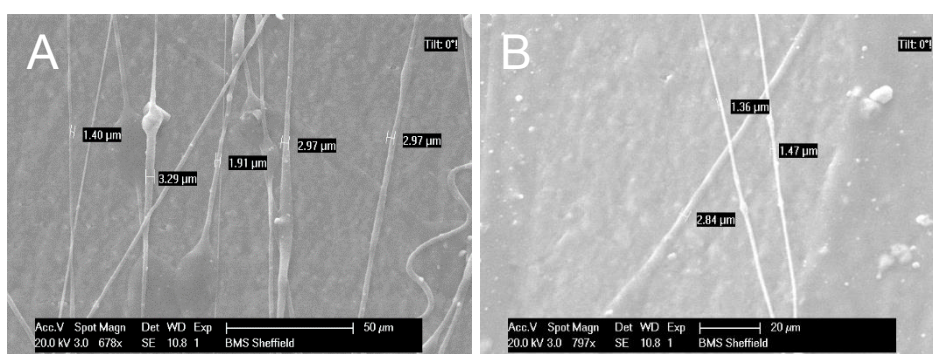


Figure 5.5 Electrospun fibres of 10 % w/v 25:75 P(3HO)/P(3HB) blends. A) Partially aligned 25:75 P(3HO)/P(3HB) fibres 10% w/v using 18 kV and 2000 rpm. B) Partially aligned 25:75 P(3HO)/P(3HB) fibres 10% w/v using 18 kV and 1500 rpm. The fibrous sheet (A) contained fibres of $1.55 \pm 0.70 \mu\text{m}$ diameter. The fibrous sheet (B) contained random fibres of $1.69 \pm 0.53 \mu\text{m}$ diameter.

Fibres made from 10% (w/v) P(3HB) presented different forms and distributions; curved (Fig. 5.6 A), random (Fig. 5.6 B), spiral shaped (Fig. 5.6 C) and aligned (Fig. 5.6 D).

No trend was observed in the P(3HB) fibre diameters when the rotator speed decreased using the applied voltages of 12kV and 18 kV (Table 5.1). For an applied voltage of 12kV the resulting fibre diameters were 1.03 ± 0.13 , 5.40 ± 1.90 and $2.21 \pm 1.82 \mu\text{m}$ for rotator speeds of 2000, 1500 and 1000 rpm respectively (Fig.5.6. A, B). When the voltage applied was 18kV, the resulting fibre diameters were 2.24 ± 1.82 , 1.38 ± 0.43 , $3.45 \pm 0.90 \mu\text{m}$ for rotator speeds of 2000, 1500 and 1000 rpm (Fig.5.6. C, D) (Table 5.1) respectively. The largest fibre diameters (5.40 ± 1.90 and $3.45 \pm 0.90 \mu\text{m}$) were obtained by electrospinning 10% (w/v) P(3HB) compared to the other polymeric solutions (0:100, 75:25, 50:50, 25:75 P(3HO)/P(3HB)) with the same polymer concentration. Additionally, aligned and homogeneous P(3HB) fibres were obtained using 18kV, 1500 rpm (Fig. 5.6 D).

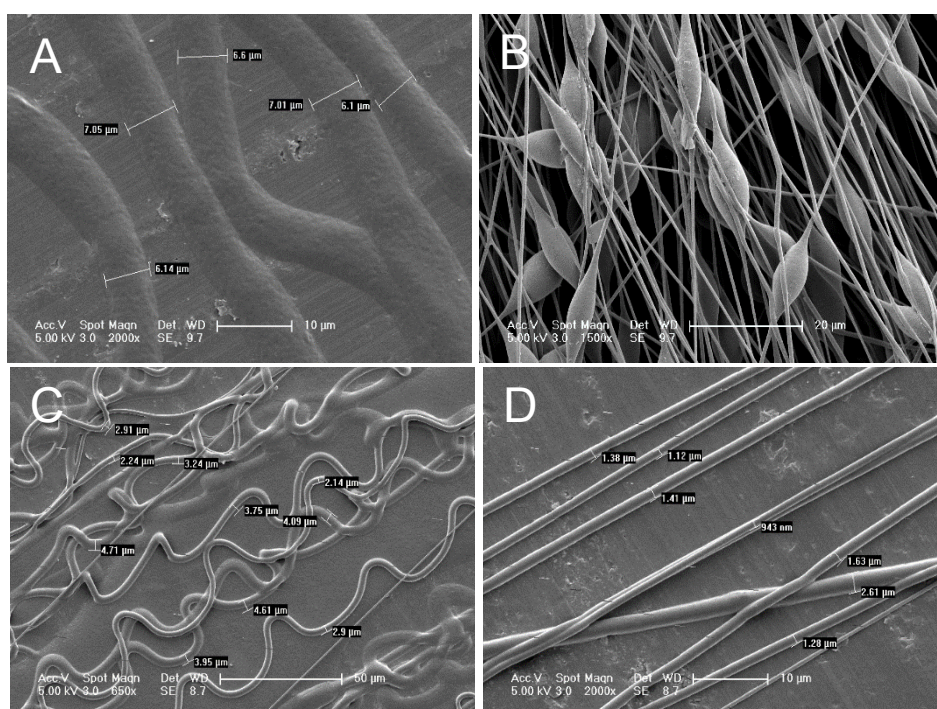


Figure 5.6 Electrospun fibres of 10 % w/v P(3HB). A) Partially aligned P(3HB) fibres 10% w/v using 12kV, 1500 rpm. B) Random fibres 10% w/v along with beads using 12kV and 2000 rpm. C) Spiral shaped P(3HB) fibres 10% w/v using 18kV, 1000 rpm. D) Aligned P(3HB) fibres 10% w/v using 18kV, 1500 rpm. The fibrous sheet (A) contained the thickest P(3HB) fibres of $5.40 \pm 1.90 \mu\text{m}$ diameter. The random fibres showed in Fig. B represented the smallest diameter of $1.03 \pm 0.13 \mu\text{m}$. Polymer beads were found on the fibrous sheet. Spiral shaped fibres in Fig. C showed a diameter of $3.45 \pm 0.90 \mu\text{m}$. Aligned fibres ($1.38 \pm 0.43 \mu\text{m}$) in Fig. D were more uniform and aligned when compared with fibres showed in Fig. A, B and C.

As in previous studies (Chapter 4) the blend 25:75 P(3HO)/P(3HB) showed higher compatibility with NG-108-15 cells when compared to the other blends (100:0, 50:50, 75:25 and 100:0 P(3HO)/P(3HB)) this blend was chosen for further fibre manufacturing studies and

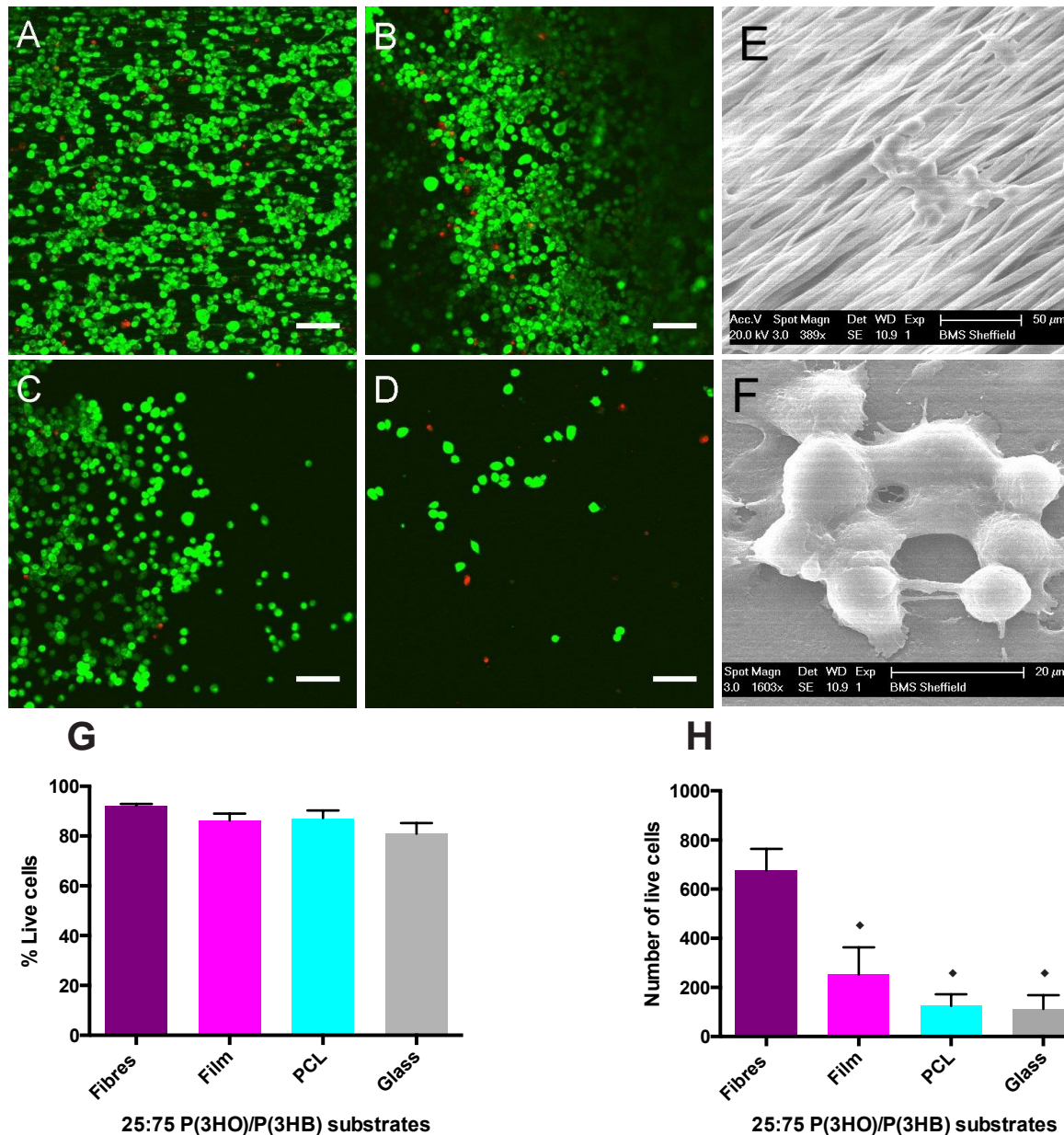


Figure 5.8 A-D) Confocal micrographs of NG108-15 neuronal cells labelled with propidium iodide (red) and Syto-9 (green) after four days in culture on both films and electrospun aligned fibres made from 25:75 P(3HO)/P(3HB) using a PCL film and glass as controls. (A) 25:75 P(3HO)/P(3HB) electrospun aligned fibres; (B) 25:75 P(3HO)/P(3HB) film (C) PCL film and D) glass. E-F) Scanning electron micrograph of neuronal cells grown on 25:75 P(3HO)/P(3HB) scaffolds. (E) Electrospun aligned fibres and F) film. (G) Live/dead analysis of neuronal cells on the 25:75 P(3HO)/P(3HB) substrates, PCL and glass (mean \pm SEM, $n = 6$ independent experiments $P < 0.05$). (H) Number of live cells on the 25:75 P(3HO)/P(3HB) substrates, PCL and glass (mean \pm SEM, $n = 6$ independent experiments $P < 0.05$).

The percentages of live/dead cells on the substrates (Fig. 5.8 G) 25:75 P(3HO)/P(3HB) electrospun fibres, 25:75 P(3HO)/P(3HB) film, PCL film and glass were $92.21 \pm 0.68\%$, $86.18 \pm 2.85\%$, $87.23 \pm 3.08\%$ and $80.94 \pm 4.30\%$ respectively. Statistical analysis showed that no significant differences were found between the live/dead cell percentages of the substrates

($P < 0.05$). The number of live cells on the 25:75 P(3HO)/P(3HB) electrospun fibers, 25/75 P(3HO)/P(3HB) film, PCL film and glass substrates were 676.00 ± 87.51 , 252.17 ± 111.03 , 124.67 ± 47.09 and 112.17 ± 56.31 respectively. In this case however, the number of live cells grown on 25:75 P(3HO)/P(3HB) electrospun fibers was higher when compared with all the other substrates ($P < 0.05$).

In order to obtain fibres with higher diameters, the polymer concentration was increased from 10% (w/v) to 20% (w/v). For the manufacture of 25:75 P(3HO)/P(3HB) electrospun fibres, voltage of 12 and 18 kV combined with 2000, 1500 and 1000 rpm were used and the resulting fibre diameter are presented in Table 5.2. For both voltages (12 kV and 18 kV), fibre diameter increased when the rotator speed decreased. When the voltage applied was 12 kV the fibre diameters were 3.61 ± 0.63 , 4.07 ± 1.12 and 4.44 ± 0.23 μm for 2000, 1500 and 1000 rpm respectively. Similarly, for voltage of 18 kV the resulting diameters were 3.73 ± 0.57 , 4.28 ± 1.55 and 5.58 ± 1.00 for 2000, 1500 and 1000 rpm respectively.

Table 5.2 Summary of electrospinning parameters used to determine the optimal conditions for the manufacture of aligned blend fibres using 20% w/v of 25:75 P(3HO)/P(3HB) blend.

% Polymer (w/v)	Voltage (kV)	Flow rate (ml/h)	Rotator speed (rpm)	Diameter of 25:75 P(3HO)/P(3HB) fibres (μm)
20	12	1	2000	3.6 ± 0.6
20	12	1	1500	4.1 ± 1.1
20	12	1	1000	4.4 ± 0.2
20	18	1	2000	3.7 ± 0.6
20	18	1	1500	4.3 ± 1.5
20	18	1	1000	5.6 ± 1.0

The fibre diameters obtained using 20 % (w/v) of 25:75 P(3HO)/P(3HB) blend (Table 5.2, Fig. 5.9) were higher as compared to the fibre diameters obtained with 10 % (w/v) of 25:75 P(3HO)/P(3HB) blend (Table 5.1, Fig. 5.4) using the equivalent electrospinning conditions. When a voltage of 12 kV was combined with rotator speeds of 2000, 1500 and 1000 rpm, the diameters obtained using 10% (w/v) of 25:75 P(3HO)/P(3HB) were 1.20 ± 0.25 , 1.46 ± 0.40 and 2.54 ± 1.22 μm (Table 5.1) whereas for 20 % (w/v) of 25:75 P(3HO)/P(3HB) blend the resulting diameters were 3.61 ± 0.63 , 4.07 ± 1.12 and 4.44 ± 0.23 μm respectively (Table 5.2). In the same way, when the applied voltage was 18 kV combined with rotator speeds of 2000,

1500 and 1000 rpm, the resulting diameters using 10% (w/v) of 25:75 P(3HO)/P(3HB) were 1.55 ± 0.70 , 1.69 ± 0.53 , $2.80 \pm 0.36 \mu\text{m}$ respectively (Table 5.1) whereas the obtained diameters for 20 % (w/v) of 25:75 P(3HO)/P(3HB) blend were 3.73 ± 0.57 , 4.28 ± 1.55 and $5.58 \pm 1.00 \mu\text{m}$ respectively (Table 5.2).

Aligned and uniform fibres were obtained using 20 % (w/v) of 25:75 P(3HO)/P(3HB) blend under all the electrospinning conditions used except for the fibres obtained when the rotator speed was 1000 rpm (Fig. 5.9 A, C).

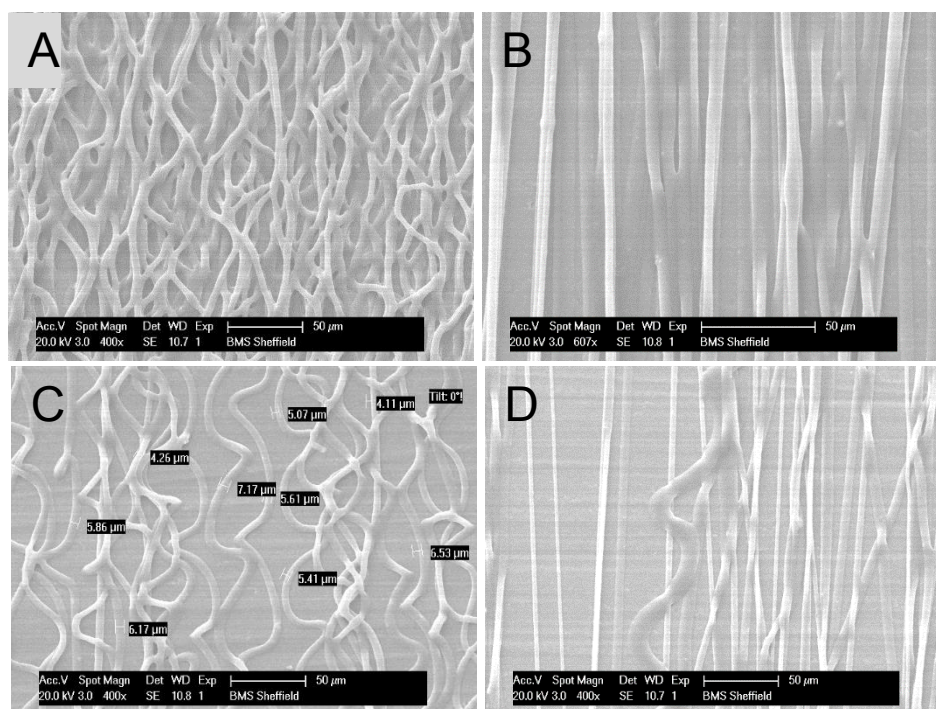


Figure 5.9 Electrospun fibres of 20 % w/v 25:75 P(3HO)/P(3HB) blends. A) Curved fibres obtained using 12kV, 1000 rpm. B) Aligned obtained using 12kV and 1500 rpm. C) Spiral shaped obtained using 18kV, 1000 rpm. D) Partially aligned fibres obtained using 18kV, 1500 rpm. The fibrous sheet (A) contained fibres of $4.44 \pm 0.23 \mu\text{m}$ diameter. The aligned fibres showed in Fig. B exhibited a diameter of $4.07 \pm 1.12 \mu\text{m}$. Spiral shaped fibres in Fig. C exhibited a maximum diameter of $5.58 \pm 1.00 \mu\text{m}$ when compared to the rest of electrospinning conditions. Partially aligned fibres presented in Fig. D exhibited a diameter of $4.28 \pm 1.55 \mu\text{m}$.

5.2.3 FABRICATION OF ALIGNED 25:75 P(3HO)/P(3HB) BLEND WITH DIFFERENT FIBRE DIAMETERS

In order to investigate the effect of fibre diameter on cell growth and differentiation of neuronal cells NG-108-15 four different concentrations of 25:75 P(3HO)/P(3HB) blend (15, 25, 30 and 35 % w/v) were used to manufacture sheets of electrospun fibres. Voltages of 12 kV and 18 kV combined with 2000 and 1500 rpm were applied for the fabrication of the varying diameter fibres and the results are shown in Table 5.3.

For all the concentrations with their respective voltages (12kV and 18kV), increments in the fibre diameter were observed when the rotator speed was decreased. All of the manufactured 25:75 P(3HO)/P(3HB) fibres under all electrospinning conditions applied (12 kV and 18 kV combined with 2000 and 1500 rpm) were aligned and uniform (Fig. 5.10, 5.11 and 5.12). Higher fibre diameter increments were observed when the concentration of 25:75 P(3HO)/P(3HB) increased compared with the increments observed when the collector speed was decreased.

Table 5.3. Summary of fibre diameters obtained using different polymer concentrations of 25:75 P(3HO)/P(3HB) blend and electrospinning conditions.

Voltage (kV)	Flow rate (ml/h)	Collector speed (RPM)	Fibre diameter μm			
			Polymer concentration			
			15 wt %	25 wt %	30 wt %	35 wt %
12	1	2000	2.4 ± 0.3	3.5 ± 0.3	4.3 ± 0.2	12.1 ± 3.6
12	1	1500	3.5 ± 0.4	4.1 ± 0.3	4.4 ± 0.3	13.5 ± 2.3
18	1	2000	3.1 ± 0.2	3.4 ± 0.3	4.4 ± 0.8	14.0 ± 3.5
18	1	1500	3.4 ± 0.2	3.7 ± 0.3	5.1 ± 0.9	15.9 ± 7.9

When the polymeric concentration of 25:75 P(3HO)/P(3HB) was 15% w/v, fibres in the range of 2.42 ± 0.34 and $3.41 \pm 0.20 \mu\text{m}$ were obtained (Table 5.3 and Fig.5.10). For an applied voltage of 12kV the resulting fibre diameters were 2.42 ± 0.34 and $3.48 \pm 0.36 \mu\text{m}$ for the rotator speeds of 2000 and 1500 respectively. When the voltage applied was 18kV, the resulting fibre diameters were 3.09 ± 0.25 and $3.41 \pm 0.20 \mu\text{m}$ for rotator speeds of 2000 and 1500 rpm.

For the polymeric concentration of 25% w/v, the resulting fibre diameters were in the range of 3.47 ± 0.34 and $3.47 \pm 0.34 \mu\text{m}$ (Table 5.3 and Fig. 5.11). When the voltage applied was 12kV the resulting fibre diameters were 3.47 ± 0.34 and $4.09 \pm 0.34 \mu\text{m}$ for the rotator speeds of 2000 and 1500 respectively. For the applied voltage of 18kV the obtained fibres diameters were 3.39 ± 0.30 and $3.68 \pm 0.26 \mu\text{m}$ when using the rotator speeds of 2000 and 1500 respectively.

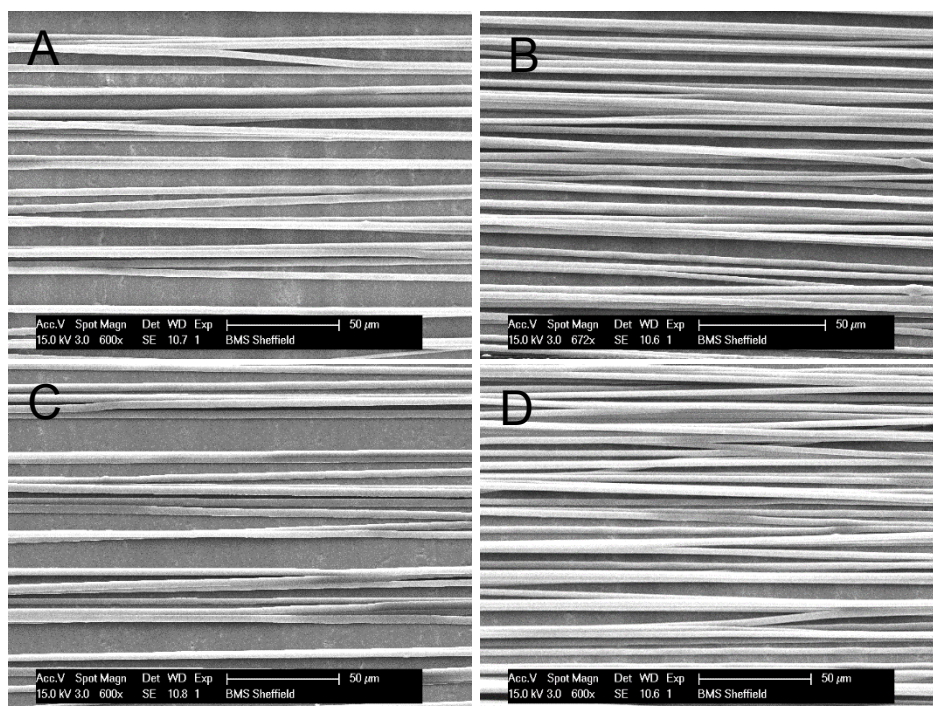


Figure 5.10 Aligned electrospun fibres using 15% w/v of 25:75 P(3HO)/P(3HB) blend. A) Aligned 25:75 P(3HO)/P(3HB) fibres using 15% w/v, 12 kV, 1500 rpm. B) Aligned 25:75 P(3HO)/P(3HB) fibres using 15% w/v, 12 kV, 2500 rpm. C) Aligned 25:75 P(3HO)/P(3HB) fibres using 15% w/v, 18 kV, 1500 rpm. The diameter showed by these fibres was $3.41 \pm 0.20 \mu\text{m}$ D) Aligned 25:75 P(3HO)/P(3HB) fibres using 15% w/v, 18 kV, 2000 rpm (Fibre diameter = $3.09 \pm 0.25 \mu\text{m}$).

When the polymeric concentration of 25:75 P(3HO)/P(3HB) was 30% w/v, fibres in the range of 4.33 ± 0.19 and $5.14 \pm 0.91 \mu\text{m}$ were obtained (Table 5.3 and Fig.5.11). For the applied voltage of 12kV the resulting fibre diameters were 4.33 ± 0.19 and $4.38 \pm 0.30 \mu\text{m}$ for the rotator speeds of 2000 and 1500 respectively. When the voltage applied was 18kV, the resulting fibre diameters were 4.44 ± 0.75 , $5.14 \pm 0.91 \mu\text{m}$ for rotator speeds of 2000 and 1500 rpm.

For the polymeric concentration of 35% w/v, the resulting fibre diameter were in the range of 12.09 ± 3.61 and $15.95 \pm 7.99 \mu\text{m}$ (Table 5.3 and Fig. 5.11). When the voltage applied was 12kV the resulting fibre diameters were 12.09 ± 3.61 and $13.50 \pm 2.33 \mu\text{m}$ for the rotator speeds of 2000 and 1500 respectively. For the applied voltage of 18kV the obtained fibres diameters were slightly higher than those obtained using 12 kV. The measured diameters for 18 kV were 14.03 ± 3.50 and $15.95 \pm 7.99 \mu\text{m}$ for the rotator speeds of 2000 and 1500 respectively.

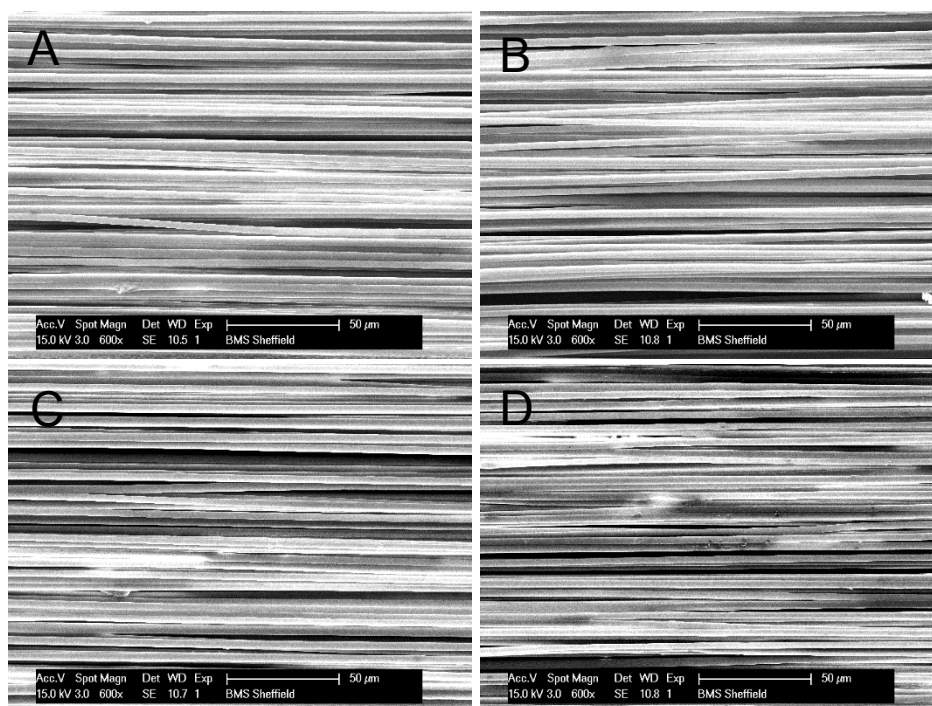


Figure 5.11 Aligned electrospun fibres using 25% w/v of 25:75 P(3HO)/P(3HB) blend. A) Aligned 25:75 P(3HO)/P(3HB) fibres using 25% w/v, 12 kV, 1500 rpm. B) Aligned 25:75 P(3HO)/P(3HB) fibres using 25% w/v, 12 kV, 2000 rpm. These fibres presented (Fig. B) a diameter of $3.47 \pm 0.34 \mu\text{m}$. C) Aligned 25:75 P(3HO)/P(3HB) fibres using 25% w/v, 18 kV, 1500 rpm (Fibre diameter = $3.68 \pm 0.26 \mu\text{m}$). D) Aligned 25:75 P(3HO)/P(3HB) fibres using 25% w/v, 18 kV, 2000 rpm (Fibre diameter = $3.39 \pm 0.30 \mu\text{m}$).

For studying the effect of diameter size on neuronal cell growth and differentiation only three scaffolds with aligned electrospun fibres of different fibre diameters were selected. The average diameter selected for the small, medium and large fibres were 2.42 ± 0.34 , 3.68 ± 0.26 and $13.50 \pm 2.33 \mu\text{m}$ respectively which were obtained using different electrospinning conditions summarized in Table 5.3.

5.2.4 PHYSICAL CHARACTERIZATION OF ALIGNED 25:75 P(3HO)/P(3HB) BLEND MICROFIBRES BY SCANNING ELECTRON MICROSCOPY

Three scaffolds consisting of aligned 25:75 P(3HO)/P(3HB) blend microfibers with varying diameters were manufactured by electrospinning using three different processing conditions, summarized in Table 5.3. The fibre architecture was studied using a field emission scanning electron microscope to analyse three physical features using the NIH Image J software: i) fibre diameter; ii) fibre density and iii) fibre alignment. SEM micrographs of small, medium and large fibres are shown in Fig. 5.13 A, B; Fig. 5.13 C, D and Fig. 5.13 E, F respectively. After analysis of the scaffolds, the resulting average fibre diameter for small,

medium and large fibre groups were 2.42 ± 0.34 , 3.68 ± 0.26 and 13.50 ± 2.33 μm respectively (Fig. 5.14 A). Statistical analysis showed that the difference in fibre diameter between each of the fibre group was significant (2.42 ± 0.34 μm versus 3.68 ± 0.26 μm , $p < 0.05$; 2.42 ± 0.34 μm versus 13.50 ± 2.33 μm , $p < 0.05$ and 3.68 ± 0.26 μm versus 13.50 ± 2.33 μm , $p < 0.05$).

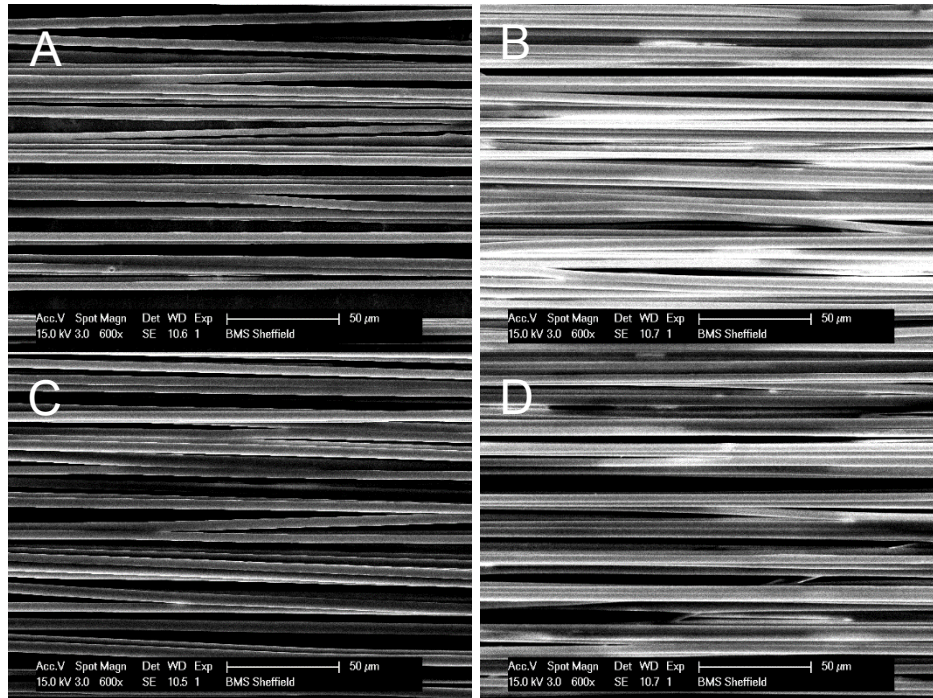


Figure 5.12 Aligned electrospun fibres using 30% w/v of 25:75 P(3HO)/P(3HB) blend. A) Aligned fibres obtained using 30% w/v, 12 kV, 1500 rpm. The average diameter was 4.38 ± 0.30 μm . B) Aligned 25:75 P(3HO)/P(3HB) fibres using 30% w/v, 12 kV, 2000 rpm. These fibres exhibited a diameter of 4.33 ± 0.19 μm . C) Aligned fibres using 18 kV, 1500 rpm. These fibres presented the largest diameter (Fibre diameter = 5.14 ± 0.91 μm) when compared with A, B and D. D) Aligned fibres using 18 kV, 2000 rpm (Fibre diameter = 4.44 ± 0.75 μm). The fibre diameters obtained in A, B and D were similar.

Fibre density determination was also carried out based on the SEM micrograph images. It can be seen in Fig. 5.14 B that the medium sized fibre group (0.30 ± 0.03 fibres/ μm) presented the highest fibre density compared to the small (0.22 ± 0.04 fibres/ μm , $*P < 0.05$) and the large fibre group (0.21 ± 0.02 fibres/ μm , $**P < 0.05$). However, no significant difference was found between the small and large fibre groups.

Fibre alignment estimation was assessed by measuring the angular difference between fibres and an assigned central reference line. For each size fibre group, an average of 27 fibres were analysed to determine the mean of each angular difference group and were presented in a histogram (Fig. 5.14 B).

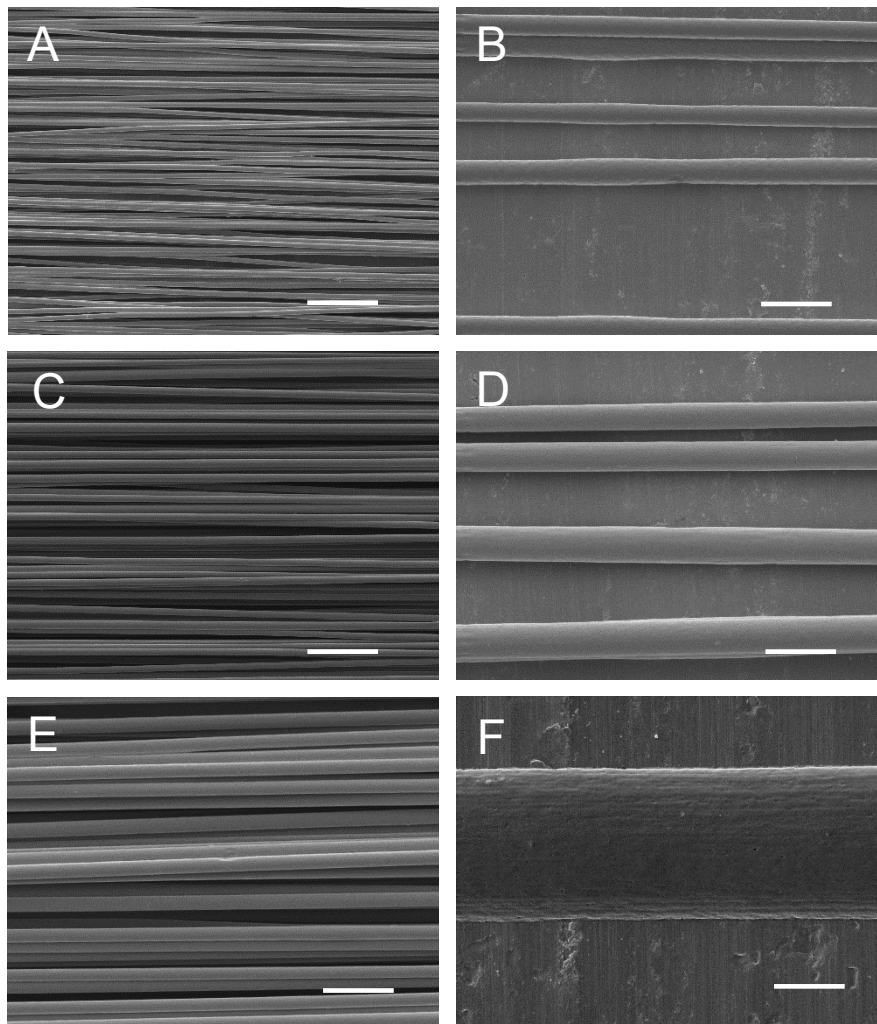


Figure 5.13 Characterization of electrospun 25:75 P(3HO)/P(3HB) fibres by scanning electron microscopy. Diameter, density and alignment of fibres were determined by image analysis. (A, B), (C, D) and (E,F) show the micrographs of the electrospun fibre mats corresponding to the small, medium and large 25:75 P(3HO)/P(3HB) fibre diameter respectively.

A greater number of the fibres for the three size groups presented an angular difference of 0° . Medium and large fibres showed the highest number of fibres with an angular difference of 0° when compared to small fibres (* $P < 0.05$ in comparison to medium fibres and large fibres). The number of fibres dropped markedly as the angle of variance increased, showing that the majority of fibres were arranged in a straight line and parallel to each other (Fig. 5.13 A, C, E and Fig. 5.14 H).

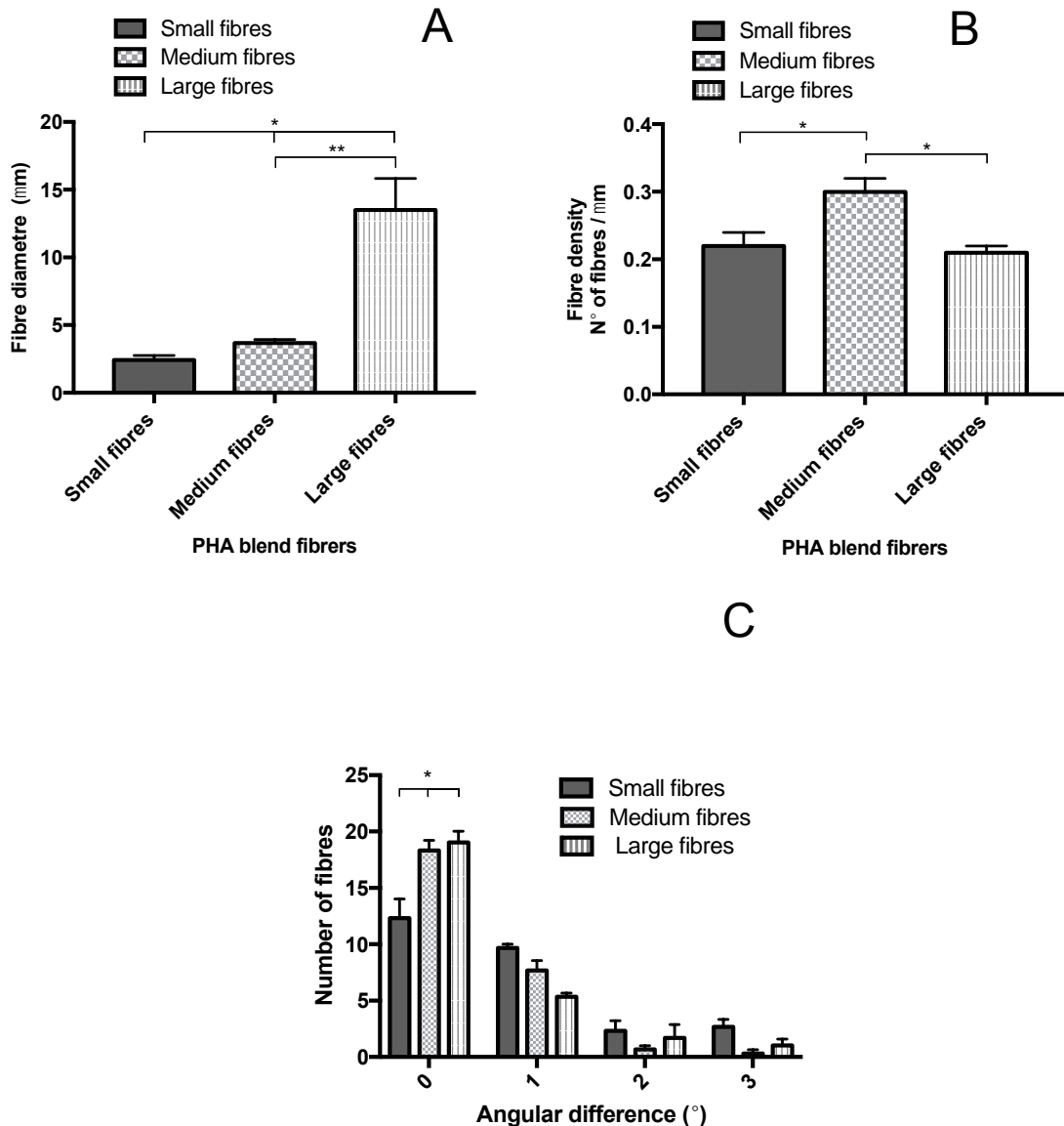


Figure 5.14 Fibre characterization. (A) The average diameter for the small, medium and large fibres were 2.42 ± 0.34 , 3.68 ± 0.26 and $13.50 \pm 2.33 \mu\text{m}$ respectively. A total of approximately 27 fibres were analysed for each fibre diameter group to determine the mean of the diameters (mean \pm SD, $n = 3$ samples independently fabricated, $*P < 0.05$ compared to small fibres, $**P < 0.05$ in relation to medium fibres). (B) Mean fibre density measurement for each fibre group. The number of fibres containing in an area of $152 \mu\text{m}$ was counted (mean \pm SEM, $n = 3$ samples independently fabricated). (C) Fibre alignment estimation. Angular difference between fibres and an assigned central reference fibre was measured. An average of 27 fibres were analysed for each size fibre group to determine the mean of each angular difference range. (mean \pm SEM, $n = 3$ samples independently fabricated, ($*P < 0.05$ in comparison to medium fibres and large fibres).

5.2.5 LIVE/DEAD MEASUREMENT OF NG108-15 NEURONAL CELLS ON PHA BLEND ELECTROSPUN FIBRES

Live/dead cell assays were performed in order to compare the attachment and survival of NG-108-15 neuronal cells on the electrospun 25:75 P(3HO)/P(3HB) blend sheets with

varying fibre diameters. In Figure 5.15, representative confocal images of neuronal cells grown on different substrates are shown.

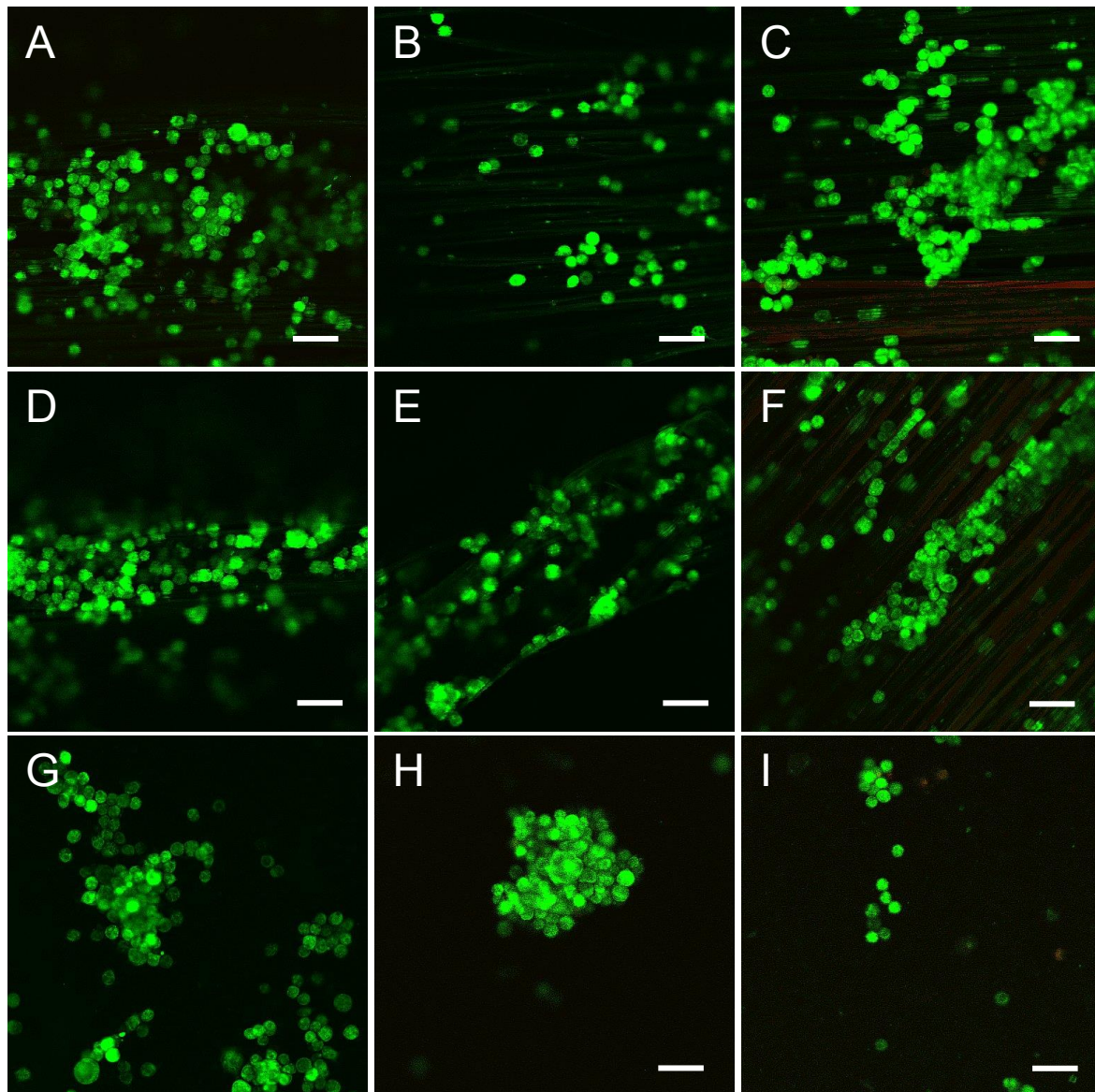


Figure 5.15. Confocal micrographs of NG108-15 neuronal cells labelled with propidium iodide (red) and Syto-9 (green) after four days in culture on aligned 25:75 P(3HO)/P(3HB) fibres. (A, D) Small fibres ($2.42 \pm 0.34 \mu\text{m}$); (B, E) Medium fibres ($3.68 \pm 0.26 \mu\text{m}$), (C, F) Large fibres ($13.50 \pm 2.33 \mu\text{m}$), and on flat substrates (controls) consisting of (G) PHA blend film (H) PCL film and (I) glass. Scale bar = $50 \mu\text{m}$

Figures 5.3 A and D; 5.3 B and D; and 5.3 C and F correspond to cells grown on the small, medium and large 25:75 P(3HO)/P(3HB) fibres respectively. It can be seen that neuronal cell growth had an aligned distribution on the three fibre groups (Fig 5.15 A-F). On the other hand, random growth of cells was observed in the flat substrates of the PHA blend

(Fig. 5.15 G), PCL (Fig. 5.15 H) and glass (Fig. 5.15 I), in which several clusters of cells were found.

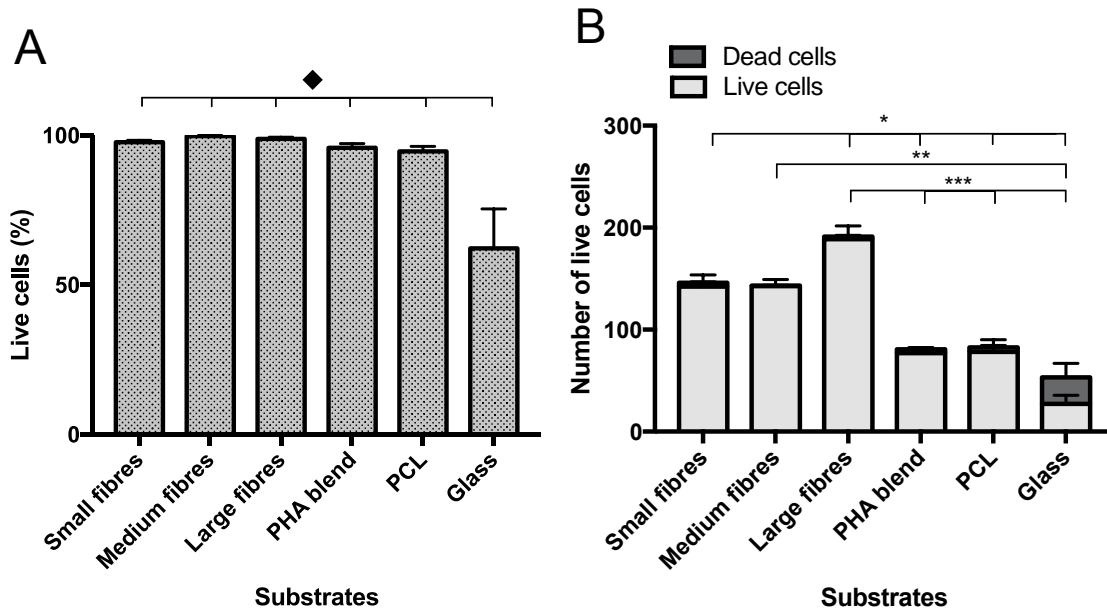


Figure 5.16. Live and dead cell test on fibres with varying diameters (A)The number of neuronal cells on fibres with varying diameters. (B) Live/dead analysis of neuronal cells on fibres with varying diameters, PHA blend film, PCL film and glass. Percentage of live neuronal cells on the fibres, PHA blend film and PCL film was higher in comparison to glass (control) (mean \pm SEM, $n = 9$ independent experiments $P < 0.05$).

The percentage of live cells on small ($97.76 \pm 0.58\%$), medium ($99.77 \pm 0.22\%$), large fibres ($98.87 \pm 0.60\%$), flat 25:75 P(3HO)/P(3HB) blend film ($95.89 \pm 1.43\%$) and flat PCL film ($94.72 \pm 1.68\%$) was higher when compared to glass ($62.28 \pm 13.16\%$, $\blacklozenge P < 0.05$) (Fig. 5.16 A). However, no significant differences in percentage of live cells were found between the fibre groups. The number of neuronal cells that grew on the small (142.2 ± 11.42 ; $*P < 0.05$), medium (142.67 ± 6.36 , $**P < 0.05$) and large (188.58 ± 13.00 , $***P < 0.05$) fibre groups was higher when compared to that obtained on the glass control (27.20 ± 8.40) (Fig. 5.16 B).

Also, the number of neuronal cells grown on the small (142.2 ± 11.42 ; $*P < 0.05$) and large (188.58 ± 13.00 , $***P < 0.05$) fibre groups were higher when compared to that obtained on the PHA blend (76.89 ± 5.60) and PCL (78.00 ± 12.04) flat substrates (Fig. 5.16 B). Large fibres supported the highest number of neuronal cells (188.58 ± 13.00) when compared to controls (PHA blend, PCL and glass; $***P < 0.05$) and small fibres ($*P < 0.05$). No significant difference was found between the number of neuronal cells that grew on the controls.

5.2.6 NEURITE OUTGROWTH ASSESSMENT ON NG108-15 NEURONAL CELL CULTURE GROWN ON PHA BLEND ELECTROSPUN FIBRES

NG108-15 neuronal cells were grown on the scaffolds and immunolabelled with the anti- β III-tubulin antibody to assess neurite outgrowth and differentiation. Figure 5.14 (A-I) shows the confocal images of immunolabelled neuronal cells grown on all the substrates.

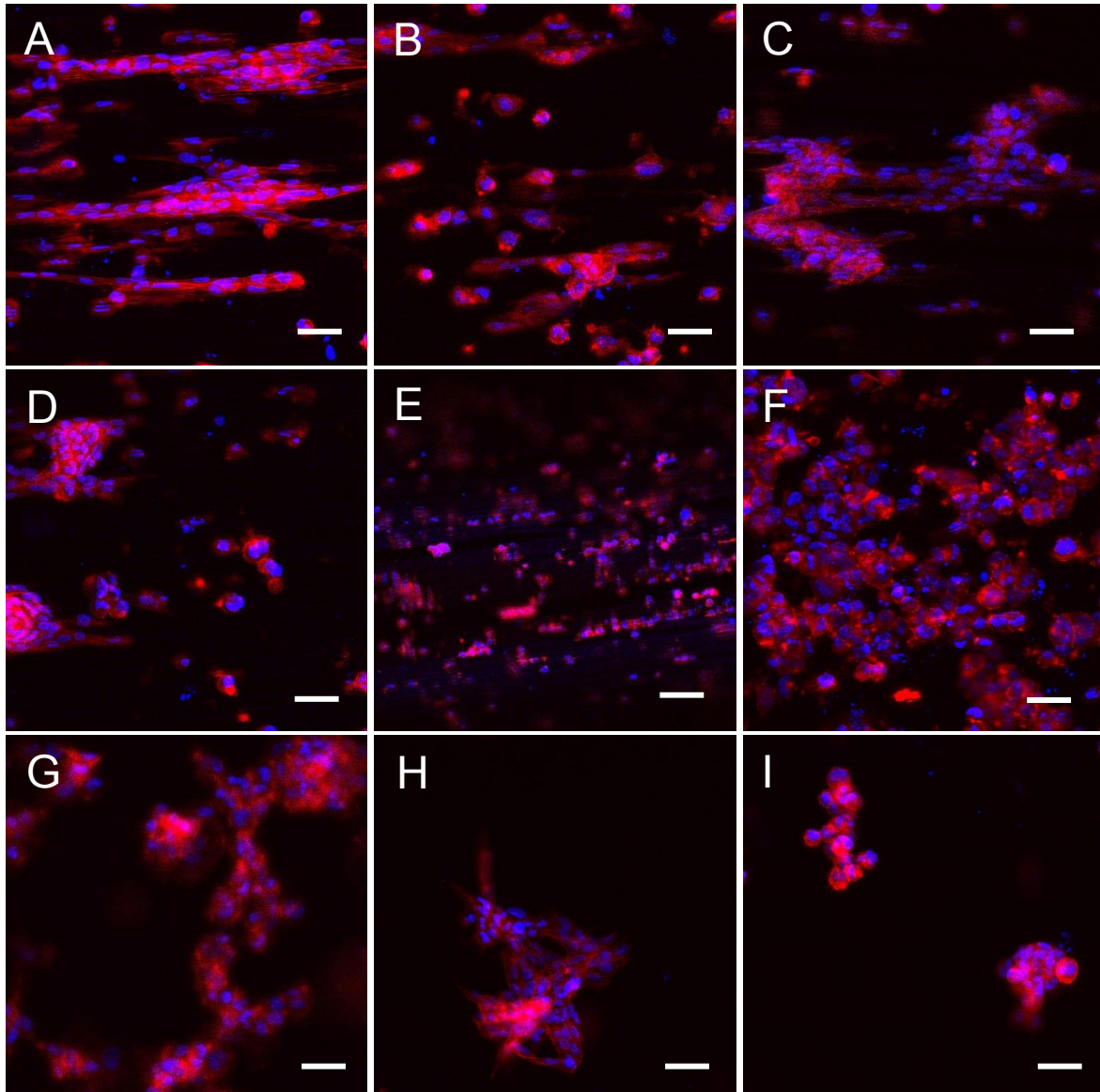


Figure 5.17. Confocal micrographs of NG108-15 neuronal cells immunolabelled for beta-III tubulin after four days in culture on aligned 25:75 P(3HO)/P(3HB) fibres, flat PHA flat film, PCL and glass. (A, D) Small fibres ($2.42 \pm 0.34 \mu\text{m}$); (B, E) Medium fibres ($3.68 \pm 0.26 \mu\text{m}$), (C, F) Large fibres ($13.50 \pm 2.33 \mu\text{m}$) and on flat substrates (controls) consisting of (G) PHA blend film (H) PCL film and (I) glass.

Differentiation was observed in all the neuronal cells which were positive for anti- β III-tubulin antibody in all the substrates including the controls PHA blend (Fig 5.17 G), PCL (Fig.

5.17 H) and glass (Fig.5.17 I). Alignment of cell growth was clearly seen on the three fibre groups; small fibres (Fig. 5.17 A, D), medium fibres (Fig. 5.17 B, E) and large fibres (Fig. 5.17 C, F) whereas a random distribution of cells was presented in the controls; PHA blend (Fig. 5.17 G), PCL (Fig. 5.17 H) and glass (Fig. 5.17 I).

Figure 5.18 shows the number of differentiated neuronal cells on each substrate. The large fibre group displayed the highest number of differentiated neuronal cells (225.67 ± 24.85) compared to the small fibre (129.13 ± 16.58 , * $P < 0.05$) and medium fibre (125.33 ± 2.40 , ** $P < 0.05$) groups. Statistical analysis showed no significant difference between the number of neuronal cells that grew on the small fibre (129.13 ± 16.58) and medium fibre (125.33 ± 2.40) groups. The number of differentiated neuronal cells on the small fibre (129.13 ± 16.58 , * $P < 0.05$) and large fibre (225.67 ± 24.85 , *** $P < 0.05$) groups were found significantly different to those measured on the flat substrates, the PHA blend (79.88 ± 24.49), PCL (51.25 ± 7.87) and glass (10.13 ± 2.96). However, no significant difference was found between the number of differentiated neuronal cells found on the medium fibre group with respect to any of the flat control substrates (Fig. 5.18). No significant difference was found between any of the flat substrates PHA blend, PCL and glass.

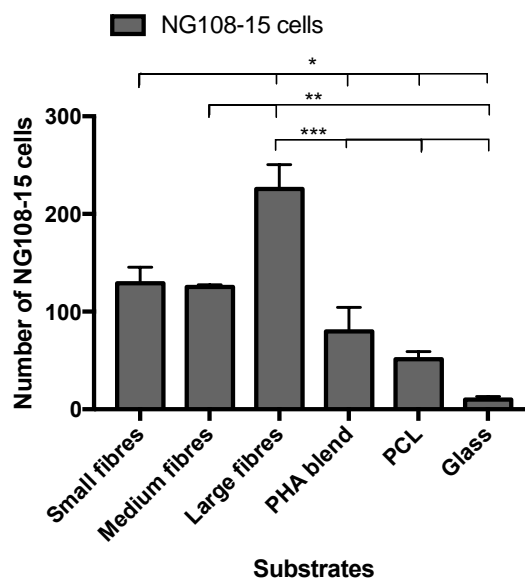


Figure 5.18. Number of cells with neurites on P(3HO)/P(3HB) fibres, PCL and glass (control). (mean ± SEM, n = 9 independent experiments, $P < 0.05$). Scale bar = 50 μ m

In the Figure 5.19, differentiated neuronal cells grown on the three fibre groups are shown with a higher magnification (40X).

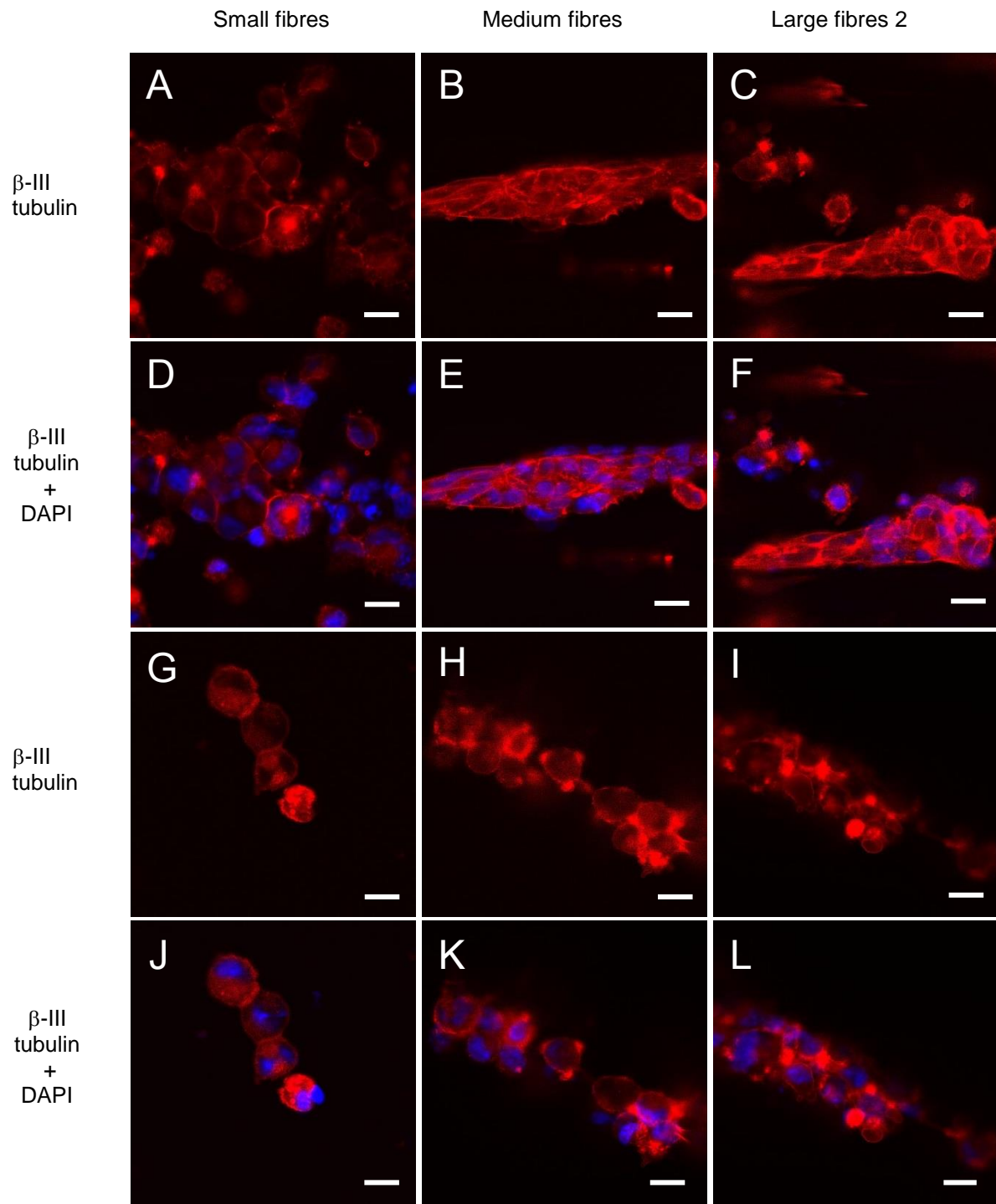


Figure 5.19. Confocal micrographs of NG108-15 neuronal cells immunolabelled for beta-III tubulin after four days in culture on aligned 25:75 P(3HO)/P(3HB) fibres. (A, G), Neuronal cells immunolabelled for beta-III tubulin grown on small fibres. (B, H), Neuronal cells immunolabelled for beta-III tubulin grown on medium fibres. (C, I) Neuronal cells immunolabelled for beta-III tubulin on large fibres 2. (D, J), Neuronal cells immunolabelled for beta-III tubulin + DAPI grown on small fibres. (E, K), Neuronal cells immunolabelled for beta-III tubulin + DAPI grown on medium fibres. (F, L) Neuronal cells immunolabelled for beta-III tubulin + DAPI grown on large fibres 2. Aligned cellular growth was clearly observed on the three different fibres diameters. Scale bar = 12.5 μ m

Figure 5.19 G-L shows a closer view of the neuronal cells grown along the fibres. Neurites bearing cells can be observed forming parallel aligned groups of cells in the three

fibre groups; small fibre (Fig. 5.19 G, H), medium fibre (Fig. 5.19 H, K) and large fibre (Fig. 5.19 I, L). On the other hand, clusters of cells were observed in the controls, P(3HB) blend (Fig. 5.16 A, D), PCL (Fig. 5.16 B, E) and glass (Fig. 5.16 C, F).

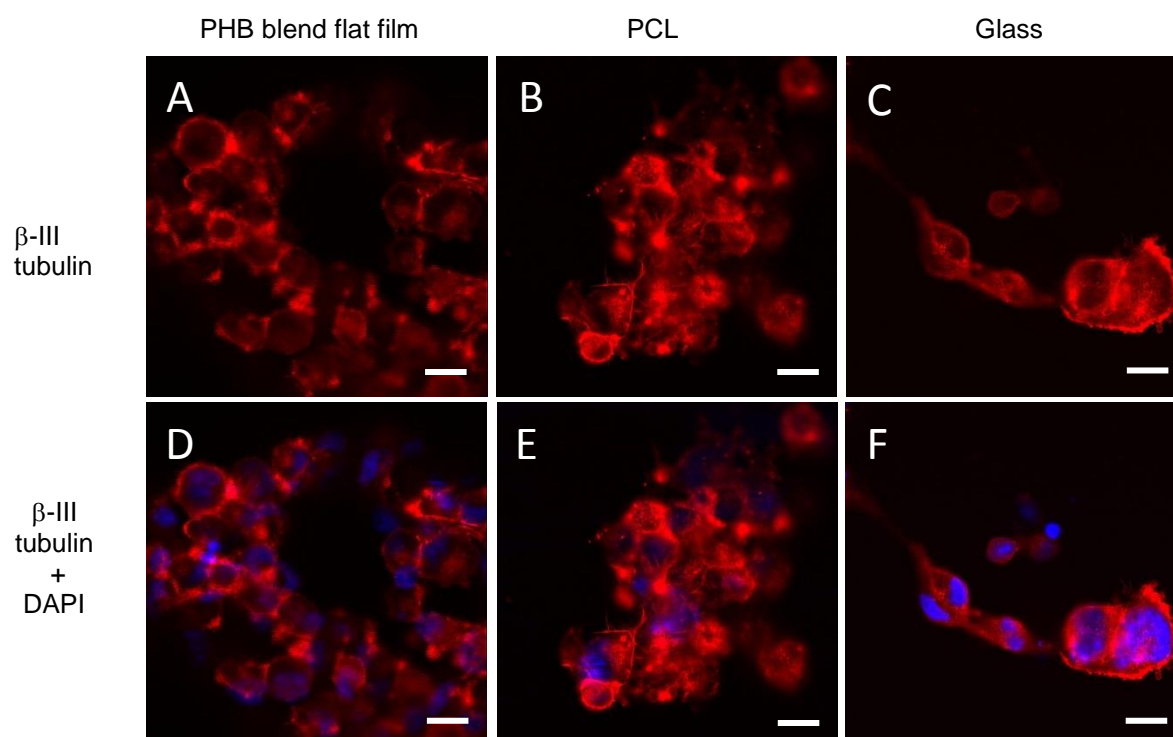


Figure 5.20 Confocal micrographs of NG108-15 neuronal cells immunolabelled for beta-III tubulin + DAPI after four days in culture on PHB blend flat film, PCL and glass. A) Neuronal cells immunolabelled for beta-III tubulin grown on PHB blend flat film. B) Neuronal cells immunolabelled for beta-III tubulin grown on PCL. C) Neuronal cells immunolabelled for beta-III tubulin grown on glass. D) Neuronal cells immunolabelled for beta-III tubulin + DAPI grown on PHB blend flat film. E) Neuronal cells immunolabelled for beta-III tubulin + DAPI grown on PCL. F) Neuronal cells immunolabelled for beta-III tubulin + DAPI grown on glass. Cell growth was randomly oriented on each of the flat surfaces and clusters of neuronal cells connected through neurites were observed. Scale bar = 12.5 μ m

5.2.7 NEURITE OUTGROWTH ASSESSMENT ON NG108-15 NEURONAL CELL/SCHWANN CELL CO-CULTURES GROWN ON PHA BLEND ELECTROSPUN FIBRES

Confocal micrograph images of NG108-15 neuronal cells (red) grown in co-culture with Schwannoma cell line RN22 (green) on small fibres (Fig. 5.21 A, D, G), medium fibres (Fig. 5.21 B, E, H) and on large fibres (Fig. 5.21 C, F, I) are shown in Fig. 5.21.

Only few RN22 cells were detected after four days of cell co-culture and were observed attached to the three fibres groups, small fibres (Fig. 5.21 D), medium fibres (Fig. 5.21 E) and large fibres (Fig. 5.21 E). Although only a few RN22 cells were detected, the cell growth of neuronal cells shows that these two cell lines were able to co-exist on all the fibre groups. Alignment of neuronal cell growth was observed in all fibre groups, small fibres (Fig. 5.21 A), medium fibres (Fig. 5.21 B) and large fibres (Fig. 5.21 C). However, random growth was

observed on the control substrates, PHA blend (Fig. 5.21 A), PCL (Fig. 5.21 B) and glass (Fig. 5.22 C). After analysis of confocal images using image J, all neuronal cells were found to be differentiated on all the substrates; small fibres (Fig. 5.21 G), medium fibres (Fig.5.21 H) large fibres (Fig.5.21 I), PHA blend (5.21 G), PCL (Fig. 5.2 H) and glass (Fig. 5.21 I).

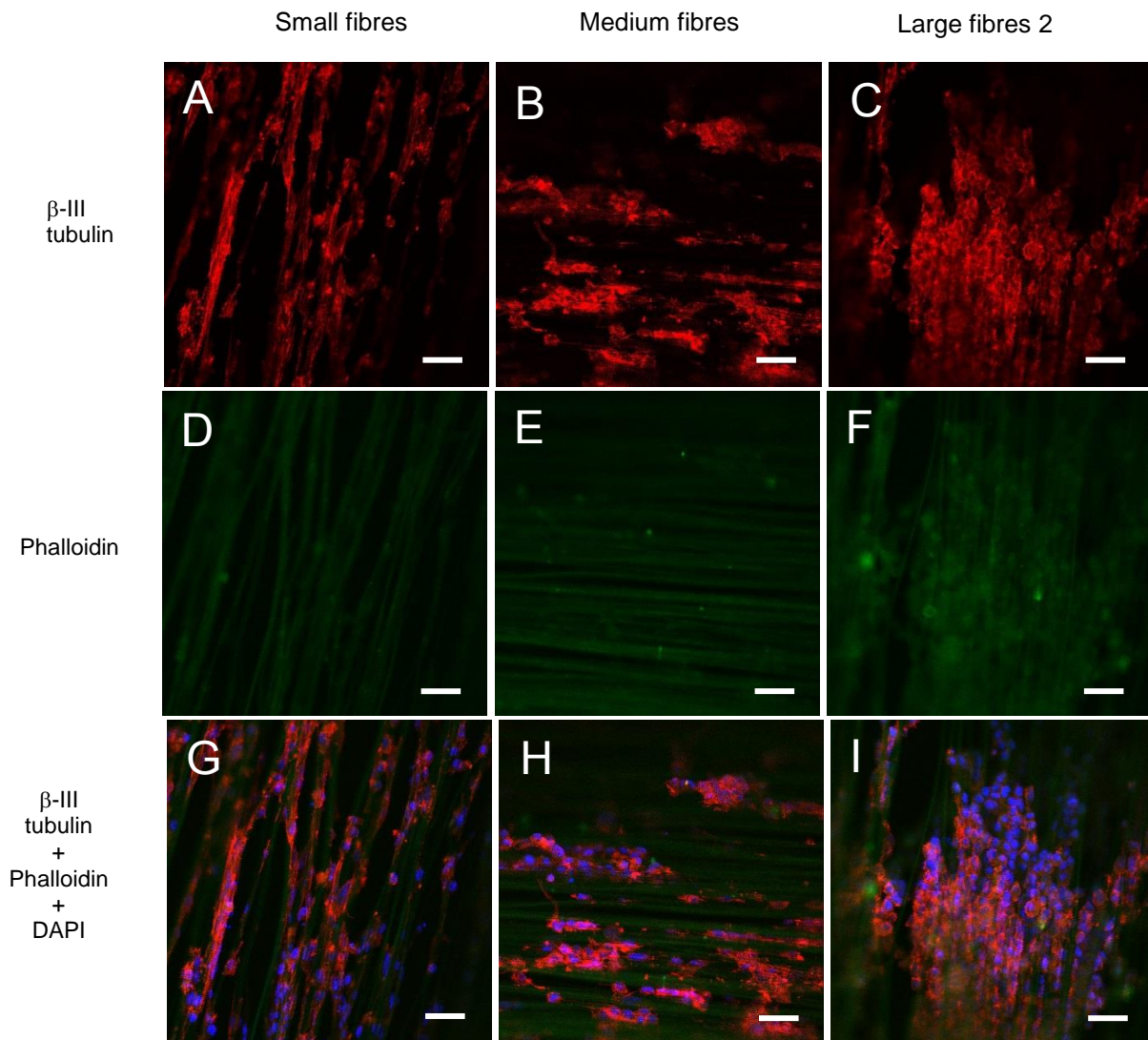


Figure 5.21 Confocal micrographs of NG108-15 neuronal cells (red) grown with RN22 Schwann cells (green) immunolabelled for beta-III tubulin and stained with phalloidin and DAPI after four days in culture on aligned 25:75 P(3HO)/P(3HB) fibres. (A,D,G) Small fibres ($2.42 \pm 0.34 \mu\text{m}$); (B, E, H) Medium fibres ($3.68 \pm 0.26 \mu\text{m}$), (C, F, I) Large fibres ($13.50 \pm 2.33 \mu\text{m}$). Alignment of neuronal cells can be appreciated in all three fibre groups. Scale bar = $50 \mu\text{m}$

Fig. 5.23 shows the number of neuronal cells grown with RN22 cells on all the substrates. Statistical analysis showed that the number of neuronal cells found on the three fibre groups were significantly different. Also, the number of neuronal cells grown on the fibre groups increased as the fibre diameter increased (5.18 J). The number of neuronal cells found

on large fibres (423.25 ± 16.90) was significantly higher than those found on small (191.00 ± 9.50 , $^*P < 0.05$) and medium fibres (274.43 ± 25.36 , $^{**}P < 0.05$).

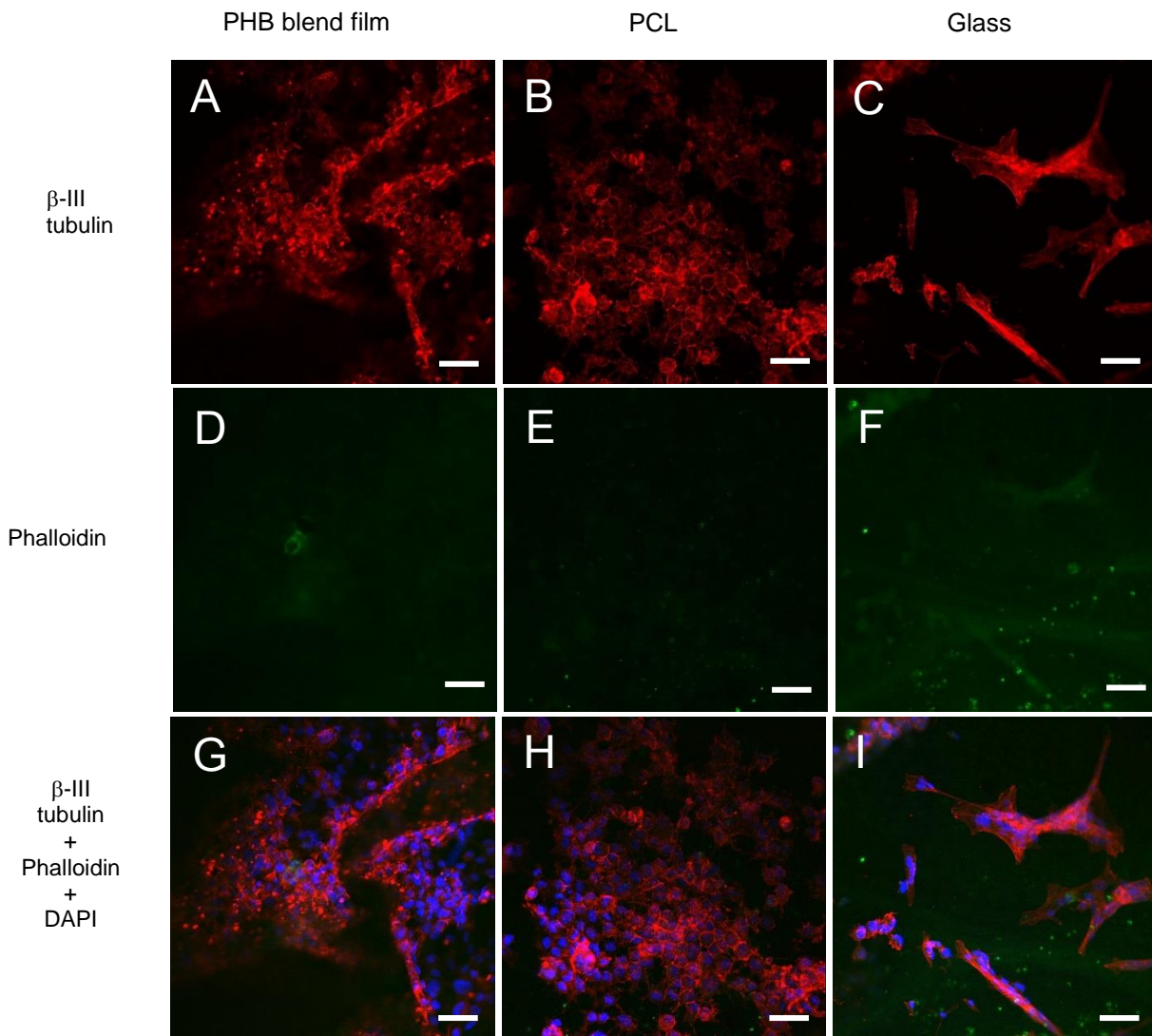


Figure 5.22 Confocal micrographs of NG108-15 neuronal cells (red) grown with RN22 Schwann cells (green) immunolabelled for beta-III tubulin and stained with phalloidin and DAPI after four days in culture on flat substrates (controls) consisting of (A, D, G) PHA blend film, (B, I, H) PCL film and (C, F, I) glass. Cell growth was randomly oriented on the flat substrates PHA blend film, PCL film and glass. Scale bar = 50 μm .

Similarly, the number of NG108-15 found on medium fibres (274.43 ± 25.36) was higher than that measured on small fibres (191.00 ± 9.50 , $^*P < 0.05$). The resulting number of neuronal cells found in medium and large fibre groups was significantly higher than those measured on the control substrates; PHA blend ($^{**}P < 0.05$). Significant differences were also found in the number of neuronal cells grown on the PHB blend (171.00 ± 2.65 , $^*P < 0.05$) and PCL (102.00 ± 27.13 $^{**}P < 0.05$) with respect to glass (16.67 ± 7.04). Figure 5.23 shows the number of neuronal cells grown on all substrates in co-culture with RN22 cells vs. the number

of neuronal cells grown on all the substrates without RN22 cells. Interestingly, statistical analysis showed that the number of neuronal cells grown on medium fibres was significantly higher when these cells were grown in co-culture with RN22 cells (274.43 ± 25.36 , $\blacksquare P < 0.05$) compared to the number of NG108-15 grown on their own (125.33 ± 2.40 , $\blacksquare P < 0.05$). Similarly, the number of neuronal cells grown on large fibres (225.6 ± 24.85 , $2\text{square}P < 0.05$) increased when they were grown with RN22 cells (423.25 ± 16.90 , $\blacksquare\blacksquare P < 0.05$).

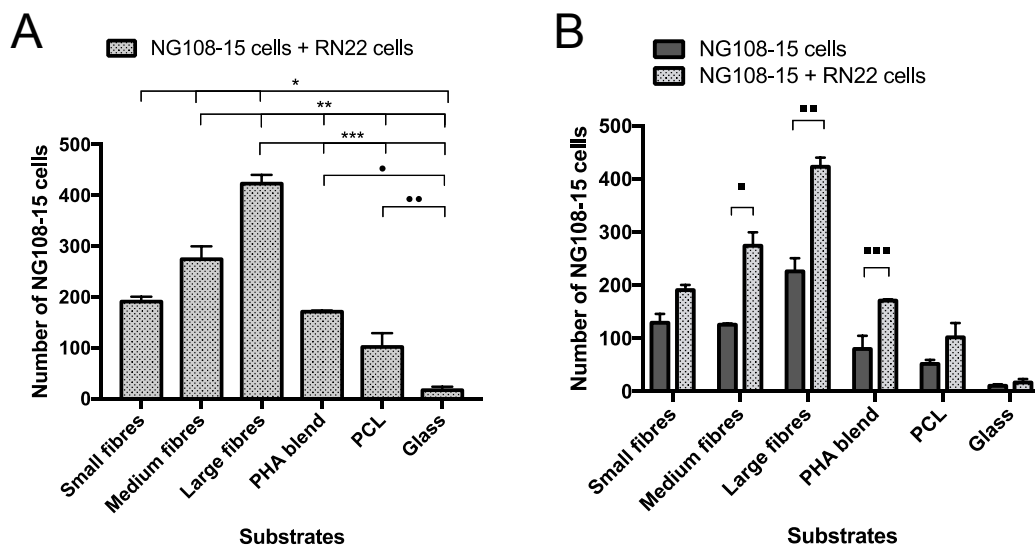


Figure 5.23 Differentiated cells NG108-15 cells in co-culture with RN22 cells. (A) Number of differentiated neuronal cells grown on fibres with varying diameters, PHA blend film, PCL film and glass. Number of differentiated neuronal cells on the fibres increased as the fibre diameter increased. (B) Comparison of differentiated neuronal cells grown in all the substrates individually and in the presence of RN22 cells (mean \pm SEM, $n = 9$ independent experiments, $P < 0.05$).

The number of neuronal cells measured on the P(3HB) blend control (79.88 ± 24.49 , $\blacksquare P < 0.05$) were also significantly different when grown along with RN22 (102.00 ± 27.13 , $\blacksquare\blacksquare P < 0.05$). No significant increments in the number of neuronal cells were found when co-cultured with RN22 cells on small fibres (129.13 ± 16.58 vs. 191.00 ± 9.50), PCL ($51.25 \pm 7.87 \pm 102.00 \pm 27.13$) and glass ($10.13 \pm 2.96 \pm 16.67 \pm 7.04$).

5.3 DISCUSSION

This investigation shows that the development of a 3D scaffold consisting of aligned microfibers results in the alignment of neuronal cell growth either, individually or in co-culture with RN22 cells. A range of PHA blends and neat PHAs were used as the base material for the manufacturing of the fibres with varying diameters; P(3HO), 75:25 P(3HO)/P(3HB) blend, 50:50 25 P(3HO)/P(3HB) blend, 25:75 P(3HO)/P(3HB) blend and P(3HB). Since 25:75 P(3HO)/P(3HB) blends had previously shown to display superior biocompatibility with neuronal NG108-15 cells compared to the other blends and neat PHAs, this blend was chosen for the fabrication of microfibers to be used for the lumen modification of NGCs. Several fibre diameters were produced using 25:75 P(3HO)/P(3HB) blends by electrospinning in order to assess the effect of the fibre diameter on the response of neuronal cells grown either individually or in the presence of RN22 Schwann cells.

As cells are organized in a three dimensional organization in natural tissues, 3D cultures provide an effective approach to develop a functional construct that mimic the natural architecture of the cell environment. In their native environment, the majority of cells are surrounded by extracellular matrix and other cells in a 3D fashion. Three dimensional scaffolds should be able to provide physical cues that promote topographic stimuli to trigger cell adhesion, growth and differentiation. Also, the spatial distribution of the scaffold should be designed to permit the interchange of vital nutrients and gases with the external environment. Development of three dimensional cultures is rapidly progressing as they mimic more accurately the native environment of cells compared to the two dimensional cultures. Drug discovery research has driven the majority of innovations in 3D culture systems over the past five years (Edmonson *et al.*, 2014). Also, tissue engineering, cancer and stem cell research have adopted and adapted 3D cultures methods to obtain more predictable *in vivo* data. It has been shown that cell responses to 2D and 3D environments are different. Focal adhesion structures, proliferation, population, differentiation and gene and protein profiles have been shown to be different for the same cell type when grown on a 3D scaffold when compared to that on a 2D environment (Sun *et al.*, 2007). In fact, it has been shown that cells in the 3D culture environment differ morphologically and physiologically from cells grown in a 2D culture environment (Edmonson *et al.*, 2014). Three dimensional cultures have been used to study more than 380 cell lines until date (Ravi *et al.*, 2015). However, the majority of cell studies are still based on the use of 2D cultures using flat and rigid substrates, which considerably differ from the native environment of the cells. As a result, it has been shown that 2D cell culture assays can provide misleading and non-predictive data for *in vivo* cell behavior.

Three dimensional cultures influence the signal transduction by affecting the spatial organization of the cell surface receptors involved in interaction with cells. This will ultimately provoke a specific gene expression profile, which will be expressed in a particular cell behavior (Edmonson *et al.*, 2014).

In spite of the fact that limitations of 2D cultures are well known, only few 3D models have been developed for nerve regeneration research. A reduced number of studies are based on the use of co-cultures models using natural polymers to investigate peripheral nerve repair with the ultimate aim of manufacturing NGCs. Several scaffolds have been developed for peripheral nerve regeneration research including porous matrices, random fibres and hydrogels (Table 1.2 and 1.3, Chapter 1). However, only few studies have described the use of aligned fibres using more than one cell type (Wang *et al.*, 2010; Daud *et al.*, 2012). In the majority of the studies aligned fibres are used and have focused on the use of a single cell type such as primary neurons extracted from dorsal root ganglia (Corey *et al.*, 2017), PC12 cells (Yao *et al.*, 2009) and primary human Schwann cells isolated from sciatic nerves of human fetuses (Chew *et al.*, 2008).

Previous studies have shown that the diameter of fibres can affect cell growth and functions not only in neuronal cells but also in different cell types such as human dermal fibroblasts (Liu *et al.*, 2009) and osteoblastic cells (Badami *et al.*, 2009). In the case of peripheral nerve repair, it still not clear whether nano-fibres or micro-fibres support better nerve regeneration. Some researchers argue that nano-fibres should be better scaffolds because their dimensions and architecture are closer to the native structure of the extracellular matrix of neurons. Nevertheless, comparative studies are not conclusive and have shown that despite the resemblance of nano-fibres to the ECM of neurons, they have not displayed a satisfactory outcome. In fact, Yao *et al.* (2009) fabricated PLLA fibres of varying diameters and found that neurite outgrowth and cell migration were inhibited when fibers of 200 nm diameter were used. Conversely, Wen and Tresco, 2005 found good alignment and outgrowth of neurites on micro-fibres with diameters ranging from 30 μm (comparable to cellular size) and below (5 μm). However, Schwann cell migration and neurite outgrowth were inhibited when the diameter of the micro-fibres was greater than 30 μm (Wen and Tresco, 2005).

In this Chapter, highly aligned and uniform fibres with varying diameters were successfully fabricated by controlling electrospinning parameters summarized in Table 5.3. In a preliminary study (Fig. 5.8), the effect of fibers on the growth of neuronal cells NG108-15 was investigated by live/dead cell test. Cell migration observed on the electrospun fibres showed directional alignment in accordance with the direction of the fibres. The distribution of cells on the electrospun fibres had a more uniform arrangement when compared with that on the 25:75 P(3HO)/P(3HB) blend film's surface. This finding agreed with previous studies in

which electrospun fibres have shown to affect cell proliferation, differentiation and migration (Daud *et al.*, 2012). Additionally, any cytotoxic effect was found when neuronal cells were grown in any of the studied substrates. Thereafter, the correlation between 25:75 P(3HO)/P(3HB) micro-fibres diameter and neuronal growth under two conditions; individually and in co-culture with RN22 Schwann cells were evaluated. This was investigated using two types of cell staining; live/dead cell test and anti-beta tubulin immunolabelling. Results displayed from both assays revealed that all 25:75 P(3HO)/P(3HB) blend fibre groups were able not only to support growth but also to guide aligned distribution of neuronal cells when grown individually and in the presence of RN22 Schwann cells. All the substrates, including the controls were found to support neurite outgrowth. Although the counting of neuritebearing cells was not possible, a more complex multi-cellular organization was observed in the fibre scaffolds (Fig. 5.14).

Results revealed a direct correlation between fibre diameter and neuronal growth and differentiation. Although neuronal cell viability was similar for all the substrates (approximately 99%) except on glass, large fibres supported the highest number of live neuronal cells grown individually compared to the rest of substrates. However, no significant difference was found between the number of live neuronal cells grown on small fibres and medium fibres. A similar outcome was found when neuronal cell differentiation was assessed in the single cell type culture. The greatest number of neuronal cells was displayed by large fibres while no significant difference was found between small and medium fibres (Fig.5.13). Interestingly, when neuronal cells were grown in co-culture with RN22 Schwann cells, the number of NG108-15 cells increased as the fibre diameter increased (Fig.5.23).

Although RN22 cells were scarcely detected, statistical analysis showed significant increments in the number of neuronal cells NG108-15 on the three substrates when grown in co-culture with this Schwann cell line (Fig. 5.22 B). The number of NG108-15 cells increased significantly on medium fibres, large fibres and PHA blend film when co-cultured with RN22 cells. These findings suggest that RN22 cells are able to significantly enhance neuronal cell growth. This could be due to the secretion of a combination of neurotrophic factors (e.g. NGF and BDNF) from RN22 cells to the culture media and these could have been metabolized by neuronal NG108-15 cells.

Chapter 6
Fabrication, chemical and biological
characterization of 25:75 P(3HO)/P(3HB)
blend/BGs composites

6 FABRICATION, CHEMICAL AND BIOLOGICAL CHARACTERIZATION OF OF 25:75 P(3HO)/P(3HB) BLEND/BGs COMPOSITES

6.1 INTRODUCTION

After injury, peripheral nerves are able to regenerate spontaneously as a result of the action of Schwann cells that promote a favorable environment for axonal growth. However, the regeneration and the recovery of nerve function depends on the injury gap length and the type of lesion. If the continuity of the endoneurial tubes is preserved, axonal regeneration is likely to be successful. In contrast, when perineurium and endoneurium are compromised, or when the nerve is transected, nerve regeneration is impeded and surgical intervention is required. For short gaps (less than 3 cm), suturing the two stumps (i.e., end-to-end suture) is a suitable and common method to bridge the gaps. On the other hand, for large gaps (more than 3 cm) implantation of an autologous nerve graft is the gold standard procedure (Novajra *et al.*, 2014). However, autografting may cause additional surgery, loss of nerve function, donor site morbidity and scar tissue formation. NGCs are a promising alternative to autografting, which prevent additional surgical intervention required to harvest autologous nerves. Furthermore, since fewer epineurial sutures are needed, less surgical trauma is generated. Moreover, fibrous scar tissue infiltration is reduced whereas accumulation of soluble factors is maximized. Also, the use of NGCs avoids mismatched fascicles between the injured nerve and the autograft (Novajra *et al.*, 2014). There are several commercial NGCs made from natural and synthetic materials, such as PLCL, PGA, PVA, COLI and EMC. Although their use is limited to short nerve gaps (max. 3 cm), their regeneration outcome is comparable with that obtained using autograft when the gap length is shorter than 3 cm. For larger gaps, nerve repair using autografting is superior compared to that displayed when NGCs are used. The major drawback when the nerve gaps are large is a deficient formation of fibrin cables between the stumps, which restricts the formation of bands of Büngner and migration of Schwann cells. As a consequence, the topographical guidance and trophic structures required for the growth of regenerating axons from the proximal stump are impeded. Also, a lack of available neurotrophic factors has been observed (Novajra *et al.*, 2014).

The majority of implants used for peripheral nerve regeneration have been made from natural and synthetic polymeric materials. Nevertheless, the use of bioactive glasses (BGs) for applications in nerve tissue engineering and specially the use of fibrous BGs has been explored in the last five years. Bioactive glasses have been extensively investigated and used in biological applications since Professor Larry Hench discovered their biological reactivity in

the late 60s (Hench, 1970). Bioactive glasses have been widely used in bone tissue regeneration since they have the ability to promote mesenchymal stem cell differentiation, osteointegration and enhanced the release of growth factors. It has been shown that BG's dissolution products have an angiogenic effect in both *in vitro* and *in vivo* experiments. Angiogenesis is a fundamental process for tissue engineering, which involves migration, growth, and differentiation of endothelial cells. This process is orchestrated by mechanical stress and chemical cues produced by surrounding tissues such as extracellular matrix proteins, growth factors and other signaling proteins (Miguez-Pacheco, 2015). Direct stimulation of fibroblast cells with BG's dissolution products triggers the production of growth factors such as vascular endothelial growth factor (VEGF) and basic fibroblastic growth factor (bFGF) (Gorustovich *et al.*, 2010).

Silicate-based BGs such as Bioglass® 45S5 are well known for their properties to support regeneration of hard tissue and are broadly used as base material for the fabrication of implants. The biological requirements for a particular tissue can be suited by adapting the physicochemical properties of BGs. Such properties can be tailored by altering the chemical composition of the bioactive glass. For instance, when the amount of borate within the borate-based BG is increased, the BG biodegradation rate increases, which is more suitable for soft tissue remodeling (Marquart *et al.*, 2014). As a consequence, the use of BGs has recently disseminated and different compositions have been developed to embrace a wider spectra of tissue regeneration including soft tissues such as intestinal epithelium, skin and peripheral nerves. Also, the addition of silver within BGs have shown to display anti-microbial properties (Blaker *et al.*, 2004). Bioglass® 45S5 has demonstrated to enhance production of bFGF in epithelial cells, which can be highly beneficial for intestinal epithelium regeneration (Moosvi and Day, 2009). Also, the increased production of VEGF and bFGF in fibroblasts when cultured with Bioglass® 45S5 have shown its ability to stimulate angiogenesis (Day, 2005 and Keshaw *et al.*, 2005). Furthermore, BG 13-93 B3 has been investigated for wound healing and have shown regenerating effects such as notable wound size reduction and recovery of sensation in the scar area (Jung, 2012).

Various types of BGs have shown to have regenerating properties in neuronal context. For example, Bioglass® 45S5 fibres are not only compatible with rat Schwann cells and fibroblasts *in vitro* but also have demonstrated to promote axonal regeneration *in vivo* (Bunting *et al.*, 2005). Also, phosphate glass fibres have demonstrated to be biocompatible with Neonatal Olfactory Bulb Ensheathing Cell Line (NOBEC) and Dorsal Root Ganglia (DRG) neurons. Additionally, these fibres provide a directional cue for growing axons (Vitale-Brovarone *et al.*, 2012). In another study, aligned phosphate glass fibres were used for the manufacturing of NGCs and showed good biocompatibility with adult dorsal root ganglion

(DRG) neurons. Furthermore, these fibres promoted neurite outgrowth when NGCs were implanted in rat sciatic nerve (Kim *et al.*, 2012). Bioactive borate glass scaffolds have also shown not only to be biocompatible with embryonic chick dorsal root ganglia (DRG) but also shown to support neurite extension (Marquardt *et al.*, 2014). Resorbable phosphate glass hollow fibers filled with hydrogel were used for the fabrication of NGCs and were found to be biocompatible with neonatal olfactory bulb ensheathing cell line (NOBEC) (Novajira *et al.*, 2014). Mohammadkhah *et al.* (2015) fabricated composites made using different BGs compositions consisting of 50 wt.% PCL combined with 50 wt.% 13–93 B3 borate glass; 50 wt.% 45S5 silicate glass and with a blend of 25 wt.% 13–93 B3 and 25 wt.% 45S5 silicate glass. The resulting composites were shown to be compatible with dorsal root ganglia isolated from embryonic chicks and had a positive effect on neurite outgrowth (Mohammadkhah *et al.*, 2015).

In this Chapter, biocompatibility and neuron regenerating properties of various BG/PHA blend composites were assessed in order to study their suitability for peripheral nerve tissue applications. BG/PHA blend composites were fabricated using Bioglass® 45S5 and 1393, named BG1 and BG2 respectively along with 25:75 P(3HO)/P(3HB) blend produced in a previous study (Lizarraga-Valderrama, 2015, Chapter 4). Bioactive glasses Bioglass® 45S5 and 1393 were chosen because of their proven bioactivity, ability to support cell proliferation and to form porous constructs. Furthermore, they are approved for *in vivo* use in humans in United States by the FDA. Additionally, 25:75 P(3HO)/P(3HB) blend has been previously proved to support neuronal growth, differentiation and neurite extension of NG108-15 cells (Lizarraga-Valderrama *et al.*, 2015). Different proportions of each BG (0.5, 1.0 and 2.5 wt %) were used to determine the BG concentration that results in superior neuronal growth and differentiation of NG108-15 in single culture and in co-culture system with Schwannoma RN22 cells.

6.2 RESULTS

6.2.1 FABRICATION OF PHA BLEND/BGS COMPOSITES

PHA blend/BGs composites were fabricated with varying amounts of two BGs, Bioglass® 4TS5 (BG1) and BG 1393 (BG2) in order to evaluate their cytotoxicity effect and to determine the appropriate BG concentration for optimal neuronal growth and differentiation. Composites of 25:75 P(3HO)/P(3HB) blend along with each of the BGs Bioglass® 4TS5 and 1393 named BG1 and BG2 respectively, were prepared with different concentrations of each BG (0.5, 1.0 and 2.5 wt %).

6.2 Characterization of the PHA blend/BGs composites

6.2.2 SCANNING ELECTRON MICROSCOPY OF PHA BLEND/BG COMPOSITES

Scanning electron micrographs of PHA blend (25/75 P(3HO)/P(3HB) (5 wt %)/BG composites were used in order to compare their surface morphology. The PHA blend/BG1 (0.5wt %) (Fig. 6.1A-B) showed an intricate porous network in which the average size of the pores were $5.4 \pm 0.7 \mu\text{m}$, ranging from 2 - 15 μm . The PHA blend/BG1 (1wt %) (Fig. 6.1 C-D) exhibited low porosity with respect to the PHA blend/BG1 (0.5wt %) which had average pore size of $3.7 \pm 1.1 \mu\text{m}$. PHA blend/BG1 (2.5 wt %) (Fig. 6.1 E and F) displayed a porous structure similar to that of the PHA blend/BG1 (0.5wt %) with pore size of $3.5 \pm 0.3 \mu\text{m}$. On the other hand, PHA blend/BG2 (0.5wt %) presented an irregular porous surface with the presence of protrusions. This composite displayed the smallest pores ($0.9 \pm 0.1 \mu\text{m}$) when compared to the rest of substrates. PHA blend/BG2 (1wt %) and PHA blend/BG2 (2.5wt %) (Fig. 6.2 E and F) had similar porous surfaces with an average pore size of 2.3 ± 0.1 and $2.1 \pm 0.1 \mu\text{m}$ respectively. The PHA blend film displayed a uniformly distributed porous surface with an average pore size of $1.6 \pm 0.2 \mu\text{m}$. The PCL control film exhibited larger pore size with an average diameter of $36.1 \pm 3.5 \mu\text{m}$. As it can be observed in Table 6.1, no relationship was found between the amount of BG and the pore size. However, the pore sizes obtained in all the BG1 composites were larger than the pore sizes observed in BG2 composites (Table 6.1).

Table 6.1 Porous size of PHA blend/BGs composites and controls

Substrates	Porous size (μm)
PHA blend/BG1 (0.5wt %)	5.4 ± 0.7
PHA blend/BG1 (1wt %)	3.7 ± 1.1
PHA blend/BG1 (2.5wt %)	3.5 ± 0.3
PHA blend/BG2 (0.5wt %)	0.9 ± 0.1
PHA blend/BG2 (1wt %)	2.3 ± 0.1
PHA blend/BG2 (2.5wt %)	2.1 ± 0.1
PHA blend	1.6 ± 0.2
PCL	36.1 ± 3.5

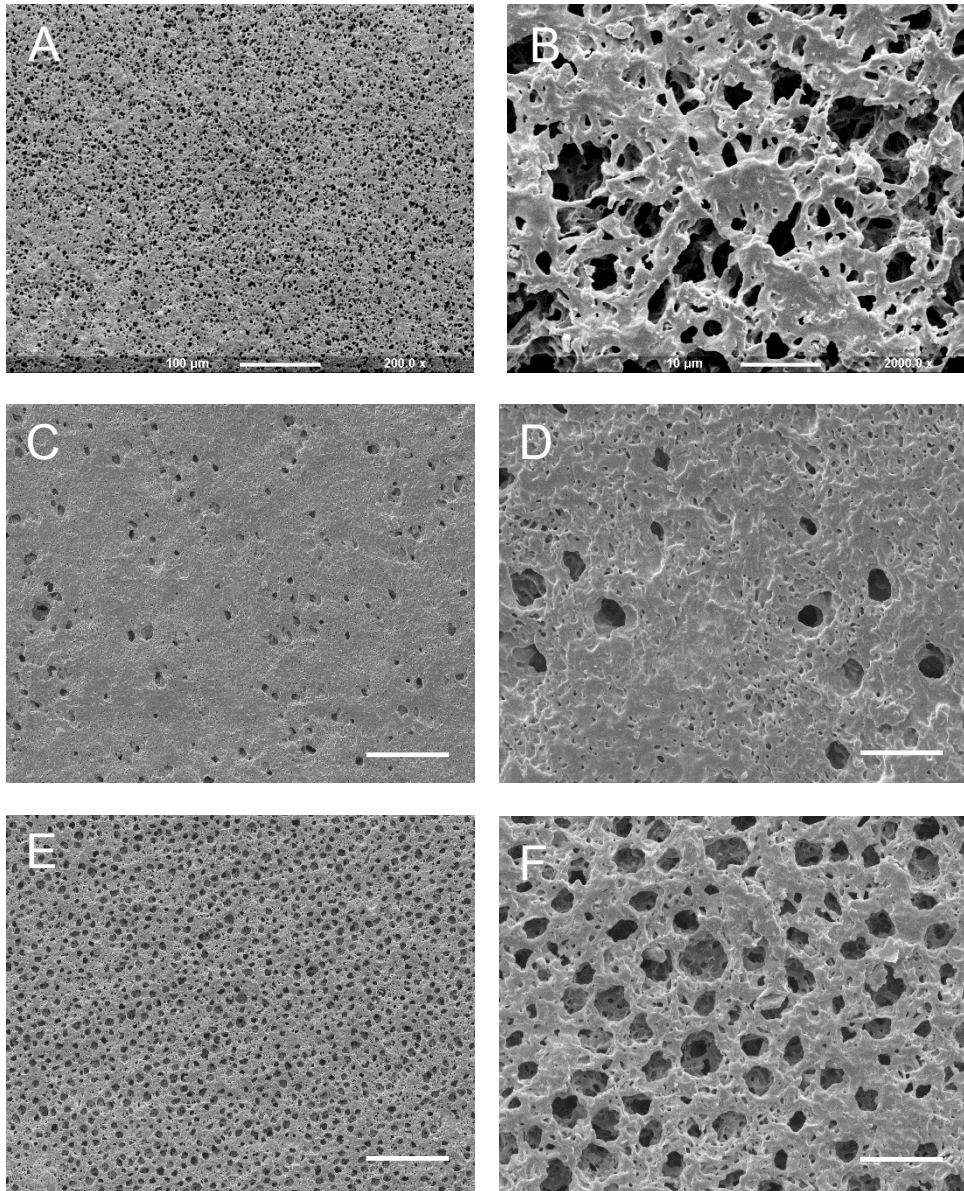


Figure 6.1. Scanning electron microscopy of PHA blend/BG1 composites. (A, B) PHA blend/BG1 (0.5 wt %) at 200X and 2000X respectively. PHA blend/BG1 (0.5wt %) showed an intricate porous network with pores of $5.44 \pm 0.71 \mu\text{m}$ of average diameter ranging from 2 - 15 μm . (C, D) PHA blend/BG1 (1 wt %) at 200X and 2000X respectively. E, F) PHA blend/BG1 (2.5 wt %) at 200X and 2000X respectively. Scale bar (A, C and E) = 100 μm ; (B, D and F) = 10 μm .

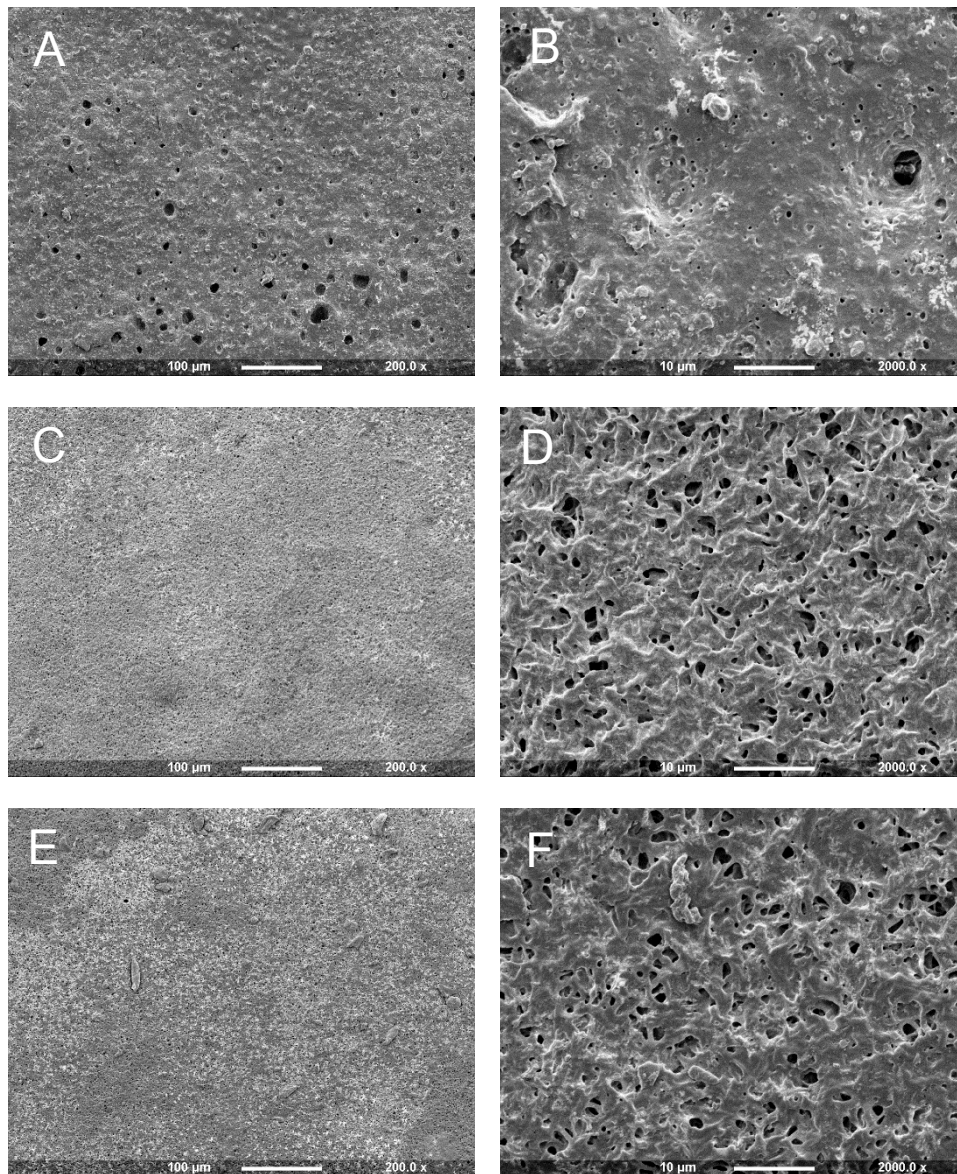


Figure 6.2. Scanning electron microscopy of PHA blend/BG2 composites. (A, B) PHA blend/BG2 (0.5 wt %) at 200X and 2000X respectively. (C, D) PHA blend/BG2 (1 wt %) at 200X and 2000X respectively, (E, F) PHA blend/BG2 (2.5 wt %) at X200 and 2000X respectively. Scale bar (A, C and E) = 100 µm; (B, D and F) = 10 µm.

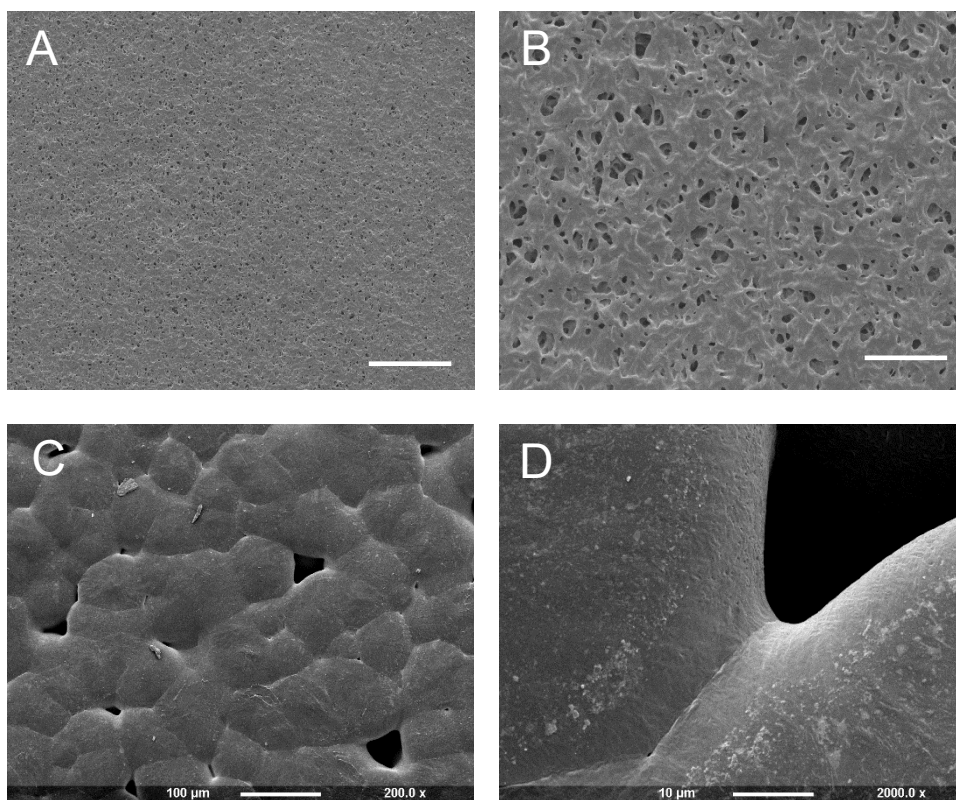


Figure 6.3. Scanning electron microscopy of PHA blend and PCL film. (A, B) PHA blend at 200X and 2000X respectively. (C, D) PCL at 200X and 2000X respectively. Scale bar (A) = 100 μm ; (B) = 10 μm .

6.2.3 PROFILOMETRIC SURFACE ANALYSIS OF PHA BLEND/BG COMPOSITES

The root mean square roughness (R_q) of the PHA blend/BG composites was measured using a laser profilometer and results are shown in Table 6.2 and Figure 6.4. The Root Mean Square (RMS) roughness (R_q) is the root mean square average of the profile height deviations from the mean line. The roughness found for PHA blend/BG1 (0.5 wt %) was not significantly different to that of PHA blend/BG1 (2.5wt %) and the glass control ($0.4 \pm 0.00 \mu\text{m}$, $0.4 \pm 0.00 \mu\text{m}$, $0.3 \pm 0.0 \mu\text{m}$ respectively, $p < 0.05$). The glass substrate displayed the lowest roughness compared to all the substrates ($0.3 \pm 0.0 \mu\text{m}$). The roughness of PHA blend/BG1 (1.0 wt %) ($1.0 \pm 0.1 \mu\text{m}$) was not significantly different to those found in PHA blend/BG2 and the PHA blend ($1.2 \pm 0.1 \mu\text{m}$, $1.3 \pm 0.0 \mu\text{m}$, $p > 0.05$). However, the R_q value of the PHA blend/BG1 (1.0 wt %) ($1.0 \pm 0.1 \mu\text{m}$) was significantly different to those measured for PHA blend/BG2 (0.5wt %) and PHA blend/BG2 (2.5wt %) ($2.6 \pm 0.1 \mu\text{m}$, $2.3 \pm 0.0 \mu\text{m}$, $p < 0.05$). The PHA blend/BG composites with the highest roughness were PHA blend/BG2 (0.5wt %) ($2.6 \pm 0.1 \mu\text{m}$) and PHA blend/BG2 (2.5wt %) ($2.3 \pm 0.0 \mu\text{m}$). The PCL substrate showed the highest roughness when compared to all other substrates ($7.2 \pm 0.1 \mu\text{m}$).

Table 6.2 Roughness of PHA blend/BGs composites and controls

Substrates	Roughness Rq (μm)
PHA blend/BG1 (0.5wt %)	0.4 ± 0.0
PHA blend/BG1 (1wt %)	1.0 ± 0.1
PHA blend/BG1 (2.5wt %)	0.4 ± 0.0
PHA blend/BG2 (0.5wt %)	2.6 ± 0.1
PHA blend/BG2 (1wt %)	1.2 ± 0.1
PHA blend/BG2 (2.5wt %)	2.3 ± 0.0
PHA blend	1.3 ± 0.0
PCL	7.2 ± 0.1
Glass	0.3 ± 0.0

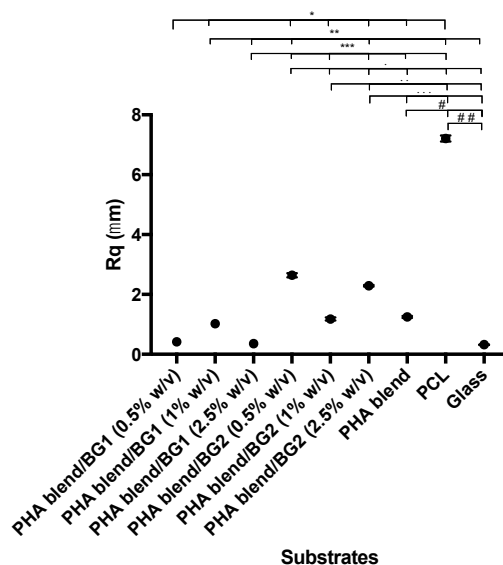


Figure 6.4. Root mean square roughness (Rq) of PHA blend/BG composites and controls.

6.2.4 DETERMINATION OF WATER CONTACT ANGLE OF PHA BLEND/BG COMPOSITES

The water contact angle of PHA blend/BG composites (Table 6.2, Fig. 6.5) decreased as the content of BG increased. The wettability found for PHA blend/BG1 (0.5wt %) was significantly different to those found on PHA blend/BG1 (1wt %) and PHA blend/BG1 (2.5wt %) ($95.7 \pm 0.6^\circ$, $65.7 \pm 0.4^\circ$, $65.3 \pm 0.5^\circ$, * $p < 0.05$). However, no significant differences were found between PHA blend/BG1 (1wt %) and PHA blend/BG1 (2.5wt %) ($65.7 \pm 0.4^\circ$, $65.3 \pm 0.5^\circ$, $p > 0.05$). Statistical analysis revealed significant differences between the three composites of PHA blend/BG2; PHA blend/BG2 (0.5wt %) ($93.5 \pm 0.8^\circ$, * $p < 0.05$), PHA blend/BG2 (1wt %) ($78.8^\circ \pm 0.2$, * $p < 0.05$) and PHA blend/BG2 (2.5wt %) ($67.0 \pm 0.3^\circ$, * $p < 0.05$). The PHA blend wettability ($61.9 \pm 0.2^\circ$) was found to be significantly different to those of displayed by PHA blend/BG1 (0.5wt %) (95.7 ± 0.6 , * $p < 0.05$), PHA blend/BG2 (0.5wt %)

($93.5 \pm 0.8^\circ$, $^*p < 0.05$), PHA blend/BG2 (1wt %) ($78.8^\circ \pm 0.2$, $^{**}p < 0.05$) and PHA blend/BG2 (2.5wt %) ($67.0 \pm 0.3^\circ$, $^{***}p < 0.05$). On the other hand, no significant differences were found between PHA blend with respect to PHA blend/BG1 (1wt %) ($65.69 \pm 0.41^\circ$, $^{**}p > 0.05$) nor to PHA blend/BG1 (2.5wt %) ($65.3 \pm 0.5^\circ$, $^{***}p > 0.05$) (Fig.6.5). The majority of the studied substrates (PHA blend/BG1 (1wt %), PHA blend/BG1 (2.5wt %), PHA blend/BG2 (1wt %), PHA blend/BG2 (2.5wt %), PHA blend and glass) displayed water contact angles lower than 90° , and hence were hydrophilic in nature. By contrast, the composites PHA blend/BG1 (0.5 wt %) and PHA blend/BG2 (0.5 wt %) were found to be hydrophobic in nature.

Table 6.3 Water contact angles of PHA blend/BG composites and controls

Substrates	Water contact angle ($^\circ$)
PHA blend/BG1 (0.5wt %)	95.7 ± 0.6
PHA blend/BG1 (1wt %)	65.7 ± 1.2
PHA blend/BG1 (2.5wt %)	65.3 ± 1.4
PHA blend/BG2 (0.5wt %)	93.5 ± 0.8
PHA blend/BG2 (1wt %)	78.8 ± 0.7
PHA blend/BG2 (2.5wt %)	67.0 ± 0.7
PHA blend	61.9 ± 0.7
PCL	81.9 ± 1.3
Glass	23.2 ± 0.5

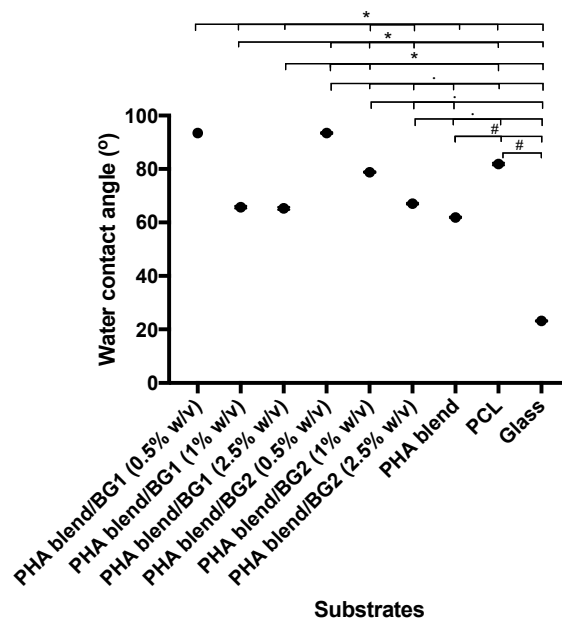


Figure 6.5. Water contact angles of PHA blend/BG composites and controls. As the content of BG increased, the wettability of PHA blend/BG composites increased.

6.2.4 STATIC TENSILE TEST OF THE FILMS

Static tensile test was used to measure the mechanical properties of the BG composites. Young's Modulus (E values), tensile strength and elongation at break of the different films are shown in Table 6.3.

The majority of E values (Table 6.3) of PHA/BG composites and controls were significantly different when compared against each other (p -value < 0.05) excepting for PHA blend/BG1 (0.5wt %) vs PHA blend/BG1 (2.5wt %); PHA blend/BG1 (0.5wt %) vs PCL; PHA blend/BG1 (1wt %) vs PHA blend/BG2 (1wt %); PHA blend/BG1 (2.5wt %) vs PCL (385.6 ± 25.8 MPa); PHA blend/BG2 (0.5wt %) vs PHA blend/BG2 (1wt %); and PHA blend/BG2 (2.5wt %) vs PHA blend.

Similarly, the majority of the tensile strength values of PHA blend/BG composites and controls were significantly different when compared against each other. However, no significant differences were found when the following substrates were compared: PHA blend/BG1 (0.5wt %) vs PHA blend/BG1 (2.5wt %); PHA blend/BG1 (1wt %) vs PHA blend/BG2 (1wt %); PHA blend/BG1 (1wt %) vs PCL; PHA blend/BG2 (0.5wt %) vs PHA blend/BG2 (1wt %); PHA blend/BG2 (0.5wt %) vs PHA blend/BG2 (2.5wt %); PHA blend/BG2 (0.5wt %) vs PHA blend; PHA blend/BG2 (0.5wt %) vs PCL; PHA blend/BG2 (1wt %) vs PCL and PHA blend/BG2 (2.5wt %) vs PHA blend. All the values of percentage strain of PHA blend/BG composites were significantly different to PCL percentage strain (p -value < 0.05). When the percentage strain values of the blends were compared against each other none significant difference was found.

Table 6.4 Mechanical analysis of the P(3HO)/P(3HB) films

Substrates	E (MPa)	Tensile strength (MPa)	Percentage strain
PHA blend/BG1 (0.5wt %)	399.8 ± 6.6	5.8 ± 0.0	35.4 ± 6.4
PHA blend/BG1 (1wt %)	853.6 ± 66.3	10.0 ± 0.6	2.5 ± 0.3
PHA blend/BG1 (2.5wt %)	385.6 ± 25.8	5.1 ± 0.7	2.3 ± 0.5
PHA blend/BG2 (0.5wt %)	1333.3 ± 100.2	16.1 ± 0.7	3.6 ± 1.2
PHA blend/BG2 (1wt %)	1057.4 ± 47.1	12.8 ± 1.4	1.7 ± 0.1
PHA blend/BG2 (2.5wt %)	1731.6 ± 76.4	19.6 ± 0.8	1.7 ± 0.2
PHA blend	1792.6 ± 189.0	19.7 ± 0.3	1.6 ± 0.1
PCL	385.6 ± 25.8	12.6 ± 0.3	123.4 ± 41.4

6.2.4 DIFFERENTIAL SCANNING CALORIMETRY OF COMPOSITES

Differential scanning calorimetry of PHA blend/BG composites was carried out to determine glass transition temperature (T_g), melting temperature (T_m) and specific enthalpy of

fusion (ΔH_f). None of the composites made from BG1 (PHA blend/BG1 (0.5wt %), PHA blend/BG1 (1wt %) and PHA blend/BG1 (2.5wt %) did not display glass transition temperature (Table 6.4). In the other hand, glass transition temperatures (T_g) displayed by PHA blend/BG1 (0.5wt %) (3.1 °C) and PHA blend/BG2 (1wt %) (3.4 °C) were similar to that of PHA blend/BG2 (2.5wt %) (3.1 °C). The melting temperatures (T_m) for all the composites and PHA blend were around 175 °C. The range of enthalpy of formation PHA blend/BG2 (0.5wt %) (65.1/87.2 Kj) and PHA blend/BG2 (2.5wt %) (66.5/90.9 Kj/g) were similar to that of the control PHB blend (65.1/90.9 Kj/g). Specific enthalpy of formation of PHA blend/BG1 (0.5wt %) (59.2/79.3Kj/g) was also in the same range as that of PHA blend/BG2 (1wt %) (60.8/81.8 Kj). The range of specific enthalpy of PHA blend/BG1 (1wt %) (42.0/56.6 Kj/g) and PHA blend/BG1 (2.5wt %) (36.8/50.3 Kj/g) were found to be lowest of all the BG composites.

Table 6.5. Differential scanning calorimetry of PHA blend/BG composites.

Substrates	Glass transition temperature (°C)	Melting temperature (°C)	Specific enthalpy of formation (Kj)
PHA blend/BG1 (0.5wt %)	-	177.6	59.2/79.3
PHA blend/BG1 (1wt %)	-	175.1	42.0/56.6
PHA blend/BG1 (2.5wt %)	-	173.0	36.8/50.3
PHA blend/BG2 (0.5wt %)	3.1	174.6	65.1/87.2
PHA blend/BG2 (1wt %)	3.4	174.3	60.8/81.8
PHA blend/BG2 (2.5wt %)	5.7	174.4	66.5/90.9
PHA blend	3.1	174.6	65.1/90.9
PCL			

6.3 LIVE/DEAD MEASUREMENT OF NG-108-15 NEURONAL CELLS ON PHA BLEND/BG COMPOSITES

The live/dead cell measurement of NG108-15 neuronal cells was carried out on PHA blend/BG composites in order to compare the survival and attachment of the neuronal cells on the different substrates. Figure 6.6 shows representative confocal images of neuronal cells grown on the composites can be observed. Growth and attachment of neuronal cells were observed in all the substrates showing no cytotoxicity effect.

Figure 6.7 A shows the percentage of live cell displayed in all the substrates. The percentages of live cells displayed by the composites PHA blend/BG1 (0.5wt %) (93.4 ± 2.7 %), PHA blend/BG1 (1wt %) (99.4 ± 0.1 %), PHA blend/BG1 (2.5 wt %) (95.5 ± 1.0 %), PHA blend/BG2 (0.5wt %) (98.0 ± 0.6 %), PHA blend/BG2 (1wt %) (96.3 ± 15.3 %), PHA blend/BG2 (2.5wt %) (95.0 ± 1.5 %) and the controls PHB blend film (94.9 ± 0.9 %) and PCL film ($92.4 \pm$

1.6 %) were found to be significantly different to those displayed by glass control (51.1 ± 26.4 %) ($^*P < 0.05$). The percentages of live cells determined for all the composites were similar, which values were found to be in the range of 99.4 ± 0.1 % to 92.4 ± 1.6 %. Significant difference was found between the percentage of live cells of the controls PHB blend film (94.9 ± 0.9 %) and PCL film (92.4 ± 1.6 %) ($^{\#}P < 0.05$).

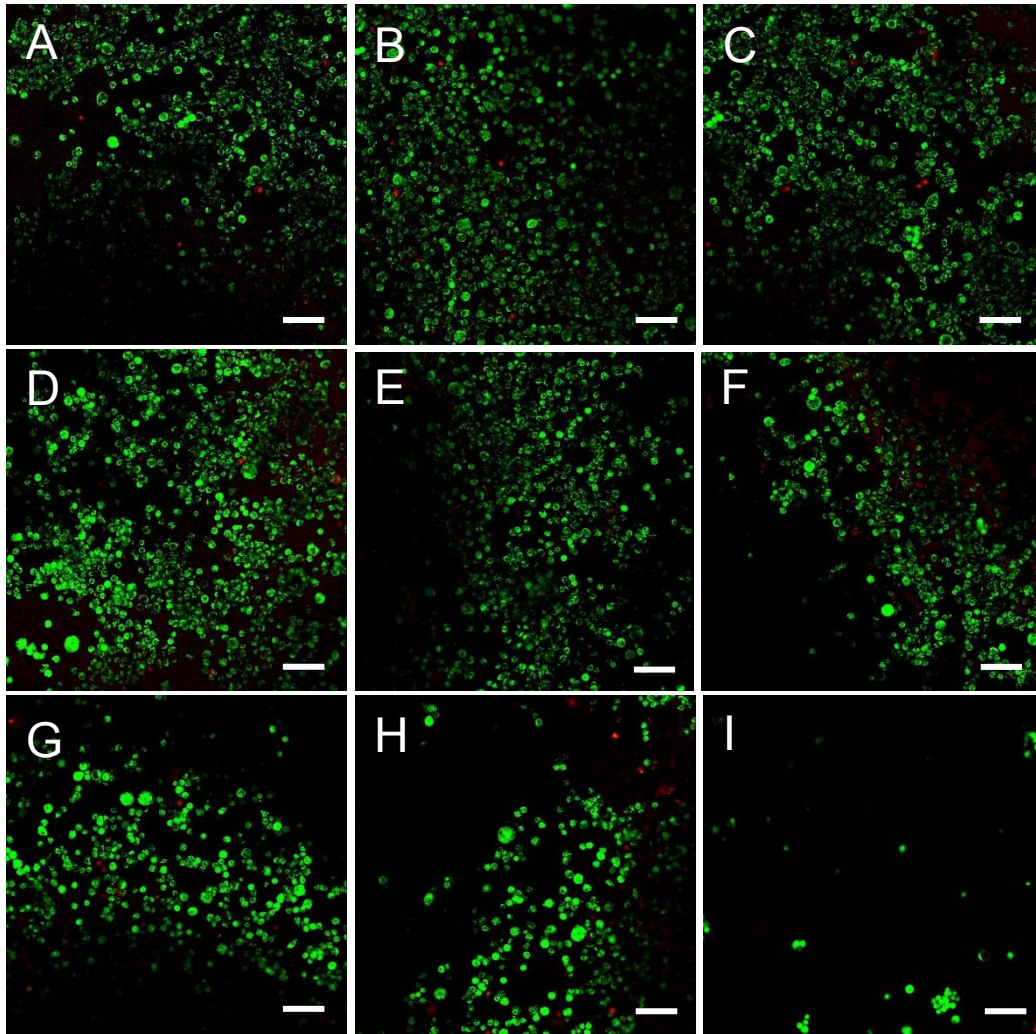


Figure 6.6. Confocal micrographs of NG108-15 neuronal cells labelled with propidium iodide (red) and Syto-9 (green) after four days in culture on P(3HO)/P(3HB)/BG composites and controls PHB blend, PCL and glass. A) PHA blend/BG1 (0.5wt %), B) PHA blend/BG1 (1wt %), C) PHA blend/BG1 (2.5wt %), D) PHA blend/BG2 (0.5wt %), E) PHA blend/BG1 (1wt %), F) PHA blend/BG2 (2.5wt %), G) PHB blend, H) PCL, I) Glass. Scale bar = 50 μ m

Although the comparison of percentage of live cells did not display significant differences, the statistical analysis of the number of neuronal cells grown on all the substrates allowed to detect cell attachment differences between the composites. In figure 6.7 B the number of neuronal cells grown on the different substrates is compared. The composite PHA

blend/BG1 (1wt %) supported the highest number of cells (760.6 ± 55.7 cells) among all the composites which was significantly different when compared to the rest of substrates ($**P < 0.05$). On the other hand, PHA blend/BG1 (1wt %) presented the lowest number of neuronal cells (215 ± 26.89 cells) among all the composites and it was significantly different only when compared to PHA blend/BG1 (1wt %) ($*P < 0.05$). The number of neuronal cells grown on PHA blend/BG1 (2.5 wt %) (317.0 ± 30.5 cells) ($***P < 0.05$) and PHA blend/BG2 (0.5 wt %) (401.33 ± 108.49 cells) ($*P < 0.05$) were significantly different when compared to the glass control (53.2 ± 17.8 cells). The number of cells grown on PHA blend/BG2 (1 wt %) (410.1 ± 68.2 cells) ($**P < 0.05$) was significantly different to the cell number grown on the controls PCL (171.3 ± 38.5) and glass (53.2 ± 17.8 cells). No significant differences were found when the number of neuronal cells grown on PHA blend/BG2 (2.5 wt %) (256.4 ± 44.7 cells), PHA blend (201.9 ± 58.3 cells), PCL (171.3 ± 38.5 cells) and glass (53.2 ± 17.8 cells) were statistically analyzed.

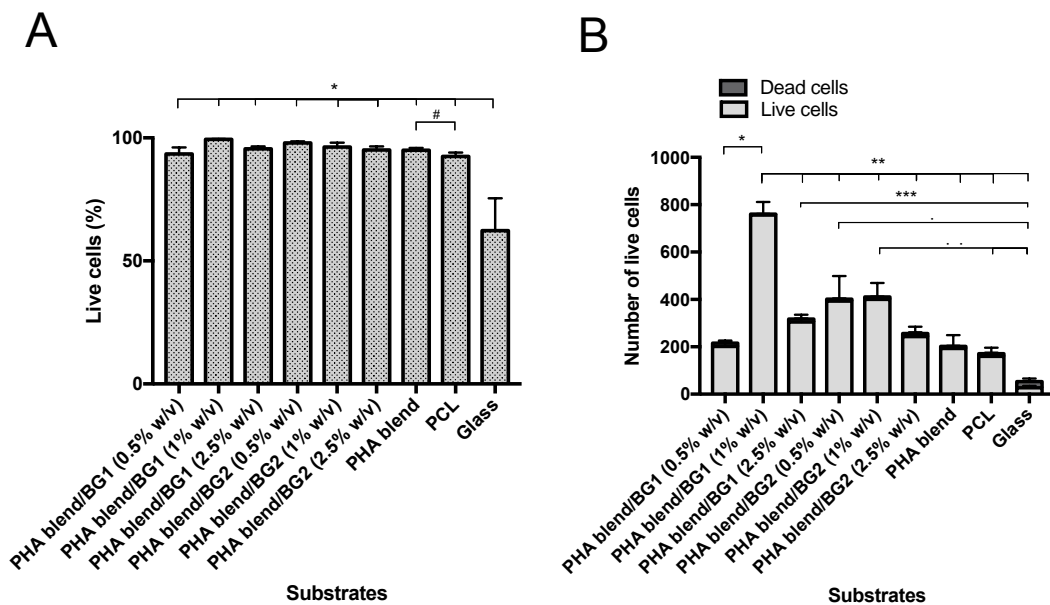


Figure 6.7. Live and dead tests of neuronal cells on PHA blend/BG substrates A) Percentage of live neuronal cells on the PHA blend/BG substrates, PCL and glass (control). B) Number of live cells on P(3HO)/P(3HB)/BG composites, PCL and glass (control). (mean \pm SEM, $n = 9$ independent experiments).

6.4 NEURITE OUTGROWTH ASSESSMENT ON NG108-15 NEURONAL CELL CULTURE GROWN ON PHA BLEND/BG COMPOSITES

NG108-15 neuronal cells were grown on PHA blend/BG composites and immunolabelled for anti- β III-tubulin to study neuronal differentiation and neurite outgrowth. Figures 6.8 (A-I) shows representative micrographs of immunolabelled neuronal cells attached

and grown on all the substrates including the controls. Differentiation was confirmed in all the neuronal cells by a positive reaction with anti- β III-tubulin antibody in all the PHA blend/BG composites; PHA blend/BG1 (0.5wt %) (Fig. 6.8A), PHA blend/BG1 (1wt %) (Fig. 6.8 B), PHA blend/BG1 (2.5wt %) (Fig. 6.8 C), PHA blend/BG2 (0.5wt %) (Fig. 6.7D), PHA blend/BG2 (1wt %) (Fig. 6.8 E), PHA blend/BG2 (2.5wt %) (Fig. 6.8 F) and the controls PHA blend film (Fig. 6.8 G), PCL film (Fig. 6.7 H) and glass (Fig. 6.8 I).

However, more uniformly distributed and higher number of differentiated cells were found on the PHA blend/BG composites (Fig. 6.8 A-F) compared to the controls PCL and glass (Fig. 6.8 H-I). As it can be observed in figures (Fig. 6.8 H-I), cells grown on PCL and glass were grouped in clusters with globular forms.

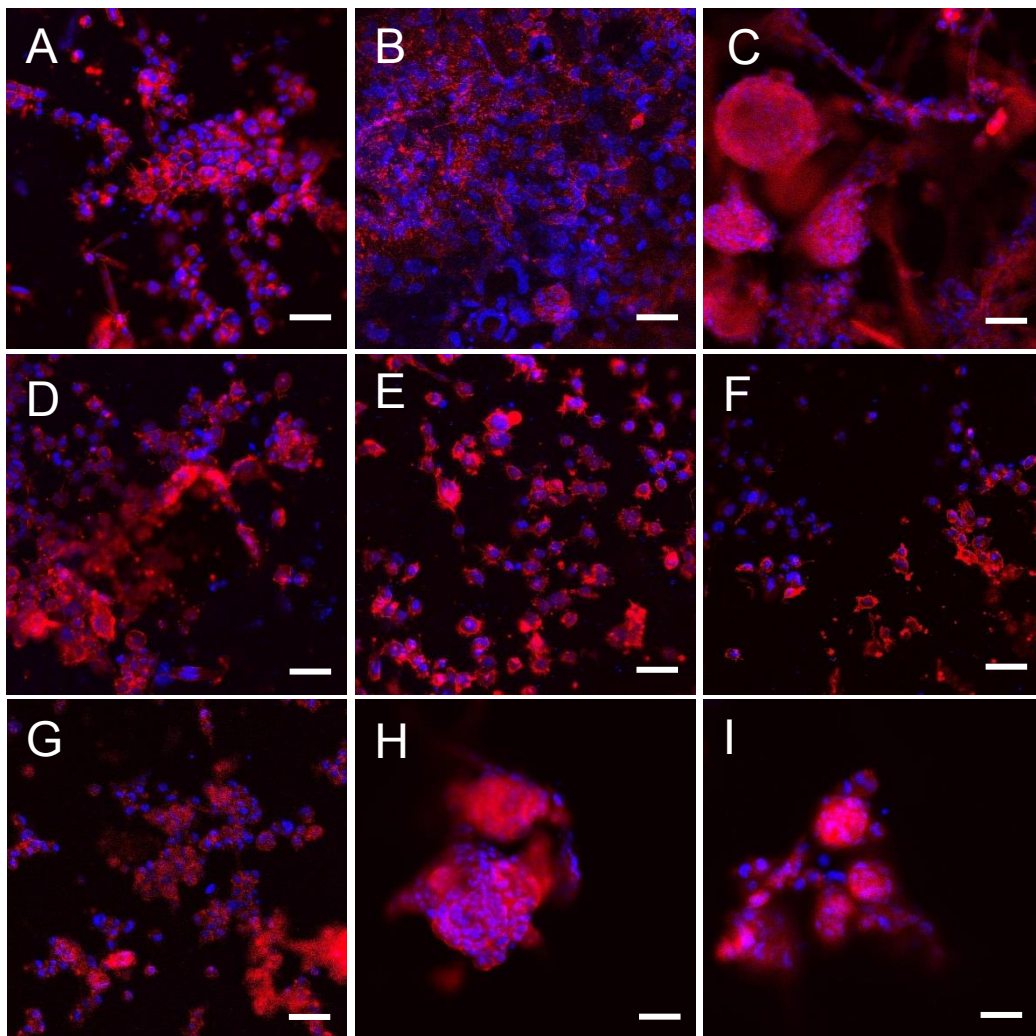


Figure 6.8 Micrographs of NG108-15 neuronal cells immunocytochemically-labelled for beta-III tubulin after 4 days culture on PHA blend composites. A) PHA blend/BG1 (0.5wt %) composite, B) PHA blend/BG1 (1wt %) composite, C) PHA blend/BG1 (2.5wt %) composite, D) PHA blend/BG2 (0.5wt %) composite, E) PHA blend/BG2 (1wt %) composite, F) PHA blend/BG2 (2.5wt %) composite; G) PHB blend, H) PCL, I) Glass. Scale bar = 50 μ m

In the live/dead cell test (Fig. 6.9), the PHA blend/BG1 (1wt %) composite supported the highest number of differentiated neuronal cells (347.5 ± 36.8 cells) in comparison to the rest of the substrates; PHA blend/BG1 (0.5wt %) (247.8 ± 26.4 cells), PHA blend/BG1 (2.5wt %) (299.4 ± 25.4 cells), PHA blend/BG2 (0.5wt %) (227.1 ± 21.7 cells), PHA blend/BG2 (1wt %) (85.7 ± 11.3 cells), PHA blend/BG2 (2.5wt %) (57.0 ± 9.0 cells) and the controls PHA blend film (79.9 ± 23.1), PCL film (51.3 ± 7.4 cells) and glass (10.1 ± 2.8 cells). However, the number of differentiated cells grown on PHA blend/BG1 (1wt %) (347.5 ± 36.8 cells) was not significantly different to that of PHA blend/BG1 (0.5wt %) (227.1 ± 21.7 cells), PHA blend/BG1 (2.5wt %) (299.4 ± 25.4 cells) and PHA blend/BG2 (0.5wt %).

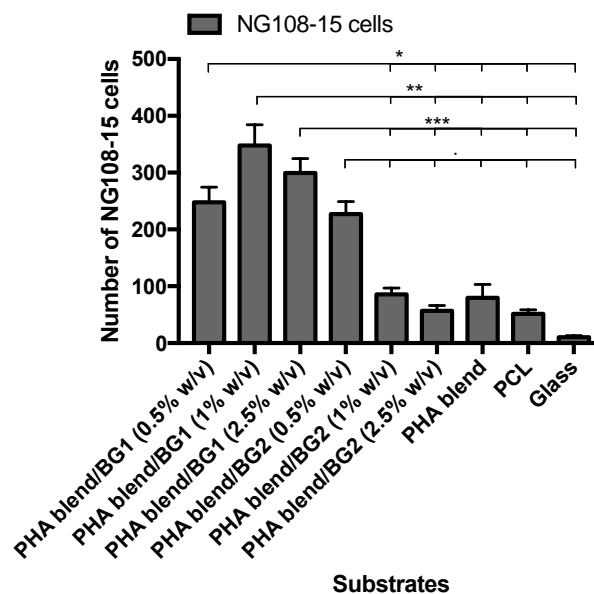


Figure 6.9 Number of differentiated NG108-15 neuronal cells (mean \pm SEM, n = 9 independent experiments)

The number of neuronal cells grown on the composites PHA blend/BG1 (0.5wt %) (227.1 ± 21.7 cells), PHA blend/BG1 (1wt %) (347.5 ± 36.8 cells), PHA blend/BG1 (2.5wt %) (299.4 ± 25.43 cells) and PHA blend/BG2 (0.5wt %) (227.1 ± 21.7 cells), were significantly different to those found on PHA blend/BG2 (1wt %) (85.7 ± 11.3 cells), PHA blend/BG2 (2.5wt %) (57.0 ± 9.0 cells) and the controls PHA blend film (79.9 ± 23.1), PCL film (51.3 ± 7.4 cells) and glass (10.1 ± 2.8 cells) (* $P < 0.05$, ** $P < 0.05$, *** $P < 0.05$, $\cdot P < 0.05$). None significant differences were found between the numbers of differentiated cells grown on the substrates PHA blend/BG2 (1wt %) (85.7 ± 11.3 cells), PHA blend/BG2 (2.5wt %) (57.0 ± 9.0 cells) and the controls PHA blend film (79.9 ± 23.1), PCL film (51.3 ± 7.4 cells) and glass (10.1 ± 2.8 cells) as shown in Fig. 6.9. Confocal micrographs of NG108-15 neuronal cells immunocytochemically-labelled for beta-III tubulin grown on PHA blend/BG1 (Fig. 6.10) and

PHA blend/BG2 composites (Fig. 6.11) were taken with higher magnification in order to observe neurites bearing neurons.

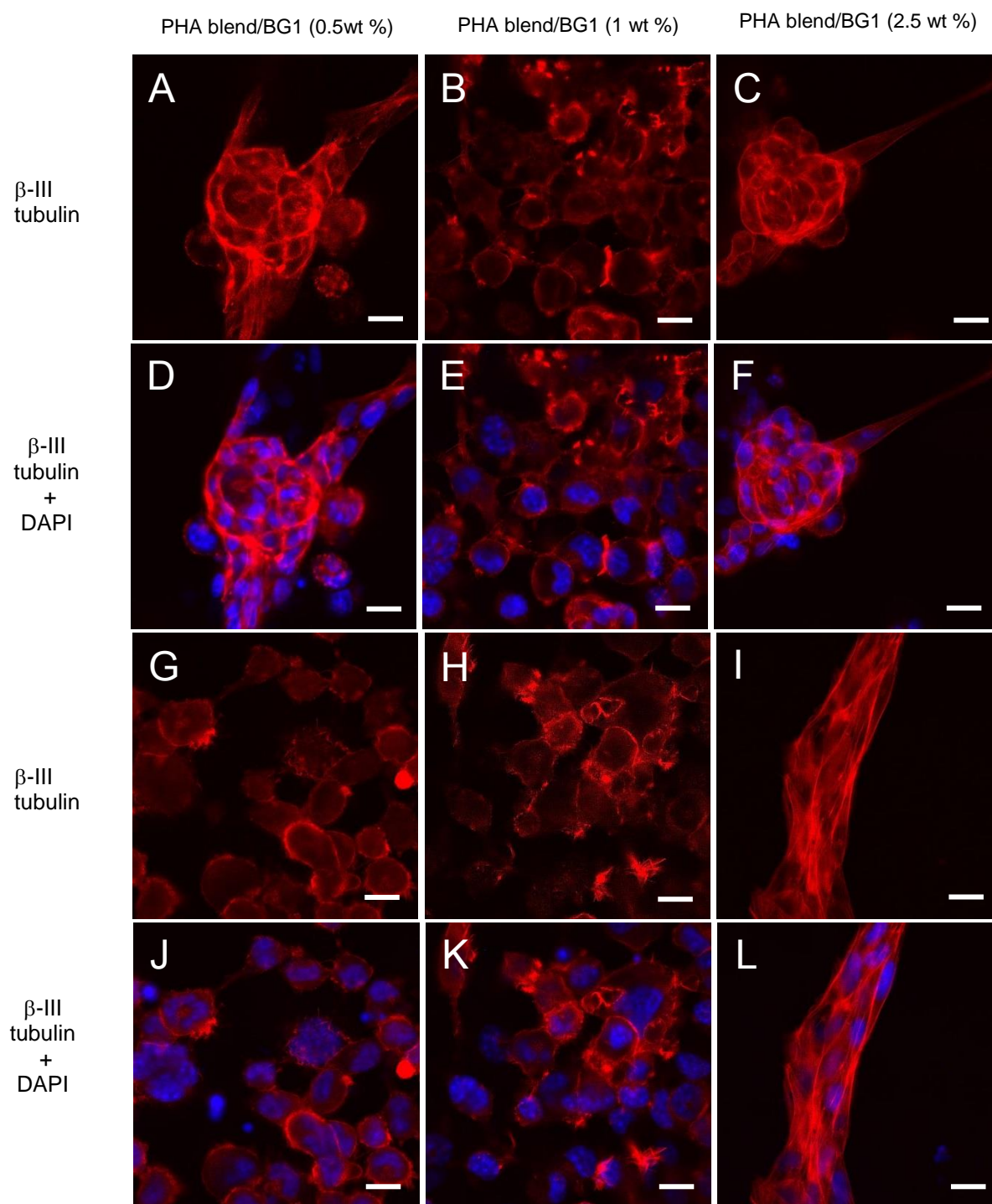


Figure 6.10. Confocal microscopy images of NG108-15 neuronal cells immunocytochemically-labelled for beta-III tubulin after 4 days culture on PHA blend/BG1 composites. (A, D, G, J) PHA blend/BG1 (0.5wt %) composite, (B, E, H, K) PHA blend/BG1 (1 wt %) composite, (C, F, I, L) PHA blend/BG1 (2.5wt %) composite. Neuronal cell differentiation (red coloured cells) could be observed in all the substrates containing BG1 at different concentrations. Neurites bearing neuronal cells were highly abundant in all PHA blend/BG1 composites. Scale bar = 12.5 μ m

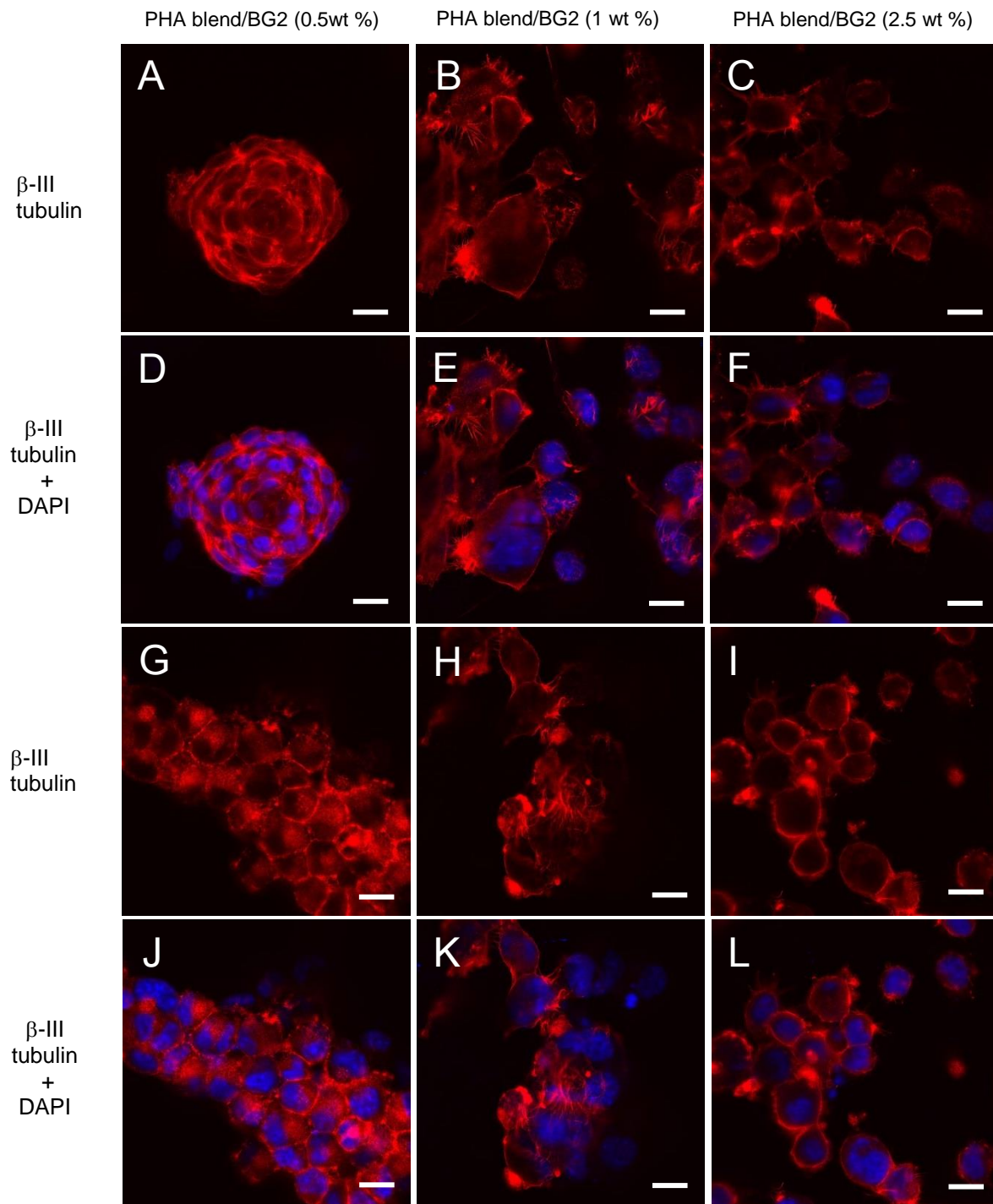


Figure 6.11 Confocal microscopy images of NG108-15 neuronal cells immunocytochemically-labelled for beta-III tubulin after 4 days culture on PHA blend/BG2 (0.5wt %) composite. (A, D, G, J) PHA blend/BG2 (0.5wt %) composite, (B, E, H, K) PHA blend/BG2 (1wt %) composite, (C, F, I, L) PHA blend/BG2 (2.5wt %) composite. Neuronal cell differentiation could be observed in all the substrates containing BG2 at different concentrations. Neurites bearing neuronal cells were observed in all BG2 substrates and cells were found in clusters. Scale bar = 12.5 μ m.

6.6 NEURITE OUTGROWTH ASSESSMENT ON NG108-15 NEURONAL CELL/SCHWANN CELL CO-CULTURES GROWN ON PHA BLEND/BG COMPOSITES

Micrographs of NG108-15 neuronal cells (red) grown in co-culture with Schwannoma cell line RN22 (green) on PHA blend/BG composites are shown in Figures 6.10, 6.11, 6.12 and 6.13. Neuronal cells were immunolabelled for β III-tubulin (red) to study the effect of RN22 cells on neuronal differentiation and neurite outgrowth. RN22 cells were stained with phalloidin (green) for visualization (Fig. 6.12 G-L).

Differentiation of neuronal cells was detected on all of the substrates using the immunolabeling with anti- β III-tubulin antibody (red). PHA blend/BG composites and controls PHA blend film, PCL film and glass (not shown). As it is shown in both figures 6.10 (G-L), only a few RN22 cells were detected after four days of cell co-culture and were observed attached to the the six PHA blend/BG composites (Fig. 6.12 G, H, I, J, K, L). Although a few RN22 cells were detected, cell growth analysis of NG108-15 demonstrated that this neuronal cell line was able to attach, grow and differentiate on all the substrates co-existing with RN22 cells. In the other hand, the low number of RN22 cells detected on all the substrates showed a lower attachment and growth performance compared to NG108-15 neuronal cells.

As in the live/dead cell test and in the neurite outgrowth assessment of NG108-15 neuronal cells, the PHA blend/BG1 (1wt %) composite supported the highest number of differentiated neuronal cells in co-culture with RN22 cells (654.8 ± 18.5 cells) when compared to the rest of substrates; PHA blend/BG1 (0.5wt %) (426.2 ± 24.0 cells) (Fig. 6.12, 6.10 (A-L)), PHA blend/BG1 (2.5wt %) (506.0 ± 29.2 cells) (Fig. 6.13 (G-L)), PHA blend/BG2 (0.5wt %) (204.38 ± 30.01 cells), PHA blend/BG2 (1wt %) (549.2 ± 20.1 cells) (Fig. 6.16 (G-L)), PHA blend/BG2 (2.5wt %) (426.13 ± 19.81 cells) (Fig. 6.16 (M-R)) and the controls PHA blend film (171.0 ± 2.7), PCL film (102.0 ± 27.1 cells) and glass (16.7 ± 7.0 cells) as shown in Fig.6.14 S.

Statistical analysis showed that the number of neuronal cells grown on PHA blend/BG2 (1wt %) (654.8 ± 18.5 cells) in the presence of RN22 cells was significantly different to that of PHA blend/BG1 (0.5wt %) (426.2 ± 24.0 cells) (* $P < 0.05$) and to those of PHA blend/BG1 (2.5wt %) (506.0 ± 29.2 cells), PHA blend/BG2 (0.5wt %) (204.4 ± 30.0 cells), PHA blend/BG2 (1wt %) (549.2 ± 20.1 cells), PHA blend/BG2 (2.5wt %) (426.1 ± 19.8 cells), PHA blend film (171.0 ± 2.7), PCL film (102.0 ± 27.1 cells) and glass (16.7 ± 7.0 cells) (** $P < 0.05$). The number of neuronal cells in co-culture with RN22 found on PHA blend/BG1 (2.5wt %) (506.0 ± 29.2 cells) was also significantly different in comparison to those found on the controls PHA blend film (171.0 ± 2.7), PCL film (102.0 ± 27.1 cells) and glass (16.7 ± 7.0 cells) (** $P < 0.05$).

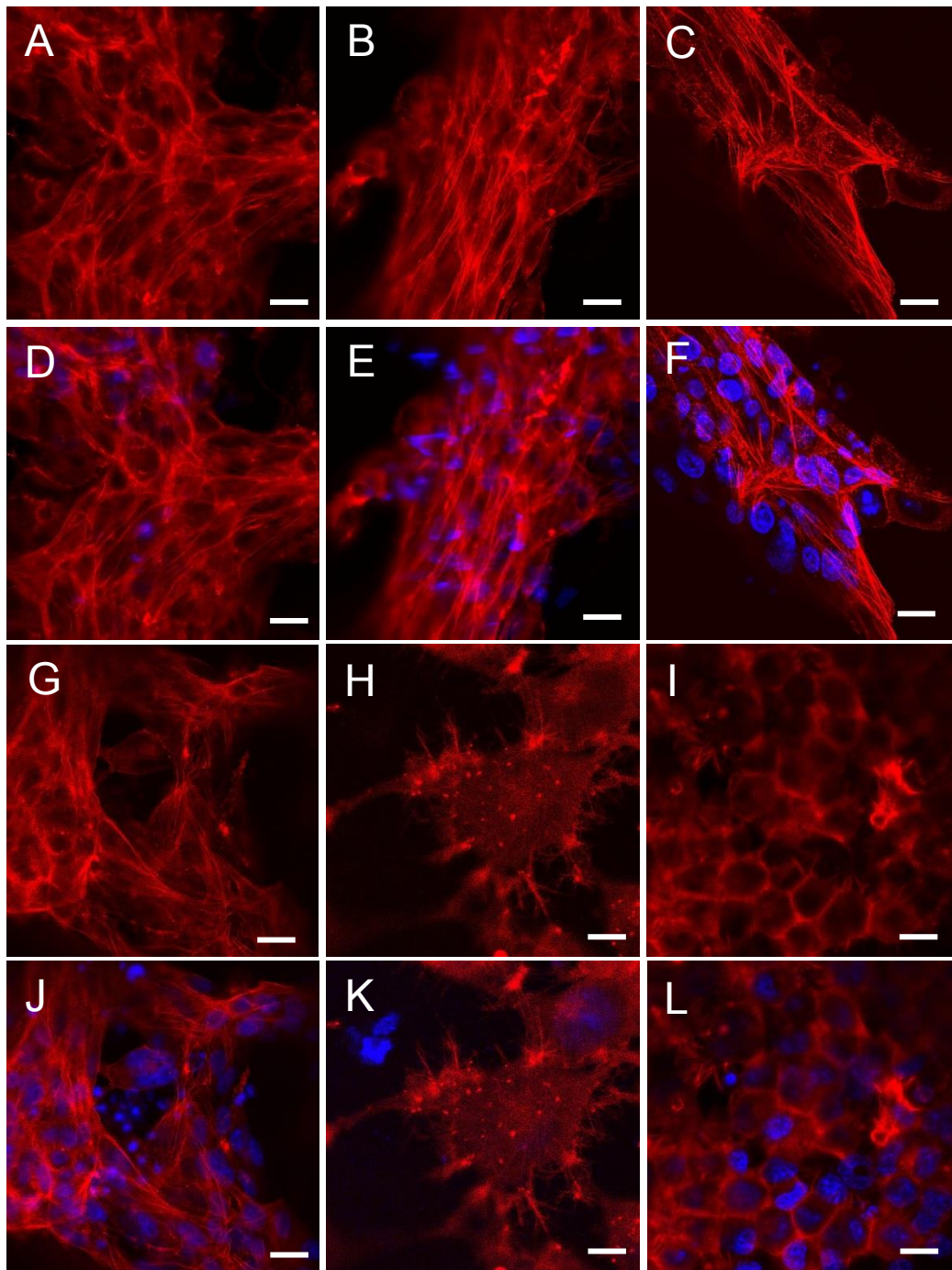


Figure 6.12. Confocal microscopy images of PHA blend/BG1 (0.5wt %). (A-L) Varying neuronal tissue-like structures were formed by NG108-15 in co-culture with RN22 cells. Neurite bearing neuronal cells were highly abundant on PHA blend/BG1 (0.5wt %) composites. Axonal extension was also evident. Scale bar = 12.5 μ m

The composite PHA blend/BG2 (0.5wt %) supported the lowest number of neuronal cells grown with RN22 cells compared to the other composites. The number of NG108-15 displayed by PHA blend/BG2 (0.5wt %) (204.4 ± 30.0 cells) was also significantly different to those presented by the rest of composites; PHA blend/BG1 (0.5wt %) (426.2 ± 24.0 cells) (* $P < 0.05$), PHA blend/BG2 (1wt %) (654.8 ± 18.5 cells) (** $P < 0.05$), PHA blend/BG1 (2.5wt %)

(506.0 ± 29.2 cells) (**P < 0.05), PHA blend/BG2 (1wt %) (549.2 ± 20.1 cells) (*P < 0.05) and PHA blend/BG2 (2.5wt %) (426.1 ± 19.8 cells) (*P < 0.05).

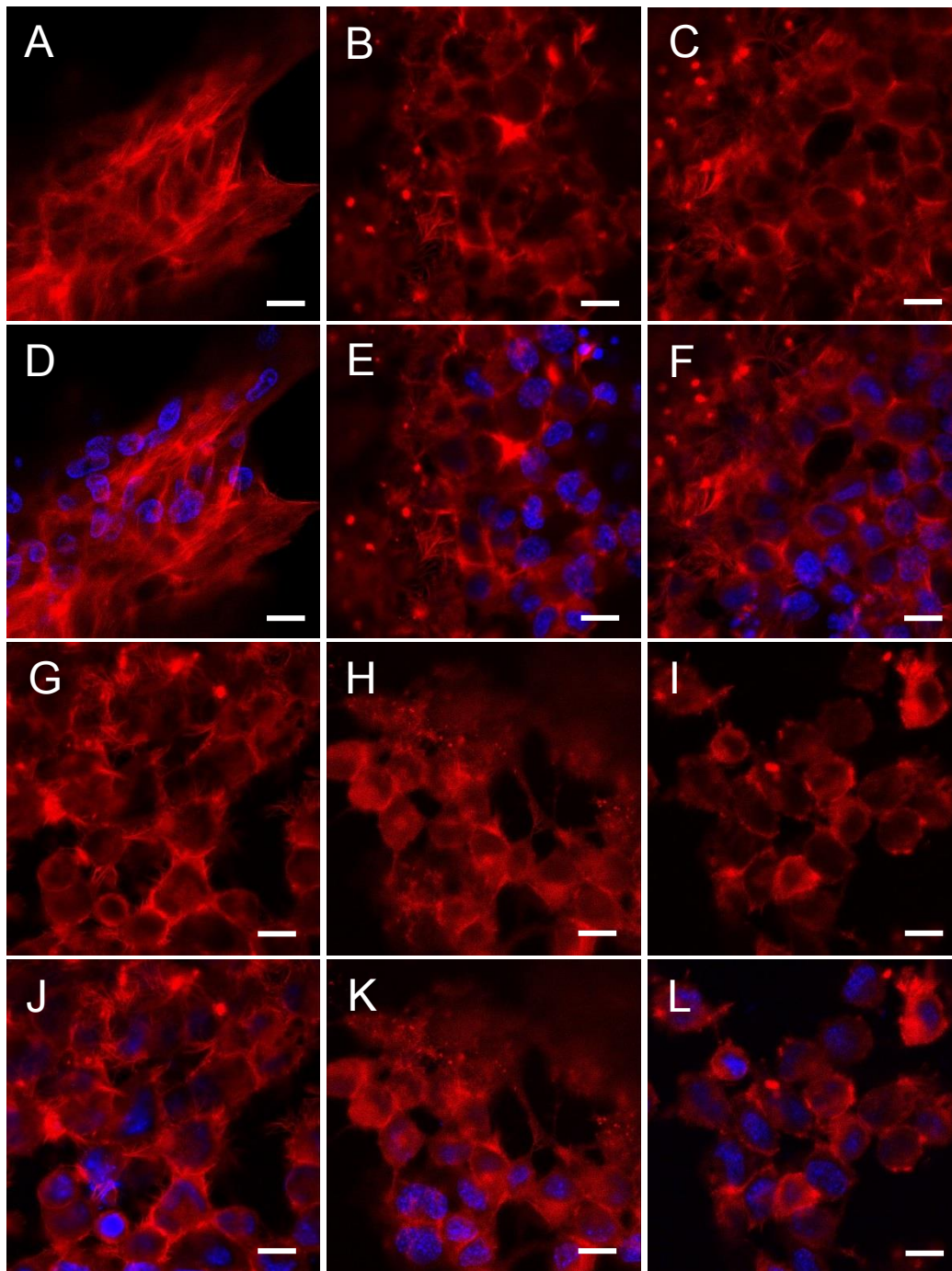


Figure 6.13. Confocal microscopy images of neuronal cells grown on PHA blend/BG1 (1 wt %) and PHA blend/BG1 (2.5 wt %). (A-F) NG108-15 cells grown in co-culture with RN22 cells on PHA blend/BG1 (1 wt %). (G-L) NG108-15 cells grown in co-culture with RN22 cells on PHA blend/BG1 (2.5 wt %). Neurites bearing neuronal cells were highly abundant on both PHA blend/BG1 (1 wt %) and PHA blend/BG1 (2.5 wt %). Axonal extension was also evident.

However, none significant differences were found when the number of NG108-15 cells grown in co-existence with RN22 on PHA blend/BG2 (0.5wt %) (204.4 ± 30.0 cells) was compared to those of PHA blend film (171.0 ± 2.7), PCL film (102.0 ± 27.1 cells). The number of neuronal cells grown on PHA blend/BG2 (1wt %) (549.2 ± 20.1 cells) in the presence of RN22 cells was significantly different to that determined for PHA blend/BG2 (2.5wt %) (426.1 ± 19.8 cells) (** $P < 0.05$).

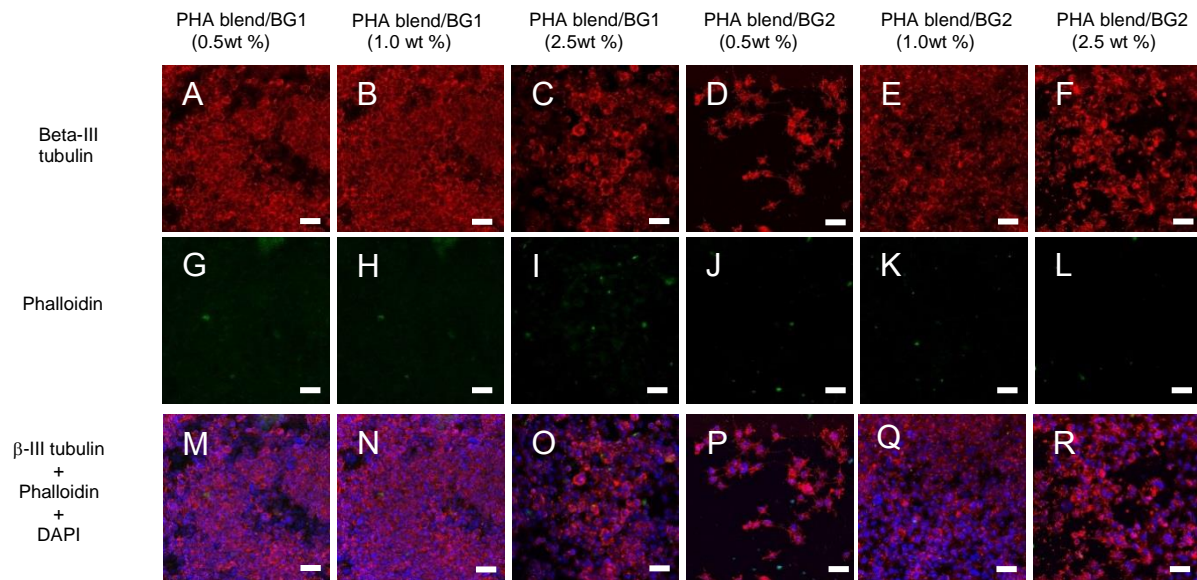


Figure 6.14. Micrographs of NG108-15 neuronal cells immunolabelled for beta-III tubulin (red) grown in co-culture with RN22 cells stained with phalloidin (green) after 4 days on PHA blend/BG composites. (A, G, M) PHA blend/BG1 (0.5wt %); (B, H, N) PHA blend/BG1 (1 wt %); (C, I, O) PHA blend/BG1 (2.5 wt %); (D, J, P) PHA blend/BG2 (0.5wt %); (E, H, Q) PHA blend/BG2 (1 wt %); (F, L, R) PHA blend/BG2 (2.5 wt %). Scale bar = 50 μ m

Also, NG108-15 cell number of cells grown in co-culture on these two composites; PHA blend/BG2 (1wt %) (549.2 ± 20.1 cells) (** $P < 0.05$) and PHA blend/BG2 (2.5wt %) (426.1 ± 19.8 cells) (***) ($P < 0.05$) were significantly different compared to those of the three controls PHA blend film (171.0 ± 2.7), PCL film (102.0 ± 27.1 cells) and glass (16.7 ± 7.0 cells). Although, the number of neuronal cells grown on PHA blend film (171.0 ± 2.7) in co-existence with RN22 was significantly different to that found on glass (16.7 ± 7.0 cells) (# $P < 0.05$), no significant difference was found between that number on PCL film (102.0 ± 27.1 cells) and glass (16.7 ± 7.0 cells).

Statistical analysis of the number of NG108-15 neuronal cells grown on PHA blend/BG composites in single culture and in co-culture with RN22 showed an increase in the number of neuronal cells when cultured with RN22 cells. This increase was statistically significant and observed in PHA blend/BG1 (0.5wt %), PHA blend/BG1 (1.0 wt %), PHA blend/BG1 (2.5 wt

%), PHA blend/BG2 (1.0wt %) and PHA blend/BG2 (2.5 wt %) (Fig. 6.10 S). The number of neuronal cells grown on PHA blend/BG1 (0.5wt %) with RN22 cells (426.2 ± 24.00 cells) was higher and significantly different to that when grown in single culture (247.8 ± 26.4 cells) (* $P < 0.05$). The number of NG108-15 presented in PHA blend/BG1 (1.0 wt %) increased significantly from (347.5 ± 36.8 cells) in single culture to (654.8 ± 18.5 cells) when grown with RN22 cells (** $P < 0.05$). In the same way, the number of neuronal cells grown on PHA blend/BG1 (2.5 wt %) (299.4 ± 25.4 cells) was increased when cultured with RN22 (506.0 ± 29.2 cells) (** $P < 0.05$). Seven-fold increase was shown in the number of neuronal cells detected in PHA blend/BG2 (1.0wt %) and PHA blend/BG2 (2.5 wt %) when cultured with RN22. The number of neuronal cells grown in single culture on PHA blend/BG2 (1.0wt %) (85.7 ± 11.3 cells) and PHA blend/BG2 (2.5 wt %) (57.0 ± 9.0 cells) increased to 654.8 ± 18.5 cells and 506.0 ± 29.2 cells respectively when grown with RN22 cells. The number of neuronal cells grown on these two composites in single culture was significantly different to those when grown in co-culture with RN22 cells (* $P < 0.05$ and ** $P < 0.05$). No significant differences were found when the number of neuronal cells grown on PHA blend/BG2 (0.5 wt %) (227.1 ± 21.7 cells) was compared to that displayed when cells were cultured with RN22 cells (204.4 ± 30.0 cells). Also, no significant differences were found when the number of NG108-15 cells grown on PHA blend (79.9 ± 23.1 cells), PCL (51.3 ± 7.4 cells) and glass (10.1 ± 2.8 cells) in single culture was compared to those displayed in co-culture with RN22 cells (171.0 ± 2.7 , 102.0 ± 27.1 , 16.7 ± 7.0 cells respectively).

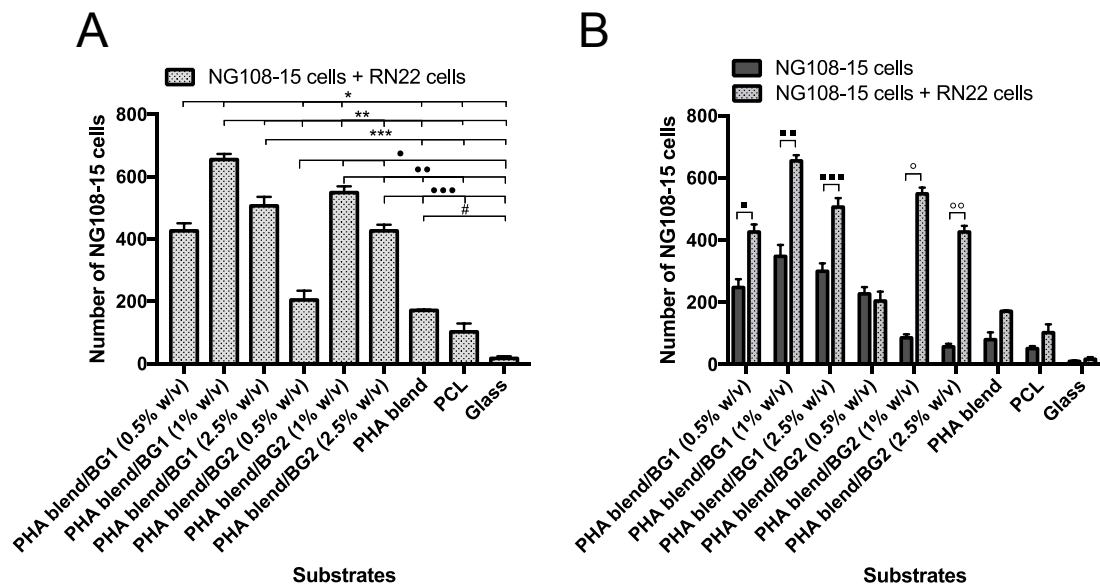


Figure 6.15. Number of NG108-15 neuronal cells grown on varying substrates with and without RN22 cells. A) Number of NG108-15 neuronal cells grown on PHA blend/BG composites, PHA blend film, PCL and glass. B) Number of NG108-15 neuronal cells grown on PHA blend/BG composites in single culture vs co-cultured with RN22 cells. mean \pm SEM, n = 9 independent experiments).

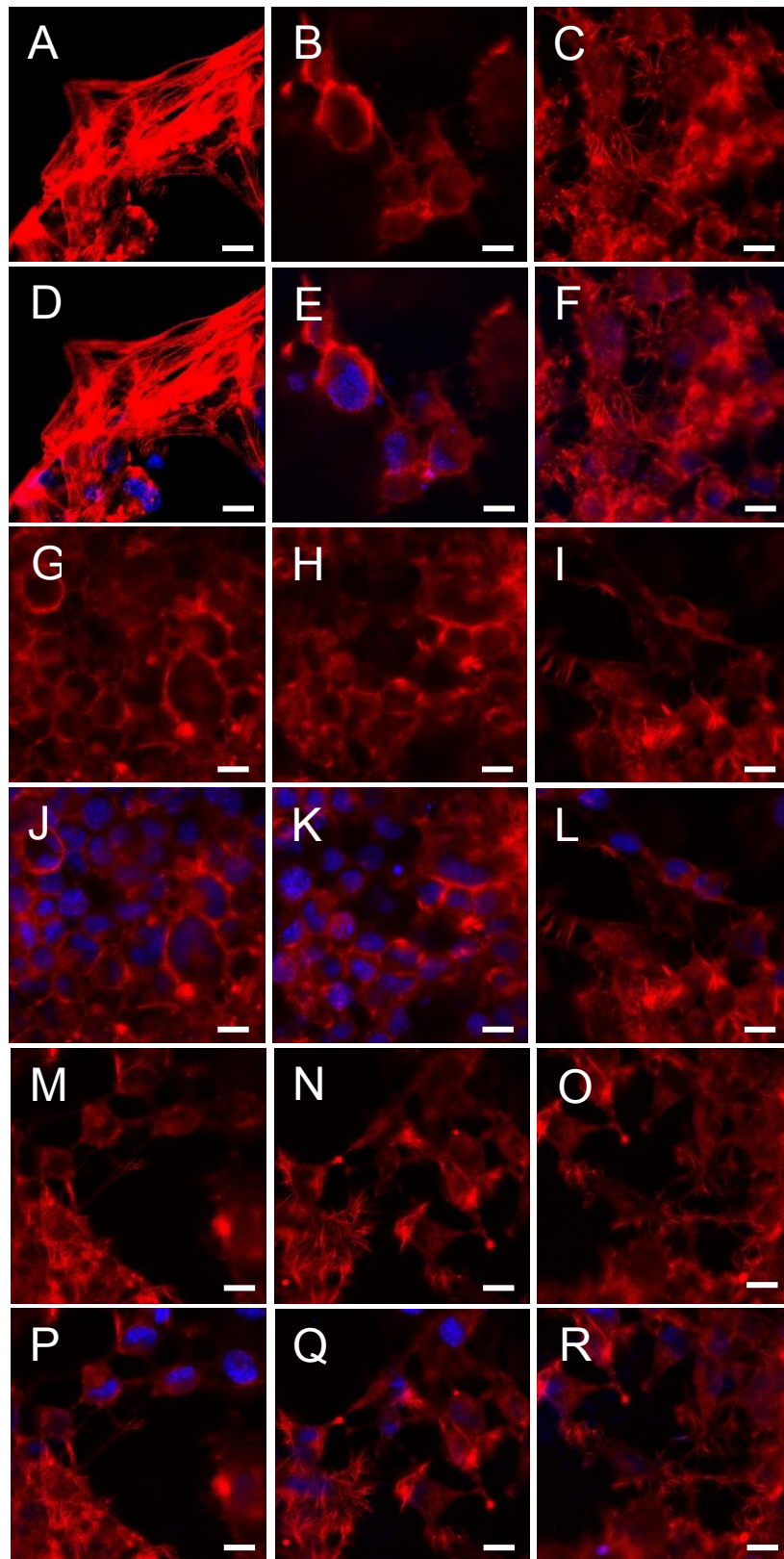


Figure 6.16. Confocal microscopy images of neuronal cells grown on PHA blend/BG2. (A - F) NG108-15 cells grown in co-culture with RN22 on PHA blend/BG2 (0.5wt %). (G - L) NG108-15 cells grown in co-culture with RN22 cells on PHA blend/BG2 (1wt %). (M-R) Neuronal cells NG108-15 grown in co-culture with RN22 cells on PHA blend/BG2 (2.5 wt %).

6.7 DISCUSSION

The modern era of tissue engineering and regenerative medicine begun only a quarter of a century ago. This scientific discipline has rapidly progressed and has involved both, the cell-based and cell-free scaffold development for *in vivo* implantation. Furthermore, the development of tunable materials has played an important role in the success of regeneration in a wide variety of tissues. This adaptability permits to obtain specific properties that match the physico-chemical characteristics of the tissue of interest. Biomaterial development is focused on surface modification of biocompatible materials in order to acquire a greater understanding of cell-surface interactions and improved biocompatibility. The surface hydrophobicity, roughness and porosity are well known as key factors that affect cell response. Greater wettability and roughness as well as the presence of pores have shown to favour cell attachment, growth and differentiation.

It has been shown that both bioactive glasses 45S5 (BG1) and 1393 (BG2) react with phosphate containing liquids *in vitro* and *in vivo*. Once these BGs are immersed in solution, cations (Na^+ , K^+ , Ca^{2+} and Mg^{2+}) are realised from the glass and dissolved in the surrounding liquid. Insoluble calcium phosphate is quickly formed by the reaction of calcium ions with available phosphate ions. This reaction continues until the phosphate and calcium ions fully react forming amorphous calcium phosphate, which would transform into non-stoichiometric hydroxyapatite (HA) (Marquardt *et al.*, 2013). Hydroxyapatite is responsible of the strong bonding that BGs have shown to form with the tissue that surrounds the place of implantation. Additionally, it has been demonstrated that some of the ions released by BGs activate the expression of osteogenic genes and stimulate angiogenesis. The bioactivity of glasses is measured by their conversion rate to HA, which ranges from hours to months (Fu *et al.*, 2010).

The microstructure of the PHA blend/BG composites was affected by the concentration of BG in the composite. The concentration of BG1 and BG2 showed an effect not only on the size of pores in PHA blend/BG composites, but also in the form of porous structures. The microstructure of PHA blend/BG1 composites with 0.5 wt % and 2.5 wt % BG1 included interconnected pores. However, although the pore size of PHA blend/BG1 1.0 wt % was similar to that found in PHA blend/BG1 2.5 wt %, it's porous interconnection was poor in comparison to those observed in PHA blend/BG1 0.5 wt % and PHA blend/BG1 2.5 wt %. The presence of BG in the PHA blend/BG2 (0.5 wt %) composite showed little effect on both pore formation and porous interconnection generation. The pores found in the PHA blend/BG2 (0.5 wt %) were the smallest and the least abundant ones when compared to the other composites. Also, non-porous interconnection systems were observed. On the other hand, the PHA

blend/BG2 composites with higher concentrations (1.0 % and 2.5 %) of BG2 presented similar pore size and pore interconnection. However, the pore interconnectivity found in these two composites was less prominent than that observed in PHA blend/BG1 0.5 wt % and in PHA blend/BG1 2.5 wt % surfaces.

It has been shown that high porosities and interconnected porous systems in scaffolds facilitate vascularization and tissue ingrowth when implanted as bone tissue engineering scaffolds. Although, vascularization in bone tissue regeneration has shown to be significantly enhanced in scaffolds containing pores with diameters higher than 250 μm , porous interconnectivity seems to be the major factor for ingrowth of tissue and blood vessels (Hoppe et al., 2014). The average size of differentiated NG108-15 in the performed experiments ranged from 10 – 15 μm . As the microstructure of PHA blend/BG1 (0.5wt %) contained pores with diameter ranging from 3 to 10 μm , this composite could potentially support tissue ingrowth of NG108-15.

In section 6.2.3, R_q of the substrates was determined by profilometric surface analysis. RMS roughness is weighted by large values of peak height and depth valleys of the substrate's surface. No relationship was found between the R_q values and the surface microstructure of the substrates observed by scanning electronic microscopy. The porous interconnection systems observed in PHA blend/BG1 (0.5wt %), PHA blend/BG1 (2.5wt %), PHA blend/BG2 (1wt %) and PHA blend/BG2 (2.5wt %) did not show a significant effect on the R_q values. PHA blend/BG1 (0.5wt %) and PHA blend/BG1 (2.5wt %) showed not only similar level of porous interconnectivity but also displayed similar roughness. This suggested that the height and depth of the peaks and valleys on their surfaces could be similar. On the other hand, a significant difference was found between the roughness of the PHA blend/BG1 (1.0 wt %) and those of PHA blend/BG1 (0.5wt %) and PHA blend/BG1 (2.5wt %), which could indicate the presence of higher peaks on the PHA blend/BG1 (1.0 wt %) surface compared to those on the PHA blend/BG1 (0.5wt %) and PHA blend/BG1 (2.5wt %). Although PHA blend/BG2 (1.0 wt %) and PHA blend/BG2 (2.5 wt %) presented the same appearance and pore size when analysed by scanning electronic microscopy, their roughness was significantly different. The higher R_q value displayed by PHA blend/BG2 (2.5 wt %) compared to that of PHA blend/BG2 (1.0 wt %) suggested the presence of higher peaks in the PHA blend/BG2 (2.5 wt %) surface compared to those on PHA blend/BG2 (1.0 wt %). In spite of the fact that PHA blend/BG2 (0.5wt %) was the least porous among all the composites, this substrate was the roughest amongst all the BG composites.

No correlation was found between the BG concentration and the R_q values. In a previous study, the 25:75 P(3HO)/P(3HB) blend film displayed a R_q value of $4.16 \pm 0.25 \mu\text{m}$ (Lizarraga-Valderrama *et al.*, 2015, Chapter 4) by using the same method of roughness

determination (profilometric analyses). This roughness value is three-fold the R_q determined in the present work ($1.25 \pm 0.03 \mu\text{m}$). This discrepancy may be due to the use of solvent casting method to prepare both films. Solvent casting of polymer solutions is a well-known method, which is routinely used in a wide variety of industrial and biological applications (Strawhecker *et al.*, 2001). It has been shown that when the solvent is rapidly evaporated, Marangoni flows are produced, impeding the appropriate level and heal of the roughness. On the other hand, when the solvent is slowly evaporated, no effect of Marangoni flow is observed and hence, the resultant film surfaces are smoother (Strawhecker *et al.*, 2001). The Marangoni effect is induced by interfacial tension gradient generated in the process of heat or mass transfer and its observed in industrial gas–liquid and liquid–liquid processes. It has been shown that the Marangoni effect can cause cellular convection, drop pulsation, localized eruption and kicking (Wang *et al.*, 2016). In this context, it seems that the evaporation rate of the PHA blend film prepared in this study was perhaps slower than that in the previous study.

It is well-known that surface hydrophobicity is a key factor that affects cell attachment and hence, cell response. In the present study (section 6.2.4), surface hydrophobicity of the PHA blend composites was assessed by measuring contact angle of a water droplet spread on the composites' surfaces. The lower the contact angle is, the more hydrophilic the surface. Previous studies have shown that cell attachment increases when hydrophilicity increases. These findings have been observed in different cells types such as osteoblasts (Goddard & Hotchkiss, 2007; Xu, 2007), fibroblasts (Tamada & Ikada, 1993; Wei *et al.*, 2009), Madin-Darby Canine Kidney (MDCK) cells (Vogler, 1999), mouse osteoblast-like cell line MC3T3-E (Wei *et al.*, 2009), 7F2 mouse osteoblasts (Yildirim *et al.*, 2010) and neurites Khorasani & Irani, 2008; Lee *et al.*, 2003).

A correlation between the concentration of BG and water contact angle was observed in both types of BGs composites; PHA blend/BG1 and PHA blend/BG2. Increments in the BG concentration resulted in a decrease in the water contact angle, which were closer to that of the PHA blend control when using 2.5 % in both BGs. The explanation to these results could be based on the solubility of these BGs in the PHA blend suspension. The BG concentration of 2.5 wt % may be too high to allow the adequate dissolution of the BG in the polymer suspension. Hence, excess of BG in the polymer suspensions could produce phase separation and the formation of two layers during solvent evaporation. As a consequence, the top layer could be probably composed of the polymer mix (PHA blend) along with the suspended BGs and the bottom layer may be formed by the excess of non-dissolved BG. As it was mentioned before, the water contact angles were measured on the top surface of the substrates. Therefore, the fact that the measured water contact angles of the PHA blend/BG composites (2.5 wt %) are closer to that of the PHA blend could prove that a phase separation

took place during the film manufacturing procedure, hence leading to a almost polymer only on the top. Furthermore, the high water contact angles found on PHA blend/BG1 (0.5 wt %) and PHA blend/BG2 (0.5 wt %) could be the result of a better dispersion of the BGs in the polymeric suspension. Therefore, the two BGs increased the hydrophobicity of PHA blends when they are well dissolved. In the present study, the water contact angle displayed by the control PHA blend ($61.90 \pm 0.70^\circ$) was different to that measured in a previous study ($77.36 \pm 0.81^\circ$) (Lizarraga-Valderrama *et al.*, 2015, Chapter 4) using the same instrument and software. This discrepancy could also be the result of insufficient control of the physical parameters during the solvent casting of these films. It has been shown that the spreading time of solutions when volatile solvents are used, is larger than the solvent evaporation time. As a consequence, the solution does not spread completely resulting in higher values of contact angles. Thus, the solution used for the manufacture of PHA blend in the previous study may not have spread completely before the wettability measurement, yielding a larger water contact angles.

The discrepancy found in the roughness and water contact angle values displayed in this study compared to previous studies exposes the great importance of considering the fluid leveling when solvent casting method is used. Strategies should be taken into account to control evaporation rates in order to have more consistent measurements.

The good growth and differentiation performance of NG108-15 cells displayed on all the PHA blend composites have shown that both BGs (BG1 and BG2) have good biocompatibility at 2.5, 1.0 and 0.5 wt % in the PHA blend solution. In all the cell culture experiments, PHA blend/BG1 (1wt %) has shown superior performance in supporting growth and neuronal differentiation of NG108-15 compared to the rest of substrates. The superior performance of PHA blend/BG1 (1wt %) was consistent in all the cell culture experiments (Live/dead cell test, neurite outgrowth assessment on NG108-15 neuronal cell and on NG108-15/Schwann cell co-cultures) supporting the highest number of neuronal cells when compared to the rest of composites. Furthermore, neurite extension found in the PHA blend/BG1 (1wt %) was very clear as observed in Fig.6.13 where neurites form a complex connection network. These neurite interconnection structures were also observed in PHA blend/BG1 (0.5wt %) (Fig. 6.12). The growth and differentiation of the NG108-15 cells on the rest of PHA blend/composites was variable in the live/dead cell test, neurite outgrowth assessment on NG108-15 neuronal cell and on NG108-15/Schwann cell co-cultures (Fig. 6.6 K, Fig. 6.7 J, Fig. 6.12 V and W). It's important to mention that this type of analyses using NG108-15 neuronal cells to measure biocompatibility on BG composites has not been reported before. Although the use of BG in nerve tissue engineering application is a recent area of investigation, it seems to be promising.

It is important to notice that despite the fact that PHA blend/BG1 (1.0 wt %) displayed a superior performance as a neuronal scaffold, this composite did not show the most favourable surface characteristics among the rest of composites. Although the water contact angle ($65.69 \pm 1.23^\circ$) corresponds to a hydrophilic substrate, the roughness was low and its microstructure did not show an interconnected porous system. Therefore, the concentration of BG1 used in PHA blend/BG1 has played an important role in the success of this composite.

In general, both BGs showed to have a significant impact on the biocompatibility of the PHA blend. In all the experiments the presence of BGs at all concentrations (0.5 wt %, 1.0 wt %, 2.5wt %) increased the number of differentiated neuronal cells with respect to both the PHA blend control and PCL control. Although 1393 BG (BG2) has shown to support neuronal regeneration, 45S5 (BG2) has demonstrated superior performance in supporting cell growth and differentiation of NG108-15 cells. To the best of my knowledge, this study is the first to evaluate the effect of PHA/1393 BG on NG108-15 and shows its potential application as base material for the manufacture of scaffolds for nerve regeneration. In the other hand, Bioglass® 45S5 has been investigated for peripheral nerve regeneration applications. Bunting *et al.* (2005) have shown that fibres of Bioglass® 45S5 are biocompatible with rat Schwann cells and fibroblasts *in vitro*. They showed qualitatively and quantitatively evidence of axonal regeneration *in vivo* by using a silastic conduit filled with Bioglass® 45S5 fibres implanted in sciatic nerves of adult rats. Additionally, Mohammadkhah *et al.* (2015) used Bioglass® 45S5 as one of the components of polymer/BG composites to be tested as biomaterials to support nerve regeneration. They used three different composite sheets made from biodegradable poly- ϵ -caprolactone (PCL) and varying types of bioactive glass to investigate nerve regeneration. The three composites consisted of 50 wt.% PCL and the other 50 wt.% was variable. The composite named as i, consisted of 50 wt.% PCL and 50 wt.% of 13–93 B3 borate glass particles. The composite ii was made from 50 wt.% PCL and 50 wt.% 45S5 silicate glass particles. Finally, the composite iii consisted of 50 wt.% PCL, 25 wt.% 13–93 B3 and 25 wt.% 45S5 glass particles. When degradation profiles were determined and compared, the composite i was found to have a higher degradation rate compared to the composite ii. For the biocompatibility study, dorsal root ganglia isolated from embryonic chicks was cultured on composite sheets and neurite outgrowth was measured. The bioactive glass particles added to the composites did not showed negative effects on neurite extension (Mohammadkhah *et al.*, 2015).

The presence of Schwannoma RN22 cells in NG108-15 cultures had a positive effect on the growth and differentiation of these neuronal cells on all the PHA blend/composites excepting for the PHA blend/BG1 (0.5wt %) (Fig. 6.12 W). In this composite, the number of differentiated NG108-15 did not increase when grown in co-culture with RN22 cells. Although

only few RN22 cells were detectable at the end of the experiment, they have shown to support not only neuronal growth but also axonal extension. Schwannoma RN22 cells have demonstrated to grow faster than NG108-15 cells and rapidly form a layer of cells that tend to easily detach. Therefore, RN22 cells could have detached during the fixation and washing process required to immunolabel the cells. Schwannoma RN22 cells are the myelin-forming cells of the PNS. The layers of myelin membrane wrap axons insulating them to allow the conduction of electric impulses. SC ensheath synaptic junctions, form myelin and bundle axons together (Fields and Stevens-Graham, 2002). Communication between neurons and SCs is essential for synaptic transmission, axonal conduction and processing of information. Signals between neurons and SCs involve ion fluxes, neurotransmitters, cell adhesion molecules and specialized signaling molecules, which are released from neurons. SCs-neuron communication is carried out through intracellular waves of calcium and via intercellular diffusion of chemical messengers. In this respect, the release of Ca^{+2} from bioactive glasses could affect SC-neuron communication affecting the intracellular waves of Ca^{+2} . SCs monitor synaptic activity by detecting neuron-glia signaling molecules and control the strength of synaptic transmission by regulating the release of neurotransmitters from the nerve terminal end. This process begins when the neurotransmitter adenosine (Ach) or extracellular ATP are released from nerve terminal end and activate G-protein-coupled receptors on the SCs (Fields and Stevens-Graham, 2002). This activation induces an increase in Ca^{2+} level in the terminal SCs enhancing nerve-stimulated transmitter release (Ca^{2+} transient), which triggers glutamate release from the SCs. As a result, metabotropic receptors are activated on the postsynaptic muscle membrane, which stimulates synthesis of NO in the muscle. The produced NO diffuses to the nerve resulting in the decrease of transmitter release (Sugiura and Lin, 2011).

Neuron-glia interactions at the node of Ranvier are essential for rapid impulse conduction. Nodes of Ranvier are rich in voltage-gated Na^+ channels, where Na^+ ions cross and depolarize the membrane between segments of compacted myelin. Channels of K^+ are highly concentrated in the juxtaparanodal region of the axon and allow K^+ ions to exit from the axon restoring the membrane potential after the impulse. Therefore, the release of Na^+ ions from bioactive glasses could affect the membrane polarization during impulse conduction.

The good growth and differentiation performance of NG108-15 cells displayed on all the PHA blend composites have shown that both BGs (BG1 and BG2) have good biocompatibility at 2.5, 1.0 and 0.5 wt % in the PHA blends.

The Young's modulus values displayed by all the PHA blend/BG composites were ranged from 385.6 MPa to 1792.6 MPa, which are much higher than that of peripheral nerves. In previous studies, a Young's modulus of $0.58 \text{ MPa} \pm 0.16 \text{ MPa}$ was found in rat peripheral nerves (Menziez and Jones, 2010). However, the tensile strength obtained in PHA blend/BG1

(1wt %) (10.0 ± 0.6 MPa) was found to be similar to that of rabbit peroneal nerve measured in another study (11.7 ± 0.7 MPa) (Al-Nasassrah *et al.*, 1998). Therefore, although PHA blend/BG1 (1wt %) does not provide the adequate elasticity, it has the appropriate strength that NGCs require.

PHA blend/BG1 (1wt %) showed the best performance in supporting growth and neuronal differentiation of NG108-15 amongst all the substrates in all the cell culture experiments (Live/dead cell test, neurite outgrowth assessment on NG108-15 neuronal cell and on NG108-15/Schwann cell co-cultures). Moreover, neurite extension found on the PHA blend/BG1 (1wt %) was remarkable as neurites formed a complex connection network. No correlation was found between the surface characteristics (roughness, hydrophilicity and porous size) of PHA blend/BGs at different concentrations of BG and cell growth and differentiation. Therefore, PHA blend/BG1 (1wt %) exhibited the best combination of surface features to display better performance supporting NG108-15 neuronal cells.

Chapter 7

Fabrication of nerve guidance conduits

7 FABRICATION OF NERVE GUIDANCE CONDUITS

7.1 INTRODUCTION

The peripheral nerve system (PNS) consists of sensory nerve cell bodies and nerves arising from the brain and the spinal cord. The PNS is connected to the central nervous system (CNS) through an intricate interconnected collection of nerves, sensory receptors and ganglia. Peripheral nerves innervate muscle tissue, transmitting sensory and excitatory inputs to and from the spinal column (Schmidt and Leach, 2003). Such anatomy makes the PNS one of the most complex and largest structures in the body. Peripheral nerve injuries (PNI) may be provoked by acute compression, blunt or penetrating trauma. Such injuries may produce loss of sensory function, motor function or both. Unfortunately, there are no recent statistical data available concerning PNI. The most recent reports, which are repeatedly found in the literature date from 1997 (Kelsey *et al.*, 1997) and 1998 (Noble *et al.*, 1998). In United States, around 360,000 people are known to suffer extremity paralytic syndromes per year. This resulted in 8,648,000 restricted activity days and 4,916,000 bed/disability days (Kelsey *et al.*, 1997). Noble *et al.* 1998 reported that 2.8% of trauma patients suffer PNI. Unfortunately, a considerable amount of these injured patients were disable during their lifetime (Noble *et al.*, 1998). In Europe, 300,000 PNI cases are reported each year (Huang *et al.*, 2012).

Regeneration and recovery of nerve function depends on the gap injury length and the type of lesion. Injured peripheral nerves are able to repair themselves when the nerve has a gap of less than 5 mm to bridge (Jiang *et al.*, 2010; Schmidt and Leach, 2003). In this case, peripheral nerves can regenerate spontaneously thanks to the action of Schwann cells, which generate a beneficial environment for axonal growth. However, misdirection of axons may occur even across short distances, preventing the nerve to recover its function. When the continuity of endoneurial tubes is preserved after injury, axonal regeneration is likely to be successful. On the other hand, when the nerve is transected compromising perineurium and endoneurium, regeneration is hampered and surgical intervention is required. When injuries consist of gaps of more than 5mm length as in the case of axonotmesis and neurotmesis, suturing of the two stumps through epineural microsutures is the standard method to bridge the gaps. Epineural repair is carried out when a tension free coadaptation can be achieved after suturing. When injuries are more severe and less than 3 cm, implantation of an autologous nerve graft is the gold standard procedure. When nerve damage is even more extreme and gaps exceed this distance, allografts, vascularised nerve grafts and nerve grafts without vessels are used (Babu *et al.*, 2008, de Ruyter *et al.*, 2009).

The use of autografts for peripheral nerve repair has various well-known limitations including scar tissue formation, donor site morbidity, lack of donor nerves, inadequate return

of function and aberrant regeneration (Babu *et al.*, 2008; Huang *et al.*, 2012). New approaches for peripheral nerve regeneration have focused on the development of nerve guidance conduits (NGCs) as alternatives of nerve autografts. During the last twenty years a large variety of materials, nano-structures and biochemical factors have been investigated in an attempt to create the ideal NGC. At present, there are several commercially available NGCs approved by U.S Food and Drug Administration (FDA) and Conformit Europe (CE). It has been previously reported that the efficiency of these commercial devices are comparable to autografting when the gap length is less than 3 cm. When the gap to bridge is longer than 3 cm, human autografts have a superior performance compared to the commercially available NGCs. These medical devices are made from either synthetic or organic materials and are available in varying designs and sizes. All of the current commercial NGCs take the form of simple hollow tubes with a single lumen without internal substructure. They are made from acellular human allograft, collagen, COLI, EMC, PLCL, PGA and PVA.

Although commercial NGCs have been shown to overcome some of the limitations of nerve autografts, they exhibit various considerable shortcomings. Common drawbacks of synthetic biodegradable NGCs include; immune response production, scar tissue formation, poor suturability and releasing of by-products that are detrimental for the regeneration process. When NGCs are made from a non-biodegradable material, follow-up surgery is often required for the removal of the conduit, comprising an additional disadvantage. Biodegradable materials are preferred over non-biodegradable materials as the former not only prevents the conduction of a second surgery to remove the implant after the treatment is completed, but also prevent chronic nerve compression and fibrotic reactions (Babu *et al.*, 2008; Midha, 2006). Additionally, biodegradable NGCs have shown less aberrant axonal growth, reduced fibrous scar tissue formation and reduced risk of neuromas when compared to non-biodegradable materials.

The parameters to consider when choosing specific materials and manufacturing techniques for the fabrication of artificial nerve conduits are; biodegradability, degradation rate, degree of swelling, toxicity, reactivity to the immune system, permeability, porosity, flexibility, ability to guide neuronal cells, resistance to high temperatures and suturability. Degradation and swelling of NGCs are very important properties to be taken into consideration. High degradation rates might cause swelling which could block the lumen and consequently prevent regeneration. This swelling is caused by water uptake following the formation of by-products that might increase the osmotic pressure of the conduit. Too slow degradation rates can induce both compression of regenerated axons or chronic immune reaction. The degradation kinetics of the tube should match the nerve regeneration rate. With an ideal degradation rate, the nerve tube should remain intact, with minimal swelling until the

axons have managed to regenerate across the nerve gap. Furthermore, the architecture of the tube should remain mechanically stable during axonal regeneration to resist tear from sutures and tissue inflammation (Keoe *et al.*, 2012).

In the present investigation, two prototypes of NGCs were fabricated using blends of PHAs as base materials. PHAs exhibit properties that could overcome some of the limitations of the available NGCs such as controllable surface erosion, lower acidity of their degradation products and longer-lasting stability compared to their synthetic counterparts. The only PHA that have been investigated for peripheral nerve regeneration application are P(3HB) and (3-hydroxybutyrate-co-3-hydroxyvalerate) (P(3HB-co-HV), which have shown to be highly biocompatible with neuronal cells in animal models (Yong *et al.*, 2002, Mohanna *et al.*, 2005, Biazar and Keshel, 2014). However, the mechanical properties of P(3HB) are unsuitable for nerve tissue engineering, in which flexible polymers are required. Since 75:25 P(3HO)/P(3HB) blend films have shown to possess the required flexibility to be implanted in peripheral nerves, this polymer blend was chosen for manufacturing of NGCs (Lizarraga-Valderrama *et al.*, 2015). Therefore, in this study, blends of PHAs that have not been used before as base material for the manufacture of NGCs were fabricated for their potential to support peripheral nerve regeneration.

The prototype 1 consisted of a nerve guidance conduit made from 75:25 P(3HO)/P(3HB) blend with luminal electrospun aligned fibres fabricated with 25:75 P(3HO)/P(3HB) blend. The prototype 2 comprised of a hollow tube made from 75:25 P(3HO)/P(3HB) blend manufactured by dip-moulding using various dipping conditions.

7.2 RESULTS

7.2.1 NERVE GUIDANCE CONDUITS MANUFACTURING

7.2.1.1 FABRICATION OF NERVE GUIDANCE CONDUITS BY ROLLING AND LIGATION OF PHA FILMS

A NGC was produced using both, 25:75 and 75:25 P(3HO)/P(3HB) blends as base materials. In a first attempt to produce a conduit with a luminal substructure, a mat consisting of two layers of electrospun fibres made from 25:75 P(3HO)/P(3HB) blend was produced. The fibre diameter chosen for the production of the mat was $5.14 \pm 0.91 \mu\text{m}$ (Chapter 5, Figure 5.11 C). Since the resulting mat was extremely thin and weak, formation of the conduit by rolling was unfeasible. In a second attempt, 25:75 P(3HO)/P(3HB) blend film was indented to use as the base material for the fabrication of the conduit (Chapter 4, Figure 4.1 F). The film was cut accordingly to be rolled around with a blunt needle (20 G). However, the brittleness of the material impeded the rolling of the film. Since the 75:25 P(3HO)/P(3HB)

blend film was shown to be more flexible in previous studies (Lizarraga-Valderrama *et al.*, 2015, Chapter 4), this material was chosen as a substrate for electrospun aligned fibers. A sheet of 75:25 P(3HO)/P(3HB) blend was attached to the collector of the electrospinning equipment and fibres were fabricated with a 25:75 P(3HO)/P(3HB) blend solution (35 wt%). After one week when the fibres were dried, a square of the film was cut, rolled into a nerve conduit and borders were joined together using polymer 25:75 P(3HO)/P(3HB) blend solution (5 wt%). Deformation of the fibres was observed after using the polymer solution to join the borders. The final inner diameter 1.08 mm was close to that required for *in vivo* studies in rats (1.1-1.3 mm).

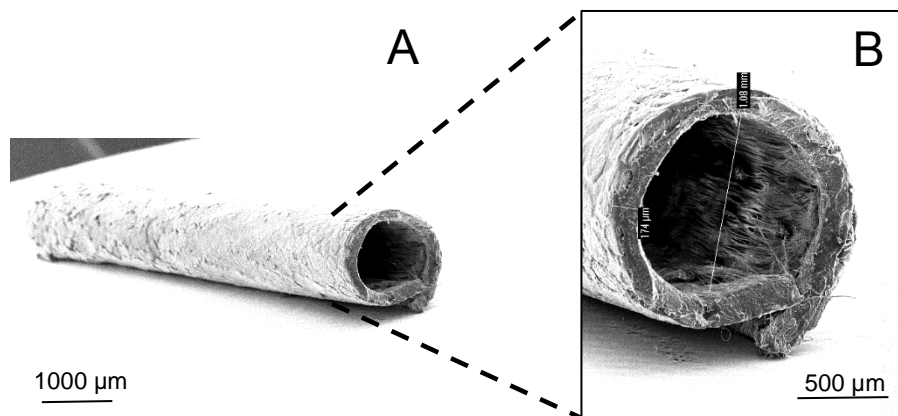


Figure 7.1. A nerve guidance conduit with luminal electrospun aligned fibres. A) External surface of the conduit. A rough surface can be observed characterized by the presence of protrusions. B) Luminal structure of the conduit. Aligned electrospun fibres can be observed aligned along the lumen. The inner diameter and the thickness were 1.08 mm and 174 µm respectively.

7.2.1.2 FABRICATION OF NERVE GUIDANCE CONDUIT BY DIP-MOULDING

Nerve guidance conduits were fabricated by the dip-moulding technique using various conditions (Table 7.1).

Table 7.1. Varying dip-moulding conditions used for fabrication of NGCs.		
NGCs	Dip-moulding conditions	Thickness (mm)
1	Condition 1	0.31
2	Condition 2	0.31
3	Condition 3	0.44
4	Condition 4	0.34

The mandrel was secured to a dipping apparatus and dipped into a 75:25 P(3HO)/P(3HB) (15 wt%) solution every 10 seconds, for a total of 10-12 dips at different rates

(Table 7.1). After dipping, the conduits were left in the fume hood for evaporation of solvent at atmospheric pressure for 10 days and the thickness was measured (Figure 7.2, Table 7.1).

After drying, 1 cm length tubes were cut for *in vivo* experiments (Figure 7.2 B). All NGCs were transparent and showed to be flexible, which are desirable features since they facilitate the suturing procedure. Moreover, all NGCs were completely dried after 10 days and no stickiness was detected.

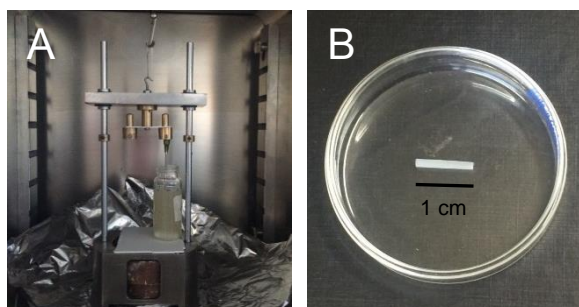


Figure 7.2. Manufacturing of NGCs by dip-moulding. A) Dip-moulding apparatus with a 75:25 P(3HO)/P(3HB) blend solution (15 % w/v). B) Dried hollow NGC fabricated using dip-moulding.

7.3 DISCUSSION

The use of nerve guidance conduits (NGCs) to re-connect peripheral nerve gaps has been extensively investigated in the last 20 years. Notable efforts have been made to overcome the limitations of using the standard treatment autografting. A diverse range of biomaterials has been investigated for their use as base materials for the manufacture of NGCs such as aliphatic polyesters, polylactic acids (PLA), polycaprolactones (PCL), polyurethanes, silicon, collagen, glycoproteins, polypeptides, polyhydroxyalkanoates, polysaccharides, proteins and acellular extracellular matrix. Although some NGCs made from natural and synthetic materials have been clinically approved, the regeneration obtained using these commercial NGCs is only comparable with that using autologous graft when the gaps are less than 3 cm. Commercial NGCs have shown to induce scar tissue formation and release of compounds that are detrimental for the nerve regeneration process. Therefore, in this study, blends of PHAs that have not been used before for the manufacturing of NGCs were fabricated. It is well-known that PHAs display properties that could overcome some of the limitations of the available NGCs. PHAs exhibit controllable surface erosion, lower acidity of their degradation products and longer-lasting stability compared to their synthetic counterparts.

The electrospinning technique as well as the solvent-casting method allowed the fabrication of a nerve guidance conduit with luminal electrospun aligned fibres (Fig. 7.1). Due

to the fact that 25:75 P(3HO)/P(3HB) blend fibres showed high biocompatibility with neuronal cells NG108-15 and support neuronal differentiation (Chapter 5), this blend was chosen to electrospin the surface of a 25:75 P(3HO)/P(3HB) blend sheet. Although this NGC shows noticeable potential because of the proven high biocompatibility of its base materials, the resulting discontinuity observed after joining its borders could have hampered the appropriate suturing of the conduit to the nerve stumps. Furthermore, deformation of the electrospun fibres was observed after using the polymer solution (25:75 P(3HO)/P(3HB) blend) to join the borders. On the other hand, NGCs produced by dip-moulding were well-shaped and reproducible under all the conditions tested (Table 7.1 and Fig. 7.2). Moreover, these NGCs exhibited the adequate transparency and flexibility required for suturing. They were found to be manoeuvrable by the surgeons which facilitated the implantation of the conduits in the rats.

The only PHAs that have been used as base material for the manufacturing of NGCs are P(3HB) and (3-hydroxybutyrate-co-3-hydroxyvalerate) (PHBV). Yong et al. (2002) fabricated P(3HB) conduits to bridge 2, 3 and 4 cm gaps and implanted in rabbit common-peroneal-nerve injury model. The regeneration outcome resulted from the P(3HB) conduits was compared to that obtained using autografting. At 42 days, the area of immunostained regenerating fibres in the P(3HB) group was found to be greater than that obtained in the nerve autograft group. P(3HB) base conduits have been shown to support peripheral nerve regeneration up to 63 days proving their suitability for long-gap nerve injury repair. Mohanna et al. (2005) compared the performance of three P(3HB) conduits to bridge both 2 cm and 4 cm nerve gaps in rabbit peroneal nerve. The P(3HB) conduits consisted of P(3HB) tubes containing glial growth factor (PHB-GGF), P(3HB) tubes containing alginate matrix (PHB-ALG), and empty P(3HB) conduits (E-PHB). At 63 days postoperatively, nerve regeneration assisted by the PHB-GGF conduit was significantly superior to that obtained with other two conduits and resulted in motor organ reinervation. Moreover, at 120 days after implantation, analysis of regenerated nerves showed that PHB-GGF conduit displayed higher number of Schwann cells and superior axonal regeneration when compared to the other conduits. Also, higher number of minifascicles with myelinated fibres were found when PHB-GGF conduit was used. PHB-GGF conduits also showed reduced muscle mass percentage loss when compared to controls. However, although P(3HB) displays high biocompatibility with neuronal cells, it lacks the mechanical properties required for peripheral nerve regeneration. P(3HB) is a well-known brittle polymer widely used in bone tissue engineering with a Young's modulus and a tensile strength of 1160 ± 185.87 MPa and 28.60 ± 1.76 MPa respectively.

Biazar and Keshel (2014) designed (3-hydroxybutyrate-co-3-hydroxyvalerate) (PHBV) conduits with nanofibrous lumen to bridge a 30-mm gap in rat sciatic nerves. The conduits consisted of either, (PHBV) conduits with nanofibrous lumen immersed in gelatin and (PHBV)

conduits with nanofibrous lumen immersed in gelatin containing Schwann cells. Nerve regeneration was compared to both, a negative control (non-grafted group) and to autografting. After 4 months of implantation, (PHBV) conduits with nanofibrous lumen immersed in gelatin containing Schwann cells showed better nerve regeneration performance when compared to control and (PHBV) conduits with nanofibrous lumen immersed in gelatin. Reconstruction of the sciatic nerve truck with restoration of nerve continuity, formation of myelinated nerve fibres and re-innervation of skeletal muscle were found superior when (PHBV) conduits with nanofibrous lumen immersed in gelatin containing Schwann cells and autografting were compared to the other conduits. Although the physical, structural and mechanical properties of these (PHBV) conduits were suitable for peripheral nerve regeneration, the results displayed by these conduits were inferior to those obtained using the gold standard treatment autografting.

Since 75:25 P(3HO)/P(3HB) blend films exhibited in previous studies the required flexibility to be implanted in peripheral nerves, this material was chosen for the fabrication of NGCs (Lizarraga-Valderrama et al., 2015). Both, Young's modulus (1.25 ± 0.18 MPa) and tensile strength (0.71 ± 0.08 MPa) of the 75:25 P(3HO)/P(3HB) blend are similar to those of peripheral nerves in rats ($0.58 \text{ MPa} \pm 0.16 \text{ MPa}$ and $1.4 \pm 0.29 \text{ MPa}$ respectively).

Further studies need to be performed to assess the efficiency of the 75:25 P(3HO)/P(3HB) NGCs in supporting peripheral nerve regeneration. Several replicates of the 75:25 P(3HO)/P(3HB) blend NGCs need to be implanted in rats and withdrawn after a period of at least 7 weeks, since animals usually start to recover after 6-7 weeks after tube implantation. Also, quantitative studies of vital parameters for nerve regeneration such as number of myelinated and unmyelinated nerve fibres need to be performed and compared with autografting outcomes.

Chapter 8

Conclusions

8 CONCLUSIONS

In this work *B. cereus* SVP and *P. mendocina* were successfully used for the production of two polyhydroxyalkanoates, P(3HB) and P(3HO) respectively. Chemical characterization of both P(3HO) and P(3HB) using ^1H NMR and ^{13}C NMR, GCMS and FTIR have allowed the identification and confirmation of the chemical structure of these polyhydroxyalkanoates. The culture conditions used for the production of these PHAs allowed the production of appropriate amounts of polymer for detailed characterisation and manufacturing of scaffolds (PHA fibres and PHA/BG composites) for tissue engineering.

The fabrication and characterization of the various P(3HO)/P(3HB) blend film compositions; neat P(3HO); 75:25 P(3HO)/P(3HB); 50:50 P(3HO)/P(3HB); 25:75 P(3HO)/P(3HB) and neat P(3HB) showed significant differences in their surface features affecting the efficiently with which neuronal cells NG-108 attached and differentiated. A correlation between the roughness presented in these films and the presence of pores was established. Most porous blend film surfaces presented higher R_q values. A decrease in wettability was observed in the blend films as the P(3HO) content increased demonstrating the higher number of hydrophobic chains present in these films. Higher Young's modulus values obtained for the P(3HO) and 50:50 P(3HO)/P(3HB) blends could be the result of variations in the molecular weight of the polymers. It has been shown that lower molecular weights of the same polymer increase Young's modulus and tensile strength values. Therefore, these results suggested that the molecular weight of the P(3HO) used could be higher than that used in previous studies confirming that fermentation conditions affect the molecular weight of PHAs. The Young's modulus of the 75:25 P(3HO)/P(3HB) blend (1.25 ± 0.18 MPa) and the tensile strength (0.71 ± 0.08 MPa) were the most similar to that of peripheral nerves in rats (0.58 MPa \pm 0.16 MPa and 1.4 ± 0.29 MPa respectively). Therefore, PHA-based blends could provide the appropriate strength and elasticity that NGCs require for adequate flexibility at the site of implantation. The 25:75 blend supported significantly better growth and differentiation of NG108-15 neuronal cells. The growth of NG108-15 neuronal cells was characterized by their irregular distribution in various layers on all substrates showing a random attachment and migration of cells.

In summary, although all of the P(3HO)/P(3HB) blends, neat P(3HO) and P(3HB) were able to support neuronal growth, the 25:75 P(3HO)/P(3HB) and P(3HB) films supported better neurite extension. Although both 75:25 P(3HO)/P(3HB) and 25:75 P(3HO)/P(3HB) blends presented suitable tensile strength and percentage of strain for their application in peripheral nerve repair, the 25:75 P(3HO)/P(3HB) blend displayed the highest biocompatibility among all the substrates.

Highly aligned and uniform fibres with varying diametres were successfully fabricated by controlling electrospinning parametres. Preliminary studies were carried out to evaluate the effect of fibers on the growth of neuronal cells NG108-15 by live/dead cell test. Cell migration observed on the electrospun fibres showed directional alignment in accordance with the direction of the fibres. The distribution of cells on the electrospun fibres had a more uniform arrangement when compared with that on the 25:75 P(3HO)/P(3HB) blend film surface. This finding agreed with previous studies in which electrospun fibres have shown to affect cell proliferation, differentiation and migration. Additionally, no cytotoxic effect was found when neuronal cells were grown in any of the studied substrates. Thereafter, the relationship between 25:75 P(3HO)/P(3HB) micro-fibres diameter and neuronal growth under two conditions; individually and in co-culture with RN22 Schwann cells was evaluated. This relationship was investigated using two types of cell staining; live/dead cell test and anti-beta tubulin immunolabelling. Results displayed from both essays revealed that all 25:75 P(3HO)/P(3HB) blend fibre groups were able not only to support growth but also to guide aligned distribution of neuronal cells when grown individually and in the presence of RN22 Schwann cells. All the substrates, including the controls were found to support neurite outgrowth. Although the counting of neurite bearing cells was not possible, a more complex multi-cellular organization was observed in the fibre scaffolds. Results revealed a direct relationship between fiber diametre and neuronal growth and differentiation. The greatest number of neuronal cells was displayed by large fibres while no significant difference was found between small and medium fibres. Interestingly, when neuronal cells were grown in co-culture with RN22 Schwann cells, the number of NG108-15 cells increased as the fibre diametre increased. Although RN22 cells were scarcely detected, statistical analysis showed significant increments in the number of neuronal cells NG108-15 in three substrates when grown in co-culture with this Schwann cell line. The number of NG108-15 cells increased significantly on medium fibres, large fibres and PHA blend film when co-cultured with RN22 cells. These findings suggested that RN22 cells are able to enhance significantly neuronal cell growth. This could be due to the secretion of a combination of neurotrophic factors (e.g. NGF and BDNF) from RN22 cells to the culture media and these could have been metabolized by neuronal NG108-15 cells.

Biomaterial development is focused on surface modifications of biocompatible materials in order to acquire a greater understanding of cell-surface interactions and improved biocompatibility. The surface hydrophobicity, roughness and porosity are well known as key factors that affect cell response. Greater wettability and roughness as well as the presence of pores have shown to favour cell attachment, growth and differentiation.

The microstructure of the PHA blend/bioglass composites was affected by the concentration of bioactive glasses in the composite. The concentration of BG1 and BG2 showed an effect not only in the pore size of PHA blend/BG composites, but also in the formations of porous systems. The discrepancy found in the roughness and water contact angle values displayed in this study compared to previous studies exposes the great importance of considering the fluid leveling when solvent casting method is used. Strategies should be taken into account to control evaporation rates in order to have more consistent measurements. The good growth and differentiation performance of NG108-15 cells displayed on all the PHA blend composites have shown that both bioactive glasses (BG1 and BG2) have good biocompatibility at 2.5, 1.0 and 0.5 % w/v in PHA blends solution. The growth and differentiation performance of NG108-15 cells on the remaining of PHA blend/composites was variable in the live/dead cell test, neurite outgrowth assessment on NG108-15 neuronal cell and on NG108-15/Schwann cell co-cultures. In general, both bioactive glasses showed to have a significant impact on the biocompatibility of the PHA blend. In all the experiments the presence of bioactive glasses at all concentrations (0.5 % w/v, 1.0 % w/v, 2.5% w/v) increased the number of differentiated neuronal cells with respect to both the PHA blend control and PCL control. Although 1393 bioactive glass (BG2) has shown to support neuronal regeneration, 45S5 (BG2) demonstrated superior performance in supporting cell growth and differentiation of NG108-15 cells. The presence of Schwannoma RN22 cells in NG108-15 cultures had a positive effect in the growth and differentiation of these neuronal cells on all the PHA blend/composites excepting for the PHA blend/BG1. In this composite the number of differentiated NG108-15 did not increase when grown in co-culture with RN22 cells. Although only few RN22 cells were detectable at the end of the experiment, they have shown to support not only neuronal growth but also axonal extension.

The electrospinning technique as well as the solvent-casting method allowed the fabrication of a nerve guidance conduit with luminal electrospun aligned fibres. NGCs were also produced using dip-moulding, which resulted to be well-shaped and reproducible under all the conditions tested. Moreover, these NGCs exhibited the adequate transparency and flexibility required for surgical suturation.

To summarize, the biocompatibility and mechanical properties of 25:75 and 75:25 P(3HO)/P(3HB) blends make these polymers excellent materials to be used for the manufacturing of scaffolds for nerve tissue engineering.

Chapter 9

Future perspectives

The results presented from Chapter 3 to Chapter 7 constitute major preliminary studies that have to be carried out for the screening of materials to be used in nerve tissue engineering with the final aim of manufacturing improved nerve guidance conduits.

Although polymer production resulted in desired amounts of both P(3HO) and P(3HB), further studies should be performed to increase these polymer yields. It is well-known that PHA production is still expensive due to the media components, consumed water and electricity. Optimization of fermentation conditions should aim to increase the polymer yields but also to decrease the cost of production. Moreover, further studies in the use of renewable sources of carbon and nutrients such as PHA production from wastes such as starch, whey, molasses, bagasse and soymeal could contribute substantially for the development of a more sustainable and cost-effective PHA production.

Biocompatibility studies of P(3HO)/P(3HB) films with varying compositions; P(3HO), 75:25 P(3HO)/P(3HB), 50:50 P(3HO)/P(3HB), 25:75 P(3HO)/P(3HB) and P(3HB); were based on live/dead cell test and immunolabelling of beta-tubulin after culturing of NG108-15 cells on films. Although the culturing of NG108-15 cells is a versatile and practical tool for the preliminary screening of materials, the results obtained by using only this cell line are not conclusive. Further studies should be performed to study the effect of Schwann cells on the growth and differentiation of neuronal cells on these composites. This could be achieved by using co-cultures of NG108-15/RN22 Schwann cells, NG108-15/primary Schwann cells and/or dorsal root ganglion/Schwann cells.

Varying concentrations of P(3HO)/P(3HB) using 5 different PHA compositions (P(3HO), 75:25 P(3HO)/P(3HB), 50:50 P(3HO)/P(3HB), 25:75 P(3HO)/P(3HB) and P(3HB)) were used for the production of varying aligned fiber diameters. Although this investigation was focused on the production of aligned fibres for nerve tissue engineering applications, further studies should be performed to evaluate their biocompatibility with other cell types. Aligned and random fibres have potential applications in other areas of tissue engineering such as cardiac tissue engineering or skin tissue engineering.

Although co-cultures of NG108-15/RN22 Schwann cells allowed to study the effect of Schwann cells on neuronal cells growth and differentiation, further studies should be performed by using co-cultures of NG108-15/RN22 Schwann cells, NG108-15/primary Schwann cells and/or dorsal root ganglion/Schwann cells. When RN22 Schwann cells were grown in co-culture with NG108-15 on fibres and bioactive glass composites, only few RN22 Schwann cells were detected after fixation treatments. Experiments using primary cells would result in more accurate estimations of neuronal regeneration as they more closely mimic nerve

tissue environment.

Solvent casting of polymer solutions is a well-known method, which is routinely used to prepare coatings in a wide variety of industrial and biological applications. This method was used for the production of all the films characterized in Chapter 3 and 6. Discrepancies were found in the roughness of films made from similar material compositions. As it has been shown that the evaporation rate of solvent affects significantly the surface roughness of the films, a more controlled solvent evaporation should be taken into consideration when using solvent casting method. This would allow the acquisition of a reproducible method that ensures the control of pores formation.

Further studies should be carried on to study the interaction of bioactive glasses with neuronal cells and Schwann cells. When bioactive glasses start to dissolve in cell cultures, they release mineral ions that can affect the cellular growth and differentiation. As composites made from bioactive glasses supported superior performance of cell growth and differentiation compared to PHA films, studies of the minerals involved in neuronal cell metabolism is vital for understanding the specific effect of bioactive glasses on neuronal regeneration. Therefore, specific compositions of bioactive glasses could be formulated specially to improve peripheral nerve regeneration.

Further studies have to be performed to assess the efficiency of 75:25 P(3HO)/P(3HB) NGCs in supporting peripheral nerve regeneration. Several replicates of 75:25 P(3HO)/P(3HB) blend NGCs should be implanted in rats to perform functional tests. Also, quantitative studies of vital parameters for nerve regeneration such as number of myelinated and unmyelinated nerve fibres must be performed and compared with autografting outcomes.

Electrospun sheet made from thick fibres of 3.68 ± 0.26 and 13.50 ± 2.33 μm diameter should be fabricated for further studies of biocompatibility using co-cultures of NG108-15/RN22 Schwann cells, NG108-15/primary Schwann cells and/or dorsal root ganglion/Schwann cells. The resulting outcome should be evaluated to choose the fibre diameter with superior performance to be used as luminal structure for the fabrication of NGCs. Thereafter, NGCs with electrospun fibres should be tested *in vivo* in order to assess their regeneration efficiency. Moreover, quantitative studies of vital parameters for nerve regeneration such as number of myelinated and unmyelinated nerve fibres must be performed and compared with autografting outcomes.

As the composite 25:75 P(3HO)/P(3HB)/BG1 presented superior performance compared to either, the rest of composites and 25:75 P(3HO)/P(3HB) blend, this material could be used as base material for the manufacturing of NGCs. In a preliminary study 25:75 P(3HO)/P(3HB)/BG1 NGCs could be manufactured by using dip-molding technique to assess their mechanical properties. Moreover, aligned fibres of 25:75 P(3HO)/P(3HB)/BG1 using

varying electrospinning conditions should be tested in order to obtain various fibres diametres for biocompatibility characterization. Finally, if mechanical properties match with those of human peripheral nerves, *in vivo* studies of the resulting NGCs should be performed.

A range of more complex designs should be developed to enhance nerve regeneration involving either, an internal microstructure or a composition of multiples components. Considering that 25:75 P(3HO)/P(3HB) displayed the most suitable mechanical properties for peripheral nerve repair, this blend should be used as the base material for the manufacturing of NGCs. As the composite 25:75 P(3HO)/P(3HB)/BG1 has shown the highest biocompatibility, fibres made from this material would be excellent lumen structures to guide neuronal growth. Biochemical components to support nerve regeneration including support cells along with growth factors could be incorporated into the nerve guidance conduit to enhance nerve repair. For example, glial cells such as primary Schwann cells (SCs) or olfactory ensheathing cells (OECs) combined with support stem cells such as neural stem cells (NSCs), bone marrow stromal cells (BMSCs), induced pluripotent stem cells (iPS), skin-derived precursor cells (SKPs) or adipose-derived mesenchymal stem cells (AMSCs) could be incorporated to the electrospun lumen surface to support cell growth and reproduce an optimal regeneration environment. Simultaneously, growth factors such as neurotrophins or neurotrophic growth factors could be integrated to the nerve constructs to support cell proliferation and cell migration. Additionally, different delivery systems could be implemented to achieve a continuous release of growth factors such as the addition of growth factor-loaded microspheres in the scaffold or direct injection of GFs using an injection device.

Chapter 10

References

10 REFERENCES

1. Agus, J., Kahar, P., Hyakutake, M., Tomizawa, S., Abe, H., Tsuge, T., Satoh, Y., & Tajima. (2010). Unusual change in molecular weight of polyhydroxyalkanoate (PHA) during cultivation of PHA-accumulating *Escherichia coli*. *Polymer Degradation and Stability*. [Online] 95 (12), 2250–2254. Available from: doi:10.1016/j.polymdegradstab.2010.09.009 [Accessed: 20 January 2017].
2. Al-Nasassrah, M.A., Podczeck, F. & Newton, J.M. (1998) The effect of an increase in chain length on the mechanical properties of polyethylene glycols. *European Journal of Pharmaceutics and Biopharmaceutics*. [Online] 46 (1), 31–38. Available from: doi:10.1016/S0939-6411(97)00151-3 [Accessed: 21 January 2017].
3. Anjum, A., Zuber, M., Zia, K.M., Noreen, A., Anjum, M. N., & Tabasum S. (2016). Microbial production of polyhydroxyalkanoates (PHAs) and its copolymers: A review of recent advancements. *International Journal of Biological Macromolecules*. [Online]. 89 pp.161–174. Available from: doi:10.1016/j.ijbiomac.2016.04.069 [Accessed: 18 January 2017].
4. Archibald, S.J., Krarup, C., Shefner, J., Li, S., Madison R. D. (1991). A collagen based nerve guide conduit for peripheral nerve repair: An electrophysiological study of nerve regeneration in rodents and nonhuman primates. *Journal of Comparative Neurology*. [Online] 306 (4), 685–696. Available from: doi:10.1002/cne.903060410 [Accessed: 18 January 2017].
5. Archibald, S.J., Shefner, J., Krarup, : C & Madison, R.D. (1995). Monkey Median Nerve Repaired by Nerve Graft or Collagen Nerve Guide Tube. *The Journal of Neuroscience*. [Online] 15 (5), 4109–4123. [Accessed: 18 January 2017].
6. Armstrong, S.J., Wiberg, M., Terenghi, G. & Kingham, P.J. (2007). ECM Molecules Mediate Both Schwann Cell Proliferation and Activation to Enhance Neurite Outgrowth. *Tissue Engineering*. [Online] 13 (12), 2863–2870. Available from: doi:10.1089/ten.2007.0055 [Accessed: 21 January 2017].

7. Ashley, W.W., Weatherly, T. & Park, T.S. (2006). Collagen nerve guides for surgical repair of brachial plexus birth injury. *Journal of neurosurgery*. [Online] 105 (6 Suppl), 452–456. Available from: doi:10.3171/ped.2006.105.6.452 [Accessed: 18 January 2017].
8. Babu, P., Behl, A., Chakravarty, B., Bhandari, P. S., Bhatti, T. S., & Maurya, S. (2008). Entubulation techniques in peripheral nerve repair. *Indian Journal of Neurotrauma*. [Online] 5 (1), 15–20. Available from: doi:10.1016/S0973-0508(08)80023-8. [Accessed: 18 January 2017].
9. Babu, P., Behl, A., Chakravarty, B., Bhandari, P. S., Bhatti, T.S., & Maurya, S. (2008) Entubulation techniques in peripheral nerve repair. *Indian Journal of Neurotrauma*. [Online] 5 (1), 15–20. Available from: doi:10.1016/S0973-0508(08)80023-8 [Accessed: 18 January 2017].
10. Badami, A.S., Kreke, M.R., Thompson, M.S., Riffle, J.S., & Goldstein AS. (2006). Effect of fiber diameter on spreading, proliferation, and differentiation of osteoblastic cells on electrospun poly(lactic acid) substrates. *Biomaterials*. [Online] 27 (4), 596–606. Available from: doi:10.1016/j.biomaterials.2005.05.084 [Accessed: 18 January 2017].
11. Barras, F.M., Pasche, P., Bouche, N., Aebischer, P., Zurn, A. D. (2002) Glial cell line-derived neurotrophic factor released by synthetic guidance channels promotes facial nerve regeneration in the rat. *Journal of Neuroscience Research*. [Online] 70 (6), 746–755. Available from: doi:10.1002/jnr.10434 [Accessed: 18 January 2017].
12. Basnett, P., Ching, K.Y., Stolz, M., Knowles, J.C., Boccaccini, A.R., Smith, C., Locke, I.C., Keshavarz, T., Roy, I. (2013) Novel Poly(3-hydroxyoctanoate)/Poly(3-hydroxybutyrate) blends for medical applications. *Reactive and Functional Polymers*. [Online] 73 (10), 1340–1348. Available from: doi:10.1016/j.reactfunctpolym.2013.03.019 [Accessed: 18 January 2017].
13. Bell, J.H., & Haycock, J.W. (2011). Next generation nerve guides - materials, fabrication, growth factors and cell delivery. *Tissue engineering Part B: Reviews*. [Online] 0 (0), 116–128. Available from: doi:10.1089/ten.teb.2011.0498 [Accessed: 21 January 2017].

14. Bertleff, M.J.O.E., Meek, M.F. & Nicolai, J.P.A. (2005) A prospective clinical evaluation of biodegradable Neurolac nerve guides for sensory nerve repair in the hand. *Journal of Hand Surgery*. [Online] 30 (3), 513–518. Available from: doi:10.1016/j.jhsa.2004.12.009 [Accessed: 18 January 2017].
15. Bian, Y.Z., Wang, Y., Aibaidoula, G., Chen, G.Q., & Wu, Q. (2009). Evaluation of poly(3-hydroxybutyrate-co-3-hydroxyhexanoate) conduits for peripheral nerve regeneration. *Biomaterials*. [Online] 30 (2), 217–225. Available from: doi:10.1016/j.biomaterials.2008.09.036 [Accessed: 18 January 2017].
16. Biazar, E. & Keshel, S.H. (2013) Chitosan-cross-linked nanofibrous PHBV nerve guide for rat sciatic nerve regeneration across a defect bridge. *ASAIO journal (American Society for Artificial Internal Organs : 1992)*. [Online] 59 (6), 651–659. Available from: doi:10.1097/MAT.0b013e3182a79151 [Accessed: 18 January 2017].
17. Bini, T.B., Gao, S., Xu, X., Wang, S., Ramakrishna, S., & K. W Leong. (2004) Peripheral nerve regeneration by microbraided poly(L-lactide-co-glycolide) biodegradable polymer fibers. *Journal of biomedical materials research. Part A*. [Online] 68 (2), 286–295. Available from: doi:10.1002/jbm.a.20050 [Accessed: 18 January 2017].
18. Binns, K.L., Taylor, P.P., Sicheri, F., Pawson, T., & Holland S.J. (2000). Phosphorylation of tyrosine residues in the kinase domain and juxtamembrane region regulates the biological and catalytic activities of Eph receptors. *Molecular and cellular biology*. [Online] 20 (13), 4791–4805. Available from: doi:10.1128/MCB.20.13.4791-4805.2000 [Accessed: 18 January 2017].
19. Blaker, J.J., Nazhat, S.N. & Boccaccini, A.R. (2004) Development and characterisation of silver-doped bioactive glass-coated sutures for tissue engineering and wound healing applications. *Biomaterials*. [Online] 25 (7–8), 1319–1329. Available from: doi:10.1016/j.biomaterials.2003.08.007 [Accessed: 18 January 2017].
20. Borkenhagen, M., Stoll, R.C., Neuenschwander, P., Suter, U.W., & P. Aebischer. (1998) In vivo performance of a new biodegradable polyester urethane system used

as a nerve guidance channel. *Biomaterials*. [Online] 19 (23), 2155–2165. Available from: doi:10.1016/S0142-9612(98)00122-7 [Accessed: 18 January 2017].

21. Borschel, G.H., Kia, K.F., Kuzon, W.M., Dennis, R.G., et al. (2003) Mechanical properties of acellular peripheral nerve. *The Journal of surgical research*. [Online] 114 (2), 133–139. Available from: doi:10.1016/S0022-4804(03)00255-5 [Accessed: 15 June 2017].
22. Brigham & Sinskey (2012) Applications of Polyhydroxyalkanoates in the Medical Industry. *International Journal of Biotechnology for Wellness Industries*. [Online] 153–60. Available from: doi:10.6000/1927-3037.2012.01.01.03 [Accessed: 18 January 2017].
23. Bryan, D.J., Tang, J.B., Holway, A.H., Rieger-Christ, K.M., Trantolo D.J, Wise D.L, & Summerhayes, I.C. (2003) Enhanced peripheral nerve regeneration elicited by cell-mediated events delivered via a bioresorbable PLGA guide. *Journal of Reconstructive Microsurgery*. [Online] 19 (2), 125–134. Available from: doi:10.1055/s-2003-37820 [Accessed: 18 January 2017].
24. Bunting, S., Di Silvio, L., Deb, S., & Hall, S. (2005) Bioresorbable glass fibres facilitate peripheral nerve regeneration. *Journal of Hand Surgery*. [Online] 30 (3), 242–247. Available from: doi:10.1016/j.jhsb.2004.11.003 [Accessed: 18 January 2017].
25. Bushnell, B.D., McWilliams, A.D., Whitener, G.B. & Messer, T.M. (2008) Early Clinical Experience With Collagen Nerve Tubes in Digital Nerve Repair. *Journal of Hand Surgery*. [Online] 33 (7), 1081–1087. Available from: doi:10.1016/j.jhsa.2008.03.015 [Accessed: 18 January 2017].
26. Cai, J., Peng, X., Nelson, K.D., Eberhart, R., & Smith, G.M. (2005) Permeable guidance channels containing microfilament scaffolds enhance axon growth and maturation. *Journal of Biomedical Materials Research - Part A*. [Online] 75 (2), 374–386. Available from: doi:10.1002/jbm.a.30432 [Accessed: 18 January 2017].
27. Cai, Y., Yan, L., Liu, G., Yuan, H., & Xiao, D. (2013). In-situ synthesis of fluorescent gold nanoclusters with electrospun fibrous membrane and application on Hg (II) sensing. *Biosensors and Bioelectronics*. [Online] 41 (1), 875–879. Available from: doi:10.1016/j.bios.2012.08.064 [Accessed: 18 January 2017].

28. Capitán, M.J., Rueda, D.R. & Ezquerro, T.A. (2004) Inhibition of the crystallization in nanofilms of poly(3-hydroxybutyrate). *Macromolecules*. [Online] 37 (15), 5653–5659. Available from: doi:10.1021/ma049576p [Accessed: 18 January 2017].
29. Cargill, R.S., Dee, K.C. & Malcolm, S. (1999) An assessment of the strength of NG108-15 cell adhesion to chemically modified surfaces. *Biomaterials*. [Online] 20 (23–24), 2417–2425. Available from: doi:10.1016/S0142-9612(99)00169-6 [Accessed: 18 January 2017].
30. Chang, C. J., S. H. Hsu, H. J. Yen, H. Chang, and S. K. Hsu. (2007). Effects of unidirectional permeability in asymmetric poly(DL-lactic acid-co-glycolic acid) conduits on peripheral nerve regeneration: an in vitro and in vivo study. *Journal of Biomedical Materials Research. Part B, Applied Biomaterials*. [Online] 83 (1), 206–215. Available from: doi: 10.1002/jbm.b.30785 [Accessed: 18 January 2017].
31. Chang, C.J. & Hsu, S.H. (2006) The effect of high outflow permeability in asymmetric poly(DL-lactic acid-co-glycolic acid) conduits for peripheral nerve regeneration. *Biomaterials*. [Online] 27 (7), 1035–1042. Available from: doi:10.1016/j.biomaterials.2005.07.003 [Accessed: 18 January 2017].
32. Charness, M.E., Safran, R.M. & Perides, G. (1994). Ethanol inhibits neural cell-cell adhesion. *Journal of Biological Chemistry*. 269 (12), 9304–9309.
33. Chen, C.-J., Ou, Y.-C., Liao, S.-L., Chen, W.-Y., Chen, S. Y., Wu, C. W., Wang, C. C., Wang, W. Y., Huang, Y. S., & Hsu, S. H. (2007) Transplantation of bone marrow stromal cells for peripheral nerve repair. *Experimental neurology*. [Online] 204 (1), 443–453. Available from: doi:10.1016/j.expneurol.2006.12.004 [Accessed: 18 January 2017].
34. Chen, G.-Q. (2010) Plastics Completely Synthesized by Bacteria: Polyhydroxyalkanoates. *Plastics from Bacteria: Natural Functions and Applications*. [Online] 14 (10), 121–132. Available from: doi:10.1007/978-3-642-03287_5 [Accessed: 18 January 2017].

35. Chen, G.Q. & Wu, Q. (2005) The application of polyhydroxyalkanoates as tissue engineering materials. *Biomaterials*. [Online]. 26 (33) pp.6565–6578. Available from: doi:10.1016/j.biomaterials.2005.04.036 [Accessed: 18 January 2017].
36. Chen, Y.S., Hsieh, C.L., Tsai, C.C., Chen, T.H., Cheng, W. C., Hu, C. L., & Yao, C. H. (2000) Peripheral nerve regeneration using silicone rubber chambers filled with collagen, laminin and fibronectin. *Biomaterials*. [Online] 21 (15), 1541–1547. Available from: doi:10.1016/S0142-9612(00)00028-4 [Accessed: 18 January 2017].
37. Cheng, B. & Chen, Z. (2002) Fabricating autologous tissue to engineer artificial nerve. *Microsurgery*. [Online] 22 (4), 133–137. Available from: doi:10.1002/micr.21740 [Accessed: 18 January 2017].
38. Chew, S.Y., Mi, R., Hoke, A. & Leong, K.W. (2007) Aligned Protein–Polymer Composite Fibers Enhance Nerve Regeneration: A Potential Tissue-Engineering Platform. *Advanced Functional Materials*. [Online] 17 (8), 1288–1296. Available from: doi:10.1002/adfm.200600441 [Accessed: 21 January 2017].
39. Chew, S.Y., Mi, R., Hoke, A. & Leong, K.W. (2007) Aligned Protein–Polymer Composite Fibers Enhance Nerve Regeneration: A Potential Tissue-Engineering Platform. *Advanced Functional Materials*. [Online] 17 (8), 1288–1296. Available from: doi:10.1002/adfm.200600441 [Accessed: 18 January 2017].
40. Chomiak, T. & Hu, B. (2009) What is the optimal value of the g-ratio for myelinated fibers in the rat CNS? A theoretical approach David Finkelstein (ed.). *PLoS ONE*. [Online] 4 (11), e7754. Available from: doi:10.1371/journal.pone.0007754 [Accessed: 17 January 2017].
41. Corey, J.M., Lin, D.Y., Mycek, K.B., Chen, Q., Samuel, S., Feldman, E.L., & Martin, D.C. (2007). Aligned electrospun nanofibers specify the direction of dorsal root ganglia neurite growth. *Journal of Biomedical Materials Research - Part A*. [Online] 83 (3), 636–645. Available from: doi:10.1002/jbm.a.31285 [Accessed: 21 January 2017].
42. Daud, M. F. (2013). An organized 3D in vitro model for peripheral nerve studies. Doctoral thesis. University of Sheffield, Sheffield, United Kingdom.

43. Daud, M.F.B., Pawar, K.C., Claeysens, F., Ryan, A.J., & Haycock, J. W. (2012). An aligned 3D neuronal-glia co-culture model for peripheral nerve studies. *Biomaterials*. [Online] 33 (25), 5901–5913. Available from: doi:10.1016/j.biomaterials.2012.05.008 [Accessed: 18 January 2017].
44. De Jaco, A., Comoletti, D., Kovarik, Z., Gaietta, G., et al. (2006) A mutation linked with autism reveals a common mechanism of endoplasmic reticulum retention for the α , β hydrolase fold protein family. *Journal of Biological Chemistry*. [Online] 281 (14), 9667–9676. Available from: doi:10.1074/jbc.M510262200 [Accessed: 18 January 2017].
45. de Ruiter, G.C.W., Malessy, M.J.A., Yaszemski, M.J., Windebank, A.J., et al. (2009) Designing ideal conduits for peripheral nerve repair. *Neurosurgical focus*. [Online] 26 (2), E5. Available from: doi:10.3171/FOC.2009.26.2.E5 [Accessed: 17 January 2017].
46. Doolabh V. B., M. C. Hertl, and S. E. Mackinnon. (1996). The Role of Conduits in Nerve Repair: A Review. *Reviews in the Neurosciences*. [Online] 7(1), 47–84. Available from: doi <https://doi.org/10.1515/REVNEURO.1996.7.1.47> [Accessed: 18 January 2017].
47. Du, G. & Yu, J. (2002) Metabolic analysis on fatty acid utilization by *Pseudomonas oleovorans*: mcl-poly(3-hydroxyalkanoates) synthesis versus oxidation. *Process Biochemistry*. [Online] 38 (3), 325–332. Available from: doi:10.1016/S0032-9592(02)00084-5 [Accessed: 18 January 2017].
48. Du, G. & Yu, J. (2002b). Green technology for conversion of food scraps to biodegradable thermoplastic polyhydroxyalkanoates. *Environmental Science and Technology*. [Online] 36 (24), 5511–5516. Available from: doi:10.1021/es011110o [Accessed: 18 January 2017]
49. Du, G., Si, Y. & Yu, J. (2001a). Inhibitory effect of medium-chain-length fatty acids on synthesis of polyhydroxyalkanoates from volatile fatty acids by *Ralstonia eutropha*. *Biotechnology Letters*. [Online] 23 (19), 1613–1617. Available from: doi:10.1023/A:1011916131544 [Accessed: 20 January 2017].

50. Edmondson, R., Broglie, J.J., Adcock, A.F. & Yang, L. (2014). Three-dimensional cell culture systems and their applications in drug discovery and cell-based biosensors. *Assay and drug development technologies*. [Online] 12 (4), 207–218. Available from: doi:10.1089/adt.2014.573 [Accessed: 21 January 2017].
51. El-Gendy, R., Kirkham, J., Newby, P.J., Mohanram, Y., Boccaccini, A. R. & Xuebin, Y. B. (2015) Investigating the Vascularization of Tissue-Engineered Bone Constructs Using Dental Pulp Cells and 45S5 Bioglass® Scaffolds. *Tissue engineering. Part A*. [Online] 21 (13–14), 2034–2043. Available from: doi:10.1089/ten.tea.2014.0485 [Accessed: 20 January 2017].
52. Evans, G.R., K. Brandt, A. D. Niederbichler, P. Chauvin, S. Herrman, M. Bogle, L. Otta, B. Wang, and C. W. Patrick Jr. (2000). Clinical long-term in vivo evaluation of poly (L-lactic acid) porous conduits for peripheral nerve regeneration. *Journal of Biomaterials Science Polymer. Edition*, 11 (8), 869-878.
53. Fansa, H., Schneider, W., Wolf, G. & Keilhoff, G. (2002) Influence of insulin-like growth factor-I (IGF-I) on nerve autografts and tissue-engineered nerve grafts. *Muscle and Nerve*. [Online] 26 (1), 87–93. Available from: doi:10.1002/mus.10165 [Accessed: 18 January 2017].
54. Fields, R.D. & Stevens-Graham, B. (2002) New insights into neuron-glia communication. *Science (New York, N.Y.)*. [Online] 298 (5593), 556–562. Available from: doi:10.1126/science.298.5593.556 [Accessed: 17 January 2017].
55. Fine, E.G., Decosterd, I., Papaloizos, M., Zurn, A.D., Aebischer, P. (2002) GDNF and NGF released by synthetic guidance channels support sciatic nerve regeneration across a long gap. *European Journal of Neuroscience*. [Online] 15 (4), 589–601. Available from: doi:10.1046/j.1460-9568.2002.01892.x [Accessed: 18 January 2017].
56. Fine, E.G., Valentini, R.F., Bellamkonda, R. & Aebischer, P. (1991) Improved nerve regeneration through piezoelectric vinylidene fluoride-trifluoroethylene copolymer guidance channels. *Biomaterials*. [Online] 12 (8), 775–780. Available from: doi:10.1016/0142-9612(91)90029-A [Accessed: 18 January 2017].

57. Förch, R., Schönherr, H., Jenkins, A. T. A. (2009). Appendix C: Contact Angle Goniometry. In: Förch, R., Schönherr, H., Jenkins, A. T. A. (Ed.), *Surface Design: Applications in Bioscience and Nanotechnology*. Weinheim: Wiley-VCH Verlag GmbH & Co. KGaA, 471-473.
58. Fu, Q., Rahaman, M.N., Fu, H. & Liu, X. (2010) Silicate, borosilicate, and borate bioactive glass scaffolds with controllable degradation rate for bone tissue engineering applications. I. Preparation and in vitro degradation. *Journal of Biomedical Materials Research - Part A*. [Online] 95 (1), 164–171. Available from: doi:10.1002/jbm.a.32824 [Accessed: 21 January 2017].
59. Furrer, P., Hany, R., Rentsch, D., Grubelnik, A., Ruth, K., Panke, S., and Manfred Z. (2007) Quantitative analysis of bacterial medium-chain-length poly([R]-3-hydroxyalkanoates) by gas chromatography. *Journal of Chromatography A*. [Online] 1143 (1–2), 199–206. Available from: doi:10.1016/j.chroma.2007.01.002 [Accessed: 18 January 2017].
60. Gamez, E., Goto, Y., Nagata, K., Iwaki, T., Sasaki, T., and Matsuda, T. (2004) Photofabricated gelatin-based nerve conduits: Nerve tissue regeneration potentials. *Cell Transplantation*. [Online] 13 (5), 549–564. Available from: doi:10.3727/000000004783983639 [Accessed: 20 January 2017].
61. Gaudet, A.D., Popovich, P.G. & Ramer, M.S. (2011) Wallerian degeneration: Gaining perspective on inflammatory events after peripheral nerve injury. *Journal of Neuroinflammation*. [Online] 8 (110), 1-13. Available from: doi:10.1186/1742-2094-8-110 [Accessed: 18 January 2017].
62. Goddard, J.M. & Hotchkiss, J.H. (2007). Polymer surface modification for the attachment of bioactive compounds. *Progress in Polymer Science (Oxford)*. [Online]. 32 (7) pp.698–725. Available from: doi:10.1016/j.progpolymsci.2007.04.002 [Accessed: 18 January 2017].
63. Gorustovich, A.A., Steimetz, T., Cabrini, R.L. & Porto López, J.M. (2010). Osteoconductivity of strontium-doped bioactive glass particles: A histomorphometric study in rats. *Journal of Biomedical Materials Research - Part A*. [Online] 92 (1), 232–237. Available from: doi:10.1002/jbm.a.32355 [Accessed: 21 January 2017].

64. Gorustovich, A.A., Steimetz, T., Cabrini, R.L. & Porto López, J.M. (2010). Osteoconductivity of strontium-doped bioactive glass particles: A histomorphometric study in rats. *Journal of Biomedical Materials Research - Part A*. [Online] 92 (1), 232–237. Available from: doi:10.1002/jbm.a.32355 [Accessed: 20 January 2017].
65. Grage, K., Jahns, A.C., Parlane, N., Palanisamy, R., Rasiah, I. A., Atwood, J. A., & Rehm, B. H. A. (2009) Bacterial polyhydroxyalkanoate granules: Biogenesis, structure, and potential use as nano-/micro-beads in biotechnological and biomedical applications. In: *Biomacromolecules*. [Online]. 13 April 2009 American Chemical Society. pp. 660–669. Available from: doi:10.1021/bm801394s [Accessed: 20 January 2017].
66. Greiner, A. & Wendorff, J.H. (2007) Electrospinning: A fascinating method for the preparation of ultrathin fibers. *Angewandte Chemie - International Edition*. [Online]. 46 (30) pp.5670–5703. Available from: doi:10.1002/anie.200604646 [Accessed: 20 January 2017].
67. Griffin, J.W., Hogan, M. V, Chhabra, A.B. & Deal, D.N. (2013) Peripheral nerve repair and reconstruction. *The Journal of Bone and Joint Surgery – American Volume*. [Online] 95 (23), 2144–2151. Available from: doi:10.2106/jbjs.l.00704 [Accessed: 17 January 2017].
68. Guénard, V., Kleitman, N., Morrissey, T.K., Bunge, R.P., et al. (1992) Syngeneic Schwann cells derived from adult nerves seeded in semipermeable guidance channels enhance peripheral nerve regeneration. *The Journal of neuroscience: the official journal of the Society for Neuroscience*. 12 (9), 3310–3320. (26)
69. Gutmann, J.S., Müller-Buschbaum, P., Schubert, D.W., Stribeck, N., Smilgies, D., & Stamm, M. (2000). Roughness correlations in ultra-thin polymer blend films. *Physica B: Condensed Matter*. [Online] 283 (1–3), 40–44. Available from: doi:10.1016/S0921-4526(99)01888-8 [Accessed: 21 January 2017].
70. Hart, A.M., Wiberg, M. & Terenghi, G. (2003) Exogenous leukaemia inhibitory factor enhances nerve regeneration after late secondary repair using a bioartificial nerve conduit. *British Journal of Plastic Surgery*. [Online] 56 (5), 444–450. Available from: doi:10.1016/S0007-1226(03)00134-6 [Accessed: 18 January 2017].

71. Haycock, J.W. (2011). *3D cell culture: a review of current approaches and techniques*. [Online]. Available from: doi:10.1007/978-1-60761-984-0_1 [Accessed: 21 January 2017].
72. Hazari, A., Wiberg, M., Johansson-Rudén, G., Green, & Terenghi, G. (1999) A resorbable nerve conduit as an alternative to nerve autograft in nerve gap repair. *British journal of plastic surgery*. [Online] 52 (8), 653–657. Available from: doi:10.1054/bjps.1999.3184 [Accessed: 18 January 2017].
73. Hench, L.L. (1970) Semiconducting glass-ceramics. *Journal of Non-Crystalline Solids*. [Online] 2 (C), 250–277. Available from: doi:10.1016/0022-3093(70)90143-2 [Accessed: 18 January 2017].
74. Hobson, M.I., Green, C.J. & Terenghi, G. (2000) VEGF enhances intraneural angiogenesis and improves nerve regeneration after axotomy. *Journal of anatomy*. [Online] 197 Pt 4591–605. Available from: doi:10.1046/j.1469-7580.2000.19740591.x [Accessed: 18 January 2017].
75. Hoppe, A., Jokic, B., Janackovic, D., Fey, Greil, P., Romeis, S., Schmidt, J., Peukert, W., Lao, J., Jallot, E., & Boccaccini A.R. (2014) Cobalt-releasing 1393 bioactive glass-derived scaffolds for bone tissue engineering applications. *ACS Applied Materials and Interfaces*. [Online] 6 (4), 2865–2877. Available from: doi:10.1021/am405354y [Accessed: 21 January 2017].
76. Hu, W., Gu, J., Deng, A. & Gu, X. (2008) Polyglycolic acid filaments guide Schwann cell migration in vitro and in vivo. *Biotechnology Letters*. [Online] 30 (11), 1937–1942. Available from: doi:10.1007/s10529-008-9795-1 [Accessed: 18 January 2017].
77. Hu, X., Cai, J., Yang, J. & Smith, G.M. (2010) Sensory axon targeting is increased by NGF gene therapy within the lesioned adult femoral nerve. *Experimental Neurology*. [Online] 223 (1), 153–165. Available from: doi:10.1016/j.expneurol.2009.08.025 [Accessed: 18 January 2017].
78. Huang, W., Begum, R., Barber, T., Ibba, V., Tee N. C. H., Hussain M., Arastoo M., Yang Q., Robson L. G., Lesage S., Gheysens T., Skaer N. J. V., Knight D. P., & Priestley J. V. (2012) Regenerative potential of silk conduits in repair of peripheral

- nerve injury in adult rats. *Biomaterials*. [Online] 33 (1), 59–71. Available from: doi:10.1016/j.biomaterials.2011.09.030 [Accessed: 18 January 2017].
79. Huebner, E.A. & Strittmatter, S.M. (2009) Axon regeneration in the peripheral and central nervous systems. *Results and Problems in Cell Differentiation*. [Online] 48, 339–351. Available from: doi:10.1007/400_2009_19 [Accessed: 18 January 2017].
80. Hynes, R.O. (2002) Integrins: bidirectional, allosteric signaling machines. *Cell*. [Online] 110 (6), 673–687. Available from: doi:10.1016/S0092-8674(02)00971-6 [Accessed: 21 January 2017].
81. Hynes, R.O., & Lander, A.D. (1992). Contact and adhesive specificities in the associations, migrations, and targeting of cells and axons. *Cell*. [Online] 68 (2), 303–322. Available from: doi:10.1016/0092-8674(92)90472-O [Accessed: 21 January 2017].
82. Itoh, S., Takakuda, K., Ichinose, S., Kikuchi, M., & Schinomiya, K. (2001) A study of induction of nerve regeneration using bioabsorbable tubes. *Journal of Reconstructive Microsurgery*. [Online] 17 (2), 115–123. Available from: doi:10.1055/s-2001-12700 [Accessed: 18 January 2017].
83. Jiang, X., Lim, S.H., Mao Hai-Quan, H.Q. & Chew, S.Y. (2010) Current applications and future perspectives of artificial nerve conduits. *Experimental Neurology*. [Online]. 223 (1) pp.86–101. Available from: doi:10.1016/j.expneurol.2009.09.009 [Accessed: 18 January 2017].
84. Jung, S. B. (2012). Bioactive Borate Glasses. In: Jones, J.R. & Clare, A.G Bio-Glasses: An Introduction. Chichester, John Wiley & Sons, Ltd. doi: 10.1002/9781118346457.ch6
85. Kai, Z., Ying, D. & Guo-Qiang, C. (2003) Effects of surface morphology on the biocompatibility of polyhydroxyalkanoates. *Biochemical Engineering Journal*. [Online] 16 (2), 115–123. Available from: doi:10.1016/S1369-703X(03)00029-9 [Accessed: 18 January 2017].

86. Kehoe, S., Zhang, X.F., & Boyd, D. (2012). FDA approved guidance conduits and wraps for peripheral nerve injury: a review of materials and efficacy. *Injury*. [Online] 43 (5), 553–572. Available from: doi:10.1016/j.injury.2010.12.030 [Accessed: 21 January 2017].
87. Kelsey, J.K., Nelson, L., Felberg, A., & Rice, D. (1997). Upper extremity disorders: frequency, impact, and cost. New York: Churchill Livingstone.
88. Khorasani, M.T., Mirzadeh, H. & Irani, S. (2008) Plasma surface modification of poly (l-lactic acid) and poly (lactic-co-glycolic acid) films for improvement of nerve cells adhesion. *Radiation Physics and Chemistry*. [Online] 77 (3), 280–287. Available from: doi:10.1016/j.radphyschem.2007.05.013 [Accessed: 18 January 2017].
89. Kiernan, J. A., & N. Rajakumar. (2014). Barr's The human nervous system, 10th ed. Baltimore: Wolters Kluwer/Lippincot Williams & Wilkins.
90. Kim, Y. tae, Haftel, V.K., Kumar, S. & Bellamkonda, R. V (2008) The role of aligned polymer fiber-based constructs in the bridging of long peripheral nerve gaps. *Biomaterials*. [Online] 29 (21), 3117–3127. Available from: doi:10.1016/j.biomaterials.2008.03.042 [Accessed: 18 January 2017].
91. Kim, Y.-P., Lee, G.-S., Kim, J.-W., Kim, M.S., Ahn, H. S., Lim, J. Y., Kim, H. W., Son, Y. J. Knowles, J. C. & Hyun, J. K. (2015). Phosphate glass fibres promote neurite outgrowth and early regeneration in a peripheral nerve injury model. *Journal of Tissue Engineering and Regenerative Medicine*. [Online] 9 (3), 236–246. Available from: doi:10.1002/term.1626 [Accessed: 20 January 2017].
92. Koudehi, M.F., Fooladi, A.A.I., Mansoori, K., Jamalpoor, Z., Amiri, A., & Nourani, M. R. (2014) Preparation and evaluation of novel nano-bioglass/gelatin conduit for peripheral nerve regeneration. *Journal of Materials Science: Materials in Medicine*. [Online] 25 (2), 363–373. Available from: doi:10.1007/s10856-013-5076-1 [Accessed: 20 January 2017].
93. Lee, A.C., Yu, V.M., Lowe, J.B., Brenner, M.J., Hunter, D. A., Mackinnon, S. E. and Sakiyama-Elbert, S. E. (2003). Controlled release of nerve growth factor enhances sciatic nerve regeneration. *Experimental Neurology*. [Online] 184 (1), 295–303. Available from: doi:10.1016/S0014-4886(03)00258-9 [Accessed: 18 January 2017].

94. Lee, J.W., Kim, Y.H., Park, K.D., Jee, K.S., Shinc, J.W., & Hahn, S. B. (2004). Importance of integrin β 1-mediated cell adhesion on biodegradable polymers under serum depletion in mesenchymal stem cells and chondrocytes. *Biomaterials*. [Online] 25 (10), 1901–1909. Available from: doi:10.1016/j.biomaterials.2003.08.037 [Accessed: 18 January 2017].
95. Lee, S.J., Khang, G., Lee, Y.M. & Lee, H.B. (2003) The effect of surface wettability on induction and growth of neurites from the PC-12 cell on a polymer surface. *Journal of Colloid and Interface Science*. [Online] 259 (2), 228–235. Available from: doi:10.1016/S0021-9797(02)00163-7 [Accessed: 21 January 2017].
96. Lee, S.Y. (1996) Plastic bacteria? Progress and prospects for polyhydroxyalkanoate production in bacteria. *Trends in Biotechnology*. [Online]. 14 (11) pp.431–438. Available from: doi:10.1016/0167-7799(96)10061-5 [Accessed: 18 January 2017].
97. Lemoigne, M. (1927). Études sur l'autolyse microbienne origine de l'acide b-oxybutyrique formé par autolyse. *Annales de l'Institut Pasteur*. 41, 148-165.
98. Li, S.T., Archibald, S.J., Krarup, C. & Madison, R.D. (1992) Peripheral nerve repair with collagen conduits. *Clinical Materials*. [Online] 9 (3–4), 195–200. Available from: doi:10.1016/0267-6605(92)90100-8 [Accessed: 18 January 2017].
99. Liu, Y., Ji, Y., Ghosh, K., Clark, R.A.F., Huang, L., & Rafailovich, M. H. (2009). Effects of fiber orientation and diameter on the behavior of human dermal fibroblasts on electrospun PMMA scaffolds. *Journal of Biomedical Materials Research - Part A*. [Online] 90 (4), 1092–1106. Available from: doi:10.1002/jbm.a.32165 [Accessed: 21 January 2017]
100. Lizarraga-Valderrama, L.R., Nigmatullin, R., Taylor, C., Haycock, J.W., Claeysens, F., Knowles, J. C. and Roy, I. (2015) Nerve tissue engineering using blends of poly(3-hydroxyalkanoates) for peripheral nerve regeneration. *Engineering in Life Sciences*. [Online] 15 (6), 612–621. Available from: doi:10.1002/elsc.201400151 [Accessed: 20 January 2017]

101. Lu, Q., Han, J., Zhou, L., Zhou, J., & Xiang, H. (2008) Genetic and biochemical characterization of the poly(3-hydroxybutyrate-co-3-hydroxyvalerate) synthase in *Haloferax mediterranei*. *Journal of bacteriology*. [Online] 190 (12), 4173–4180. Available from: doi:10.1128/JB.00134-08 [Accessed: 20 January 2017].
102. Luis, A.L., Rodrigues, J.M., Lopes, M.A., Amado, S., et al. (2007) Evaluation of two biodegradable nerve guides for the reconstruction of the rat sciatic nerve. *Bio-medical Materials and Engineering*. [Online] 17 (1), 39–52. Available from: <http://www.ncbi.nlm.nih.gov/pubmed/17264386> [Accessed: 18 January 2017].
103. Lundborg, G., Dahlin, L., Dohi, D., Kanje, M., & N.Terada. (1997). A new type of "bioartificial" nerve graft for bridging extended defects in nerves. *The Journal of Hand Surgery: British & European Volume*. [Online] 22 (3), 299-303.
104. Mackinnon, S.E. & Dellon, A.L. (1990) Clinical nerve reconstruction with a bioabsorbable polyglycolic acid tube. *Plastic and reconstructive surgery*. [Online]. 85 (3) pp.419–424. Available from: doi: 10.1097/00006534-199003000-00015 [Accessed: 18 January 2017].
105. Mackinnon, S.E., Dellon, A.L., Hudson, A.R. & Hunter, D.A. (1985) A primate model for chronic nerve compression. *J Reconstr Microsurg*. [Online] 1 (3), 185–195. Available from: doi:10.1055/s-2007-1007073 [Accessed: 18 January 2017].
106. Madison, L.L. & Huisman, G.W. (1999) Metabolic engineering of poly(3-hydroxyalkanoates): from DNA to plastic. *Microbiology and molecular biology reviews* : *MMBR*. [Online] 63 (1), 21–53. Available from: doi:<p></p>. [Accessed: 18 January 2017].
107. Mao, C., Chen, X., Miao, G. & Lin, C. (2015) Angiogenesis stimulated by novel nanoscale bioactive glasses. *Biomedical materials*. [Online] 10 (2), 25005. Available from: doi:10.1088/1748-6041/10/2/025005 [Accessed: 20 January 2017].
108. Marchesini, S., Erard, N., Glumoff, T., Hiltunen, J.K., & Poirier, Y. (2003) Modification of the Monomer Composition of Polyhydroxyalkanoate Synthesized in *Saccharomyces cerevisiae* Expressing Variants of β -Oxidation-Associated Multifunctional Enzyme.

Applied and Environmental Microbiology. [Online] 69 (11), 6495–6499. Available from: doi:10.1128/AEM.69.11.6495-6499.2003 [Accessed: 18 January 2017].

109. Marquardt, L.M., Day, D., Sakiyama-Elbert, S.E. & Harkins, A.B. (2014). Effects of borate-based bioactive glass on neuron viability and neurite extension. *Journal of Biomedical Materials Research – Part A*. [Online] 102 (8), 2767–2775. Available from: doi:10.1002/jbm.a.34944 [Accessed: 21 January 2017].
110. Marquardt, L.M., Day, D., Sakiyama-Elbert, S.E. & Harkins, A.B. (2014) Effects of borate-based bioactive glass on neuron viability and neurite extension. *Journal of Biomedical Materials Research – Part A*. [Online] 102 (8), 2767–2775. Available from: doi:10.1002/jbm.a.34944 [Accessed: 20 January 2017].
111. Matsumoto, K., Ohnishi, K., Kiyotani, T., Sekine, T., Ueda, H., Nakamura, T., Endo, K., & Shimizu, Y. (2000) Peripheral nerve regeneration across an 80-mm gap bridged by a polyglycolic acid (PGA)-collagen tube filled with laminin-coated collagen fibers: A histological and electrophysiological evaluation of regenerated nerves. *Brain Research*. [Online] 868 (2), 315–328. Available from: doi:10.1016/S0006-8993(00)02207-1 [Accessed: 20 January 2017].
112. Menzies, K.L. & Jones, L. (2010). The impact of contact angle on the biocompatibility of biomaterials. *Optometry and vision science: official publication of the American Academy of Optometry*. [Online] 87 (6), 387–399. Available from: doi:10.1097/OPX.0b013e3181da863e [Accessed: 21 January 2017].
113. Mescher, A. L. (2010). *Junqueira's Basic Histology. Text and Atlas*, 14th Ed. Texas: Mc Graw Hill Education. Lange.
114. Midha, R. (2006) Emerging techniques for nerve repair: nerve transfers and nerve guidance tubes. *Clinical neurosurgery*. 53, 185–190.
115. Midha, R., Munro, C.A., Dalton, P.D., Tator, C.H., & and Shoichet, M. S. (2003) Growth factor enhancement of peripheral nerve regeneration through a novel synthetic hydrogel tube. *Journal of neurosurgery*. [Online] 99 (3), 555–565. Available from: doi:10.3171/jns.2003.99.3.0555 [Accessed: 18 January 2017].

116. Superb K. Misra, †, Sabeel P. Valappil, †,‡, Ipsita Roy, ‡ and & Aldo R. Boccaccini*, † (2006) Polyhydroxyalkanoate (PHA)/Inorganic Phase Composites for Tissue Engineering Applications. [Online] Available from: doi:10.1021/BM060317C [Accessed: 15 June 2017].
117. Miguez-Pacheco, V., Greenspan, D., Hench, L.L. & Boccaccini, A.R. (2015). Bioactive glasses in soft tissue repair. *American Ceramic Society Bulletin*. 94 (6).
118. Mohammadkhah, A., Marquardt, L.M., Sakiyama-Elbert, S.E., Day, D.E., & Harkins, A.B. (2015) Fabrication and characterization of poly-(ε)-caprolactone and bioactive glass composites for tissue engineering applications. *Materials Science and Engineering C*. [Online] 49632–639. Available from: doi:10.1016/j.msec.2015.01.060 [Accessed: 18 January 2017].
119. Mohanna, P.-N., Terenghi, G. & Wiberg, M. (2005) Composite PHB-GGF conduit for long nerve gap repair: a long-term evaluation. *Scandinavian journal of plastic and reconstructive surgery and hand surgery / Nordisk plastikkirurgisk forening [and] Nordisk klubb for handkirurgi*. [Online] 39 (3), 129–137. Available from: doi:10.1080/02844310510006295 [Accessed: 20 January 2017].
120. Moosvi, S.R. & Day, R.M. (2009). Bioactive glass modulation of intestinal epithelial cell restitution. *Acta Biomaterialia*. [Online] 5 (1), 76–83. Available from: doi:10.1016/j.actbio.2008.08.003 [Accessed: 18 January 2017].
121. Mosahebi, A., Fuller, P., Wiberg, M. & Terenghi, G. (2002) Effect of allogeneic Schwann cell transplantation on peripheral nerve regeneration. *Experimental neurology*. [Online] 173 (2), 213–223. Available from: doi:10.1006/exnr.2001.7846 [Accessed: 18 January 2017].
122. Mosahebi, A., Wiberg, M. & Terenghi, G. (2003) Addition of Fibronectin to Alginate Matrix Improves Peripheral Nerve Regeneration in Tissue-Engineered Conduits. *Tissue Engineering*. [Online] 9 (2), 209–218. Available from: doi:10.1089/107632703764664684 [Accessed: 18 January 2017].

123. Mosahebi, A., Woodward, B., Wiberg, M., Martin, R., & Terenghi, G. (2001) Retroviral labeling of Schwann cells: in vitro characterization and in vivo transplantation to improve peripheral nerve regeneration. *Glia*. [Online] 34 (1), 8–17. Available from: doi:10.1002/glia.1035 [pii] [Accessed: 18 January 2017].
124. Nilsson, A., Dahlin, L., Lundborg, G. & Kanje, M. (2005) Graft repair of a peripheral nerve without the sacrifice of a healthy donor nerve by the use of acutely dissociated autologous Schwann cells. *Scandinavian journal of plastic and reconstructive surgery and hand surgery*. [Online] 39 (1), 1–6. Available from: doi:10.1080/02844310410017979 [Accessed: 18 January 2017].
125. Noback, C. R. (1967). Human nervous system, New York: McGraw-Hill.
126. Noble, J., Munro, C.A., Prasad, V.S. & Midha, R. (1998). Analysis of upper and lower extremity peripheral nerve injuries in a population of patients with multiple injuries. *The Journal of trauma*. [Online] 45 (1), 116–122. Available from: doi:10.1097/00005373-199807000-00025 [Accessed: 21 January 2017].
127. Noda, I., Dowrey, A. E., Haynes, J. L., & Marcott, C. (2007). Group frequency assignments for major infrared bands observed in common synthetic polymers. In: Marck, J. I. (Ed.), *Physical Properties of Polymers Handbook*. New York: Springer, pp. 405-406.
128. Novajra, G., Tonda-Turo, C., Vitale-Brovarone, C., Ciardelli, G., Geuna, S. & Raimondo, S. (2014) Novel systems for tailored neurotrophic factor release based on hydrogel and resorbable glass hollow fibers. *Materials Science and Engineering C*. [Online] 36 (1), 25–32. Available from: doi:10.1016/j.msec.2013.11.035 [Accessed: 18 January 2017].
129. Ohta, M., Suzuki, Y., Chou, H., Ishikawa, N., Suzuki, S., Tanihara, M., Mizushima, Y., Dezawa, M. and Ide, C. (2004) Novel heparin/alginate gel combined with basic fibroblast growth factor promotes nerve regeneration in rat sciatic nerve. *Journal of Biomedical Materials Research - Part A*. [Online] 71 (4), 661–668. Available from: doi:10.1002/jbm.a.30194 [Accessed: 20 January 2017].
130. Ouyang, S.P., Luo, R.C., Chen, S.S., Liu, Q., Chung, A., Wu, Q., & Chen, G.Q. (2007) Production of polyhydroxyalkanoates with high 3-hydroxydodecanoate monomer

content by *fadB* and *fadA* knockout mutant of *Pseudomonas putida* KT2442. *Biomacromolecules*. [Online] 8 (8), 2504–2511. Available from: doi:10.1021/bm0702307 [Accessed: 18 January 2017].

131. Philip, S., Keshavarz, T. & Roy, I. (2007) Polyhydroxyalkanoates: Biodegradable polymers with a range of applications. *Journal of Chemical Technology and Biotechnology*. [Online]. 82 (3) pp.233–247. Available from: doi:10.1002/jctb.1667 [Accessed: 20 January 2017].
132. Phillips, J.B., Bunting, S.C.J., Hall, S.M. & Brown, R.A. (2005) Neural tissue engineering: a self-organizing collagen guidance conduit. *Tissue Engineering*. [Online] 11 (9), 1611–1617. Available from: doi:10.1089/ten.2005.11.1611 [Accessed: 18 January 2017].
133. Poli, A., Di Donato, P., Abbamondi, G.R. & Nicolaus, B. (2011). Synthesis, production, and biotechnological applications of exopolysaccharides and polyhydroxyalkanoates by Archaea. *Archaea*. [Online]. 2011 p.693253. Available from: doi:10.1155/2011/693253 [Accessed: 20 January 2017].
134. Poon, C.Y. & Bhushan, B. (1995). Comparison of surface roughness measurements by stylus profiler, AFM and non-contact optical profiler. *Wear*. [Online] 190 (1), 76–88. Available from: doi:10.1016/0043-1648(95)06697-7 [Accessed: 18 January 2017].
135. Quillaguamán, J., Guzmán, H., Van-Thuoc, D. & Hatti-Kaul, R. (2010) Synthesis and production of polyhydroxyalkanoates by halophiles: Current potential and future prospects. *Applied Microbiology and Biotechnology*. [Online] 85 (6), 1687–1696. Available from: doi:10.1007/s00253-009-2397-6 [Accessed: 18 January 2017].
136. Rai, R., Keshavarz, T., Roether, J.A., Boccaccini, A.R., & Roy, I. (2011) Medium chain length polyhydroxyalkanoates, promising new biomedical materials for the future. *Materials Science and Engineering R: Reports*. [Online] 72 (3), 29–47. Available from: doi:10.1016/j.mser.2010.11.002, [Accessed: 18 January 2017].
137. Rai, R., Yunos, D.M., Boccaccini, A.R., Knowles, J.C., Barker I.A., Howdle S.M., Tredwell G.D., Keshavarz T., & Roy, I. (2011). Poly-3-hydroxyoctanoate P(3HO), a medium chain length polyhydroxyalkanoate homopolymer from *Pseudomonas*

- mendocina. *Biomacromolecules*. [Online] 12 (6), 2126–2136. Available from: doi:10.1021/bm2001999 [Accessed: 21 January 2017].
138. Randriamahefa, Solo Estelle Renard, Philippe Guérin, Valérie Langlois. Reddy, C. S. K., Ghai, R., Rashmi, and Kalia, V. C. (2003). Polyhydroxyalkanoates: an overview. *Bioresource Technology*, 87, 137-146.
139. Randriamanhefa, S., Renard, E., Guérin, P. & Langlois, V. (2003). Fourier transform infrared spectroscopy for screening and quantifying production of PHAs by *Pseudomonas* grown on sodium octanoate. *Biomacromolecules*. [Online] 4 (4), 1092–1097. Available from: doi:10.1021/bm034104o [Accessed: 18 January 2017].
140. Ravi, M., Paramesh, V., Kaviya, S.R., Anuradha, E., & Solomon, F.D. (2015). 3D cell culture systems: Advantages and applications. *Journal of Cellular Physiology*. [Online] 230 (1), 16–26. Available from: doi:10.1002/jcp.24683 [Accessed: 21 January 2017].
141. Reddy, C.S.K., Ghai, R., Rashmi & Kalia, V.C. (2003) Polyhydroxyalkanoates: An overview. *Bioresource Technology*. [Online]. 87 (2) pp.137–146. Available from: doi:10.1016/S0960-8524(02)00212-2.
142. Robinson, P.H., Van Der Lei, B., Hoppen, H.J., Leenslag, J.W., Pennings, A. J. & Nieuwenhuis, P. (1991) Nerve regeneration through a two-ply biodegradable nerve guide in the rat and the influence of ACTH4-9 nerve growth factor. *Microsurgery*. [Online] 12 (6), 412–419. Available from: doi:10.1002/micr.1920120608 [Accessed: 18 January 2017].
143. Ronchi, G., Jager, S.B., Vaegter, C.B., Raimondo, S., Giacobini-Robecchi, M.G, & Geuna S. J. (2014). Discrepancies in quantitative assessment of normal and regenerated peripheral nerve fibers between light and electron microscopy. *Journal of the Peripheral Nervous System*. [Online] 19 (3), 224–233. Available from: doi:10.1111/jns.12090 [Accessed: 21 January 2017].
144. Sangkharak, K. and Prasertsan, P. (2008). Nutrient optimization for production of polyhydroxybutyrate from halotolerant photosynthetic bacteria cultivated under aerobic-dark condition. *Electronic Journal of Biotechnology*. [Online] 11 (3). Available from: doi: 10.2225/vol11-issue3-fulltext-2 [Accessed: 18 January 2017].

145. Sato, H., Murakami, R., Padermshoke, A., Hirose, F., Senda, K., Noda, I., & Ozaki, Y. (2004). Infrared spectroscopy studies of CH \cdots O hydrogen bondings and thermal behavior of biodegradable poly(hydroxyalkanoate). *Macromolecules*. [Online] 37 (19), 7203–7213. Available from: doi:10.1021/ma049117o [Accessed: 18 January 2017].
146. Schmidt, C.E. & Leach, J.B. (2003). Neural Tissue Engineering: Strategies for Repair and Regeneration. *Annual Review of Biomedical Engineering*. [Online] 5 (1), 293–347. Available from: doi:10.1146/annurev.bioeng.5.011303.120731 [Accessed: 17 January 2017].
147. Shoichet, M.S. (2010). Polymer scaffolds for biomaterials applications. *Macromolecules*. [Online] 43 (2), 581–591. Available from: doi:10.1021/ma901530r [Accessed: 20 January 2017].
148. Shrivastav, A., Mishra, S.K., Shethia, B., Pancha, I., Jain, D., & Mishra, S. (2010) Isolation of promising bacterial strains from soil and marine environment for polyhydroxyalkanoates (PHAs) production utilizing Jatropha biodiesel byproduct. *International Journal of Biological Macromolecules*. [Online] 47 (2), 283–287. Available from: doi:10.1016/j.ijbiomac.2010.04.007 [Accessed: 18 January 2017].
149. Snaidero, N. & Simons, M. (2014) Myelination at a glance. *Journal of cell science*. [Online] 127 (Pt 14), 2999–3004. Available from: doi:10.1242/jcs.151043 [Accessed: 17 January 2017].
150. Stang, F., Fansa, H., Wolf, G., Reppin, M., & Keilhoff, G. (2005) Structural parameters of collagen nerve grafts influence peripheral nerve regeneration. *Biomaterials*. [Online] 26 (16), 3083–3091. Available from: doi:10.1016/j.biomaterials.2004.07.060 [Accessed: 18 January 2017].
151. Sterne, G.D., Brown, R.A., Green, C.J. & Terenghi, G. (1997) Neurotrophin-3 delivered locally via fibronectin mats enhances peripheral nerve regeneration. *European Journal of Neuroscience*. [Online] 9 (7), 1388–1396. Available from: doi:10.1111/j.1460-9568.1997.tb01493.x [Accessed: 18 January 2017].

152. Strauch, B., Rodriguez, D.M., Diaz, J., Yu, H.L., Kaplan, G., and Weinstein, D. E. (2001) Autologous Schwann cells drive regeneration through a 6-cm autogenous venous nerve conduit. *Journal of Reconstructive Microsurgery*. [Online] 17 (8), 589–595. Available from: doi:10.1055/s-2001-18812 [Accessed: 20 January 2017].
153. Strawhecker, K.E., Kumar, S.K., Douglas, J.F. & Karim, A. (2001). The Critical Role of Solvent Evaporation on the Roughness of Spin-Cast Polymer Films. *Macromolecules*. [Online] 34 (14), 4669–4672. Available from: doi:10.1021/ma001440d [Accessed: 21 January 2017].
154. Sufan, W., Suzuki, Y., Tanihara, M., Ohnishi, K., Suzuki, K., Endo, K., Nishimura, Y. (2001) Sciatic nerve regeneration through alginate with tubulation or nontubulation repair in cat. *Journal of neurotrauma*. [Online] 18 (3), 329–338. Available from: doi:10.1089/08977150151070991 [Accessed: 20 January 2017].
155. Sugiura, Y., Lin, W., Sanes, J.R., Lichtman, J.W., et al. (2011) Neuron-glia interactions: the roles of Schwann cells in neuromuscular synapse formation and function. *Bioscience reports*. [Online] 31 (5), 295–302. Available from: doi:10.1042/BSR20100107 [Accessed: 17 January 2017].
156. Sun, T., Jackson, S., Haycock, J.W. & MacNeil, S. (2006) Culture of skin cells in 3D rather than 2D improves their ability to survive exposure to cytotoxic agents. *Journal of Biotechnology*. [Online] 122 (3), 372–381. Available from: doi:10.1016/j.jbiotec.2005.12.021 [Accessed: 18 January 2017].
157. Sun, T., Jackson, S., Haycock, J.W. & MacNeil, S. (2006) Culture of skin cells in 3D rather than 2D improves their ability to survive exposure to cytotoxic agents. *Journal of Biotechnology*. [Online] 122 (3), 372–381. Available from: doi:10.1016/j.jbiotec.2005.12.021.
158. Suzuki, K., Suzuki, Y., Tanihara, M., Ohnishi, K., Hashimoto, T., Endo, K., Nishimura, Y. (2000) Reconstruction of rat peripheral nerve gap without sutures using freeze-dried alginate gel. *Journal of biomedical materials research*. [Online] 49 (4), 528–533. Available from: doi:10.1002/(SICI)1097-4636(20000315)49:4<528::AID-JBM11>3.0.CO;2-1 [pii] [Accessed: 20 January 2017].

159. Tamada, Y. & Ikada, Y. (1993) Effect of preadsorbed proteins on cell adhesion to polymer surfaces. *Journal of Colloid and Interface Science*. [Online]. 155 (2) pp.334–339. Available from: doi:10.1006/jcis.1993.1044 [Accessed: 18 January 2017].
160. Tian, P.-Y., Shang, L., Ren, H., Mi, Y., Fan D., & Jiang, M. (2009) Biosynthesis of polyhydroxyalkanoates: Current research and development. *African Journal of Biotechnology*. [Online] 8 (5), 709–714. Available from: <http://www.academicjournals.org/AJB> [Accessed: 20 January 2017].
161. Tian, W., Hong, K., Chen, G.Q., Wu, Q., Zhang, R. Q.; Huang, W. (2000). Production of polyesters consisting of medium chain length 3-hydroxyalkanoic acids by *Pseudomonas mendocina* 0806 from various carbon sources. *Antonie van Leeuwenhoek, International Journal of General and Molecular Microbiology*. [Online] 77 (1), 31–36. Available from: doi:10.1023/A:1002099023046 [Accessed: 20 January 2017].
162. Toba, T., Nakamura, T., Shimizu, Y., Matsumoto, K., et al. (2001) Regeneration of canine peroneal nerve with the use of a polyglycolic acid-collagen tube filled with laminin-soaked collagen sponge: A comparative study of collagen sponge and collagen fibers as filling materials for nerve conduits. *Journal of Biomedical Materials Research*. [Online] 58 (6), 622–630. Available from: doi:10.1002/jbm.1061 [Accessed: 18 January 2017].
163. Tojima, T., Yamane, Y., Takahashi, M. & Ito, E. (2000). Acquisition of neuronal proteins during differentiation of NG108-15 cells. *Neuroscience Research*. [Online] 37 (2), 153–161. Available from: doi:10.1016/S0168-0102(00)00110-3 [Accessed: 21 January 2017].
164. Tomizawa, S., Hyakutake, M., Saito, Y., Agus, J., Mizuno, K., Abe, H., & Tsuge, T. (2011). Molecular weight change of polyhydroxyalkanoate (PHA) caused by the PhaC subunit of PHA synthase from bacillus cereus YB-4 in recombinant *Escherichia coli*. *Biomacromolecules*. [Online] 12 (7), 2660–2666. Available from: doi:10.1021/bm2004687 [Accessed: 21 January 2017].

165. Valentina Miguez-Pacheco, David Greenspan, Larry L. Hench, and Aldo R. Boccaccini. Bioactive glasses in soft tissue repair. *American Ceramic Society Bulletin*, 94 (6) 27-31.
166. Valero-Cabré, A., K. Tsironis, E. Skouras, G. Perego, X. Navarro, and W. F. Neiss. (2001) Superior muscle reinnervation after autologous nerve graft or poly-L-lactide- ϵ -caprolactone (PLC) tube implantation in comparison to silicone tube repair. *Journal of neuroscience research*. [Online] 63 (2), 214–223. Available from: doi: 10.1002/1097-4547(20010115)63:2<214::AID-JNR1014>3.0.CO;2-D [Accessed: 18 January 2017].
167. Vitale-Brovarone, C., Novajra, G., Lousteau, J., Milanese, D., Raimondo, S. & Fornaro, M. (2012) Phosphate glass fibres and their role in neuronal polarization and axonal growth direction. *Acta Biomaterialia*. [Online] 8 (3), 1125–1136. Available from: doi:10.1016/j.actbio.2011.11.018 [Accessed: 18 January 2017].
168. Vleggeert-Lankamp, C.L.A.M., De Ruitter, G.C.W., Wolfs, J.F.C., Pego, A.P., van den Berg, R. J., Feirabend, H. K. P., Malessy, M. J. A., & Lakke, E. A. J. F. (2007) Pores in synthetic nerve conduits are beneficial to regeneration. *Journal of Biomedical Materials Research - Part A*. [Online] 80 (4), 965–982. Available from: doi:10.1002/jbm.a.30941 [Accessed: 20 January 2017].
169. Wang, H.B., Mullins, M.E., Cregg, J.M., McCarthy, C.W., & Gilberta, R. J. (2010) Varying the diameter of aligned electrospun fibers alters neurite outgrowth and Schwann cell migration. *Acta Biomaterialia*. [Online] 6 (8), 2970–2978. Available from: doi:10.1016/j.actbio.2010.02.020 [Accessed: 18 January 2017].
170. Wang, J., Liu, G., Fang, Y. & Li, W. (2016). Marangoni effect in nonequilibrium multiphase system of material processing. *Reviews in Chemical Engineering*. [Online] 32 (5), 551–585. Available from: doi:10.1515/revce-2015-0067 [Accessed: 21 January 2017].
171. Wang, S., Cai, Q., Hou, J., Bei, J., et al. (2003) Acceleration effect of basic fibroblast growth factor on the regeneration of peripheral nerve through a 15-mm gap. *Journal of biomedical materials research. Part A*. [Online] 66 (3), 522–531. Available from: doi:10.1002/jbm.a.10008 [Accessed: 18 January 2017].

172. Waxman, S. G., & Bennett, M. V. L. (1972). Relative Conduction Velocities of Small Myelinated and Non-myelinated Fibres in the Central Nervous System. *Nature New Biology*. [Online] 238, 217-219. Available from: doi:10.1038/newbio238217a0 [Accessed: 17 January 2017].
173. Weber, R.A., Breidenbach, W.C., Brown, R.E., Jabaley, M.E., et al. (2000) A randomized prospective study of polyglycolic acid conduits for digital nerve reconstruction in humans. *Plastic and reconstructive surgery*. [Online] 106 (5), 1036–1045. Available from: doi:10.1097/00006534-200109150-00056 [Accessed: 18 January 2017].
174. Wei, J., Igarashi, T., Okumori, N., Igarashi, T., Maetani, T., Liu, B., & Yoshinar, M. (2009). Influence of surface wettability on competitive protein adsorption and initial attachment of osteoblasts. *Biomedical materials (Bristol, England)*. [Online] 4 (4), 45002. Available from: doi:10.1088/1748-6041/4/4/045002 [Accessed: 21 January 2017].
175. Wells, M.R., Kraus, K., Batter, D.K., Blunt, D.G., Weremowitzd, J., Lynchd, S.E., Antoniadesd, H.N., & Hanssone H.-A. (1997) Gel matrix vehicles for growth factor application in nerve gap injuries repaired with tubes: a comparison of biomatrix, collagen, and methylcellulose. *Experimental neurology*. [Online] 146 (2), 395–402. Available from: doi:10.1006/exnr.1997.6543.
176. Wen, X. & Tresco, P.A. (2006) Effect of filament diameter and extracellular matrix molecule precoating on neurite outgrowth and Schwann cell behavior on multifilament entubulation bridging device in vitro. *Journal of Biomedical Materials Research - Part A*. [Online] 76 (3), 626–637. Available from: doi:10.1002/jbm.a.30520 [Accessed: 21 January 2017].
177. Whitworth, I.H., Brown, R.A., Doré, C., Green, C.J., & Terenghi, G. (1995) Orientated mats of fibronectin as a conduit material for use in peripheral nerve repair. *Journal of Hand Surgery*. [Online] 20 (4), 429–436. Available from: doi:10.1016/S0266-7681(05)80148-2 [Accessed: 20 January 2017].
178. Wood, M.D., Moore, A.M., Hunter, D.A., Tuffaha, S., Borschel G. H., Mackinnon, S. E., & Sakiyama-Elbert, S. E. (2009) Affinity-based release of glial-derived neurotrophic

- factor from fibrin matrices enhances sciatic nerve regeneration. *Acta Biomaterialia*. [Online] 5 (4), 959–968. Available from: doi:10.1016/j.actbio.2008.11.008.
179. Wu, Q., Tian, G., Wu, Q., Sun, S. Q, Noda, I., & Chen, G-Q. (2001) Study of microbial polyhydroxyalkanoates using two-dimensional Fourier-transform infrared correlation spectroscopy. *Journal of Applied Polymer Science*. [Online] 82 (4), 934–940. Available from: doi:10.1002/app.1925 [Accessed: 21 January 2017].
180. Xu, X., Yee, W.C., Hwang, P.Y.K., Yu, H., Wan, A. C. A, Gao, S., Boon K. –L., Mao, H. –Q., Leong, K. W, & Wang, S. (2003) Peripheral nerve regeneration with sustained release of poly(phosphoester) microencapsulated nerve growth factor within nerve guide conduits. *Biomaterials*. [Online] 24 (13), 2405–2412. Available from: doi:10.1016/S0142-9612(03)00109-1.
181. Xu, Z., Choudhary, S., Okada, Y., Voznesensky, O., Alandera, C., Raisza, L., Pilbeam, C. (2007). Cyclooxygenase-2 gene disruption promotes proliferation of murine calvarial osteoblasts in vitro. *Bone*. [Online] 41 (1), 68–76. Available from: doi:10.1016/j.bone.2007.03.009 [Accessed: 21 January 2017].
182. Yang, Y., Ding, F., Wu, J., Hu, W., Liu, W., Liu, J., & Gu, X. (2008) Development and evaluation of silk fibroin-based nerve grafts for peripheral nerve regeneration. In: *IFMBE Proceedings*. [Online]. 2008 Berlin, Heidelberg, Springer Berlin Heidelberg. pp. 4–8. Available from: doi:10.1007/978-3-540-79039-6-2 [Accessed: 20 January 2017].
183. Yao, L., de Ruiter, G.C.W., Wang, H., Knight, A.M., Spinner, R. J., Yaszemski, M. J., Windebank, A. J., & Pandit, A. (2010) Controlling dispersion of axonal regeneration using a multichannel collagen nerve conduit. *Biomaterials*. [Online] 31 (22), 5789–5797. Available from: doi:10.1016/j.biomaterials.2010.03.081.
184. Yao, L., Wang, S., Cui, W., Sherlock, R., O’Connellb, C., Damodarana, G., Gormanc, A., Windebanke, A., & Pandita, A. (2009) Effect of functionalized micropatterned PLGA on guided neurite growth. *Acta Biomaterialia*. [Online] 5 (2), 580–588. Available from: doi:10.1016/j.actbio.2008.09.002.
185. Yildirim, E.D., Besunder, R., Pappas, D., Allen, F., Güçeri, S., & Sun, W. (2010). Accelerated differentiation of osteoblast cells on polycaprolactone scaffolds driven by

- a combined effect of protein coating and plasma modification. *Biofabrication*. [Online] 2 (1), 14109. Available from: doi:10.1088/1758-5082/2/1/014109 [Accessed: 21 January 2017].
186. Young, R.C., Wiberg, M. & Terenghi, G. (2002). Poly-3-hydroxybutyrate (PHB): a resorbable conduit for long-gap repair in peripheral nerves. *British journal of plastic surgery*. [Online] 55 (3), 235–240. Available from: doi:10.1054/bjps.2002.3798.
187. Yu, J. & Wang, J. (2001). Metabolic flux modeling of detoxification of acetic acid by *Ralstonia eutropha* at slightly alkaline pH levels. *Biotechnology and Bioengineering*. [Online] 73 (6), 458–464. Available from: doi:10.1002/bit.1080 [Accessed: 20 January 2017].
188. Yu, X. & Bellamkonda, R. V. (2003) Tissue-Engineered Scaffolds Are Effective Alternatives to Autografts for Bridging Peripheral Nerve Gaps. *Tissue Engineering*. [Online] 9 (3), 421–430. Available from: doi:10.1089/107632703322066606 [Accessed: 18 January 2017].
189. Zhang, J., Lineaweaver, W.C., Oswald, T., Chen, Z., Chen, Z., & Zhang, F. (2004). Ciliary Neurotrophic Factor for Acceleration of Peripheral Nerve Regeneration: An Experimental Study. *Journal of Reconstructive Microsurgery*. [Online] 20 (4), 323–327. Available from: doi:10.1055/s-2004-824891 [Accessed: 18 January 2017].